Application of Tree Barks to the Removal of Arsenic(V) and Selenium(IV) Species from Coal Fly Ash Leachates

By

Zahra Khamseh Safa

A Dissertation

Submitted in fulfilment of the requirements for the degree of

Doctor of Philosophy

Department of Chemistry and Biomolecular Sciences

Faculty of Science and Engineering

Macquarie University

Sydney, New South Wales, Australia

30 June 2017

Abstract

Coal fly ash is generated during the combustion of coal for energy production in thermal power plants. Approximately more than 50% worldwide of all coal fly ashes is either stored in stockpiles, or disposed in ash landfills or lagoons. Fly ash is recognised as an environmental contaminant because of its high concentration of trace elements, such as As and Se, and the potential for leaching these elements into the wider environment. Several methods, excluding biosorption have already been reported for elemental removal from fly ash.

Biosorbents, which refer to a group of compounds derived from the inactive, dead or microbial biomass, have the capacity to bind and potential utility in removing trace elements from wastewater systems. Tree bark as non-living biomass materials, contain proteins, carbohydrates and phenolic compounds, which can provide a wide variety of ion exchange sites. Additionally, tree barks as an environmentally friendly low cost biosorbents are readily available, renewable resource with a large surface area, and able to potentially regenerate for metal recovery.

In this study, the feasibility of using the outer layer of selected tree barks as biosorbents for removing the most abundant arsenic and selenium speciation, arsenic(V) and selenium(IV), from fly ash leachate was investigated, and the results reveal that the selected tree barks are well effective for specified biosorption.

In the beginning, three class F fly ash samples, including two acidic and one alkaline samples, have been assessed to characterise their physical (pH, moisture%, Brunauer-Emmett-Teller (BET) surface area and percentage of loss on ignition (LOI%)), chemical (major and minor elements) and morphological properties. Additionally, we have performed in this study a selection of leaching experiments under variable conditions (pH: 4, 7 and 11, solid: liquid ratios of 1:3.5 and 1:10, and contact time 1 and 24 h) in order to determine the amount of As(V) and

Se(IV) present in fly ash leachates. Acidic fly ashes were found to release nearly 10% of As, twice the corresponding level in the alkaline fly ash leachate, whilst more than 50% of Se was removable from alkaline fly ash, nearly 10-fold the level in acidic fly ash leachate. Leaching experiments determined that fly ashes would tend to maintain its natural pH level regardless of the initial pH of the solutions used in leaching test. However, the initial pH exhibited a major but variable effect on As(V) and Se(IV) mobility. The mobility of both As(V) and Se(IV) at a lower solid-to-liquid ratio of 1: 10 was found to be reduced by half in some cases. Nonetheless, during the early stage of leaching, As(V) and Se(IV) were quickly removed from enriched fine particles with great surface areas, whilst the mobility of these elemental species decreased with time, which may be due to sorption and/or co-precipitation of elements 'back into' the solid phase.

Following the above study, a series of adsorption experiments was conducted on selected tree barks in order to assess the effects of bark-type, pH, contact time, biosorption dosage, and initial As(V) and Se(IV) concentration on adsorption process. In this study, barks of *Eucalyptus deanei* (*Ed*) and *Melaleuca quinquenervia* (*Mq*) have been applied as potential biosorbents for both As(V) and Se(IV) removal. The sorption of these elementals species on bark was found to be highly dependent on solution pH. With increases in pH, sorption of As(V) and Se(IV) followed several increasing and decreasing trends which may be due to changes of an element-bark bond, which may exist as strong inner-sphere covalent bonds and weak outer-sphere hydrogen bonds at different pH conditions. Specifically, the maximum sorption of As(V) occurred at pH 5 at *Eucalyptus deanei* bark (47.7%), and at pH 4 at *Melaleuca quinquenervia* bark (56.8%), while Se(IV) was sorbed mostly at pH 6 at *Eucalyptus deanei* bark (85.8%), and at pH 5 at *Melaleuca quinquenervia* bark (84.5%). The sorption of both As(V) and Se(IV) was then determined to increase as a function of bark dosage and contact time, but decreased with a higher initial As(V) and Se(IV) concentration. The data for equilibrium sorption showed good fit to the Sips model for As(V) sorption, whilst the Langmuir and the Sips isotherm models

showed better fit compared to the Freundlich model for Se(IV) sorption. Accordingly, we have proposed here a sorption model consisting of a monolayer on a homogeneous bark surface in higher element concentration, whilst in solutions with lower element concentration a multilayer sorption on the heterogeneous surface of bark may have occurred. A pseudo-second-order kinetic model was found to correlate most strongly with the experimental data for As(V) and Se(IV) sorption from aqueous solutions. Therefore, surface sorption is crucial in the As and Se sorption process. Desorption experiments indicated that sorption of As(V) and Se(IV) might follow an ion-exchange and strong physical-chemical sorption, which led to low percentage desorption of both elements.

Finally, the removal of As(V) and Se(IV) from the acidic and alkaline fly ash leachates was demonstrated using tree bark species of *Eucalyptus deanei* and *Melaleuca quinquenervia* under optimised conditions of the biosorption process. It was found that approximately 69% to 100% As(V) can be removed from fly ash leachate in using *Ed*, and from 86% to 100% in using *Mq*. Moreover, 65% to 100% Se(IV) were removed from selected fly ash leachate using *Ed* bark, and from 63% to 85% in using *Mq* bark. Overall, the present study has demonstrated that both the *Eucalyptus deanei* bark and *Melaleuca quinquenervia* bark are effective sorbents for As(V) and Se(IV) removal from fly ash leachates.

Dedication

This dissertation is dedicated to my parents for supporting me to achieve my goals in life.

Acknowledgements

I would like to take this opportunity to thank faculty, staff, friends and family whose endless support and help has led me to where I am today. I would like to extend my gratitude to my principal supervisor, Dr Christopher McRae, for his enthusiasm, patience and encouragement throughout my PhD study. He has provided me invaluable assistance to the development of my research, which I am very grateful.

I would also like to thank my associate supervisor, Dr Danny Wong, for his outstanding advice, warm support and great encouragement during the preparation time of my thesis. He has as always managed to find time for our interactions for which I am very appreciative. Without his help, it would have been difficult for me to finalise and submit my dissertation.

I would like to thank Macquarie University for funding this research through a MQRES scholarship, and HDR staffs especially Ms. Jane Yang, Faculty of Science and Engineering HDR manager, for their great assistance during my study.

I would like to thank Delta Energy and Energy Australia for providing free coal fly ash samples. Special thanks to Dr Jane Aiken and Stephen Galway for their assistance during my visit at Mount Piper and Vales Point Power Stations, and collecting fly ash samples.

I would like to express my deep gratitude to Nicole Vella from Department of Biology, Microscopy Unit at Macquarie University, for her immense help in analysing samples using SEM-EDS. I would also like to thank Mark Tran from Department of Chemistry and Biomolecular Sciences, for his great support in using HG-AAS and FTIR-ATR, and Anthony Gurlica, Research Laboratory Manager, for his help in the maintenance of laboratory supplies.

My thanks are also due to Peter Wieland from Department of Earth and Planetary Science, Macquarie University, for countless help in analysing samples using XRF and ICP-MS, and Dr.

Jason Scott from Particles and Catalysis Research Group, the University of New South Wales, for excessive help in performing BET surface area analysis. Their valuable assistance and advice have contributed to achievements reported in my research.

My special thanks to Dr David Cantor, who has provided valuable comments and suggestions on my dissertation format. I would also like to thank the Department of Chemistry and Biomolecular Sciences for supporting me as a graduate student at the Macquarie University.

I would like to thank my current and former colleagues: Nathan Camilleri for his great help in analysing samples using CNH analyser, Dr Sahar Farzadnia, Dr Shabnam Tarahi Tabrizi, Dr Seyed Mohammad Hashemi Kavouei, Dr Nima Sayyadi, and Dr Mehdi Mirzayi for their enthusiastic discussions and encouragements on my research project.

Finally, I would like to thank my parents, my sister, her two gorgeous daughters, my brother-in-law, all my family members and friends for supporting me throughout and helping me overcome the difficulties of studying abroad and making it a wonderful experience.

Declaration

I hereby declare that this thesis represents my own work and effort in its entirety, and has not been submitted for a higher degree or otherwise at any other university, or institution.

Zahra Khamseh Safa **Date**

Table of Contents

List of Tables

List of Figures

Chapter 1

Introduction to Biosorbents and Coal Fly Ash

1.1 General Introduction

Biosorbents refer to a group of compounds derived from the inactive, dead or microbial biomass that has the capacity to bind, sequester and concentrate trace elements from dilute aqueous solutions (Gadd, 2009, Michalak *et al.*, 2013, Fomina and Gadd, 2014). Biosorbents are typically derived from one of the following three sources:

- Non-living biomass (*e.g.*, bark, lignin, shrimp, krill, squid, crab shell);
- Algal biomass;
- Microbial biomass (*e.g.*, bacteria, fungi and yeast).

Biosorbents are a focus of interest for their potential utility in removing trace elements from wastewater systems. In particular, the wide array of compounds found within non-living biomass materials, such as tree bark, has been widely investigated in recent decades (Michalak *et al.*, 2013). Due to their heterogeneous constituents of proteins, carbohydrates and phenolic compounds, these biomaterials offer numerous molecular groups to provide a wide variety of ion exchange sites for hydroxyl, carboxyl, sulfate, phosphate, and amine groups (Gaballah and Kilbertus, 1998). The high abundance of tannin, lignin and cellulose within tree bark are primarily responsible for their biosorptive properties (Wan Ngah and Hanafiah, 2008).

Moreover, tree barks are readily available, low cost, and they are a renewable resource with a large surface area. In conjunction with the possibility of regeneration and metal recovery, the preferential use of tree barks can often be justified as an environmentally friendly biosorbent.

Coal fly ash is generated as a by-product during the industrial combustion of coal for energy production in thermal power plants. In 2011, these plants annually produce approximately 780 million tons worldwide (Heidrich *et al.*, 2013) of coal combustion products including fine, powdery particles that are released into the environment. Australia, with its 40 thermal power plants, produces between 12-14.5 million tonnes of fly ash every year. Globally, between 3-57% of all fly ash (with average of 25%) are re-used in the form of cement and concrete, mine backfill, land filling, soil treatment, production of synthetic zeolites, ceramic filters for hot gas cleaning, and adsorbents (Blissett and Rowson, 2012). However, the remaining masses of fly ash (up to 75%) are either temporarily stored in stockpiles or simply disposed off in ash landfills or lagoons. This can have wide-spread environmental consequences as fly ash has been recognised as an environmental contaminant due to its high concentrations of toxic metals, and the potential for the leaching of these metals into the wider environment. There is an array of methods currently employed to remove these metals from coal fly ash; such as acid washing (Kashiwakura *et al.*, 2010), supercritical fluid extraction with CO_2 and organic ligands, and bacterial bioextraction. However, these methods are expensive and can generate additional waste disposal issues. Amongst the toxic elements in fly ash, As and Se are particularly concerning. In their oxyanionic forming species, As and Se are highly soluble in water, with their maximum leachability in the pH 7–10 range (Jankowski *et al.*, 2006), and as such, their mobility in surface and ground waters is high. Therefore, the current study investigates the potential utility of biosorbents for removing both As and Se from dilute aqueous solutions.

In this Chapter, a literature review is presented to describe: i) biosorbents in general, their varieties, properties, usage, and biosorption mechanisms, and more specifically tree bark; and

ii) coal fly ashes, their classifications, properties, disposal, reutilisation, and the environmental concerns related to their storage. Chapter 1 concludes with an outline of the current study and aims.

1.2 Biosorption

Biosorption is a physico-chemical process that can be defined as the binding and removal of specified compounds from an aqueous solution through the use of a solid surface derived from a biological material (Blissett and Rowson, 2012). Biosorption utilises mechanisms such as absorption, adsorption, precipitation, surface complexation and ion exchange in order to bind a variety of compounds including particulates, colloids, metal or metalloid species, organic compounds, phthalates, fluoride, dyes and even pharmaceutical compounds (Blissett and Rowson, 2012, Michalak *et al.*, 2013).

As a subcategory of adsorption, biosorption employs a solid phase derived from a biological matrix (the biosorbent) and a liquid phase solvent (typically water) containing the suspended species to be sorbed to the matrix (the sorbate) (Matsunaga *et al.*, 2002). This process results in the rapid and reversible binding of the sorbate to a variety of functional groups (*e.g.*, amino, carboxyl, ester and hydroxyl groups) located on the biomass surface (Michalak *et al.*, 2013).

The biosorption phenomena have been the subject of ongoing investigation since the first publication in 1951 (Michalak *et al.*, 2013). More than 61,600 scientific papers have hitherto been published in peer-reviewed journals (Google Scholar search of "biosorption of heavy metals" as of 12/02/2016), with the review 'Biosorption of Heavy Metals' by Volesky and Holan being cited 2,161 times (Volesky and Holant, 1995).

It must be recognised that the rationales for a number of these biosorptive studies are not robust, particularly when based on commercial development and applications (Gadd, 2009). However, the importance of biosorption in the environment and of conventional biotreatment processes

suggests that further, more robust research must be directed to these areas in order to fully utilise this phenomenon (Gadd, 2009, Fomina and Gadd, 2014) as biosorption offers several advantages over conventional treatment methods (Michalak *et al.*, 2013). Biosorption methods are simple, relatively low-cost, methods that perform well and are available in large quantities (Michalak *et al.*, 2013, Fomina and Gadd, 2014). Biosorption effectively minimises the generation of chemical or biological sludge. Another key strength is that biosorbents do not require additional nutrients to be capable of metal recovery along with regenerating the sorbent (Michalak *et al.*, 2013, Fomina and Gadd, 2014).

1.2.1 Classification of Biosorbents

Biosorption is an intrinsic property of both living and dead microorganisms at both the whole-organism and cellular level. As such, this process is highly applicable to the treatment of contaminants, specifically the removal and/or recovery of contaminant compounds from a solution as well as environmental clean-up and health protection (Gadd, 2009, Michalak *et al.*, 2013, Fomina and Gadd, 2014).

In effect, all biological materials (*i.e.*, plant, animal and macro-algae biomass) and even their derived products (*e.g.*, chitosan) are capable of biosorption (Fomina and Gadd, 2014). In Table 1.1 several examples of biomaterial are tabulated. A range of microbial biomass types has been investigated to determine their utility as biosorbents. These have included mixed biomass/organism systems of bacteria, cyanobacteria, archaea, microalgae, macroalgae (*e.g.*, seaweed), unicellular yeasts, lichens and fungi in either filamentous or fruiting forms (*e.g.*, mushrooms) (Volesky and Holant, 1995, Gadd, 2009, Michalak *et al.*, 2013). In addition to the use of whole organisms, multiple biomaterials have also been studied to determine their utility as biosorbents. Numerous examples of such biosorbents are also tabulated in Table 1.1.

Generally, most biosorbents are derived from dead biomass as they afford specific advantages over the use of living microorganisms (Michalak *et al*., 2013). For example, dead cells are easily stored and are able to be used for extended periods of time, without being subjected to the limitations of metal toxicity or the availability of nutrients. Once used, metal ion-bound biosorbents from dead biomass can then be easily desorbed and reused (Baysal *et al.*, 2009, Selatnia *et al.*, 2004). Dead biomass can be used either in its natural state (*i.e.*, unprocessed) or may be chemically modified through methods such as an alkali wash in order to increase biosorption efficiency (Gadd, 2009). Notably, such physico-chemical manipulations to improve biosorption (*i.e.*, increasing selectivity, capacity, kinetics and re-use) may increase the cost of production and may even raise environmental issues (Gadd, 2009, Fomina and Gadd, 2014).

Table 1.1 Different types of biomaterials used as biosorption

Source	Biomaterial	Target Elements	Reference
Microbial biomass	Bacteria, archaea, filamentous fungi, yeast, algae.	Au, Al, As, Cd, Co, Cr, Cu, Hg, Mg, Mn, Ni, Pb, Sr, Zn	(Park *et al.*, 2010, Dhankhar and Hooda, 2011, Srivastava *et al.*, 2015)
Agricultural wastes	Cocoa shells, coconut shells, fruit or vegetable waste, grape stalk waste, olive pomace, pinus cone biomass, rice husks, rice straw, seaweed biomass, soybean hull, sugar beet pulp, sunflower stalks, wheat bran.	Ag, Al, As, Cd, Co, Cr, Cu, Fe, Hg, Mg, Mn, Ni, Pb, Sr, Zn	(Kratochvil *et al.*, 1998, Sun and Shi, 1998, Ucun *et al.*, 2002, Meunier *et al.*, 2003, Pagnanelli *et al.*, 2003, Villaescusa *et al.*, 2004, Amin *et al.*, 2006, Michalak *et al.*, 2013, Fomina and Gadd, 2014, Srivastava *et al.*, 2015)
Animal materials	Crustaceans, hair, feather.	Al, Cu, Fe, Mn, Ni, U, Zn	(Ramírez-Paredesa, 2013)
Plant materials	Sawdust, sphagnum peat moss, tree barks, weeds, plant seed.	As, Cd, Cr, Cu, Hg, Mg, Mn, Mo, Ni, Pb, Se, U, V, Zn	(Kumari *et al.*, 2006, Fomina and Gadd, 2014, Srivastava *et al.*, 2015)
Industrial wastes	Activated and aerobic sludges, fermentation and food wastes.	As, Cd, Cr, Cu, Mo, Pb, Zn	(Yang, 2010, Fomina and Gadd, 2014)
Other materials	Cellulose, chitosan.	Cd, Cr, Co, Cu, Hg, Ni, Pb, Zn	(Krishnamurthy and Frederick, 1994, Cervera *et al.*, 2003)

1.2.2 Properties of Biosorbents that Influence their Functions

The applicability of biosorbents to remove contaminants such as trace elements is governed by several properties of the material employed. These include physico-chemical properties such as biosorbent size, surface area, structure of the biomass, the presence of functional groups upon the cell wall of the biosorbent, pH and the point zero charge (pH_{pzc}). These properties greatly influence the biosorption process and must be accounted for accordingly. The size and surface area of the biosorbent particles are highly important in selecting a particular biosorbent as these features influence the total adsorption capacity of the material. An important feature to note is that the surface-to-volume ratio is inversely related to particle size, thus the smaller particles possess the greatest surface areas for adsorption.

Morphology of a biosorbent surface is also an important parameter for consideration to gain further understanding of its biosorbent properties. Scanning electron microscopy is a valuable tool in this pursuit, particularly in an attempt to distinguish any changes to the cell wall architecture that have resulted from the biosorption/adsorption process.

As well as physical properties, the functional groups, pH and pH_{pzc} of a biosorbent greatly influence its capacity to bind contaminants such as trace elements. The cell wall surface of a biosorbent such as tree bark generally contains an array of functional groups (amino, carboxyl, carbonyl and ester) with acidic or basic properties. The availability of these functional groups plays a crucial role in the biosorption of ions from aqueous solutions, although this is strongly influenced by the pH of both the biosorbent and the solution. The pH_{pzc} is another important factor which indicates the surface of the adsorbent is globally neutral, hence, at the pH below this value, the surface is positively charged, whilst at pH beyond this value, it is negatively charged (Ebrahimian *et al.*, 2014). Depending upon the pH of the biosorbent and/or the solution, different functional groups will participate in metal/metalloid binding (Michalak *et al.*, 2013). For example, cationic dye can be adsorbed at pH greater than pH_{pzc} as a result of negative surface charge of adsorbent due to the presence of OH^- and COO^-, Whilst anionic dye will be

adsorbed on positively charged surface at pH lower than pH_{pzc} (Ebrahimian *et al.*, 2014). Thus, these properties must be carefully considered in order to optimise metal or metalloid binding to the functional groups present within the biosorbent.

1.2.3 Analytical Techniques for Probing Biosorption Mechanisms

The binding of a sorbate on the biosorbent surface that occurs during biosorption is a complex mechanism (Michalak *et al.*, 2013). In the case of metal ions, the net binding of these contaminants to natural materials is governed by physical interactions that can be mediated through electrostatic interaction and van der Waals forces, or through chemical processes such as the displacement of a proton or of a bound metal cation, through chelation resulting in either ionic or covalent interaction, or through complexation (Volesky, 1990, Crist *et al.*, 1999, Davis *et al*., 2003). In addition to the properties of a particular biosorbent, the biosorption process is strongly influenced by chemical properties of the metal ions being sorbed, for example, molecular weight, oxidation status and ionic radius.

According to a review by Michalak, *et al.*, 2013, a biosorption is also strongly influenced by the parameters of the process, particularly temperature, pH and the concentrations of both biosorbents and sorbates. Among them, pH is a critical factor in the biosorption mechanism as it influences the solution chemistry of the metal ions and their dissociation from the binding sites, as well as redox reactions, hydrolysis, precipitation, complexation by organic/inorganic ligands in addition to the speciation and affinity of metal ions (Yang and Volesky, 1999, Esposito *et al*., 2002, Gavrilescu, 2004).

Some of the analytical techniques that have been employed to explore the biosorption mechanisms and their targeted applications are summarised in Figure 1.1 below.

To elucidate the mechanism of biosorption, it is paramount to firstly identify the sorbent functional groups involved in the process. Fourier transformed infrared spectroscopy (FTIR) is a valuable tool in this pursuit, revealing critical information regarding the nature of bonds, while allowing for the identification of different functional groups upon the cell wall architecture (Michalak *et al.*, 2013). In applying FTIR, the magnitude of band-shifting between the natural and metal-bound forms of the biomass provides reliable insight into the extent of the interactions between the functional groups of the biomass and the bound metal cations (Murphy *et al.*, 2007). For example, the FTIR spectra of native tapioca peel (trace A) and Ni(II)-loaded (trace B) are illustrated in Figure 2, demonstrating the presence of a variety of functional groups (Promthet and Mungkarndee, 2015). In trace A of Figure 1.2, Promthet and Munkarndee determined that the absorption peak at 3,431 cm^{-1} was the result of hydroxyl (-OH) groups, whilst the peak at 2,929 cm^{-1} was due to the presence of γ(C–H) bonds in a carboxyl group (–COOH). Trace A also displayed a peak at 1,760 cm^{-1} that was the product of the stretching vibration of a C=O bond due to non-ionic carboxyl groups (–COOH, –COOCH), and therefore might be allocated to carboxylic acids or their esters. Furthermore, the peak observed at 1,652 cm^{-1} indicated C=O stretching in carboxyl groups, whereas the peak observed at 1,031 cm^{-1} was attributable to C–O stretching of alcohols and carboxylic acids (Promthet and Mungkarndee, 2015).

By comparing to the FTIR spectrum of nickel-loaded tapioca peel in trace B to trace A of Figure 2, Promthet and Munkarndee reported that the stretching vibration at 3,431 cm^{-1} has shifted to 3,426 cm^{-1}. They also observed that the peak of carboxyl shifted from 2,929 cm^{-1} to 2,922 cm^{-1} while the stretching vibration observed at 1,760 cm^{-1} shifted to 1,748 cm^{-1} (Promthet and Mungkarndee, 2015). The nickel-loaded tapioca peel also demonstrated a shift in the stretching vibration from 1,652 cm^{-1} to 1,637 cm^{-1}, while the peak of the C-O group shifted from 1,031 cm^{-1} to 1,034 cm^{-1}.These shifts following the biosorption of nickel to the tapioca peel was suggested to be the result of ion exchange between hydrogen atoms of hydroxyl and carboxyl

groups on the peel surface, and in such biosorption process, nickel ions were primarily involved (Promthet and Mungkarndee, 2015).

Another useful tool in the determination of the architecture of the biomass surface is scanning electron microscopy (SEM). This technique enables the highly-resolved investigation of the biosorbent surface before and after metal ion absorption, enabling researchers to visualise any changes to surface morphology following heavy metal exposure, particularly for modifications to the cell wall (Michalak *et al.*, 2013). As an example, the scanning electron micrographs of *Lessonia nigrescens* kelp, obtained by Reategui *et al*., are reproduced in Figure 1.3(a). According to the authors, the heterogeneity in mercury sorption on the surface of *Lessonia nigrescens* kelp might be due to heterogeneities in the composition of the sorbent cell wall, which depends on its growth stage (Reategui *et al.*, 2010). Another example of the application of SEM in this area has been demonstrated by (Michalak and Chojnacka, 2009). In their scanning electron micrographs of *Ulva prolifera* biomass displayed in Figure 1.3(b), they identified small changes and deformation in the morphology of the surface of *Ulva prolifera* biomass following Cr(III) exposure. The native biomass shows a rough surface with pores and cavities, which indicates a possibility for metal ions adsorption onto the surface. Although SEM provides interesting insights into cellular architecture, it is only capable of qualitative evaluation of a surface structure and as such requires additional, quantitative support (Michalak *et al.*, 2013).

SEM is often complemented by energy dispersive X-ray (EDS) spectroscopy to provide even more detailed information, enabling investigators to visualise the distribution of various elements upon the biomass surface (Suganya *et al.*, 2016). The EDS spectra of native and Cr(VI) loaded *Caryota urens* seeds, reproduced in Figure 1.4, was obtained by Suganya *et al.* (2016). The authors determined from these spectra that Cr(VI) was biosorbed on the surface of the biomass.

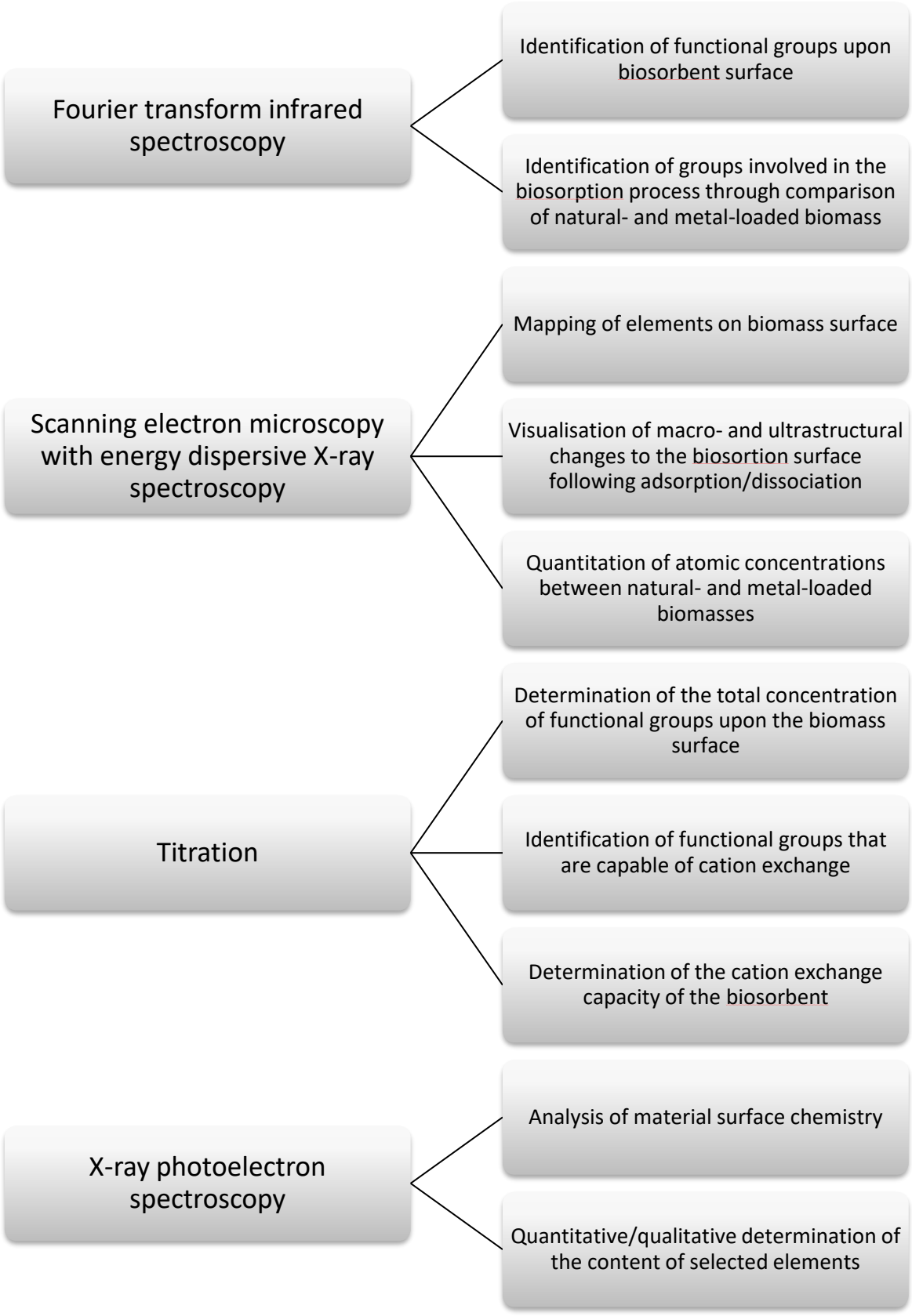

Figure 1.1 Techniques previously employed to elucidate the biosorption mechanism; adapted from (Michalak *et al.*, 2013).

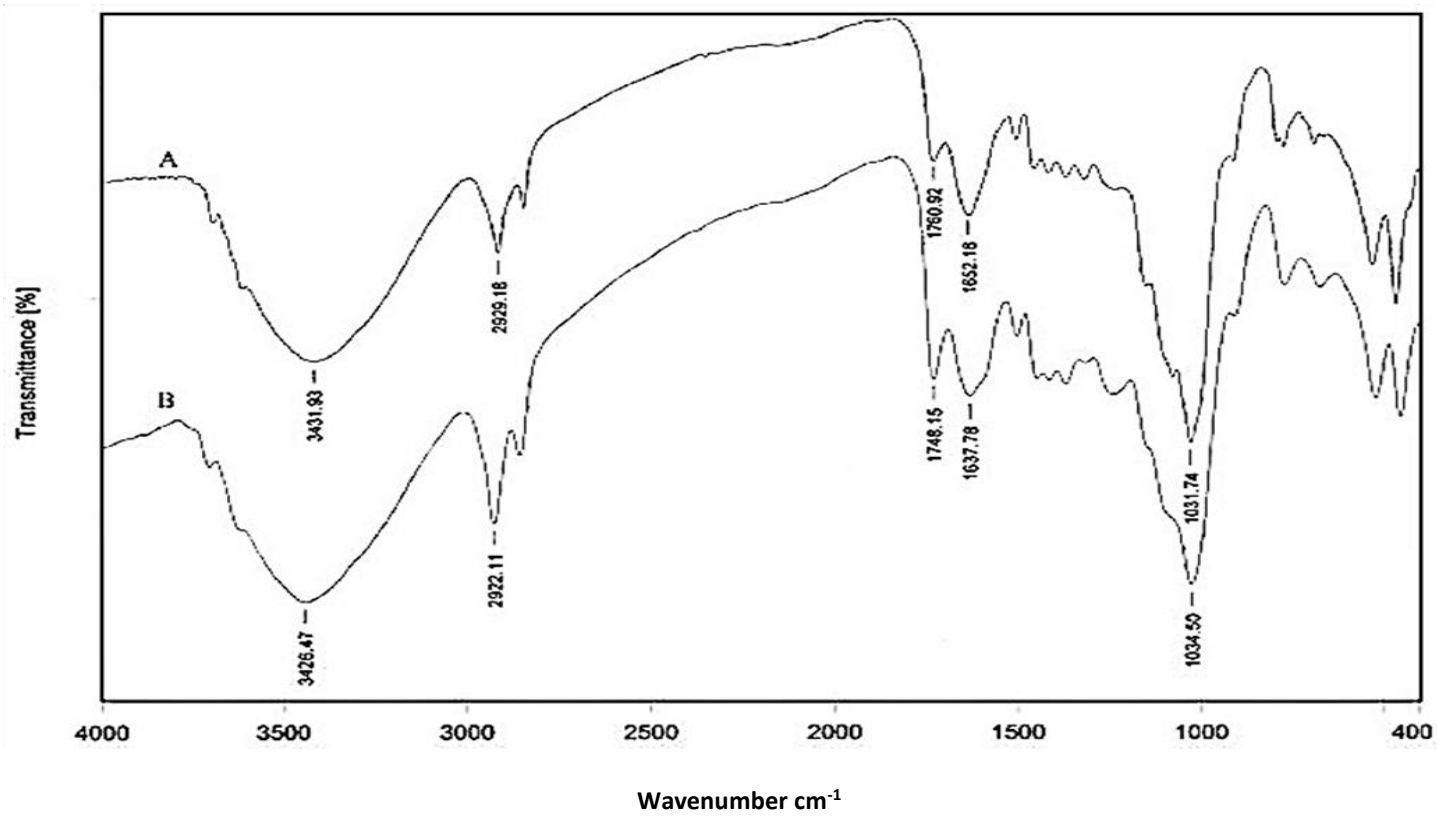

Figure 1.2 FTIR spectra of (A) native and (B) Ni(II)-loaded tapioca peel. Figure source: (Promthet and Mungkarndee, 2015).

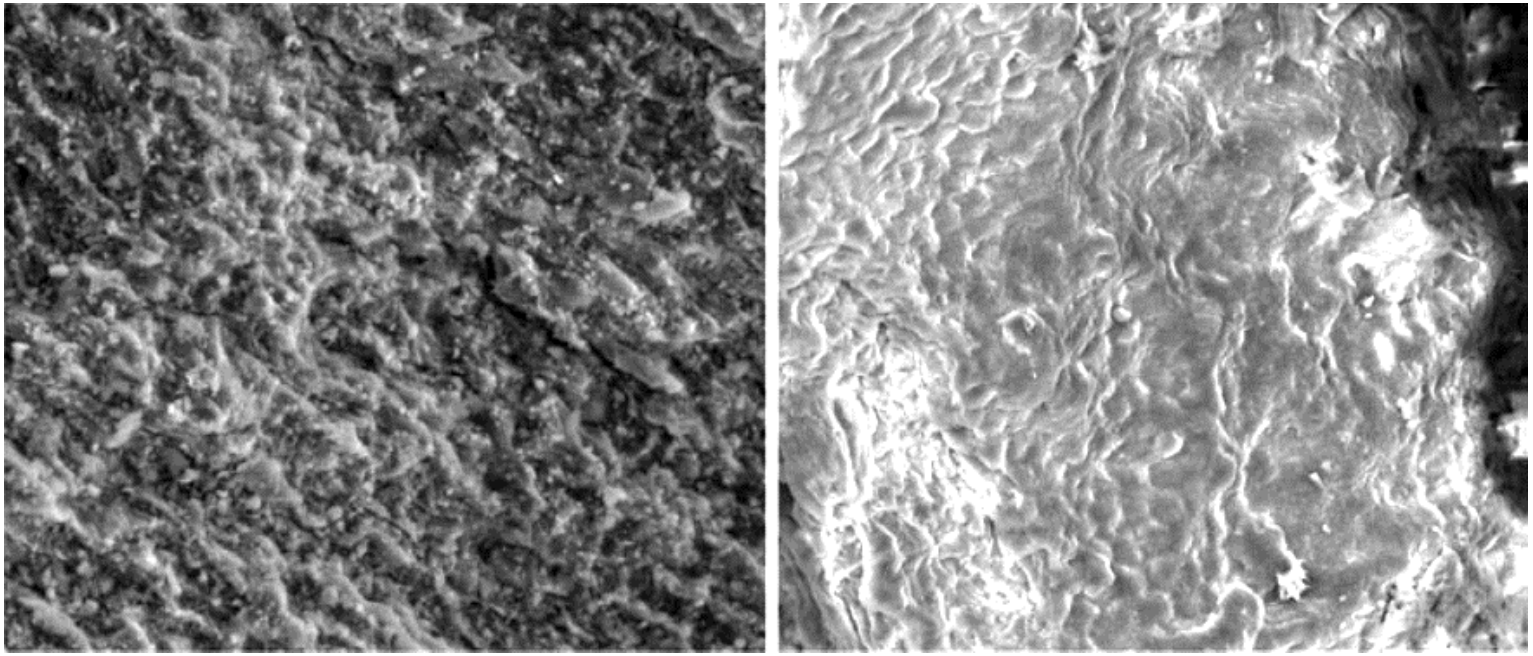

Figure 1.3(a) Scanning electron microphotograph (secondary electrons) of *Lessonia nigrescens* (left) before and (right) after Hg (II) sorption; Image source: (Reategui *et al.*, 2010)

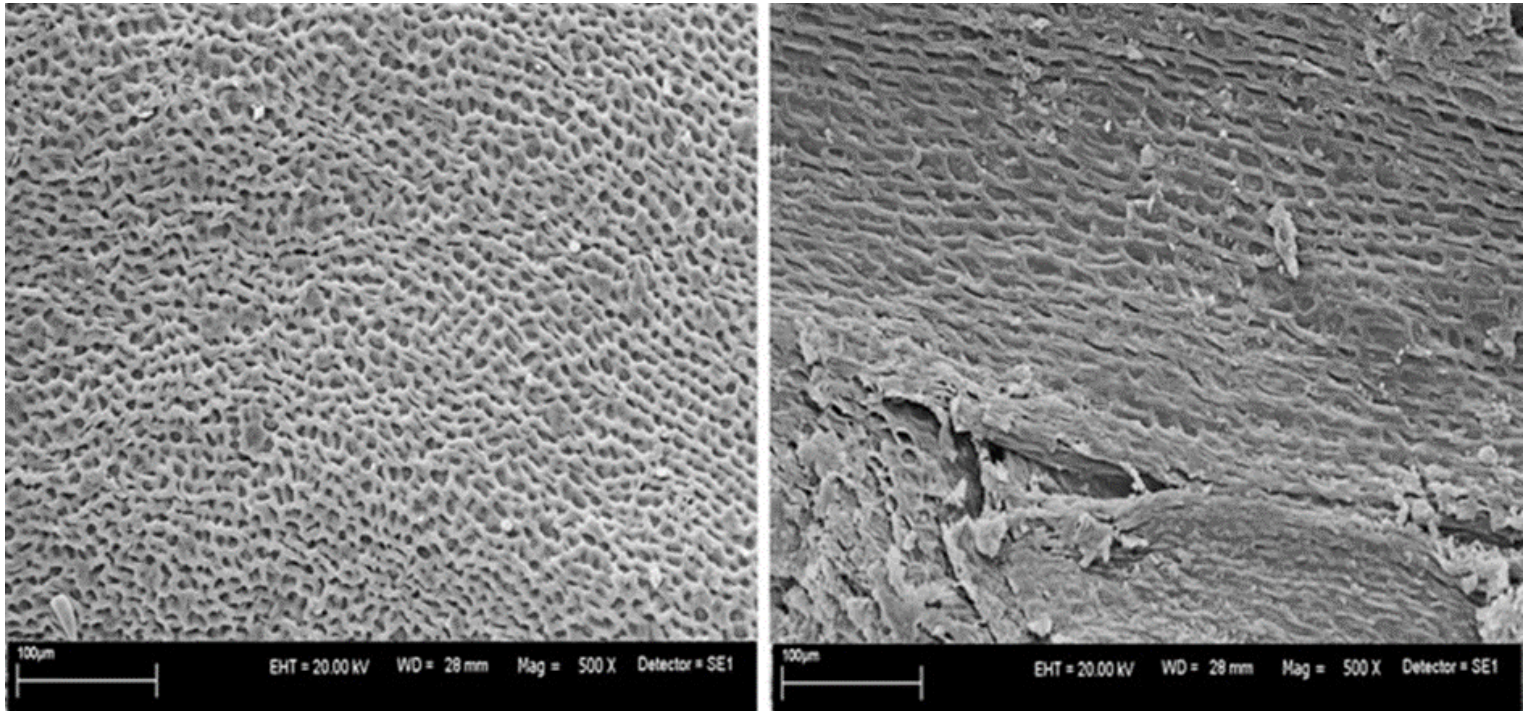

Figure 1.3(b) Scanning electron micrographs comparing the surface structure of (left) native and (right) Cr(III)-enriched *Ulva prolifera* biomass; Image source: (Michalak and Chojnacka, 2009)

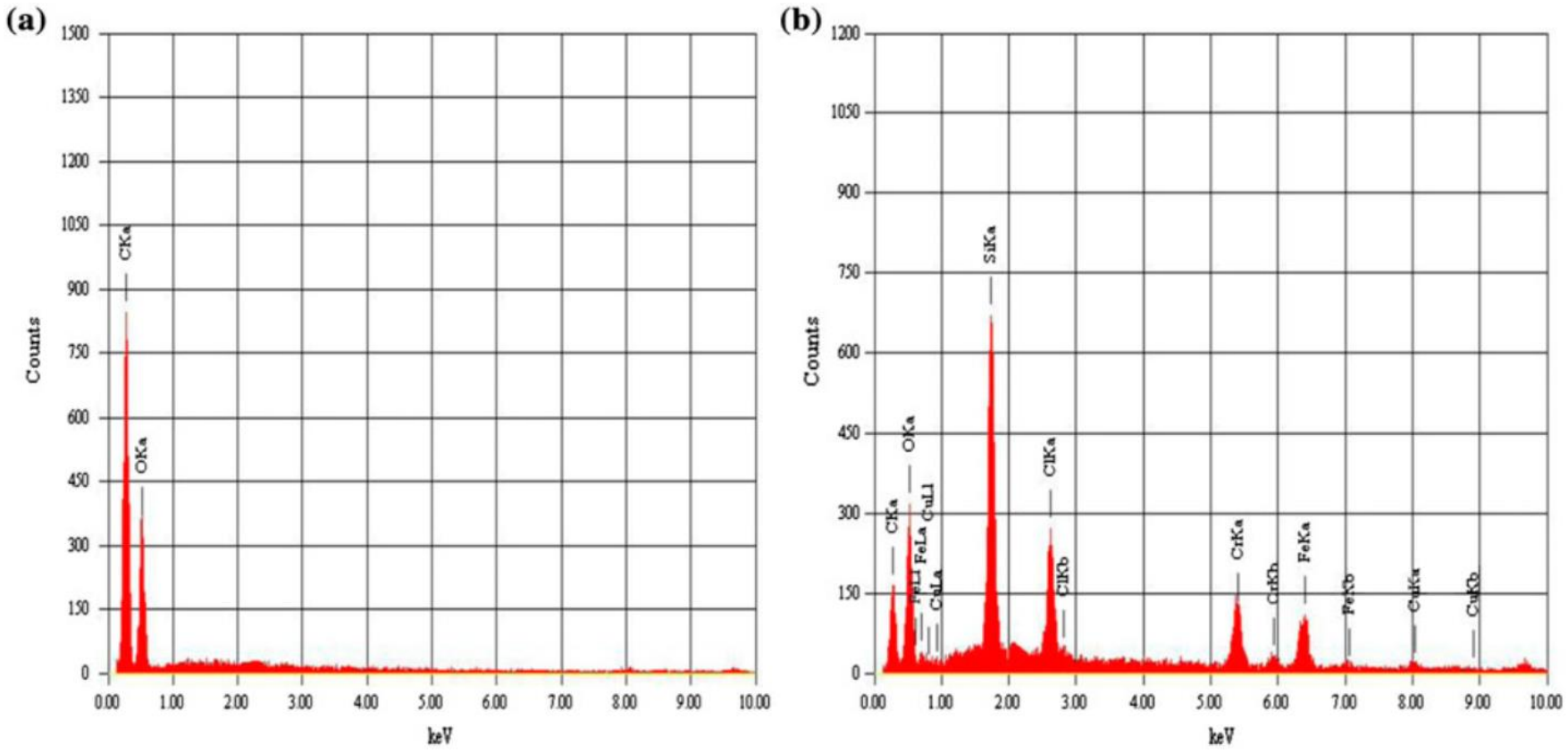

Figure 1.4 EDS elemental spectra of *Caryota urens* seeds (a) native and (b) Cr(VI)-loaded; Image source: (Suganya *et al.*, 2016)

Evidently, the identification of functional groups on the biosorbent surface will also aid in elucidating the sorption mechanisms. Determination of the functional groups present on a biomass surface can be achieved through potentiometric titration or the Boehm method, which identifies the acidic, basic or ion exchange properties of the surface (Momčilović *et al*., 2011, Michalak *et al.*, 2013). Based on the Boehm method, the acidic sites of a biomass are determined, for example, through treatment of small quantities of the biosorbent (0.1 g) with 10 mL of assorted bases of different strength (*e.g.*, 0.1 M NaOH, 0.1 M $NaHCO_3$, 0.05 M Na_2CO_3). These biosorbent samples would then be sealed and subjected overnight agitation, followed by filtration and titration with 0.05 M H_2SO_4 or 0.1 M HCl (Michalak *et al*., 2013). The number of acidic sites is evaluated according to the neutralisation of all carboxylic, phenolic, and lactonic groups by NaOH, both carboxylic and lactonic groups by Na_2CO_3, and only carboxylic groups by $NaHCO_3$ (Momčilović *et al.*, 2011). Basic functional sites are identified using a similar method in which 0.1 g of biosorbent would be treated with 10 mL of 0.1 M HCl before the samples are sealed, shaken overnight, filtered and titrated with 0.1 M NaOH (Michalak *et al.*, 2013). The number of the surface basic sites is determined from the titration of the filtrated HCl with NaOH (Momčilović *et al.*, 2011).

X-ray photoelectron spectroscopy analysis (XPS) is another quantitative method that enables the spectroscopic analysis of biosorbent surface chemistry. XPS provides valuable insight into the electronic state and composition of the elements that comprise a biosorbent material, in addition to their empirical formula (Michalak *et al.*, 2013). As such, XPS is often employed in biosorption studies in order to ascertain information regarding the biosorptive mechanism and of the oxidation state of the sorbed heavy metal. For instance, Park *et al.* 2008 used XPS on Cr- loaded brown seaweed, *Ecklonia* specie, and noticed that Cr(VI) was reduced to Cr(III) during biosorption process, while Li *et al.* 2014, obtained same result in Cr(VI) reduction during adsorption from water using buckwheat hull (Park *et al.*, 2008, Li *et al.*, 2014).

1.2.4 Biosorption Kinetics and Isotherms

1.2.4.1 Biosorption Kinetics

The kinetics of biosorption quantify the rate of solutes binding and dissociating from biomaterials (Michalak *et al.*, 2013). During a liquid-solid sorption process, the transfer of a solute is generally represented by one of two of the following processes that can occur either individually or in combination (Wang and Wu, 2006b):

a) External mass transfer, also referred to as film diffusion or boundary layer diffusion, refers to the transport of a solute suspended in solution to the exposed surface of the adsorbent through a liquid film.
b) Intraparticle diffusion, also referred to as pore diffusion, wherein the solute diffuses into the pore of the adsorbent, excluding a small amount of sorption exposed on biosorbent surface.

These processes of dynamic sorption are slow, with the slowest step (either film or pore diffusion) dictating the rate of sorption (Wang and Wu, 2006b). Following these processes, the solute is transported to the interior surfaces of the pores and capillary spaces within the architecture of the biosorbent. This final rapid step is regarded as an equilibrium reaction (Wang and Wu, 2006b). In Crini and Badot's study, the authors assumed an additional chemical reaction step, wherein the solute adsorbs via ion-exchange, chelating or complexation on the active sites of the biomaterial (Crini and Badot, 2008).

Multiple models have been proposed to characterise biosorption (Michalak *et al.*, 2013). However, the appropriateness of these kinetic models is largely dependent upon the nature of the biosorbent being investigated, the solutes being targeted and the experimental conditions that have been applied to investigate the process (Michalak *et al.*, 2013). Among the models that have been proposed, those that are based upon the order of chemical reaction are held as being particularly relevant to the rate of sorption, especially the Lagergren pseudo-first order

(Equation 1.1) and HO pseudo-second-order (Equation 1.2) kinetics models (Wang and Wu, 2006b, Michalak *et al.*, 2013).

$$q_t = q_e\,(1 - e^{-k_1 t}) \qquad \text{Equation 1.1}$$

$$q_t = \frac{q_e\left(q_e k_2 t\right)}{1 + q_e k_2 t} \qquad \text{Equation 1.2}$$

where, k_1 is the pseudo-first order rate constant (min) and k_2 is pseudo-second order rate constants (g/mg/min), q_e is the quantity of solute sorbed at equilibrium (mg/g), and q_t is the quantity of solute sorbed at any time t (Promthet and Mungkarndee, 2015).

Notably, in these models, the rate of sorption is assumed to be proportional to the number of available sites upon the biosorbent surface, which is denoted by the reaction order (*i.e*. the first or second order) (Michalak *et al.*, 2013). Contrary to this assumption, it has been more recently contended that the majority of the biosorption process follows the pseudo-second-order model (Reddy *et al.*, 2012, Witek-Krowiak *et al*., 2013, Witek-Krowiak, 2013). Despite this proposed model, biosorption remains a complex process, resulting in the simultaneous functioning of different mechanisms, and as such, researchers are often unable to sufficiently determine the order of reaction (Michalak *et al.*, 2013).

The main objectives of performing kinetic experiments are

(i) to determine the contact time required for a given biosorbent to reach sorption equilibrium,

(ii) to assess the relative impact of factors such as temperature, pH, initial concentration of metal ion (C_0), the concentration of adsorbent (C_s), on the equilibrium concentration in solid phase (q_e) and the rate constant (k) upon kinetic models, and

(iii) to evaluate the biosorption properties of a certain biosorbent (Promthet and Mungkarndee, 2015, Michalak *et al.*, 2013). The best model is chosen following linear regression of the

experimental data for the boundary conditions; t = 0 to t and q = 0 to qt, based upon the value of determination coefficients (Michalak *et al.*, 2013). Most natural biosorbents applied to bind and remove metal ions displayed the greatest R^2 value when adopting the pseudo-second order model (Aksu, 2001).

A generalised experimental procedure employed for the assessment of biosorption kinetics is illustrated below in Figure 1.5. The experiments were performed in Erlenmeyer flasks containing metal ion solution (*i.e.* 300 mg/L Cr(III)) initially) and biosorbent (*i.e.* 1 g/L microalga) at adjusted pH level. The solution was agitated in a water bath. After several defined intervals (*i.e.*, 5 min to several hours), the solutions were separated by filtration then analysed to determine metal ion concentration in solution after adsorption process (Michalak, 2010).

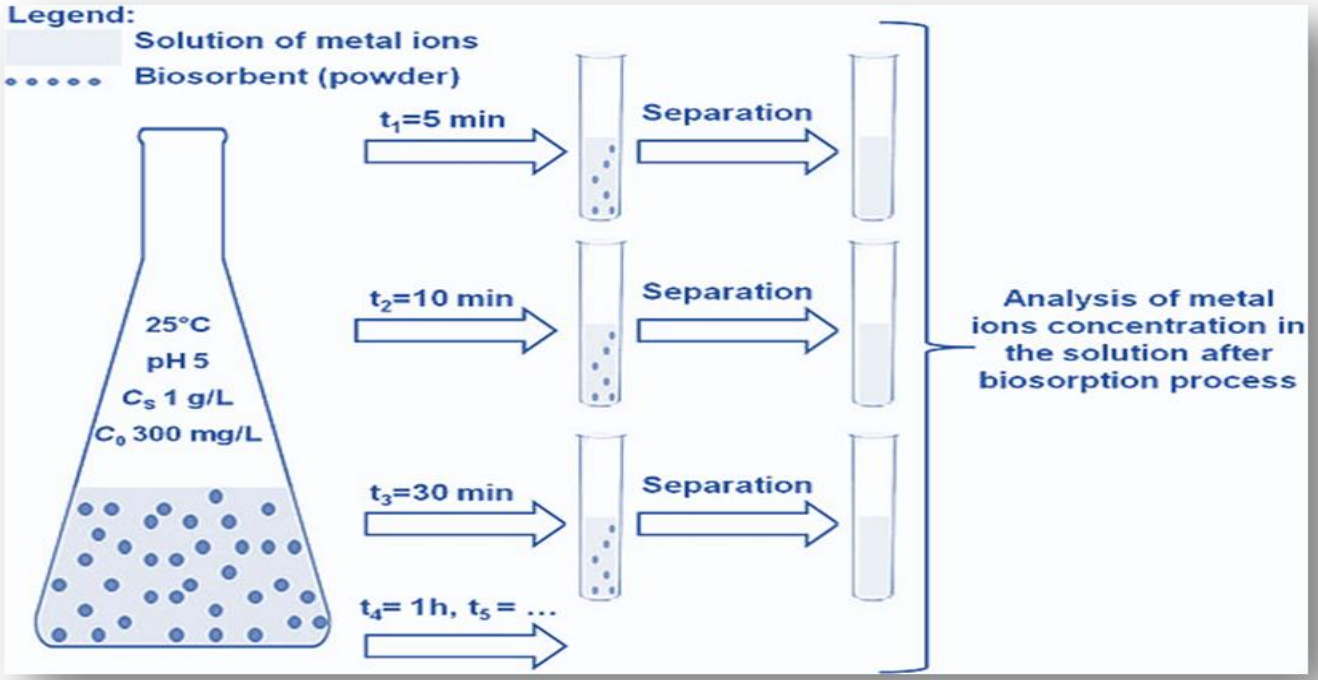

Figure 1.5 Generalised experimental scheme determining the kinetics of biosorption (*i.e.*, 25°C, pH 5, biomass concentration (C_s) 1.0 g L^{-1} and initial metal ion concentration (C_0) 300 mg L^{-1} for microalga *Ulva prolifera*, (Michalak and Chojnacka, 2009, Michalak, 2010). Figure adapted from (Michalak *et al.*, 2013).

1.2.4.2 Biosorption Isotherms

The biosorption process at equilibrium is described by sorption isotherms. These isotherms describe the relationship between the mass of the bound metal ion by the unit mass of the biosorbent, in addition to the equilibrium concentration of the target ion in the test solution (Michalak *et al.*, 2013). Linear and non-linear mathematical models have become available in literature to describe the isotherms of biosorption (Aksu, 2001, Michalak, 2010, Promthet and Mungkarndee, 2015). The most common of isotherm models are Langmuir model (Equation 1.3) and Freundlich model (Equation 1.4), as shown below in their nonlinear forms:

$$q_e = \frac{q_{max}\, b c_e}{1 + b c_e} \qquad \text{Equation 1.3}$$

$$q_e = k_F C_e^{(1/n)} \qquad \text{Equation 1.4}$$

where q_e is equilibrium concentration in solid phase (mg/g), q_{max} is maximum quantity of metal ions (mg/g) likely bound on the surface of biosorbent in the equilibrium state, b is the Langmuir constant (L/mg), C_e is equilibrium concentration in liquid phase (mg/L), k_F is biosorption capacity, and n is biosorption intensity. Accordingly, in a linear form of Langmuir model, the q_{max} and b were obtained from slope and intercept of plot of $1/q_e$ vs. $1/C_e$ whilst, k_F and 1/n could be obtained from slope and intercept of plot of log q_e vs. log C_e in a linear form of Freundlich model (Promthet and Mungkarndee, 2015). However, note that the Langmuir model is based on the theory of the coverage of adsorbate over a consistent biosorbent surface in monolayer. It means, one adsorbate molecule interacts with only one active site of biosorbent surface. In contrast, the Freundlich model is based upon a multilayer adsorption on a heterogeneous surface of biosorbent (Promthet and Mungkarndee, 2015).

In general, the equilibrium between the solid and liquid phases of a given biosorbent is better described by the Langmuir equation, rather than the Freundlich equation, while the most

attractive biosorbents display the greatest possible q_{max} with the greatest coefficient of the Langmuir constant b, which indicates the highest affinity of biosorption (Davis *et al.*, 2003).

Another useful isotherm model is the Sips isotherm, which is a combination of the Langmuir and Freundlich models including three parameters as shown in following nonlinear equation:

$$q_e = \frac{q_{max}\, K_s C_e^{\frac{1}{n_s}}}{1 + K_s C_e^{\frac{1}{n_s}}} \qquad \text{Equation 1.5}$$

where K_s is the Sips isotherm model constant (L/g), n_s is Sips isotherm exponent, and q_{max} is Sips maximum adsorption capacity (mg/g). This model is able to predict both the homogenous or heterogeneous adsorption system. This is because at low concentration of adsorbate, Sips isotherm reduces to Freundlich, whilst at high adsorbate concentrations, it predicts an adsorption in monolayer of Langmuir isotherm (Foo and Hameed, 2010).

Notably, a comparison between two biosorbents at low equilibrium concentration of the solute may yield differing uptake values relative to a high solute concentration. As such, it is crucial to determine an appropriate concentration range when comparing potential biomaterials and their respective biosorption capacities (Michalak *et al.*, 2013).

Biosorption equilibrium processes are routinely performed in batch reactors, where Erlenmeyer flasks containing a metal ion solution are placed within a temperature-controlled shaking water bath. Here, the pH of each solution would be adjusted with a 0.1 M solution of either HCl or NaOH to a desired value (Michalak *et al.*, 2013). Using the optimal contact time identified from previous kinetic experiments, these studies would be performed for the optimal process parameters in biosorption experiment (Michalak *et al.*, 2013). After a biosorption process, the solutions are separated by filtering and then analysed to determine metal ion concentration in solution. A generalised procedure for performing equilibrium sorption isotherms is illustrated in Figure 1.6. The experiments were performed in Erlenmeyer flasks containing metal ion

solution (*i.e.* from 10 mg/L to 300 mg/L Cr(III) initially) and biosorbent (*i.e.* 1 g/L microalga) at adjusted pH level at controlled temperature of 25°C. After a given time (*i.e.*, optimum contact time found from kinetic experiment), the solutions were separated by centrifuge then analysed to determine remained metal ion concentration in solution (Michalak *et al.*, 2013).

1.2.4.3 Biosorption Thermodynamics

To understand biosorption mechanism, thermodynamic parameters including the change of Gibbs free energy (–ΔG°), change of enthalpy (ΔH°), and of entropy (ΔS°) can be estimated using the following equations:

$$\Delta G^0 = -RT\,lnK_0 \qquad \text{Equation 1.6}$$

$$\Delta G^0 = \Delta H^0 - T\Delta S^0 \qquad \text{Equation 1.7}$$

$$-RT\,lnK_0 = \Delta H^0 - T\Delta S^0 \quad \text{or} \qquad \text{Equation 1.8}$$

$$lnK_0 = -\Delta H^0/RT + \Delta S^0/R \qquad \text{Equation 1.9}$$

Accordingly, a plot of ln K_0 versus 1/T in Equation 1.9 will yield an ordinate intercept of (ΔS^0 /R) and a slope of ($-\Delta H^0$/R). If a negative value of Gibbs free energy is obtained, the process can be developed spontaneously. Otherwise, the system is in equilibrium or nonspontaneous once $\Delta G^0 = 0$ or $\Delta G^0 < 0$, respectively. Additionally, the positive ΔH^0 value indicates the process of biosorption is endothermic, and the positive value of entropy ΔS^0 implies the rise of the degrees of freedom on the surface of the sorbent during the adsorption of sorbent (Witek-Krowiak, 2012).

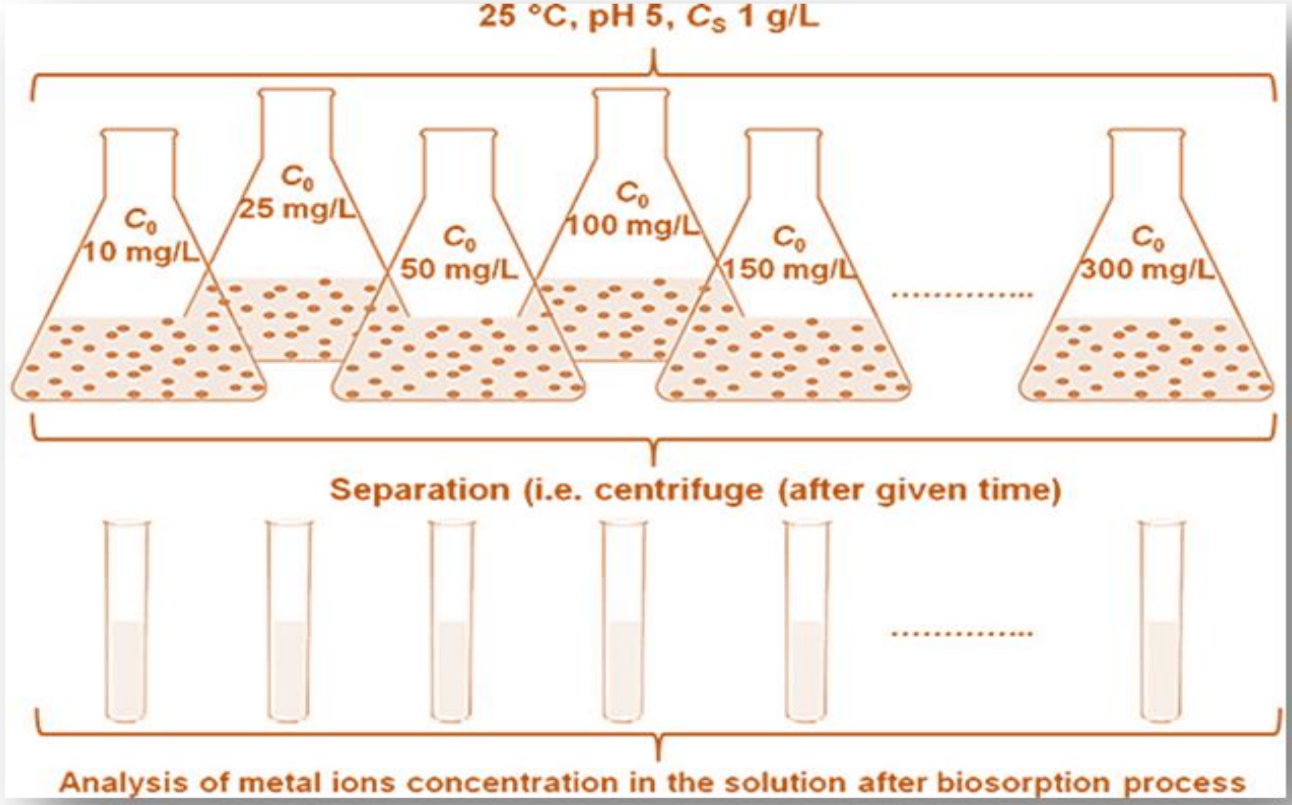

Figure 1.6 Generalised scheme for experiments to determine equilibrium of biosorption (*i.e.*, 25°C, pH 5, C_s 1.0 g L^{-1} and several solutions of C_0 from 10 mg/L to 300 mg/L for macroalga *Ulva prolifera*, (Michalak and Chojnacka, 2009, Michalak, 2010). Image adapted from (Michalak *et al.*, 2013).

1.2.5 Tree Barks

The term “tree bark” refers to tissues outside of, and surrounding, the vascular cambium of trees. Tree barks generally consist of two distinct layers, the inner bark and the outer bark that is referred to as the rhytidome. The inner bark is comprised of living tissue in older stems, while the outer bark is comprised of dead tissue on the surface of the old stems. This outer layer covers the trunks of trees and is formed from cells that have died as a result of not receiving any water or nutrients. The outer bark is usually thickest at the trunk or bole, which refers to the area of the tree between the ground and the beginning of main branching.

Bark tissues account for approximately 10-20% of the weight of woody vascular plants, and consist of various organic components that are displayed in Figure 1.7 (Gaballah and Kilbertus, 1998). These compounds can be classified as being either extractable or non-extractable components of tree bark. Extractable components can be obtained by using sequential extraction solvents with different polarities. For example, nonpolar solvents (petroleum ether and diethyl ether) can extract less polar compounds such as waxes, resin, lipid, higher fatty acid and terpenes. However, ethanol and water will dissolve polar compounds such as flavonoids, phenolics, condensed tannins and sugars. Non-extractable components include polysaccharides such as cellulose, hemicellulose and pectic substances, then phenolic polymers such as lignin, high molecular weight tannins and less cross-linked polyesters such as suberin and cutin.

Up to 40% of the bark tissue is composed of lignin, which provides the necessary structural support by crosslinking between different polysaccharides, such as cellulose (Gaballah and Kilbertus, 1998). These polysaccharides are of particular interest for applications as biosorbents as the chemical structures of polysaccharides and polyphenolic compounds suggest that these compounds may be capable of chelating heavy metal ions (Gaballah and Kilbertus, 1998), such as those found in polluted effluents. An example of such structures is depicted in

Figure 1.8, which illustrates the chemical structure of a part of lignins derived from beech, *Fagus sylvatica* (Nimz, 1974). This figure shows that the phenylpropanoid units making up lignin are linked in a complex way. The lignin of beech contains derivative units from coniferyl alcohol, sinapyl alcohol, and para-coumaryl alcohol (Sinha, 2004, Larcher, 2003). Additionally, the functional groups, for instance, free aliphatic and aromatic hydroxyl groups, benzyl alcohol or ether groups, carbonyl and methoxyl groups can be identified in the structure of lignin (Gaballah and Kilbertus, 1998, Sakai, 2000).

According to Gaballa and Kilbertus, (Gaballah and Kilbertus, 1998), tree bark is regarded as a massive waste with a density of 0.8 g/cm^3 and a moisture content of ~50%. As such, tree bark is generally incinerated in order to recover its calorific value or disposed of and left to decompose naturally. Thus, the application of routinely destroyed/discarded tree barks as ion exchangers for chelating heavy metal contaminants may increase its value by 5 to 50 folds (Gaballah and Kilbertus, 1998).

The applications of barks and woods as heavy metal ion scavengers have been an area of increasing investigation in recent years. Some examples of biosorption reports of trace elements using natural and/or pre-treated bark from early 1974 up to recent years are summarised in Table 1.2. In this table, the removal % of trace elements varied from 30% for As^{5+} to 99% for Pb^{2+}. The ability for tree bark to remove heavy metal ions from an aqueous solution depends largely upon the individual tree species and/or their pre-treatments, the pH of the solution, contact time, temperature and both the concentration and properties of the heavy metal ion tested (Gaballah and Kilbertus, 1998). For example, the rate of removal of Cu^{2+} were varied from approximately 52% using non-treated *Sequoia sempervirens* bark to 98% using formaldehyde treated *Techtona grandis* bark (Randall *et al.*, 1974, Randall *et al.*, 1976, Kumar and Dara, 1980, Kumar and Dara, 1982).

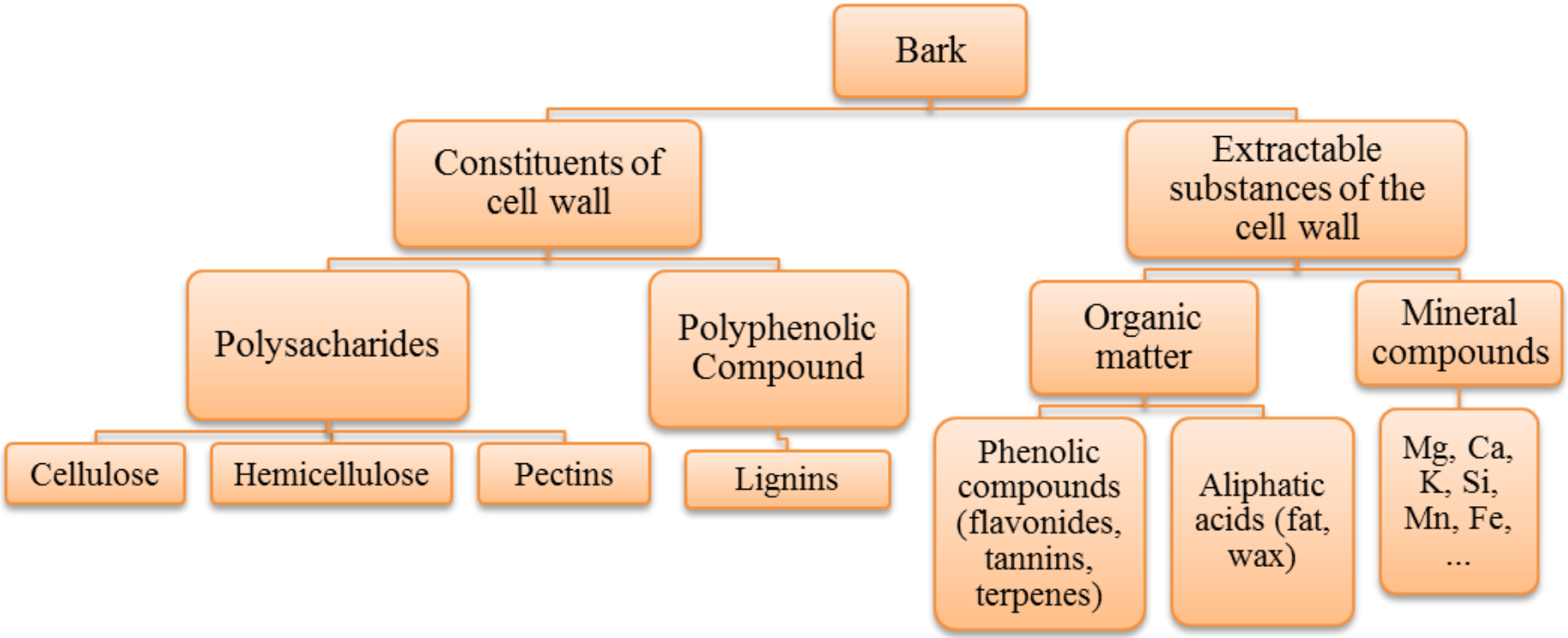

Figure 1.7 Organic components of tree bark. Adapted from (Gaballah and Kilbertus, 1998).

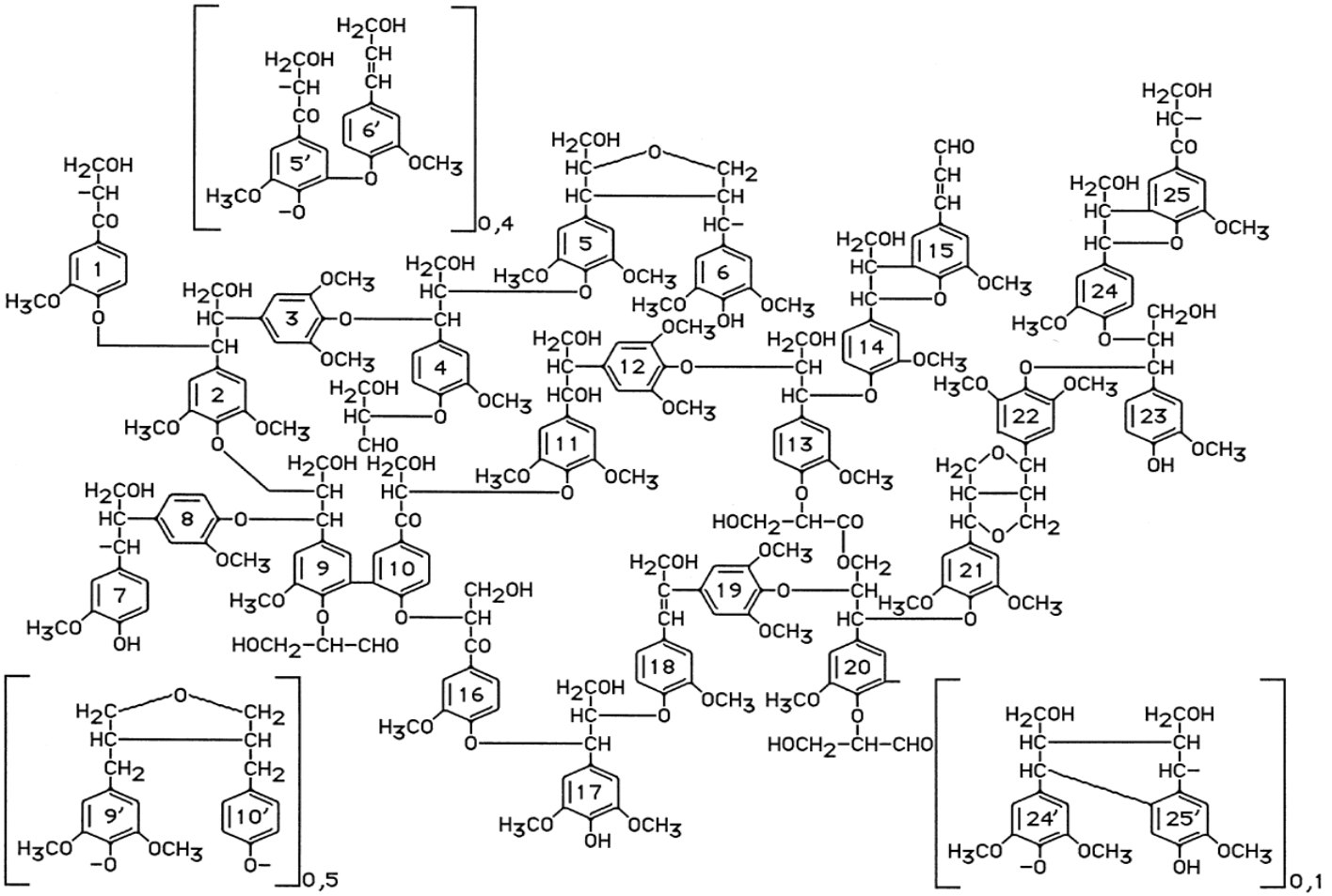

Figure 1.8 The chemical structure of a part of lignin derived from beech, *Fagus sylvatica* (Nimz, 1974). Adapted from (Gaballah and Kilbertus, 1998).

Table 1.2 Summary of reports by various researchers using tree bark for removal of trace elements

Bark	Heavy Metal	Initial Concentration	Treatment of Bark	Removal %	References
Sequoia sempervirens **(not treated)**	Ag^{+} Cu^{2+} Cd^{2+} Zn^{2+}	44 mg/L 90 mg/L 56 mg/L 31 mg/L	none	76% 52% 85-97% 73%	(Randall *et al.*, 1974, Randall *et al.*, 1976, Randall and Hautala, 1977)
Techtona grandis **(formaldehyde treated)**	Cu^{2+} Hg^{2}	40 mg/L 800 mg/L	HCHO + HNO_3	98% 99%	(Kumar and Dara, 1980, Kumar and Dara, 1982)
Terminalia tomentosa **(formaldehyde treated)**	Cr^{6+} Ni^{2+}	50 mg/L 75 mg/L	HCHO + HNO_3	94% 56%	(Kumar and Dara, 1982)
Cryptomeria japonica **(formaldehyde treated)**	Cu^{2+}	635.4 mg/L	HCHO + HNO_3	N/A	(Morita *et al.*, 1987)
Hardwickia binata **(formaldehyde treated)**	Hg^{2+}	100 mg/L	HCHO + HNO_3	92-97%	(Deshicar *et al.*, 1990)
Pinus sylvestris **(formaldehyde treated)**	As^{5+}, Cd^{2+}, Cr^{3+}, Cr^{6+}, Cu^{2+}, Fe^{2+}, Fe^{3+}, Ni^{2+}, Hg^{2+}, Pb^{2+}, Zn^{2+}.	100 mg/L of each ion	HCHO + HNO_3	30%, 99%, 97%, 99%, 95%, 99%, 95%, 98%, 100%, 100%, 99%	(Gaballah and Kilbertus, 1998)
Pinus radiata **(formaldehyde treated)**	As^{5+}, Cd^{2+}, $Hg^{2+,}$ Al^{3+}, Pb^{2+}, Fe^{2+}, Fe^{3+}, Cu^{2+}	1000 mg/L of each ion	35% HCHO + 3% HNO3 at 80°C	34%, 47%, 78%, 59%, 84%, 33%, 26%, 44%	(Palma *et al.*, 2003)
Eucalyptus camaldulensis **(not treated)**	Hg^{2+}	100 mg/L	none	N/A	(Ghodbane and Hamdaoui, 2008)
Eucalyptus globules **(carbonised)**	Cd^{2+}	100 mg/L	$HNaCO_3$ at 600°C	73%	(Kannan and Veemaraj, 2010)
Moringa oleifera **(not treated)**	Ni^{2+}	50 mg/L	Boiling double distilled water	93-95%	(Reddy *et al.*, 2011)
Pinus pinaster **(not treated)**	Pb^{2+} Cu^{2+} Cd^{2+} Zn^{2+} Ni^{2+}	0.75 mM	none	98-99% 83-84% 78-84% 77-83% 70-75%	(Cutillas-Barreiro *et al.*, 2014)
Eucalyptus sheathiana **(NaOH treated)**	Zn^{2+}	20 mg/L	0.1 M NaOH	69%	(Afroze *et al.*, 2016)
Pinus pinaster **(not treated)**	Pb, Cu, Ni, Zn and Cd		none	N/A	(Cutillas-Barreiro *et al.*, 2016)

Table 1.2 shows that in addition to the variety of species, chemical pre-treatments of biosorbent may enhance their adsorption capacities. For example, formaldehyde treatment with immobilising the phenolic polymers within the bark can reduce a number of functional groups which acts as sorption sites. Such treatments may decrease the molecular weight of the macro-molecules of barks and/or enrich their heavy metal ion chelating capacities. However, most reports offer limited documentation of either the experimental conditions or the experimental range of the tested parameters (Gaballah and Kilbertus, 1998). Additionally, the bulk of the relevant literature originated from the USA, Russia, Japan and India, leaving many widely-available Australian species such as gumtree, paperbark and brush box untested.

As stated in Section 1.2.2, the ability of cheaply recovered metal contaminants from industrial effluents or the synthetic solutions cycle makes these biomaterials highly attractive to researchers. These investigations have included both equilibrium- and column-based methodologies (Gaballah and Kilbertus, 1998).

Similar to that outlined in Section 1.2.4, batch equilibrium studies have been performed by shaking 1-10 g samples of ground wood/bark in 0.1-1 L of a 1-200 ppm metal ion solution. As before, the mixture is filtered and the solution analysed to determine the metal ion content (Gaballah and Kilbertus, 1998). Using a different methodology, column-based experiments are performed by placing between 10-50 g of ground wood/bark into glass tubes, followed by the introduction of a heavy metal solution whose concentration is known (Gaballah and Kilbertus, 1998). These solid residues are subsequently analysed (*i.e.*, digested with concentrate HNO_3, diluted and then analysed using atomic absorption spectroscopy) in order to establish their adsorbed metal ion load and their retention capacity (Cutillas-Barreiro *et al*., 2016).

Some of these studies have investigated the adsorption of chromium–copper–arsenic compounds by wood, resulting in the proposal of a number of mechanisms that may be

responsible for the adsorption of such metals (Gaballah and Kilbertus, 1998). Some have suggested that these metals react with cellulose on the wood surface (Belford and Preston, 1960, Flomina, 1967, Plackett *et al.*, 1987), whereas alternate reports proposed that these ions react with the non-cellulose components such as lignins and tannins (Bayley and Rose, 1960, Bland, 1963, Peters and Parameswaran, 1980, Kübel and Pizzi, 1982).

Despite insight into these mechanisms, the heavy metal ion reaction sites upon the wood/bark surface and the structures to which they bind remain poorly characterised.

1.3 Coal Fly Ash

Following power generation adopted wide-scale coal firing in the 1920s (Wang and Wu, 2006a), millions of tons of solid coal-combustion products such as fly ash, bottom ash, boiler slag and flue gas desulfurisation materials are annually generated from coal-fired power plants (Kalyoncu, 2001). Of these by-products, coal fly ash comprises the vast majority of coal-combustion products (~85-90%) (Ward *et al.*, 2009). These products are fine, effectively silt-sized particles of inorganic matter that are collected through mechanical processes, electrostatic precipitators and fabric filters from flue gas that is produced as a result of igniting pulverised coal in the boiler assembly (Neupane and Donahoe, 2013, Ward *et al.*, 2009). These compounds are generated from the inorganic and organic constituents of the feed coal when heated between 1,200-1,700^{o}C (Blissett and Rowson, 2012). Figure 9 illustrates the workflow of a typical coal fired power station. Usually, coal is primary pulverised to make powder for quick burning. The coal powder then is burnt in furnace at around 1100°C temperature, and the produced heat converts the water in boiler into high-pressure steam that is passed into the turbine. The steam causes high speed

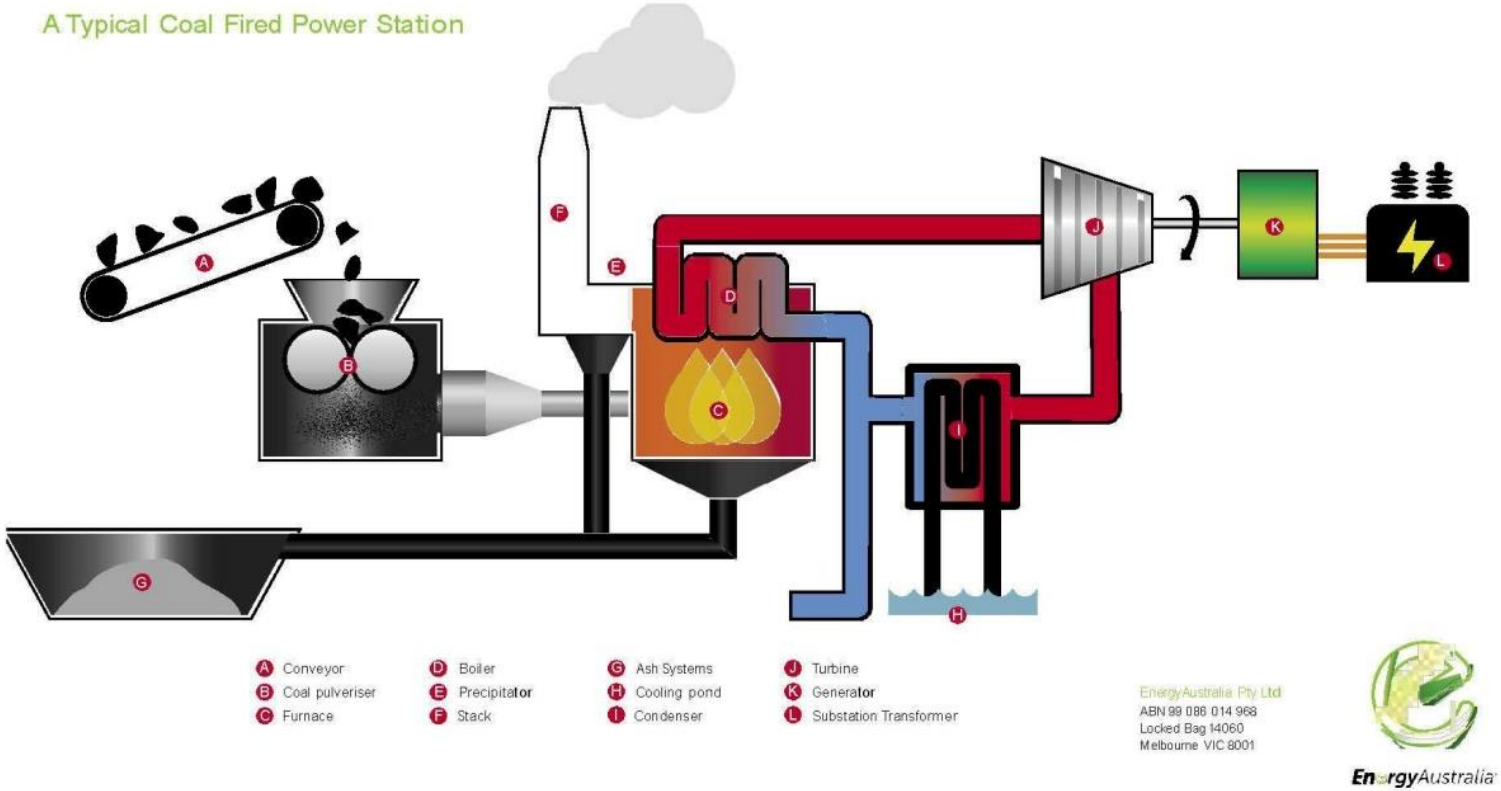

Figure 1.9 Schematic workflow of a typical coal-fired power station. During incineration, fly ashes are collected from the boiler and are eventually collected downstream through either mechanical or electrostatic precipitation. Image source: (EnergyAustralia, 2016)

rotation (≈ 3000 rotations per minutes) of turbine shafts to generate energy. Finally, this energy through a generator and electricity grid is converted to electricity (EnergyAustralia). During combustion, the generated bottom ash and fly ash are collected in ash system from boiler and stack, respectively.

The developed world has produced a staggering amount of fly ash in recent decades, with global production estimated at 349 Mt in 2000 (Wang and Wu, 2006a). In 1997, the European Coal Combustion Products Association generated 37 million tons of fly ash, which increased to 60 million tonnes in 2001 (Otero-Rey *et al.*, 2005). On the other hand, in Australia during 2010-2011, coal-fired power generation of fly ash was reported around 14 Mt (Arulrajah *et al.*, 2016). In another example, India generated approximately 118 Mt of coal ash each year up to 2008 from its 80 thermal power plants, after which it was predicted to increase to 170 Mt by 2012 and 440 Mt by 2030 (Patra *et al.*, 2012). In the United States, 67.7 million short tons of coal fly ash was generated in 2010 (Neupane and Donahoe, 2013), whilst Japan produced approximately 10 Mt of coal ash in 2011 (Kashiwakura *et al.*, 2011). More recent estimates place global coal fly ash production closer to 500 million tonnes per annum, however these estimates are recognised as being based upon data that are at least a decade old (Ahmaruzzaman, 2010). Largely due the significant economic growth of China, coal consumption increased by 50% in the period between 2002-2011 (Ahmaruzzaman, 2010), however there was a 1% decrease in 2012 (International Energy Statistics, 2012). Therefore, a more contemporary estimate of global coal combustion production would indicate that more than 750 million tonnes is generated per year (Blissett and Rowson, 2012). A comparison of national coal-combustion production in 2010 has been displayed graphically in Figure 1.10a and 1.10b, so that the estimated annual production (Mt) and utilisation rates (%) of coal-combustion products by country can be easily visualised during the same period. In 2010, Japan was ranked as demonstrating the highest coal-combustion products utilisation rate of 96.4%, followed by Europe 90.9%, China 67% and Other Asia 66% (Heidrich *et al.*, 2013). By comparison, coal-

combustion products of Australia utilisation rate was only 45.9%, below that of the global average (53%) (Heidrich *et al.*, 2013).

Coal combustion products can be reutilised in the concrete and cement industries, or through civic works such as road construction, structural fill, mining backfill and soil conditioner (Openshaw, 1992, Reijnders, 2005, Ward *et al.*, 2009, Blissett and Rowson, 2012). The relative proportions of coal combustion products utilisation evaluated by Blisset are displayed in Figure 1.11. The pie charts illustrate that from approximately 47% of fly ash utilised in Europe in 2009, mostly were used in the concrete and cement industries.

As the expansion of coal combustion has occurred faster than the development of applications to utilise its by-products, great quantities of fly ash are expected to have accumulated during the previous decade and therefore a significant proportion of the annual production of coal fly ash must be disposed of (Otero-Rey *et al.*, 2005, Blissett and Rowson, 2012). Discarded fly ash is generally buried along with other unused coal combustion products, either under water in impoundment lagoons or above the water table in dry landfills (Ward *et al.*, 2009, Neupane and Donahoe, 2013). This disposal method requires the sequestration of large lagoons and land areas and have the potential to generate possible environmental issues due to the presence of toxic elements, which possess the intrinsic ability to leach out and contaminate proximal groundwater sources (Neupane and Donahoe, 2013, Blissett and Rowson, 2012, Ward *et al.*, 2009, Otero-Rey *et al.*, 2005). Such a possible contamination system is illustrated in Figure 1.12. The contaminants including toxic metals (*e.g*. arsenic and selenium), radioactive elements and organic compounds (*e.g*. polycyclic aromatic hydrocarbons) may enter the environment through leaching into groundwater, overflow releases into surface waters, or through dust into soil. By such ways, inhabitants near a power plant can be exposed to the contaminants by consuming contaminated groundwater, ingesting agricultural products growing in contaminated soil, inhaling contaminated dust, and consuming local water products, for

example, contaminated fish (Keating *et al*., 2000). In a study of water qualities in surrounded fly ash facilities presented by Ward *et al*., 2009, it was found that among 26 water samples, the ash pond had higher concentration of many elements than ground and surface water system (Ward *et al.*, 2009). Moreover, concentration of Se, Mo and V was high up to several hundreds of µg/L, whilst As concentration were up to 3.3 µg/L in most sampling areas. However, some samples of ground water was grouped with the ash pond water, which could be a possible suggestion of ground water contamination (Ward *et al.*, 2009).

To understand the potential environmental impacts of fly ash contamination of groundwater sources, it is crucial to understand its chemical composition, physical properties and other relevant characteristics. This especially requires a detailed understanding of the mobilisation of potentially toxic elements from the discarded ash residue and the environmental impacts of their respective disposal (Meij, 1994, Gibbs *et al.*, 2008, Goodarzi *et al.*, 2008, Patra *et al.*, 2012).

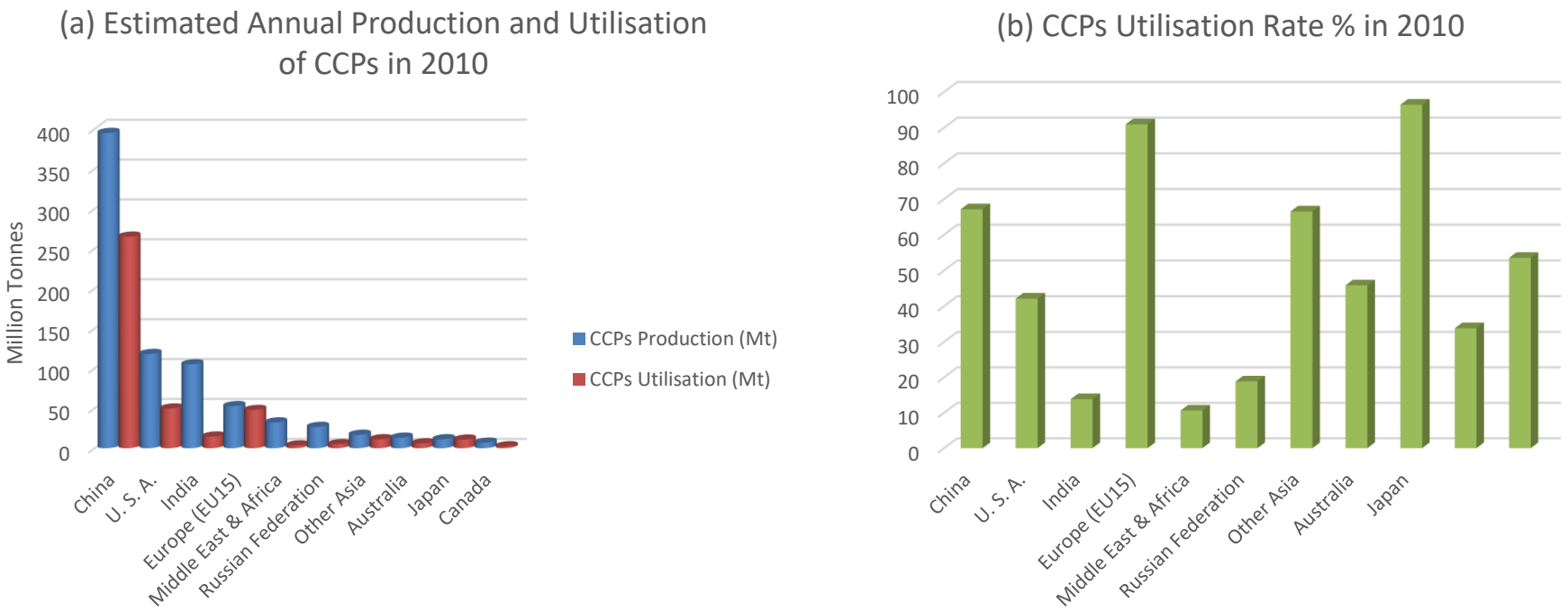

Figure 1.10 (a) Estimated annual production and utilization of coal-combustion products in Mt by country, and (b) coal-combustion products utilisation rates (%) by country in 2010 (Heidrich *et al.*, 2013).

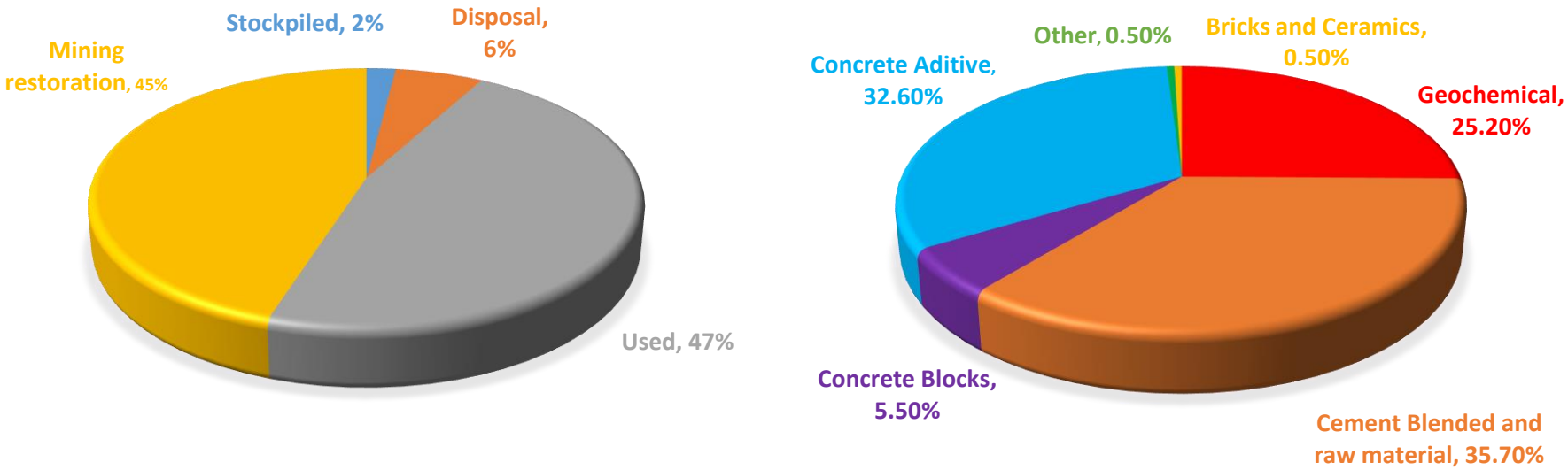

Figure 1.11 Current coal fly ash (CFA) utilisation trends in Europe in 2009. The left-hand chart demonstrates the main areas of CFA utilisation, whilst the right-hand chart offers a more detailed breakdown of the 'used' sector which accounts for 47% of the left-hand chart (Blissett and Rowson, 2012).

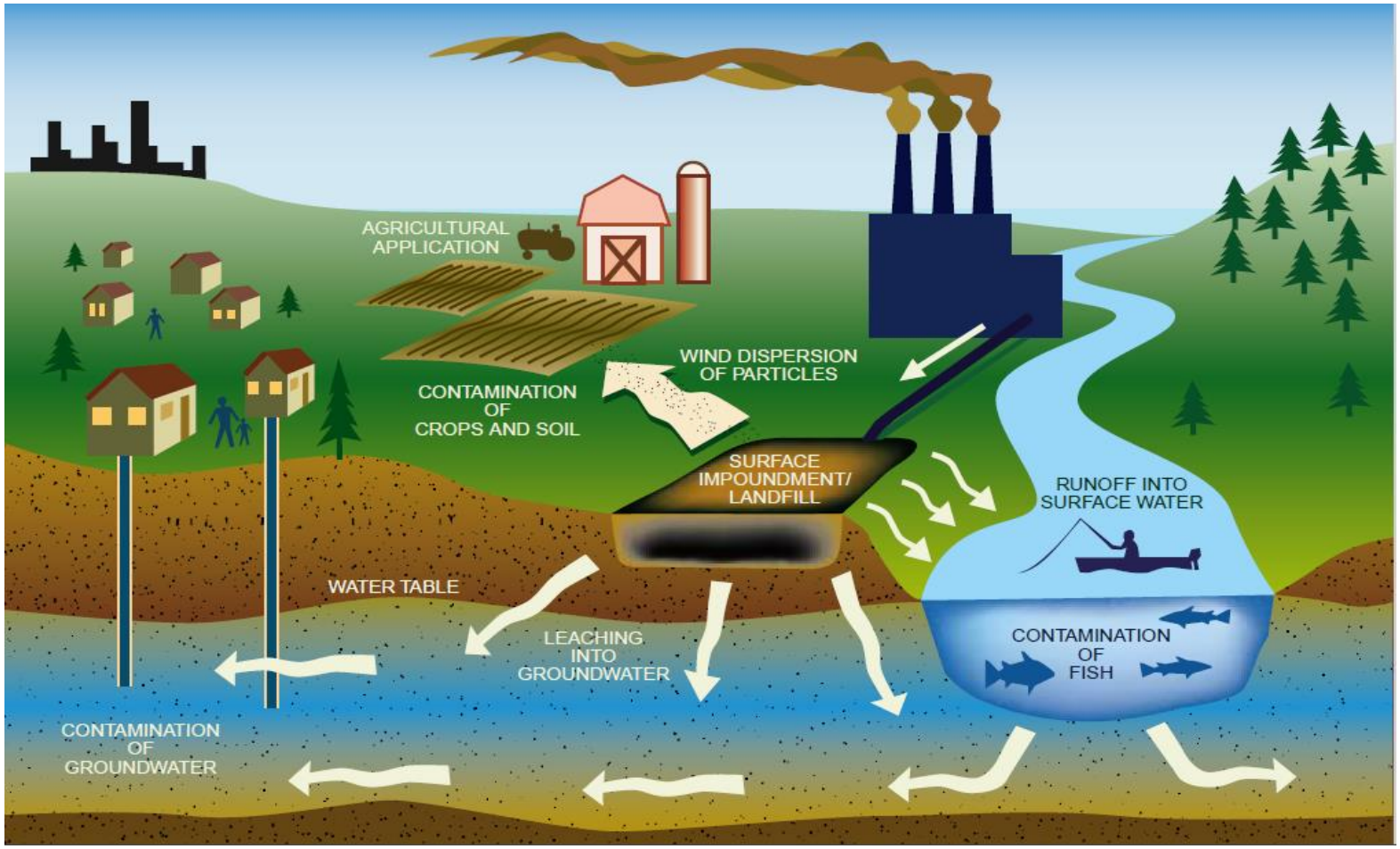

Figure 1.12 Potential environmental impacts of improperly disposed of fly ash; Image source (Keating *et al.*, 2000)

Coal fly ash is a vastly heterogenous material that primarily consists of amorphous aluminosilicate spheres, comprised of silicon dioxide and aluminium oxide, with minor amounts of iron oxide-rich spheres, minor amounts of unburnt carbon and assorted crystalline phases (Kutchko and Kim, 2006, Jegadeesan *et al.*, 2008a). Coal fly ash also contains a variety of other elements including Ba, Br, Ca, Cl, F, Fe, K, Mg, Na, Mn, P and S (Jegadeesan *et al.*, 2008b, Neupane and Donahoe, 2013, Otero-Rey *et al.*, 2005). In addition to these, coal fly ash generally contains minor quantities of toxic elements including As, Se, Pb, B, Be, Bi, Cd, Co, Cr, Cu, Ga, Li, Mo, Hg, Ni, Sb, V, W, and Zn (Neupane and Donahoe, 2013). The concentrations of these elements are tabulated in Table 1.3, which also illustrates that there are multiple environmentally-available major, minor, and trace elements within two acidic (sample 1 and sample 2) and one alkaline (sample 3) fly ash samples, which were collected from three different coal-fired power plants located in the South-eastern United States (Neupane and Donahoe, 2013). Note that As were detected at as high as 158 mg/kg while maximum Se detection was 14 mg/kg, both in the acidic MA fly ash sample.

A concerning observation made by Fernández-Turiel *et al.* (Fernández-Turiel *et al.*, 1994), suggested that 1.5-36.4% of the total concentration of each element detected in fly ash samples was extractable under natural leaching conditions. This could have far reaching impacts given the global production of coal fly ashes. Another important observation by Jankowski *et al.* (Jankowski *et al.*, 2006) proposed that As, Se and Mo ions from either acidic or alkaline fly ash samples became more mobile following high initial pH conditions. Long-term leaching of alkaline fly ash samples have also demonstrated an initial increase in the concentration of As, Se and B in the leachate towards maximum values, which was followed by a decrease, likely due to the formation of ettringite, ($Ca_6[Al(OH)_6]_2(SO_4)_3.26H_2O$), and substitution of those elements for solfate (Hassett *et al.*, 2005, Jankowski *et al.*, 2006).

Table 1.3 Environmentally available element concentrations (mg/kg) in two acidic (Sample 1 and 2) and one alkaline (Sample 3) fly ash samples (Neupane and Donahoe, 2013)

Element	Fly ash		
	Sample 1	Sample 2	Sample 3
Al	21,800	9,310	19,210
As	82	158	17
B	166	117	903
Ba	312	316	217
Ca	4860	5730	32,350
Co	19	13	4.6
Cr	50	30	18
Cu	73	63	23
Fe	19,590	12,110	16,140
K	3160	1570	638
Mg	1890	1130	5060
Mn	74	71	62
Mo	13	12	5.4
Na	722	616	1910
Ni	37	34	7.5
Pb	27	24	12
Sb	3.7	2.7	1.5
Se	7.7	14	12
Si	7290	3880	3110
Sr	287	317	538
Ti	713	615	579
V	103	90	56
Zn	67	103	69

Moderate leaching of Cr, Fe and Pb has been reported from fly ash samples under acidic conditions by Jegadeesan *et al.*, although this was paired with a significant release of As due to dissolution at a pH below 4 and desorption at a pH above 9 (Neupane and Donahoe, 2013). Although strongly influenced by pH, metal ion release is also influenced by their geochemical association and distribution within the fly ash, and their long-term availability under environmentally-relevant conditions *(*Jegadeesan *et al.*, 2008b*).* Mobile elements such as these pose significant long-term concerns when considering a pollution or sustainability perspective as they are non-degradable, and thus will simply accumulate (Reijnders, 2005).

Therefore, there is an unmet need to characterise the chemical and physical properties of coal fly ash in order to better understand its behaviour after being released into the environment. Further knowledge of the elemental composition, mineralogy, organic components and solubility of fly ash particles is essential for the development of both effective and economical remediation techniques to contain toxic trace elements within fly ash and protect ground and surface water resources from contamination (El-Mogazi *et al.*, 1988, Neupane and Donahoe, 2013). For these reasons, the following sections will discuss the physical and chemical characterisations of coal fly ash, leaching behaviour and appropriate fly ash utilisation methods.

1.3.1 Classification of Fly Ash

A number of classification methods have been proposed to distinguish fly ashes, with each method having been designed in order to fulfil an individual purpose (Openshaw, 1992). For example, two methods were established based on either their respective chemistry, pH, particle size and hydration profile (Roy *et al.*, 1981), or by the suitability of fly ashes as cementous or pozzolanic materials (Marttigod *et al.*, 1990). A separate classification method differentiates

fly ashes in relation to how they are handled in either a dry-, conditioned or wet-form (Ahmaruzzaman, 2010).

The American Society for Testing and Materials recognises two generalised classes of fly ash based upon the specified major element oxide content and the source of the coal, which whether the coal is bituminous, sub-bituminous or lignite (Marttigod *et al.*, 1990, Openshaw, 1992). The major constituents of fly ash that are generated from power stations are silica (SiO_2), alumina (Al_2O_3) and iron oxides (Fe_2O_3) (Wang and Wu, 2006a). In addition to these constituents, varying amounts of C, Ca, Mg and S (Wang and Wu, 2006a), in the order of SiO_2 > Al_2O_3 >Fe_2O_3 > CaO > MgO > K_2O > Na_2O > TiO_2 are recognisable (Blissett and Rowson, 2012).

In greater detail, the American Society for Testing and Materials groups coal fly ash into one of two classes, Class C and Class F (Blissett and Rowson, 2012). These classes are primarily differentiated according to the quantity of calcium, silica, alumina and iron present in the ash (Ahmaruzzaman, 2010). Class C fly ashes are high in lime and are composed of between 50-70 wt.% of SiO_2 + Al_2O_3 + Fe_2O_3. These fly ashes are high in calcium (30-40%, in the form of calcium oxide) and are normally generated from the combustion of low-rank coals such as lignites of other sub-bituminous coals. Class C fly ashes display cementous properties by self-hardening when reacted with water (Ahmaruzzaman, 2010). On the other hand, Class F fly ashes are low in lime and contain >70 wt.% SiO_2 + Al_2O_3 + Fe_2O_3. These fly ashes are low in calcium (1-12%, in the form of calcium hydroxide calcium sulfate and glassy components, in combination with silica and alumina) and are generated from the combustion of higher-ranked coals such as bituminous coals or anthracites. Class F fly ashes are pozzolanic in nature means hardening when reacted with $Ca(OH)_2$ in the presence of water (Ahmaruzzaman, 2010). Class C and F fly ashes can also be distinguished by the concentration of sodium and potassium

alkalis, and of sulfates, which are generally higher in Class C fly ash samples when compared to Class F (Ahmaruzzaman, 2010).

An alternate to this method of classification resulted from the analysis of 41 European coal fly ashes (Vassilev and Vassileva, 2007, Blissett and Rowson, 2012). This system grouped the majority bulk oxides together in order to establish a four-tier classification system; i) sialic, ii) calsialic, iii) ferrisialic and iv) ferricalsialic oxides. This system also distinguished between the mineralogical composition and phase of the coal fly ash as the major phases are composed of quartz, mullite and hematite (Vassilev and Vassileva, 2007, Wang, 2008, Blissett and Rowson, 2012). Furthermore, the mineralogical classification system was able to segregate four phase-mineral fly ash types. These were termed Pozzolanic, Active, Inert and Mixed, based upon the distinctive behaviours of glass, mullite with quartz or the sum of other mineral-bearing phases (*e.g.*, Fe, Ca, Mg, K, Na, Ti or Mn carbonates, sulfates, silicates or oxyhydrides) (Blissett and Rowson, 2012).

1.3.2 Physical Characteristics

By collecting from the electrostatic precipitator, a typical coal fly ash aggregate is composed of fine, powder-like particles that are primarily spherical and glassy (or amorphous) in appearance (Ahmaruzzaman, 2010, El-Mogazi *et al.*, 1988). These particles may be either hollow or solid and, depending upon the amount of unburnt carbon within the ash, can vary in colour from tan, to grey, to black (Ahmaruzzaman, 2010, El-Mogazi *et al.*, 1988). It is important to note that despite the variability of the physical characteristics of fly ash between samples, some generalisations can be made regarding properties such as the distribution of size, particle morphology and surface area and density.

1.3.2.1 Size

Fly ash generally consists of finely grained particles that fall within the silt range, with diameters between 2-74 μm (Openshaw, 1992). Another study determined that the majority (63%) of fly ash particles were between 2-50 μm in diameter, with 33% being >50 μm and 4% being <2 μm, respectively (El-Mogazi *et al.*, 1988). Interestingly, most bituminous coal fly ash particles are similar to silt (being less than a 0.075 mm or No. 200 sieve), whilst sub-bituminous coal fly ash, though similarly sized, is generally coarser (Ahmaruzzaman, 2010).

There are three standard methods to determine particle size, (1) volume median diameter, which is determined through Coulter analysis, (2) mass median diameter that is estimated from Stokes' law of settling in aqueous dispersion, and (3) the widely-adopted count median diameter, which is estimated from scanning electron micrographs (Openshaw, 1992). Particle size is an important factor as it can influence the concentration of elements; *i.e.*, as particle size is reduced, volatilisation can result in an increase in concentration of particular elements (Openshaw, 1992). Additionally, smaller particles may exhibit varying levels of enrichment for elements including As, B, Ba, Br, Cd, Cl, Co, Cu, Cr, Fe, Ga, Hg, I, In, Mg, Mn, Mo, Ni, Pb, Po, Rb, S, Sb, Sc, Se, Sr, TI, W, V, and Zn (Roy *et al.*, 1981, Openshaw, 1992).

1.3.2.2 Morphology

The overall structure of a fly ash particle is a useful feature to investigate to better understand its physical properties and its potential to undergo leaching (Openshaw, 1992). The vast majority of fly ash particles (67-95%) exhibit non-opaque, Class G or I spherical morphologies (Fisher *et al.*, 1978, Openshaw, 1992). In general, Class G morphology describes fly ash with large particles between 20-74 μm in diameter whilst Class I morphology stands for fly ash with most silt-sized particles of <10 μm in diameter (Roy *et al.*, 1981, Openshaw, 1992).

Coal fly ash particle morphology is generally determined by the combination of the combustion temperature and the following cooling rate (Blissett and Rowson, 2012). Scanning electron microscopy of coal fly ash samples has demonstrated that these populations are comprised of solid or hollow spheres (cenospheres), and irregular unburnt carbon structures (Blissett and Rowson, 2012), as displayed in Figure 1.13.

Morphology studies have also identified spherical quartz, corundum and magnetite particles within fly ash samples (Kutchko and Kim, 2006). As noted in Figure 1.13, the cenosphere fly ash is predominantly spherical (Matsunaga *et al.*, 2002), whilst the unburnt carbon is larger and more porous, resulting in an irregular particle surface due to the incomplete oxidation of the precursor coal (Blissett and Rowson, 2012).

A schematic for the formation of fly ash particles is illustrated in Figure 1.14. The initial step in the coal combustion mechanism is the material matter conversion of coal to char, which burns out at much higher temperatures (Tomeczek and Palugniok, 2002). The fine minerals that are included within the coal gradually begin to reduce at these higher temperatures, becoming released from within the char as fragments. Then, the minerals begin to decompose, being converted to gases which will eventually condense upon cooling to form the solid ash particles (Blissett and Rowson, 2012). When condensation is homogenous, 0.02-0.2 μm diameter ash particles are formed, while fragmentation of any included mineral matter will produce particles between 0.2-10 μm in size (Tomeczek and Palugniok, 2002). Any excluded mineral matter during this process is subjected to a series of complex transformations, resulting in the generation of spherical particles between 10-90 μm in size (Sarkar *et al.*, 2005).

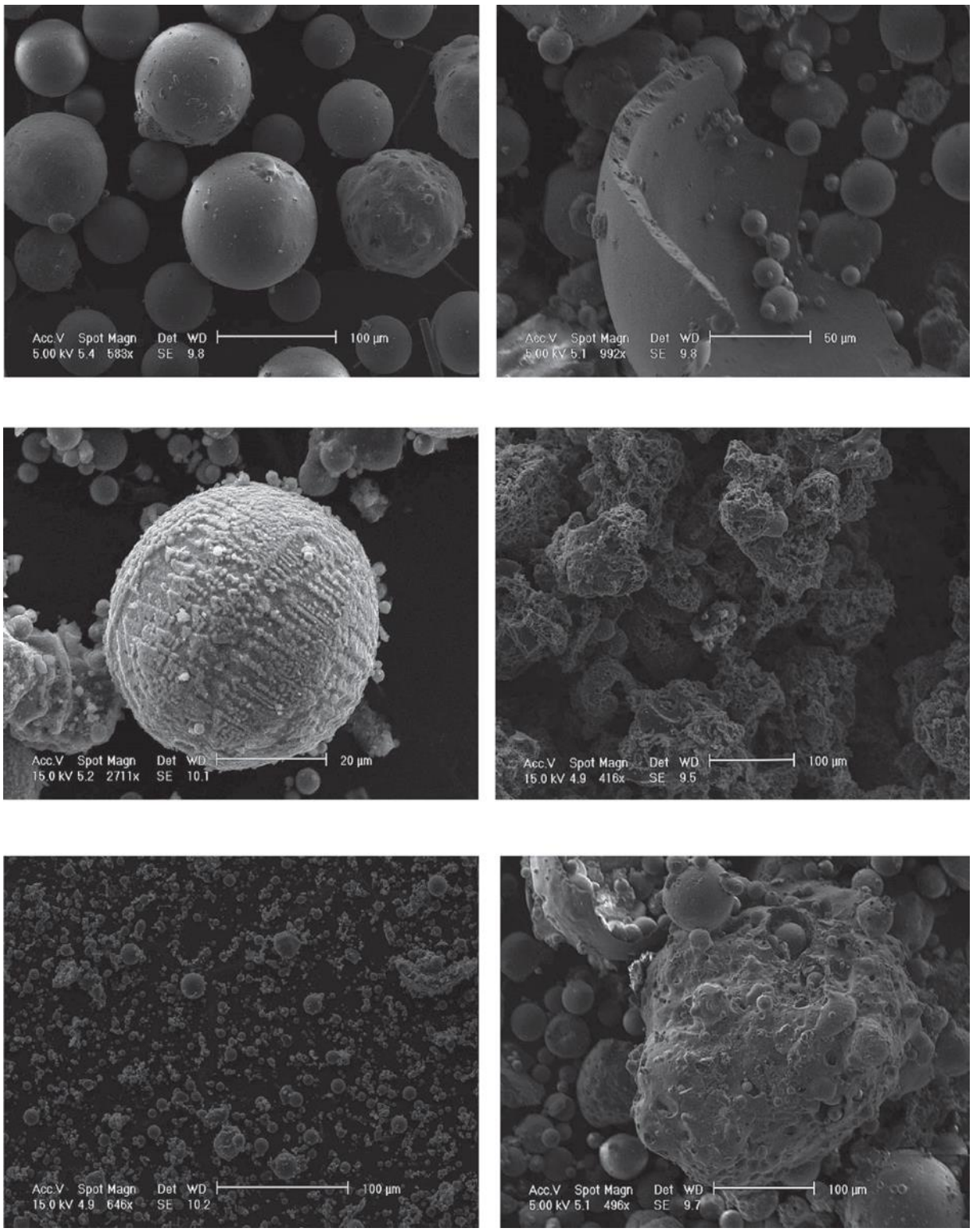

Figure 1.13 Scanning electron micrographs of coal fly ash fractions. From top-left to bottom-right, (cenospheres, broken cenosphere, magnetic sphere, carbon, fine fly ash residue and coarse fly ash residue). Image source: (Blissett and Rowson, 2012).

1.3.2.3 Surface Area

Particle surface area is another important characteristic of fly ash as it influences the total adsorption capacity of the particle, without necessarily impacting the desorption rate. The surface area of a fly ash particle is inversely related to particle size, wherein smaller particles exhibit greater surface areas (Openshaw, 1992). These surface areas can be vast, for example, the fly ash-specific surface area has been estimated to vary between 170-1,000 m^2/kg (El-Mogazi *et al*., 1988). In one study, diameters of 63% of examined particles was found in the range of 2-50 μm (Chang *et al*., 1977). In another study investigating the surface area and porosity of western coal fly ash, fly ash particles that were up to 75 μm in diameter exhibited a surface area between 0.45-1.27 m^2/g and confirmed that surface area decreased with greater particle size (Schure, 1985).

However, as a result of the large and irregular morphology of porous carbonaceous particles, fly ash particles with diameters greater than 75 μm displayed unusually high surface areas (El-Mogazi *et al.*, 1988, Openshaw, 1992). It is important to note that different studies have reported great differences in surface area. For instance, a study by Mattigod *et al.* indicated a wider surface area range of between 0.2-3.06 m^2/g, whilst Theis and Gardner reported a far greater 1-9.44 m^2/g (Mattigod, 1983, Theis and Gardner, 1990). Despite these varied results, these studies also reported a wide range of particle sizes, ranging between 0.01-125 μm, which may be the result of samples being collected from different stages of the combustion process (El-Mogazi *et al.*, 1988, Openshaw, 1992, Ahmaruzzaman, 2010).

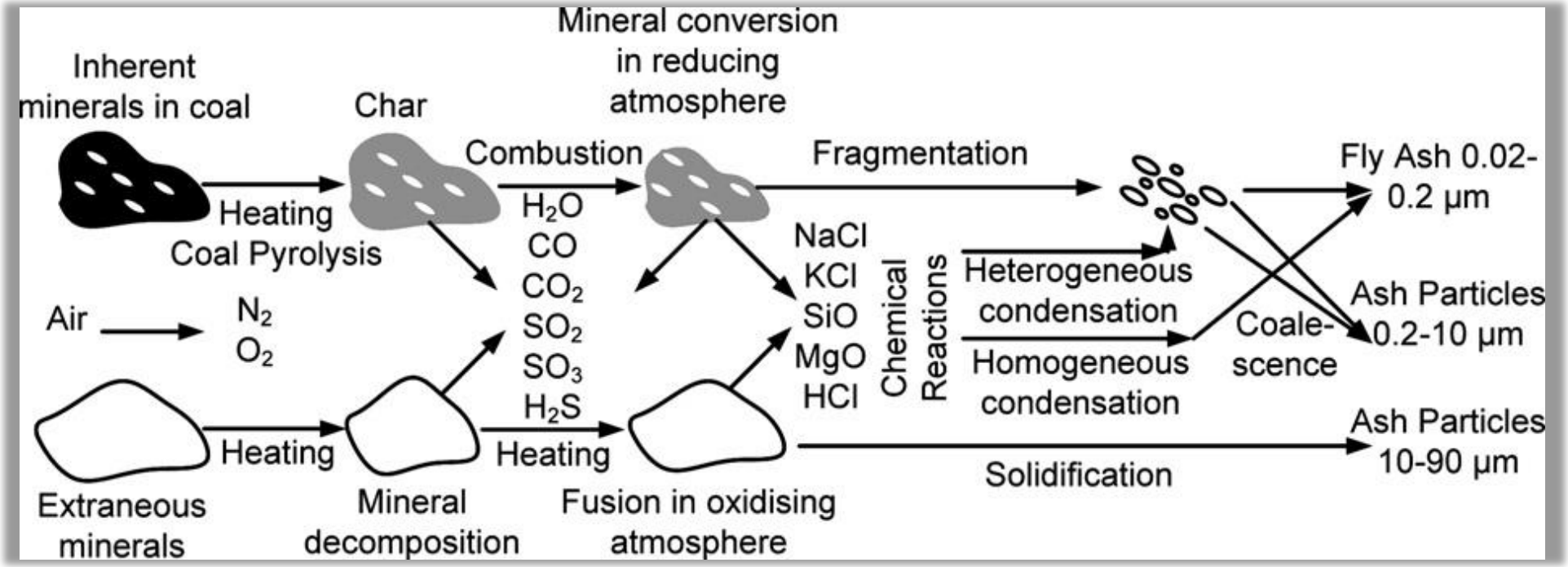

Figure 1.14 Simplified mechanism of coal fly ash formation from pulverised coal combustion (Tomeczek and Palugniok, 2002); Adapted from (Blissett and Rowson, 2012).

1.3.2.4 Density

Density, or the mass per unit of volume, is another important characteristic of fly ash. According to Matsunaga *et al.* (Matsunaga *et al.*, 2002), the solid, spherical fly ash particles are named precipitator ash and possess a density between 2-2.5 g/cm^3 . On the other hand, the hollow cenosphere fly ash particles have a density of <1 g/cm^3. Density is influenced by compaction, for example, laboratory testing of eastern bituminous coal fly ash reached a density of 1.3 g/gm^3 when compacted to 95% of maximum, whilst at the disposed state (85% of maximum density) the density was 1.1 g/cm^3 (Openshaw, 1992).

The reported specific gravity of fly ash varies between 2.1-3.0, and as fly ash possesses such a low bulk density, it can be employed for the synthesis of ultra-light composite materials or introduced into soil in order to reduce soil density (Chang *et al.*, 1977, Adriano *et al.*, 1980, Openshaw, 1992, Matsunaga *et al.*, 2002, Ahmaruzzaman, 2010).

1.3.3 Chemical Properties

The chemical properties of a given coal fly ash are greatly influenced by the properties of the type of precursor coal that was burnt (Ahmaruzzaman, 2010). Coal fly ashes that are produced from sub-bituminous or lignite coals can be distinguished by decreased SiO_2 and Al_2O_3 concentrations, paired with elevated CaO, SO_3 and MgO concentrations when compared to the higher-grade bituminous or anthracite coal fuels (Ahmaruzzaman, 2010, Blissett and Rowson, 2012).

The following section explores some of the chemical properties of coal fly ash such as pH, solubility, leachate, toxicity, and radioactivity.

1.3.3.1 pH

As with most of its chemical properties, the pH of fly ash varies based on the precursor coal source, with fly ashes being known to have been either acidic or alkaline (Roy and Berger, 2011). When mixed with water, the pH of the coal fly ash extract or leachate can either be strongly acidic (pH ~4) due to the sorption of SO_2 through condensation of gas stream-suspended sulfuric acid onto the surface of fly ash particles (Spears and Lee, 2004), or through hydrolysis of Al^{3+} that was derived from aluminium sulphates aluminium-potassium sulphate phase (Fishman *et al.*, 1999).

A coal fly ash leachate can also be rendered strongly alkaline (pH >12) by the hydrolysis of Ca- and Mg-oxides formed during coal combustion (Roy and Berger 2011). Despite these differences, the pH of fly ash-water systems may alter over time, for example, two acidic fly ash extracts that had been generated during the combustion of bituminous coal increased in pH from 4.1 to ~7 after 21-36 days (Roy and Griffin, 1984). This observation was believed to be the result of gradual neutralisation of a finite amount of sulfuric acid within the fly ash (Roy and Berger, 2011). On the other hand, introducing CO_2 into alkaline fly ash samples has been observed to reduce pH as a result of calcite ($CaCO_3$) precipitation, suggesting that geochemical buffers may restrict this broad pH range to between pH ~7-9 (Schramke, 1992). Globally, acidic fly ashes range between pH 3-5, whilst alkaline fly ashes range between pH 10-12 (Openshaw, 1992). For example, in the United States, eastern bituminous coal fly ash was observed to range between pH 4.3-4.9 (Peffer, 1982), whilst western coal fly ash were more alkaline, ranging between pH 8.16-12.4 (Theis and Gardner, 1990).

In aquatic environments, coal fly ash can dramatically alter freshwater pH, primarily due to the presence of acidifying oxalate-extractable iron or alkalising water-soluble calcium (Theis and Wirth, 1977, Openshaw, 1992). This is of great importance as pH is a critical factor in the control of metal desorption from the surfaces of fly ashes, wherein as desorption increases, the

solution becomes more acidic (Theis and Wirth, 1977, Hollis *et al.*, 1988). Another example of this was demonstrated using boron, whose concentration increased 100-fold by neutralising the pH from 12.5 to 7.0 (Hollis *et al.*, 1988). These findings raise important environmental concerns as it indicates that coal fly ashes can result in the creation of low-pH environments (Openshaw, 1992, Roy and Berger, 2011).

1.3.3.2 Solubility

Fly ash solubility is dependent upon the physico-chemical disintegration of the particles (Jala and Goyal, 2006). Essentially, fly ash particles are insoluble glasses, the external surface of which is Mg-enriched, while the dominant proportion of total potassium is sequestered within the interior glassy matrix (Openshaw, 1992, Jala and Goyal, 2006). Enriched surface elements are generally soluble (Roy *et al.*, 1981), however the composition of leachate depends upon the solubility of present trace elements or other components, and ranges between 0.5-3% on the basis of total mass in aqueous solutions (Theis and Gardner, 1990, Openshaw, 1992). When the role of pH was assessed, acidic conditions were found to enhance the solubilisation of trace cations, whilst basic conditions favoured the solubilisation of trace anions such as As, B, Cr, Mo, Se (Theis and Gardner, 1990, Openshaw, 1992). It was noted that these results were dependent upon the extraction procedure that was utilised, namely the properties of the extractant, pH, number of extractions performed, length of extraction period and the ratio of ash-to-solution that was employed (El-Mogazi *et al.*, 1988, Openshaw, 1992).

Due to their elevated abundance in fly ash, it was unsurprising that inorganic species derived from C, Ca, Fe, K, Mg, Na and S were abundant in aqueous fly ash systems (Mattigod, 1983, El-Mogazi *et al.*, 1988). Trace elements that were most soluble under alkaline conditions were B, F, Mo and Se, whereas highly volatile elements such as As, Cd, F, Mo, and Se were easily

extracted from acidic solutions following the combustion process (Openshaw, 1992). Interestingly, semi- and non-metals were found to be more soluble than metals while additional studies demonstrate that the dominant elements upon the surface layer of the fly ash exhibit significant solubility (El-Mogazi *et al.*, 1988, Openshaw, 1992, Jala and Goyal, 2006).

1.3.3.3 Leachate Compositions

Fly ash leachability varies greatly as a result of the coal type burnt and the method of combustion, the fly ash collection method and desulfurisation process (Neupane and Donahoe, 2013). Leachability of elements within coal fly ash is further compounded by the properties of the element, pH, particulate surface areas, contact time, leaching method and the variety of fly ash tested (Openshaw, 1992, Neupane and Donahoe, 2013). Unsurprisingly, coal fly ash leachate is highly variable, although routinely high in total dissolved solids, Al, B, Ca, Fe and SO_4 (Openshaw, 1992). Furthermore, fly ash leachate often exceeded the United States Environmental Protection Agency drinking water quality levels, which limited the maximum level of contaminants in drinking water, for example, maximum contaminants level are reported for arsenic 0.010 mg/L and for selenium 0.05 mg/L (USEPA, 2009). Total dissolve substances, pH and the concentration of Cd, Cr, Fe, Mn and Pb were frequently more than the standard levels (Openshaw, 1992). When investigating leachability, it has been suggested that elements which are abundant upon the particle surface begin to solubilise once they have achieved a physical location or chemical form that is conducive to leaching (Openshaw, 1992).

Acidic fly ash samples have been reported to produce a higher metal concentration in leachate samples relative to alkaline fly ashes (Marttigod *et al.*, 1990). Acidic conditions have been suggested to encourage trace metal leaching, although arsenic does not follow this trend, instead favouring extraction under alkaline conditions (Roy *et al.*, 1981). Alkaline fly ash has also

been reported to increase the leaching of oxyanion-forming trace elements due to the elevated solubility of these elements in high pH conditions (Neupane and Donahoe, 2013). The method of leaching has also been demonstrated to significantly influence the leachability of elements from coal fly ash (Table 1.4). For example, the aggressive synthetic acid rain leaching solution resulted in significantly lower leachabilities for most elements within column leaching experiments as opposed to doubly-deionised water that was employed for serial batch leaching tests (Neupane and Donahoe, 2013). In this serial batch leaching study, Neupane and Donahoe determined that higher element mobilities were due to longer leachant-ash contact times under constant agitation. The result from Killingley *et al.* confirmed that the amount of trace elements in column leach were approximately three times lower than the leachate from the standard batch method for alkaline fly ash but were the same for acidic ashes (Killingley *et al.*, 2000).

Another leaching method that was used by Neupane and Donahoe to study the long-term leaching behaviour of fly ash was the column leaching method (Neupane and Donahoe, 2013). This method involves the wash of a fly ash sample column with an aqueous solution over an extended period of time. When leached continuously with distilled water, there was a steady decrease in pH and in the concentration of Na and K, paired with a rapid decrease in Ca carbonate, hydroxide and sulfate leaching (Dudas, 1981). The concentration of bicarbonate increased steadily, prior to levelling off. Al and Mg leaching increased to its peak during the first 12 months, followed by a steady decrease (El-Mogazi *et al.*, 1988). In another study, long term column leaching of fly ashes collected from 9 power stations in Australia was conducted over 24 months (Killingley *et al.*, 2000). The results for B, Se, Mo and V showed high concentrations, up to 40 time more than other elements. Additionally, As, Cd, Cu, Ni and Zn were considerably leached from some acidic fly ashes (Killingley *et al.*, 2000).

Another leaching method that is employed to study the long-term leaching characteristics of fly ash is the use of a moderately-acidic leaching reagent to accelerate the solubilisation of fly ash constituents in a shorter period of time (El-Mogazi *et al.*, 1988). The use of a leaching agent was also employed in the columnar study of Neupane and Donahoe, who employed the more aggressive acidic solution as a strong leaching agent (Neupane and Donahoe, 2013). In a different study, lignite fly ash was treated with 0.1 M HCl for three hours, which resulted in the near-complete removal of Cd within 5 mins and the gradual leaching of Mn throughout the three hour period (Austin and Newland, 1985). As Cd is a surface concentrated element, it was expected to be more rapidly removed than Mn, which is matrix-associated (El-Mogazi *et al.*, 1988).

A third method to study long-term leaching is the use of simulation modelling, wherein a mathematical model is constructed to calculate the leaching times of particular trace elements from hypothetical ash deposits (Liem *et al.*, 1983). This simulation modelling has been utilised to predict leachate characteristics over ten years and found that <10% of the As, Cd, Cr, Mo, Ni, Se, and Zn would leach out from the original deposit (Openshaw, 1992).

Table 1.4 Summary of leaching methods and related outcomes

Leaching methods	Solution	Leachate composition	References
Serial batch	doubly-deionised water	Higher element mobilities	(Neupane and Donahoe, 2013)
column	Synthetic acid rain	Lower leachabilities for most elements	(Killingley *et al.*, 2000).
Long-term column (12 months)	distilled water	Decrease in pH, decrease in concentration of Na, K, Ca Increase in concentration of Al and Mg	(Neupane and Donahoe, 2013)
Short-term column (3 hour)	Moderately to more aggressive acidic solution	Complete removal of Cd in 5 min, Gradual leaching Mn within 3 hour	(Austin and Newland, 1985)
Simulation modelling (mathematically predict over 10 years)	distilled water	<10% of As, Cd, Cr, Mo, Ni, Se, and Zn would leach out	(Liem *et al.*, 1983)

However, some long-term column and batch leaching studies indicate that the concentration of several elements increases with time, suggesting that the long-term environmental challenge for coal fly ash management is the control of potential leachate leakage from the fly ash disposal facilities, into the environment (Neupane and Donahoe, 2013). Upon reaching ground or surface water, the fly ash leachate plume has the real potential to contaminate drinking water supplies, particularly in the case of older, unlined, disposal facilities which lack the additional barriers of newer, lined, facilities. Thus, there remains a need for the development of efficient and economical methods of containing the potentially hazardous trace elements stored within fly ash disposal facilities (El-Mogazi *et al.*, 1988, Openshaw, 1992, Neupane and Donahoe, 2013).

1.3.3.4 Toxicity

Fly ash as a hazardous waste generally contains toxic substances such as trace elements (Pb, Zn, As, Se, and etc.), and organic compounds including dioxins, furans, polychlorinated biphenyl (PCBs), volatile organic compounds (VOCs) and polycyclic aromatic hydrocarbons (PAHs) (Huang *et al.*, 2017, Chen *et al.*, 2017). Dioxins, which are relatively resistant to biodegradation, are formed by combustion processes, generally by incomplete combustion of coal. These substances accumulate in food such as eggs, dairy products, animal fat and fish (Chen *et al.*, 2017). High levels of total dissolved substances, elevated pH or a bioaccumulation can have toxic effects upon organisms and human health (Openshaw, 1992). For example, in landfills, human health was found to be associated with genetic abnormalities (Giusti, 2009).

Given the variability of fly ashes that has been previously described, each fly ash possesses individual characteristics and must be identified in both the field and the laboratory to ensure that it is handled safely (Openshaw, 1992). For example, Roy *et al.* observed high levels of

cadmium (1.38 ppm) when performing the extraction procedure toxicity test upon fly ash samples (Roy and Griffin, 1984).

Element speciation is very relevant to fly ash toxicity as particular forms of elements may exhibit greater toxicity, biological availability or mobility (Openshaw, 1992). For example, one of the toxic form of arsenic is the As (III) oxidation state, which generally occurs in very low concentrations over a broad pH range. Although it is technically challenging to determine the speciation of all potentially toxic elements present in fly ash samples, such information could differentiate two different fly ashes with the same concentrations (Openshaw, 1992).

1.3.3.5 Radioactivity

Some trace elements found within coals (*e.g.* uranium, thorium) are naturally radioactive, including their numerous decay products (*e.g.* radium and radon) (Zielinski and Finkelman, 1997). Interestingly, these elements are less chemically toxic than other trace elements found within coal, for example, As, Se, and Hg (Zielinski and Finkelman, 1997). The United States Geological Survey maintains an extensive database regarding the chemical composition of U.S.-produced coal, including data concerning uranium and thorium content (East and Matthias, 2016). Most coal samples contain concentrations of uranium between ~1-4 ppm, which are similar to the concentrations observed in various common soils and rocks. The concentration of thorium in coals also fall within the ~1-4 ppm range, despite a greater average abundance in the Earth's crust of ~10 ppm (Zielinski and Finkelman, 1997). As such, it is extremely rare for U.S. coals to contain >20 ppm of either uranium or thorium. Furthermore, almost 100% of radon gas that is present in the feed coal is transferred into the gas phase to be released in stack emissions (Zielinski and Finkelman, 1997).

However, the less volatile elements (uranium, thorium and most degeneration products) are sequestered within solid combustion wastes, resulting in a 10-fold greater concentration when compared to the original coal (Zielinski and Finkelman, 1997). Although this may sound somewhat alarming, this concentration is still within the range observed in certain shales, granitic and phosphate rocks (Zielinski and Finkelman, 1997).

In fly ash, uranium atoms are concentrated within the core of fine-sized particles rather than upon the particle surface. Furthermore, water that has contacted fly ash contains very low concentrations of uranium or radium, which are below the contemporary drinking water standard for uranium, 30 µg/L (Frisbie *et al.*, 2013), or radium, 5 picocuries per litre (Zielinski and Finkelman, 1997).

Although the U.S. Resource Conservation and Recovery Act does not provide radioactivity guidelines, fly ash would be considered as radioactive waste provided the average ^{226}Ra concentration exceeded 5 picocuries per gram, or if a leachate consisted of 50 picocuries per litre of combined ^{226}Ra and ^{228}Ra (Roy *et al.*, 1981). As such, fly ash radioactivity is only a concern with fly ash re-use in situations where coal fly ash had been incorporated into concrete products, which may potentially emanate radiation (Krieger and Jacobs, 1978). However this represents a minor possibility as the majority of radiation concentrates within the bottom ash, particularly in the airborne emissions in flue gas rather than the fly ash itself (Torrey, 1978, Openshaw, 1992).

In summary, the concentration of radioactive elements or associated radioactivity in coal and fly ash are relative to common rocks and soils. From this, it becomes apparent that there is less of a human health concern in the form of radioactivity compared to potential environmental contamination (Openshaw, 1992, Zielinski and Finkelman, 1997).

1.3.4 Chemical Composition of Fly Ash

As coal contains every naturally-occurring element, it is reasonable that coal fly ash contains many trace elements. As mentioned previously, the elemental composition of fly ash is highly variable, which is directly related to the source of the coal, pre-treatment processing (if performed) and the combustion conditions within the power plant (El-Mogazi *et al.*, 1988, Openshaw, 1992).

The following section provides an introduction into the elements, mineralogy and organic contents of fly ash. However, due to the vast heterogeneity between fly ash samples, it would be imprudent to assume that accurate assumptions can be made regarding an individual fly ash variant without performing relevant, individualised testing.

1.3.4.1 Elemental Composition (Major and Minor)

The elements that are observed within coals at >1% (*i.e.*, comprising >1 wt. %) are classified as major elements, whilst those that comprise 0.1-1% wt. are termed minor elements and those that compose <0.1% wt. are regarded as trace elements (Akinyemi *et al.*, 2012). The respective quantities of major elements in their oxide status (wt. %) within fresh fly ash that was produced by an Australian power station have been listed in Table 1.5, along with the abundance of selected minor or trace elements dry ash in mg/kg.

In order of decreasing abundance, the major elements of fly ash are Si, Al, K, Fe, Ti, Na, Ca, Mg, S, P and Mn. These elements are present in fly ash in their oxidised states in average concentrations >0.1% (El-Mogazi *et al*., 1988).

The major elements generally reside within the more stable particle cores as opposed to the surface of the particles where physico-chemical reactions more easily occur (Klein *et al.*, 1975,

Hansen and Fisher, 1980, El-Mogazi *et al.*, 1988). In order to explain these results, it has been suggested that these elements are not volatilised during combustion but rather melt to remain in a condensed form which proceeds to collection (Klein *et al.*, 1975, Page *et al.*, 1979).

The relative quantities of major oxides vary depending on the source coal type that was used. Table 1.6 compares the wt.% of major oxides from three different coal sources (Neupane and Donahoe, 2013). According to these data, bituminous and sub-bituminous coal produce fly ashes with higher quantities of SiO2, Al2O3 and Fe2O3 but lower CaO, MgO and SO3 in comparison with lignite.

In relation to minor elements, multiple studies suggest that several trace elements that are of environmental concern are localised to the surface of fly ash particles (*e.g.*, As, Se, Mo, Cd and Zn) rather than within the core of the structure (Page *et al.*, 1979). In comparison, Cr, Cu and Pb were found to be more evenly distributed throughout the fly ash particle whilst Ni was mostly observed to be associated with the particle core (Theis and Wirth, 1977, Page *et al.*, 1979). Furthermore, the concentration of As, Se, Cd, Zn, Ni, Cr, and Pb has been observed to increase with decreasing particle size (El-Mogazi *et al*., 1988).

These observations are compounded by the findings that the concentration of As, Se, Cd, Zn, Pb, Cu, and Mo increase as the ash sampling position moves downstream from the boiler (Klein *et al.*, 1975, Page *et al.*, 1979). An explanation for these findings may be that certain elements are volatilised during combustion which then condense upon the surface of fine ash particles as the flue gas cools. Trace elements are then concentrated upon smaller particles due to their greater surface area for the vapor to condense upon (El-Mogazi *et al*., 1988). Taken together, this suggests that particular trace elements are held within the fly ash particle, in a position that favours mobility and eventual release into the surrounding ecosystem (El-Mogazi *et al*., 1988, Akinyemi *et al.*, 2012).

Table 1.5 Major element (oxide wt.%) and trace element (mg/kg) data for dry ash samples (Ward *et al.*, 2009)

Major Oxides	Fresh fly ash / wt. %	Minor elements	Fresh fly ash / mg/kg
SiO_2	59.95	**As**	11
Al_2O_3	25.06	**Ba**	490
TiO_2	1.01	**Cd**	1
Fe_2O_3	1.67	**Co**	20
CaO	0.33	**Cr**	70
MgO	0.33	**Cu**	66
MnO	0.03	**Mo**	3
K_2O	2.56	**Ni**	77
Na_2O	0.50	**Pb**	75
P_2O_5	0.12	**Se**	6
SO_3	0.22	**Zn**	150

Table 1.6 Normal range of major elements in their oxide states in fly ash produced from different coal types, (Heidrich *et al.*, 2013)

	Components / wt.%							
Coal Type	**SiO_2**	**Al_2O_3**	**Fe_2O_3**	**CaO**	**MgO**	**SO_3**	**Na_2O**	**K_2O**
Bituminous	20-60	5-35	10-40	1-12	0-5	0-4	0-4	0-3
Sub-bituminous	40-60	20-30	4-10	5-30	1-6	0-2	0-2	0-4
Lignite	15-45	10-25	4-15	15-40	3-10	0-10	0-6	0-4

1.3.4.2 Mineralogy

Fly ashes can be segregated into three major matrices; glass, mullite-quartz and magnetic spinel (Hulett *et al.*, 1980). The dominant crystalline components of fly ash are quartz (SiO_2), mullite ($3Al_2O_3{\cdot}2SiO_2$) and maghemite γ-Fe_2O_3 (Silva *et al.*, 2010). Some fly ash samples contained traces of anhydrite, hematite (Fe_2O_3) and rutile (TiO_2), although these were rare (Silva *et al.*, 2010). The magnetic matrix of fly ash is of particular interest as a result of its greater reactivity and potential to carry and release toxic elements (El-Mogazi *et al.*, 1988). Fly ash also contains less abundant mineral forms such as gypsum, ferrous carbonates, calcite and manganese oxides (El-Mogazi *et al.*, 1988). As the quantities and forms of particular trace elements are determined by their association with a given matrix or mineral, mineralogical information can provide useful insight into predicting fly ash behaviour (El-Mogazi *et al*., 1988, Silva *et al.*, 2010).

X-ray diffraction revealed that pulverised feed coal was primarily composed of siliceous minerals (*e.g*. quartz (SiO_2), kaolinite [$Al_2(SiO_2O_5)(OH)_4$)]) and non-siliceous minerals such as potassium selenium chloride (K_2SeCl_6) with minor quantities of pyrite (FeS_2) (Akinyemi *et al.*, 2012). Kaolinite contains water that is bound within its lattices and was found to be uniformly distributed in tested coal samples. Water that was bound within kaolinite was lost during ashing (Akinyemi *et al.*, 2012). Pyrite was observed to be the main species of sulfur oxidation within the tested coal samples, while quartz was confirmed to be the most common mineral, likely as the result of detrital genesis (Vassilev *et al.*, 1997). The quartz content of coal fly ash was also suggested to be high as this mineral is stable/inert during combustion temperatures (Akinyemi *et al.*, 2012). In summary, the mineralogy of coal combustion products such as fly ashes is dependent upon factors such as the nature of the combustion process, the type of coal employed and its chemical interactions with infecting rainwater and accesses CO_2 (Akinyemi *et al.*, 2012).

1.3.4.3 Organic Compounds

It is commonly understood that fly ash particles are associated with a complex mixture of organic particles (El-Mogazi *et al*., 1988). The precursor coal structure undergoes extensive physico-chemical changes during combustion, leading to the release of organic fractions which are subjected to subsequent reactions, culminating in the formation of polycyclic aromatic hydrocarbons and other organic compounds (Liu *et al*., 2000, Ribeiro *et al.*, 2014). These organic compounds are suspected to be adsorbed onto the surfaces of particles within the stack system of the power plant (El-Mogazi *et al.*, 1988). Although the interactions between fly ash particles and organic compounds is poorly characterised, their adsorption is profoundly influenced by the large surface area of carbonaceous particles that act similarly to activated carbon (Greist and B.A. Tomkins, 1986, El-Mogazi *et al.*, 1988).

The organic soluble phase of fly ash samples includes a wide variety of compounds that may pose a potential risk to the environment, such as aliphatic and aromatic compounds (Ribeiro *et al.*, 2014). Fly ash samples were found to contain increased levels of aliphatic compounds such as long-chain n-alkanes, pentacyclic terpanes and regular steranes (C-27, C-28, C-29), paired with decreased tricyclic terpanes (Ribeiro *et al.*, 2014). Fly ash samples were also found to contain polycyclic aromatic hydrocarbons (PAHs) such as fluoranthene (four rings) as well as mutagenic/carcinogenic organic compounds such as benzo[a]anthracene (four rings), benzo[b]fluoranthene (four rings), indeno[123-cd]pyrene (five rings), benzo[ghi]perylene (five rings), and dibenzo[ah]anthracene (six rings). Although this study did not detect polycyclic aromatic hydrocarbons with 2 or 3 aromatic rings, it is possible that these compounds were lost due to their volatilisations (Ribeiro *et al.*, 2014).

The aliphatic and aromatic compounds observed within fly ash extracts represent a complex mixture of compounds that are derived in combination from either the precursor coal (*i.e*. petrogenic source) or the result of the heat of combustion (*i.e*. pyrolyic source) (Ribeiro *et al.*,

2014). These thermal transformations to the organic compounds present in coals are the product of a complex network of factors such as oxygen availability, combustion temperature and residence time (El-Mogazi *et al.*, 1988, Ribeiro *et al.*, 2014).

1.3.5 Fly Ash Disposal

Coal fly ash is disposed of or re-utilised according to the by-product type, processes available at the power plant and the relevant regulations governing that plant's activities (USEPA, 2016a). As discussed previously in Section 1.3, coal fly is deposited according to the 'dry' method (Figure 1.15a), or 'wet' method (Figure 1.15b). During dry disposal, the fly ash particles are held within dry surface impoundments, landfills or fly ash basins. In comparison, the wet method washes fly ash waste out with water into a neighbouring waterway such as a settling pond or an artificial lagoon (Patra *et al.*, 2012).

Some countries maintain quantitative disposal data for these processes. In 1998, 66% of fly ash and 69% of bottom ash produced from coal combustion were discarded in such ways, mostly in the form of landfill (Clark *et al.*, 2001). India, on the other hand, generated 90-100Mt of coal fly ash, of which >85% was discarded (Vageesh and Siddaramappa, 2002, Kumar *et al.*, 2003). These disposal methods ultimately result in the dumping of vast quantities of fly ash onto open land, leading to air pollution in the form of particulate contaminants being blown into the air as dust, and water table pollution in the form of leaking/leaching contaminants entering into surface or groundwater sources (Reijnders, 2005, Patra *et al*., 2012, USEPA, 2016a, USEPA, 2016b).

Figure 1.15 a) Fly ash disposal in dry method: left, the disposal site in La Belle, Fayette County, Pennsylvania, United States (Templeton and Hopey, 2010), and right, dry ash site near Mount Piper power station, NSW Australia., 2012.

Figure 1.15 b) Fly ash disposal in wet method: left, the wet disposal of ash into ash ponds adapted from (tradelink, 2015), and right, Coal ash ponds on Mountain Island Lake near Charlotte, NC, retrieved from (Dunn, 2015).

1.3.6 Re-Utilisation

Coal combustion by-products such as fly ash can be re-utilised as an alternative industrial resource, or on certain processes or applications (Wang and Wu, 2006b). As previously mentioned, fly ash can be reutilised in infrastructure to create concrete, cement roadway and pavement products, structural fill and cover materials, light-weight aggregate, subterranean void filling and infiltration barriers (Wang and Wu, 2006b, Patra *et al.*, 2012). Fly ashes can also be reused in agriculture as soil fertilisers, agriculture stakes or acid-neutralisers in soil (Patra *et al.*, 2012). Fly ashes also present a low cost adsorbent that can be employed for organic gas adsorption, flue gas cleaning and wastewater treatment by removing toxic metal ions, organic matter and dyes (Wang and Wu, 2006b, Ahmaruzzaman, 2010, Wang and Wu, 2006a). Based upon the properties of a given fly ash, a number of potential re-utilisation options are available, which are summarised in Figure 1.16 (Wang and Wu, 2006b, Ahmaruzzaman, 2010, Patra *et al*., 2012). For example, based on chemical composition, fly ash may be used as source of silica, aluminium and iron, raw material for cement, ceramic raw material for bricks and glass, *etc*.

The physico-chemical properties of fly ash such as particle size, porosity bulk density, surface area and its capacity to hold water, make it an attractive material for utilization as an adsorbent (Patra *et al.*, 2012). Although a potential use of fly ash has been suggested as a soil fertilizer, fly ash is rarely used for this purpose as it contains quantities of non-essential elements such as As, B, Cd and Se, which have an adverse effect upon soil, crop and ground/surface water quality (Patra *et al.*, 2012). Notably, water-related reutilisation of fly ash may result in the leaching of certain elements into the water table, thereby creating a potential for environmental pollution which must be accounted for (Ahmaruzzaman, 2010). As a result, before fly ash can be repurposed as an adsorbent for water treatment, a number of measures must be taken to ensure environmental safety. These include testing to characterize leaching behaviour in a given water

system, forced extraction of any mobile substances within the repurposed fly ash, immobilization and capture of mobile metals or other hazardous elements, followed by the destruction of any remaining organic contaminants. It has also been suggested that chemical modification studies should be performed on fly ash samples in order to boost their respective adsorption capacities and efficiency of contaminant removal (Ahmaruzzaman, 2010).

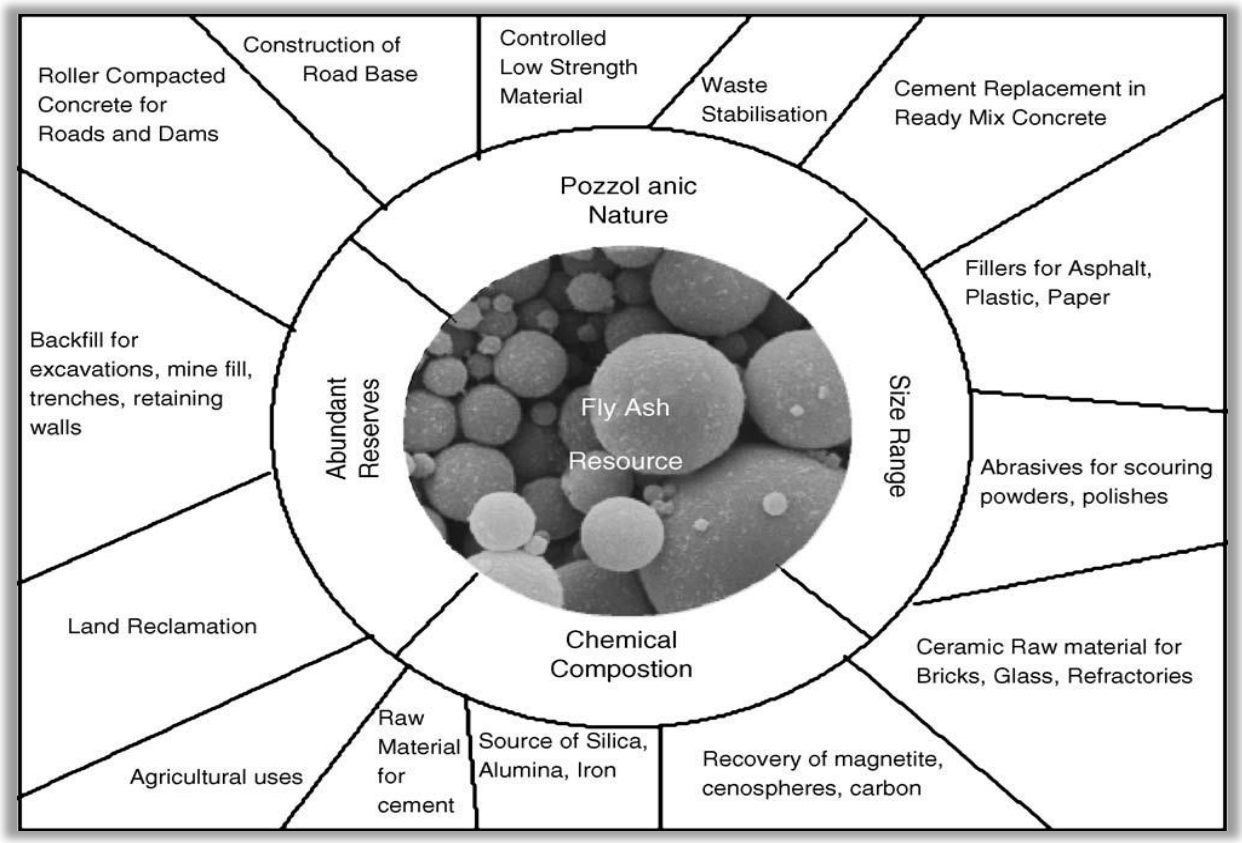

Figure 1.16 Potential avenues for fly ash reutilization, based upon the intrinsic advantages of the type of fly ash material. Image source: (Wang and Wu, 2006a).

1.3.7 Effect of Fly Ash on the Environment (Plants and Animals)

The environmental concerns of fly ash disposal reutilisation are legitimate issues regarding the mobilisation of toxic elements into water sources, the impact upon microbial populations and biota, managing the handling risks and ensuring adherence to rigorously-defined industry regulations (Openshaw, 1992). The routine disposal of fly ashes into landfills are particularly concerning as they may give rise to the release of organic compounds such as polycyclic aromatic hydrocarbons which can adversely impact water, soil, plants, biodiversity and human health due to their toxicity and mutagenic/carcinogenic activities (Ribeiro *et al.*, 2014). These activities depend greatly upon a number of factors including their concentrations, physico-chemical properties, chemical or photo-oxidation, volatilisation, adsorption characteristics in soil, microbial degradation and leaching (Wild and Jones, 1995), as well as extent and mechanism of exposure, for example, ingestion, skin contact or inhalation (Ribeiro *et al.*, 2014).

The disposal of fly ash also has the potential to adversely affect plant life within the surrounding ecosystem. For example, if grown in a mixture of soil and ash, plants that are grown in closed landfill are potentially more likely to come into contact with toxic concentrations of trace elements, boron and soluble salts, particularly if the plants possess deep roots (El-Mogazi *et al.*, 1988). Plants that have been grown in fly ash-amended soils were found to have absorbed elevated concentrations of particular elements, of which, As, Mo and Se had achieved concentrations that were potentially toxic to grazing animals (El-Mogazi *et al.*, 1988). A concerning observation here was that the concentrations of these elements in plant tissues demonstrated strong correlation with their respective concentrations in the soil/fly ash mixture (Furr *et al.*, 1976, Furr *et al.*, 1981). When fly ash was added to soil at a rate of ≤10%, plant tissues displayed elevated levels of As, Mo and Se (Furr *et al.*, 1976, El-Mogazi *et al.*, 1988). Therefore, it is reasonable to suggest that plants exposed to greater amounts of fly ash in soils

(>10% fly ash content) would accumulate even greater concentrations of these toxic elements (El-Mogazi *et al*., 1988).

Some studies have suggested that the supply of As from fly ash may be a short-term occurrence, although the supply of Se from fly ash to plants such as grasses and vegetables has been demonstrated to be both continuous and long-term (Furr *et al*., 1976, Furr *et al.*, 1979, Gutenmann and Lisk, 1979). Certain wild plants found growing in fly ash have been found to accumulate Se, resulting in a 10-fold biomagnification of the original Se concentrations within the fly ash (El-Mogazi *et al.*, 1988). This potentially dangerous accumulation of trace elements by wild plants that have adapted to growing on fly ash-heavy soils represents an environmental hazard, particularly if these elements are capable of additional biomagnification within the food chain. As such, it is important to analyse plants that have grown upon fly ash and animals that have either been exposed to fly ash or in order to determine the movement of these elemental components throughout the ecosystem (El-Mogazi *et al.*, 1988). When considering the impact of fly ash upon local fauna, it is essential to establish the immediate effects of fly ash upon wild/domestic animal growth and elemental retention, as well as the potential effects that fly ash will exert upon animal and human life. These effects are predicted using assays to determine mutagenicity and other deleterious biological activity (El-Mogazi *et al.*, 1988).

According to El-Mogazi *et al.*, immediate impacts of fly ash on local fauna include:

- Abnormally-elevated concentrations of elements such as Se, which are bio-accumulated within animals that consume plants grown in fly ash;
- Increased concentrations of such elements within the meat, milk and eggs of these animals;
- No immediately-apparent signs of damage or toxicity to the animals;
- A wide range of animal species are affected by elemental intake resulting from fly ash disposal operations.

The potential effects of fly ash extracts and particles must be individually assessed in order to establish their biological activities. A key test employed to this end are mutagenicity studies, which are greatly important to public health as fly ash mutagenicity indicates the potential for carcinogenicity (Li *et al*., 1983). The mutagenic activities of fly ash extracts are primarily attributed to nitro-substituted organic compounds, particularly nitro-polycyclic aromatic hydrocarbons, while whole-ash particles are suspected to carry inorganic mutagens (Wei *et al.*, 1982, Li *et al.*, 1983, Harris *et al*., 1984). As is often the case with coal fly ash, mutagenic activity might be influenced by the source coal combustion method, namely temperature and the point of ash sampling (El-Mogazi *et al.*, 1988). Mutagenicity is not the only biological activity tested for fly ash, whose samples are also assessed for cellular toxicity, effects upon the interferon system and hemolytic activity (Garrett *et al.*, 1981, Mumford and Lewtas, 1982, Liu *et al*., 1986). Such studies have determined that fly ash contains biologically-active compounds which may induce changes in animal and human tissues, however, short-term animal studies have found that these do not occur to a significant extent. Given the findings discussed here, it is important to note that the long-term release and bioaccumulation of compounds originating from fly ash may pose a risk of future damage to humans and animals, therefore further research into their mechanisms of action must be performed (El-Mogazi *et al.*, 1988).

1.3.8 Arsenic and Selenium in Fly Ash

As a by-product of coal combustion, coal fly ash contains elevated concentrations of hazardous As and Se, which can be classified as being ‘semi-volatile elements’ (Otero-Rey *et al.*, 2005, Kashiwakura *et al.*, 2011). Semi-volatile elements volatilise during the combustion process, accumulating within the coal fly ash particles that are produced, resulting in varied concentrations of As and Se within fly ashes (Theis and Gardner, 1990, Kashiwakura *et al.*, 2011). The United States Environmental Protection Agency Primary Drinking Water Standards

regulates the concentration of As and Se in water sources with maximum contaminant levels of 10 µg/L and 50 µg/L, respectively (USEPA, 2009). Given the variability between specimens, coal fly ashes have been reported to contain between <35–2,000 ppm total As and <10–200 µg/g Se (Otero-Rey *et al.*, 2005). Furthermore, three decades of the Electrical Power Research Institute data in the United States has determined that the 90th percentile values of As and Se contents within fly ashes were 261 mg/kg and 18 mg/kg, respectively (EPRI, 2010). Although the total amounts of these toxic and potentially hazardous elements are relatively low in coal fly ash, the vast amounts of coal fly ash deposited in wet and dry disposal each year represents significant contributions to the environment (Otero-Rey *et al.,* 2005). Furthermore, between 30-35% of environmentally available As, and 42-63% of environmentally available Se has been demonstrated to be mobilised from a fly ash sample during a leaching test (Neupane and Donahoe, 2013).

As and Se mobility and environmental toxicity is influenced by its oxidation state and chemical forms within coal fly ash (Otero-Rey *et al.*, 2005). Within coal fly ashes, As(V) and Se(IV) are the dominant species, with 93% of total arsenic in fly ash leachate consisting of arsenate, whist selenium almost entirely leaches in the form of selenite (Van Der Hoek *et al.*, 1994, Jackson and Miller, 1998, Huggins *et al*., 2007a, Shah *et al.*, 2007, Su and Wang, 2011). Adsorption/desorption is the predominant control mechanism for the leaching of As and Se from bituminous fly ashes (El-Mogazi *et al.*, 1988, Van Der Hoek *et al.*, 1994, Wang and Wu, 2006b, Wang *et al.*, 2008, Jegadeesan *et al.*, 2008a, Kashiwakura *et al.*, 2010). It is also important to note that sorption reversibility reflects the sorbed contaminant to be leached, under changing conditions, into the aqueous phase (Van Der Hoek *et al.*, 1994, Otero-Rey *et al*., 2005, Su and Wang, 2011).

As mentioned earlier in this section, though As and Se were observed to be released during serial batch and leaching tests of fly ash samples, the column leaching method proved to yield

higher proportions of the environmentally-available As and Se (Neupane and Donahoe, 2013). Class F coal fly ashes have shown greater release of As when subjected to aggressive conditions (pH<4 and pH>9), which is consistent with its intrinsic oxyanionic behaviour (Jegadeesan *et al.*, 2008a). It has been suggested that the likely mechanism controlling metal release is the partial dissolution of the acid-exchangeable fraction at an acidic pH, the desorption of oxyanions at an alkaline pH or the adsorption/co-precipitation of metals with iron (hydr)oxides (Jegadeesan *et al.*, 2008a). Furthermore, As and Se have been demonstrated to interact with a number of compounds, for example, with iron oxides such as magnetite and hematite under acidic conditions, with clay minerals such as mullite at neutral pH and with $CaCO_3$ or portlandite under alkaline conditions (Van Der Hoek *et al.*, 1994). Of these interactants, magnetite and hematite are the predominant iron-bearing minerals in unweathered fly ash, whilst lime is the most abundant Ca-phase (Van Der Hoek *et al.*, 1994, Jegadeesan *et al.*, 2008b).

Arsenic was found to be distributed primarily to the iron oxide fractions (51%, 82 mg/kg), the sulfidic/residual fractions (40%, or 64 mg/kg) and the labile arsenic fractions (total of aqueous, exchangeable, and carbonate fractions; 9%, 10.8mg/kg) (Jegadeesan *et al.*, 2008a). Once more, As was predominantly associated with iron minerals on coal fly ash samples when examined by X-ray absorption near-edge spectroscopy (Huggins *et al.*, 2007b, Zielinski *et al.*, 2007). Within the labile fractions, As appeared to be most closely associated with the carbonate fraction (9.7 mg/kg), which was suspected to be due to its presence with calcium arsenates (Jegadeesan *et al.*, 2008a). Furthermore, Jegadeesan *et al.*, suggest that the amouphous, crystalline iron oxide is likely the controlling influence behind As release and that the majority of metals were distributed in the residual and sulfidic fractions, where they would be unavailable for leaching (Jegadeesan *et al.*, 2008b).

A study investigating British fly ash determined that as pH increase from pH 4.6 to 9.3, the concentration of As also increased (El-Mogazi *et al*., 1988). When pH is increased to between pH ~4-10, As and Se leaching for acidic fly ash samples can be described by employing a simplified model of surface complexation with the iron oxides present in fly ash (Van Der Hoek *et al.*, 1994).

When under highly acidic conditions (pH 3), the X-ray absorption near-edge structure and extended X-ray absorption fine structure spectra of fly ash showed that 95% of arsenic is present as As(V), arsenate oxyanion and As in association with an assortment of ferric oxides/oxyhydroxides and iron sulphates. However, when under highly alkaline conditions (pH 12.7), the X-ray absorption near-edge structure and extended X-ray absorption fine structure spectra of fly ash suggest that As is primarily present as As(V) in calcium arsenate (Zielinski *et al.*, 2007).

As and Se concentrations increased within leachate over time, with long-term batch-leaching tests indicating that these oxyanion-forming trace elements resulted from the dissolution of glassy fly ash particles (Neupane and Donahoe, 2013). However, it was also found that although As and Se were released in the early-phases of column leaching and serial batch tests, their respective concentrations proceeded to decrease overtime (Neupane and Donahoe, 2013).

It has also been reported that As and Se leaching from acidic fly ash is not homogenous, rather it is once again under the influence of the particular properties of the fly ash, for example, conditions of combustion, elemental composition, pH and collection method (Otero-Rey *et al.*, 2005). This study also determined that from the disposed of coal fly ash, <20% of the total As and Se constituents underwent leaching under tested environmental conditions (Otero-Rey *et al.*, 2005). On the other hand, the use of a carbonate buffer solution (pH 10) to selectively extract these elements removed 49% of total As, whilst extraction with an $HCl–NH_2OH$

solution dissolved 79% of the total As by targeting amorphous, poorly crystalline iron oxides (Otero-Rey *et al.*, 2005, Zielinski *et al.*, 2007).

In summary, the total leachable mass and the adsorption constants of As and Se are the key parameters that must be addressed in order to determine their leachability from coal fly ash deposits (Su and Wang, 2011).

1.4 Aims and Scope of this Study

This project overall aim is determining the feasibility of applying selected tree barks to the biosorption of As(V) and Se(IV) from fly ash leachate prior to reutilisation or disposal of fly ash in landfills or detention lagoons.

This study was carried out to achieve three main objectives. The first was to experimentally determine the mobility of As(V) and Se(IV) in fly ash samples. The first section of Chapter 2 sought to describe the physical, chemical and morphological properties of three fly ash samples, two acidic and one alkaline. In Chapter 2, batch leaching tests will be employed to monitor the mobility of As(V) and Se(IV) from coal fly ash samples under varied pH, solid: liquid ratios, leaching times, and ash types.

The second objective of this research was to determine the possibility of using tree bark as a biosorbent to remove As(V) and Se(IV) from synthetic solutions. Chapter 3 sought to describe the physical, chemical and morphological properties of outer bark tissue derived from three different tree species including *Eucalyptus deanei* (Mountain Blue Gum), *Lophostemon confertus* (Brush Box) and especially *Melaleuca quinquenervia* (Paperbark). In Chapter 3, batch adsorption experiments will also be conducted to monitor the adsorption capacity of barks for As(V) from synthetic solutions under varied conditions such as pH, contact time, bark dosage, and the initial concentration of elements. We will also report in Chapter 4 results

obtained in batch adsorption experiments for determination the adsorption capacity of barks for Se(IV) from synthetic solutions under varied conditions such as pH, contact time, bark dosage, and the initial concentration of elements.

The third objective of this research was to experimentally test and evaluate the possibility of removing As and Se from fly ash leachate using selected bark species under optimum pH, contact time and bark dosage conditions. The latter sections of Chapter 3 are aimed at describing the biosorption of As(V) from highly concentrated leachate from each of the two acidic and one alkaline fly ash samples previously tested. The latter sections of Chapter 4 contain descriptions of the biosorption of Se(IV) from the fly ash sample leachates using selected bark species under optimum conditions.

Finally, Chapter 5 sought to conclude this project achievements.

Chapter 2

Leaching Properties of Fly Ash

2.1 Introduction

This project began by conducting a series of experiments that investigated arsenic and selenium leachability from three Class F fly ash samples including two acidic and one alkaline type. Prior to leachability testing, physical, chemical and morphological analyses of fly ash samples were performed. Batch leaching experiments were then performed to assess the role of pH, contact time and the solid-to-liquid ratio of the total concentration of As and Se in the fly ash leachate.

Therefore, the specific objectives of work reported in this chapter are:

- To determine targeted physical (pH, moisture%, BET surface area, and LOI%) and chemical properties (major and minor elements) of the fly ash samples and to characterise particulate morphology;
- To conduct individual batch leaching experiments on each fly ash sample to estimate the quantity of arsenate and selenite removed from fly ash leachates;
- To assess how changes in pH, exposure time, and dosage of fly ash influence As and Se leaching.

2.2 Experimental Method

In 2008, 2012 and 2013, Class F fly ash samples were collected from Mount Piper, Wallerawang and Vales Point coal power stations, located in central-west the state of New

South Wales, Australia. In this study, the corresponding fly ash samples collected from the three sites were referred to as MPFA, WWFA and VPFA. After collection, physical properties including pH measurement, moisture %, Brunauer-Emmett-Teller (BET) surface area were evaluated (Section 2.2.1). Prior to chemical analysis of fly ash samples, acid digestion and leaching experiments were performed (Section 2.2.2). Furthermore, chemical analysis including determination of major elements in fly ash samples (Section 2.2.3.1) using X-ray fluorescence (XRF), spectrometry, and minor elements in acid digested fly ash samples (Section 2.2.3.2) using induction coupled plasma mass spectrometry (ICP-MS) were conducted. Additionally, the total As and Se concentration in digested and leachate samples was determined (Section 2.2.3.3) using hydride generation atomic absorption spectroscopy (HG-AAS) due to availability of the instrument in Department of Chemistry and Biomolecular Science, and presenting highly reliable method for measuring As and Se species in µg/L solutions. Moreover, scanning electron microscopy with energy dispersive X-ray spectrometry (SEM-EDS) was carried out to study morphological and surface texture and for quantitative measurements of elements in fly ash particles (Section 2.2.3.4).

2.2.1 Physical Properties of Fly Ash

In our work, pH measurements were acquired using a Beckman pH meter with automated pH procedure based on a two-standard point calibration. To determine the pH of the fly ash samples, 5 g fly ash was added to 25 mL of Milli-Q water and stirred for 24 h according to EPA method 103 (NEPA, 1999).

To determine the moisture of the sample, 10 g of fly ash was placed in a 105°C oven for 24 h (Ward *et al.*, 2009). The dried fly ash samples were left to cool in a desiccator and then

weighed. This process was repeated until a stable dry weight (g) was obtained. Moisture % was then evaluated using Equation 2.1.

$$Moisture(\%) = \left(\frac{initial\,weight - final\,weight}{initial\,weight} \right) \times 100 \qquad \text{Equation 2.1}$$

The BET surface area, pore volume and pore size distribution of each fly ash samples were measured using a Micromeritics Tristar II Plus surface area and porosity analyser. All samples were degassed under vacuum for 12 h prior to analysis on a Micromeritic Smart VacPrep unit at Particle and Catalysis Research Group, The University of New South Wales, Sydney, Australia. The standard technique is based on determination of the surface area by N_2 adsorption technique. The BET model was also used to determine the specific surface area by applying the BET equation to the adsorption data.

To determine the loss on ignition (LOI), which represents unburned carbon in fly ash sample, the powdered sample was initially dried at 110 °C overnight. Then, approximately 1 g of the sample was placed in a weighed crucible, heated for 1 h at a minimum of 550°C, cooled in a desiccator and weighed again. The percentage difference between initial (pre-ignition) weight, W_i (g) and final (post-ignition) weight, W_f (g) is LOI (%) as expressed in Equation 2.2.

$$LOI(\%) = \left(\frac{W_i - W_f}{W_i} \right) \times 100 \qquad \text{Equation 2.2}$$

2.2.2 Analytical Procedures

In this work, preliminary acid digestion of fly ash samples was performed in Teflon beakers at 90-100°C. Briefly, 0.2 g of each fly ash sample was treated with 10 mL of aqua regia (1 volume

HNO_3 + 3 volume HCl), and 4 mL HF in a 100 mL polytetrafluoroethylene (Teflon) beaker. The beaker was covered with a watch glass and then heated to 90-100^oC for 1 h, followed by the addition of 5 mL of fresh aqua regia and this was heated for another hour at 90-100^oC. The digestion was then left to cool to room temperature before being treated with 6 g of H_3BO_3. The digested sample was then filtered through a Whatman Grade 1 filter and diluted to 100 mL with Milli-Q water in a volumetric flask. Finally, the solution was stored in a sealed 100 mL plastic bottle at 4°C.

Leaching tests were carried out in a batch mode (Ward *et al*., 2009). In brief, plastic beakers containing fly ash samples were stirred at 300 rpm using a magnetic stirrer at room temperature (23±2^oC) for a desired time. In this test, two dried fly ash samples of 14.5 g and 5 g of each were added to 50 mL leaching solutions at different pre- adjusted pH of 4, 7, and 10. This was performed to prepare two dissimilar concentrations; high concentrated 290 g/L with solid: liquid ratios of (1:3.5) and low concentrated 100 g/L with solid: liquid ratio of (1:10) fly ash. The pH of initial leaching solutions was adjusted to the required value by adding 0.01 M NaOH or 0.01 M HCl. All samples were then stirred using a magnet stirrer (300 rpm) at room temperature (23±2^oC) for either 1 h or 24 h. Following this, the samples were allowed to settle for 2 h prior to centrifugation for 10 min at 3,000 rpm. Next, the leachate supernatant was collected and 30 mL of each leachate sample was filtered separately using a 0.45 µm syringe filter. The final pH of these solutions was then measured. In the next step, 6 drops of concentrated HNO_3 (15.9 M) was added to the leachate sample to acidify the pH below pH 2, which was then stored in a sealed 100 mL plastic bottle at 4°C.

All chemical reagents employed in this study were of AR grade and were obtained from Sigma-Aldrich, Australia.

2.2.3 Instrumental Analysis

2.2.3.1 XRF

For chemical analysis (*i.e.*, major element analysis), XRF spectrometry was performed using a PANalytical Axios 1kW X-ray Fluorescence Spectrometer at the Department of Earth and Planetary Science, Macquarie University, Australia. The accuracy of element quantitation was assessed by comparing to an Australian reference coal ash material, ASRM 010-2, which prepared and evaluated by Australian Standards Committee MN-001, Coal and Coke. Prior to performing XRF spectrometry, glass discs or fused beads were prepared to give a homogenous representation of the sample free of mineral structures, which leads to more accurate analyses. In this respect, 10.00 g of 12:22 (lithium tetraborate: lithium metaborate) was well-mixed with 1.00 g of fly ash sample or standard in a platinum crucible using a wooden spoon. The crucible was then placed in a rocking furnace at 1,050 ˚C for 20 min. After heating, an ammonium iodide tablet was added and the sample re-heated in the furnace for a further 5 min. Then, the sample was removed from the furnace and poured into a platinum mould, forming discs that were 4 cm in diameter, and left to stand for 5 min. Once the glass had formed, the disc was removed from the mould, left to cool further, labelled and was ready for use.

2.2.3.2 ICP-MS

ICP-MS was employed for trace element analysis, which was performed using an Agilent quadrupole ICP-MS 7500cs at the Geochemical Analysis Unit, Macquarie University, Australia. The accuracy of element quantitation was again determined according to the same fly ash standard mentioned in Section 2.2.3.1.

Prior to ICP-MS, the samples were digested and diluted. For digestion purpose, 0.1g of fly ash sample was placed in a vial, and a few drops of 2% HNO_3 was added. Then, 2 mL of concentrated 30% HF and 2 mL of 15.9 M HNO_3 were added to the fly ash sample. After sealing the vials with lids, they were placed were heated on a hot plate to 130-140°C for 48 h. Vials were then left to cool for 30 mins. Uncovered vials were left to dry in a fume hood overnight at 100°C. To dissolve fluorides, 1 mL of 30% HF and 1 mL of $HClO_4$ were added to the sample, which was then sealed and heated on a hot plate overnight at 130°C. Then, uncovered samples were dried by heating to 200°C for 24 h. After cooling down, 2-3 mL of 6 M HCl was added to the sample. The vials were re-sealed and once more heated overnight to 130-150°C, and the uncovered sample was dried by heating to 150-170°C overnight. After cooling down to room temperature, the sample was treated with 6 M HNO_3 and left on the hot plate overnight at 130-150°C to be dried down to a paste.

For dilution purpose, the digested fly ash samples were rehydrated with 4-5 mL of 2% HNO_3 and 0.5% HF, transferred into 100 mL polypropylene bottle and filled with 2% HNO_3 and traces of HF until reaching 100 ± 1 g. Later, 20 µL of Li_6RhIn was spiked to 5 mL of the diluted sample in a 5 mL vial.

Rock powders were analysed in solution as an internal standard using an Agilent 7500 Series instrument. Instrument drift was corrected for using an internal standard containing ^6Li, Rh and In, while elemental concentrations were calibrated using an international U.S. Geochemical Reference Materials (BCR-2) and were blank corrected. Three international U.S. Geochemical Reference Materials (BCR-2, BIR-1, and BHVO-2) were processed in each batch of samples as a certified microanalytical reference material to validate element quantitation.

2.2.3.3 HG-AAS

A hydride generation atomic absorption spectrometer (AAS model GBC 908/909 and HG-3000) was the primary instrument employed for arsenic and selenium analysis from all leachates. A 10 mA As hollow cathode lamp at wavelength 193.7 nm and an 8 mA Se hollow cathode lamp at wavelength 196.0 nm were used. Additionally, an air-acetylene flame with an air flow rate of 14.0 L/min and fuel flow rate of 1.80 L/min was used in As analysis, and air flow rate of 10.0 L/min and fuel flow rate of 1.80 L/min in Se analysis.

For the hydride generation process, 500 mL of concentrated 37% HCl (~10.2 M), and 500 mL of 0.6% $NaBH_4$ were prepared according to HG-3000 manufacturer's instructions to react with the samples. Additionally, 50 mL of each As(V) standard solution (0, 5, 10, 20, 30, 40 and 50 ppb (µg/L)) and 50 mL of each Se(IV) standard solution (0, 5, 10, 20, 40, 80, and 100 ppb (µg/L)) were prepared.

Prior to undertaking HG-AAS, samples were pre-reduced in order to reduce As(V) to As(III) and Se(VI) to Se(IV). In this respect, according to HG-3000 manufacturer's instructions, arsenic reduction was performed by adding 0.5 mL of concentrated HCl and 1 mL of a mixture of 10% KI and 10% ascorbic acid to 5 mL of each sample, standard and blank. After 1 h, the sample was diluted to 10 mL and analysed within 24 h. Selenium reduction was also performed by adding 5 mL of concentrated (~10.2 M) HCl to 5 mL of each sample, standard and blank in plastic tubes, to yield a 50% v/v or 5 M solution. These were then sealed with a screw cap lid and heated to 70-80°C for 1 h. After heating, the samples were left to cool to room temperature. All samples and standards were then stored at 4°C until measured within 24 h.

2.2.3.4 SEM-EDS

A JEOL-JSM-6480 LA scanning electron microscope equipped with an EX-94300 SDD energy dispersive X-ray analyser (SEM-EDS) was employed for morphological and surface texture study of fly ash particles, and for quantitative measurements of several elements in fly ash samples. This method utilised a silicon drift detector for EDS analysis, which enables high count rates, high energy resolution and rapid data acquisition.

In this study, backscattered electron imaging and EDS were used to characterise the fly ash samples. Prior to SEM/EDS, all fly ash samples were heated overnight at 105°C, followed by evaporative carbon coating, which was performed using a QUORUM Q150T Sputter Coater/Turbo Evaporator at the Microscopy Unit, Macquarie University.

2.3 Results and Discussion

Work reported in this chapter is aimed, firstly, at determining some physical and chemical properties along with morphology of fly ash samples. Secondly, the quantity of As and Se, separately, in ash leachates were estimated. Finally, the effect of pH, contact time and dosage of fly ash were assessed on such leachabilities. We will achieve this by comparing the outcomes with literature information to draw conclusions.

2.3.1 General Properties of Fly Ash

In this work, we have determined the pH, moisture%, BET surface area, and LOI% of the three fly ash samples, MPFA, WWFA and VPFA. According to the results tabulated in Table 2.1, the MPFA and WWFA samples both were acidic kind of fly ash with pH 4.7 and 3.6, respectively, whilst the VPFA sample was an alkaline type with pH of 11.5.

The moisture of the fly ash samples appears to vary indirectly with pH in the order of MPFA>WWFA>VPFA. In terms of BET surface area and LOI, the fly ash samples follow the same order of WWFA>MPFA>VPFA, which is in agreement with previous studies (Wang *et al.*, 2005, Wang and Zhu, 2007, Luo *et al.*, 2011). LOI represents the quantity of unburned carbon in fly ash sample, which is correlated with surface area. Therefore, a greater surface area was observed with a higher LOI (Luo *et al.*, 2011).

Table 2.1 Fly ash sample pH, moisture (%), BET surface area (m^2/g) and LOI (%).

Fly ash sample	**pH**	**Moisture / %**	**BET Surface Area / m^2/g**	**LOI / %**
MPFA	4.7	10.5	0.73	2.05
WWFA	3.6	8.8	1.11	2.67
VPFA	11.5	0.4	0.53	1.24

We then sought to identify the major elements and their oxides that were present in these samples by XRF and the results are shown in Table 2.2. As a result of using black coal (bituminous and sub-bituminous coal) in selected power stations, more than 70 wt.% of the fly ash samples were expected to be comprised of SiO_2, Al_2O_3 and Fe_2O_3 (Neupane and Donahoe, 2013). Collectively, these three oxides composed 93.53% of MPFA, 91.82% of WWFA and 90.55% of VPFA, demonstrating their overwhelming majority within the particles. Moreover, CaO was found to compose <3 wt.% of tested fly ash samples. By these results, we can verify that all these samples were classified as Class F fly ashes. Interestingly, in acidic fly ash samples, a higher content of Fe_2O_3 and SiO_2 and a lower content of Al_2O_3, CaO and MgO were observed in MPFA in comparison to WWFA.

Following these data, minor or trace element analysis was performed on fly ash digestions, using ICP-MS. The results obtained are tabulated in Table 2.3. Notably, 3.44-7.45 mg/kg of arsenic were assessed in fly ash samples, in the order of MPFA > WWFA > VPFA, while the total selenium within the fly ash samples was estimated to be between 2.05-3.78 mg/kg, in the order of WWFA > MPFA > VPFA. The lowest arsenic and selenium contents detected in the VPFA sample could be explained by the alkaline nature of this fly ash sample.

According to Neupane, *et al.*, more than 50% of the total As and Se in fly ash are concentrated mainly in non-silicate material, while other minor and major elements, except Ca, are naturally related to silicates (Huggins *et al.*, 2007b). Thus, the total concentrations of major (excluding Ca), minor, and trace elements such as As and Se in the alkaline fly ash samples could be more than the amount removed by the digestion method (Neupane and Donahoe, 2013).

Moreover, the higher amount of As in MPFA may be related to the higher amount of Fe_2O_3 in this sample, while the highest Se in WWFA sample may be due to the higher amount of Al_2O_3 and CaO (Van Der Hoek *et al*., 1994, Iwashita *et al.*, 2005).

As mentioned previously in Chapter 1, section 1.3.4, the elemental composition of a given fly ash is highly variable, which is directly influenced by the properties of the source of the coal, pre-treatment processing, and the combustion conditions within the power plant (El-Mogazi *et al.*, 1988, Openshaw, 1992, Ahmaruzzaman, 2010). During combustion both As and Se are volatised, therefore, in addition to the original amount of these elements in coal, probably a major element such as Fe in bituminous fly ash or Ca in sub-bituminous fly ash can control the capture of these elements by fly ash (Huggins *et al.*, 2007b). Thus, it is not surprising if there is no particular correlation between minor and major elements in fly ash samples were found.

Table 2.2 Quantitative results (wt. %) of major element analysis of fly ash samples by XRF.

Fly ash samples	Major Oxide / wt.%												
	SiO_2	Al_2O_3	Fe_2O_3	MgO	CaO	Na_2O	Mn_3O_4	K_2O	P_2O_5	SO_3	TiO_2	SrO	BaO
MPFA	68.59 (0.10)	23.71 (0.16)	1.23 (0.24)	0.25 (0.59)	0.20 (1.04)	0.09 (1.11)	0.06 (0.95)	1.88 (0.39)	0.07 (1.97)	0.07 (1.47)	0.90 (0.50)	0.02 (2.50)	0.03 (1.54)
WWFA	64.26 (0.10)	27.00 (0.15)	0.56 (0.34)	0.30 (0.55)	0.34 (0.84)	0.15 (1.02)	0.03 (1.04)	2.66 (0.33)	0.07 (1.92)	0.32 (0.92)	1.11 (0.46)	0.03 (2.53)	0.03 (1.55)
VPFA	64.09 (0.10)	23.81 (0.16)	2.65 (0.17)	0.47 (0.49)	2.57 (0.33)	0.59 (0.70)	0.16 (0.81)	1.01 (0.52)	0.83 (0.63)	0.07 (1.48)	0.89 (0.51)	0.11 (2.12)	0.06 (1.47)

Measurement uncertainty presented as standard deviation relative % in parenthesis for 5 consecutive measurements

Table 2.3 Minor/trace element quantitation within fly ash samples (mg/kg dry basis) using ICP-MS.

Fly ash sample	Minor elements / mg/kg											
	Mg	V	Cr	Ni	Cu	Zn	As	Se	Ag	Cd	Ba	Pb
MPFA	846	70	12	28	38	83	7.5	3.6	1.3	1	140	45
WWFA	969	83	15	14	40	60	4.9	3.8	1.1	1	145	43
VPFA	1526	62	13	14	34	95	3.4	2.1	0.7	0	257	49

2.3.2 Fly Ash particle morphology is highly variable but follows some observable trends

Next, we sought to perform physical and chemical characterisation of fly ash samples using SEM with a backscattered electron imaging mode and EDS. Backscattered electron imaging provides grey-scale visual information wherein the intensity of colour depends on chemical phase of the sample. The greater the atomic number, the greater the number of backscattered electrons, resulting in a brighter particle being observed. For example, iron with atomic number 26, yields a brighter image in a particle than carbon with atomic number of 6 (Kutchko and Kim, 2006)

According to Kutchko and Kim (2006), the morphology of fly ash particle is related to both combustion temperature and the rate of cooling. During the combustion process, the inorganic mineral may become fluid or volatile or reacted with oxygen as a result of heat. During the cooling process, the fluid mineral might change to crystalline solids or spherical amorphous particles and/or a layer of condensed volatile mineral cover the surface of the particles.

Several scanning electron micrographs of selected fly ash particles are shown in Figure 2.1 and 2.2. As can be seen in Figure 2.1(a), (b) and (c), the majority of fly ash particles in all MPFA, WWFA and VPFA, respectively, show similar spherical shapes. Moreover, coal fly ash samples contain light-weight solids hollow spheres known as cenospheres (Figure 2.2a)), minerals such as quartz (Figure 2.2(b)), irregularly and cluster-shaped amorphous particles (Figure 2.2(c)), and magnetic particles (Figure 2.2(d)). Such morphologies are commonly observed features in scanning electron micrographs obtained in backscattered electron imaging mode. The formation of irregularly and cluster-shaped amorphous particles in Figure 2.2(c) may have resulted from ‘inter-particle contact’ or high cooling rate (Kutchko and Kim, 2006). Additionally, Figure 2.2(d) shows a rough surface on fly ash particle, which contained iron

crystals set in a matrix of amorphous alumina-silicate. This observation is in a good agreement with previous reports (Kutchko and Kim, 2006, Luo *et al.*, 2011, Blissett and Rowson, 2012).

According to the SEM results, the particles were found to exhibit ~1-100 μm in average diameters. Blissett and Rowson (2012) had previously mentioned that the larger particles were mostly made of the unburnt coal (char) components or the organic base material, while the finer particles were likely formed due to homogenous condensation (converting minerals to gas and condensing to form solid particles), destruction of the 'included mineral matters', and complex transformations of the 'excluded mineral matters' (Blissett and Rowson, 2012).

EDS analysis was then employed to determine the oxide form of the elements present on the surface of respective fly ash particles. The results presented in Table 2.4 indicate that the major elements in the fly ash samples were silicon, aluminium, iron, calcium and oxygen (in several compounds), which were consistent with the elemental compositions determined by XRF quantitative results (wt. %) for major element analysis in Table 2.2.

According to earlier studies, aluminium could be mainly associated with silicon in the form of alumino-silicate spheres, whereas iron primarily exists as iron oxide on the surface and inside of iron spheres (Kutchko and Kim, 2006). Potassium, magnesium, sodium, titanium, and sulfur were observed with the aluminium and silicon but in less significant amounts. Several trace elements including Ba (Mass % = 3.90% & 5.35%), Sr (0.35% & 0.48%), Ce (1.69% & 2.31%), Nb (1.79% & 2.46%) were identified in only a few samples and were undoubtedly linked with oxygen. In Kutchko and Kim's study, calcium was observed primarily with sulfur or with phosphorus; it was not observed associated with alumino-silicate in any of the samples of class F fly ash but in sub-bituminous Class C fly ash (Kutchko and Kim, 2006). The aluminium and silicon contents were found to vary from one sphere to another, along with the size of fly ash particles. The backscattered electron micrographs and their corresponding spectra of amorphous alumino-silicate spheres of selected fly ash samples are depicted in Figure 2.3. As

can be seen in Figure 2.3(a), (b), and (c), although the comparative amount of aluminium and silicon were varied in different sphere along with the size of fly ash particles, these two elements were the major constituents in fly ash samples. Nevertheless, in all three spectrums of fly ash samples in Figure 2.3, magnesium, potassium, calcium, titanium, and iron have moderately weak signal intensity, indicating a low abundance of these elements in the particles. These observations from stated spectra are consistent with the XRF results in Table 2.2.

In Figure 2.4, the backscattered electron micrographs and EDS spectra of the magnetic spheres of selected fly ash samples with particle size greater than 10 μm in diameter, are shown. The brighter spots in spectra indicates areas of greater iron content, whilst the darker spots are related to alumino-silicate. As can be realised in Figure 2.4(a), (b), and (c), in all selected fly ash samples, the iron spheres consisted of mostly iron oxide and different amount of silicon and aluminium. From the appearance of the spheres, it is unclear whether the iron oxide exists as surface condensation or is mixed with the alumino-silicate. However, the obtained spectrum of iron sphere of MPFA particle in high magnification (see Figure 2.5) showed that iron oxide formed an essential component of such fly ash particles. As can be seen in elemental spectra in Figure 2.5, the proportion of Fe, Si, and Al varied from one spot to another. For instance, in elemental spectra of the bright spot of 032, the quantity of iron is approximately twice the amount of silicon and three times of the amount of aluminium. In contrast, in darker spot of 034, the quantity of silicon is higher than that of iron.

Volatile elements such as As and Se, which enter the vapour phase through combustion, were expected to be detectable as discrete coatings on the surface of fly ash particles. However, SEM-EDS results failed to detect significant evidence for their presence in the fly ash samples. This was most likely due to the trace levels of arsenic and selenium (up to 10 ppm) in the samples, which were under detection limit of the instrument (3000 ppm).

In summary, regardless of the variety of fly ash samples, SEM-EDS analysis indicated that fly ashes display common morphological trends. Alumino-silicates were found to be amorphous particles, while iron-rich particles were observed as a mixture of iron oxide with alumino-silicate.

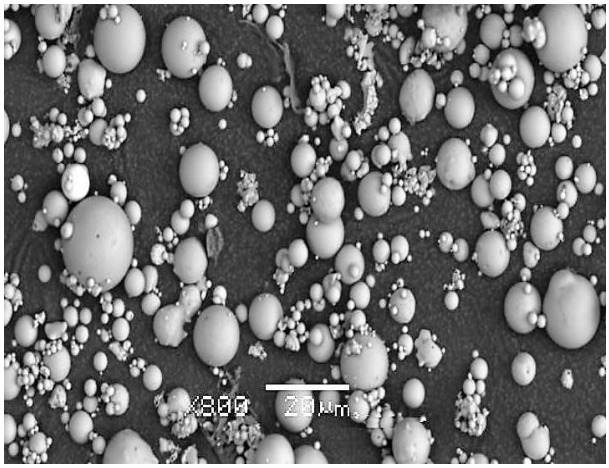

(a)

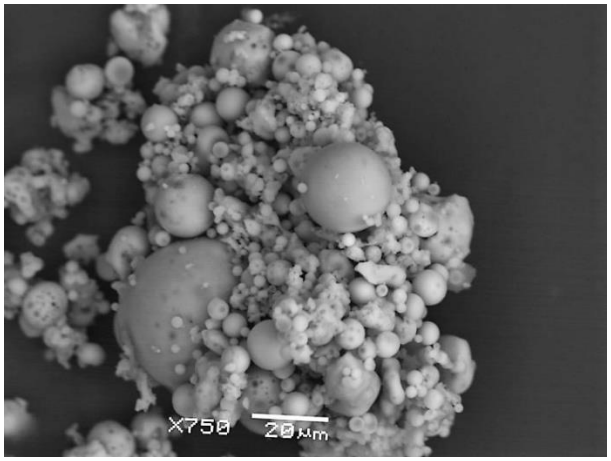

(b)

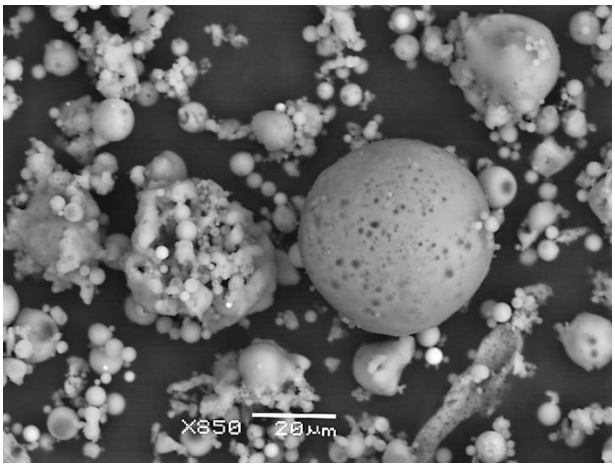

(c)

Figure 2.1 Backscattered electron micrographs of spherical fly ash particles from (a) MPFA, (b) WWFA and (c) VPFA.

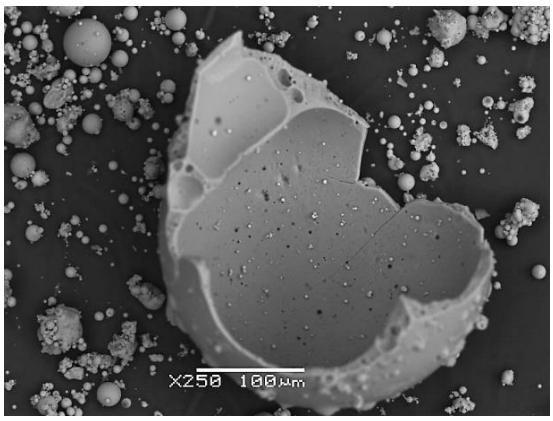

(a)

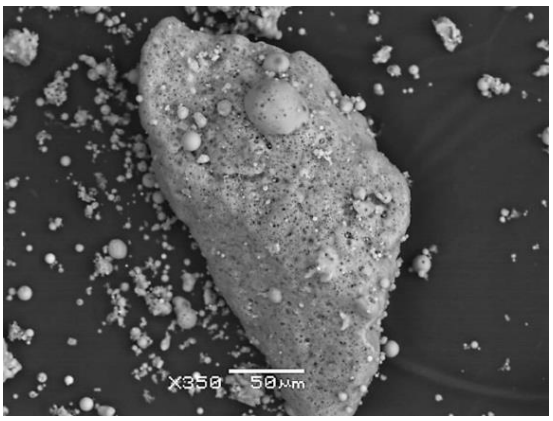

(b)

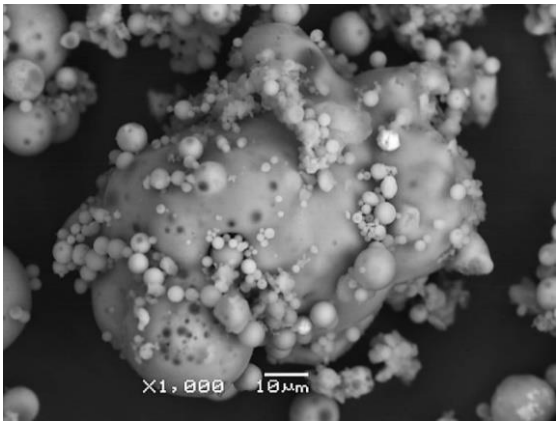

(c)

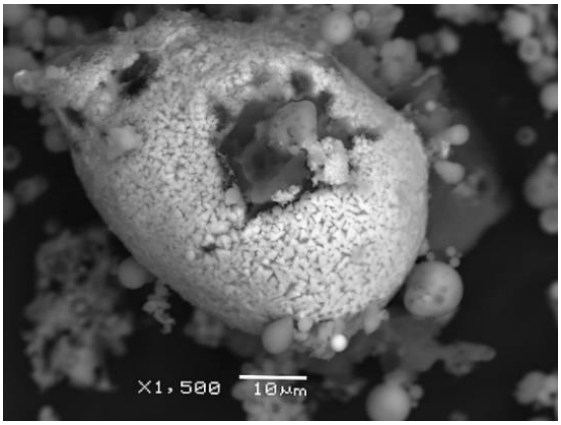

(d)

Figure 2.2 Representative backscattered electron micrographs of (a) hollow cenospheres observed within fly ash samples; (b) minerals observed within fly ash samples; (c) irregularly- and cluster-shaped amorphous particles observed within fly ash samples; (d) magnetic particles observed within fly ash samples.

Table 2.4 Major oxides present within fly ash samples, that have been determined from 3-5 spots for each EDS image. EDS results are presented as the mass % for each respective fly ash type.

	Major Oxides / mass%									
Fly ash sample	SiO_2	Al_2O_3	Fe_2O_3	CaO	MgO	MnO	Cr_2O_3	CuO	TiO_2	K_2O
MPFA	29.32 (12.4)	5.15 (0.1)	39.97 (16.1)	ND	ND	ND	ND	ND	0.38 (0.0)	0.67 (0.1)
WWFA	30.93 (5.3)	9.13 (1.1)	49.90 (4.0)	ND	ND	1.21 (0.9)	4.83 (0.1)	0.47 (0.0)	0.65 (0.3)	0.72 (0.1)
VPFA	23.44 (2.8)	5.24 (1.0)	42.85 (0.1)	1.52 (0.1)	4.99 (0.1)	1.74 (0.0)	ND	ND	0.74 (0.0)	0.27 (0.1)

ND denotes not detected; Measurement uncertainty presented as standard deviation in parenthesis for 2 consecutive measurements

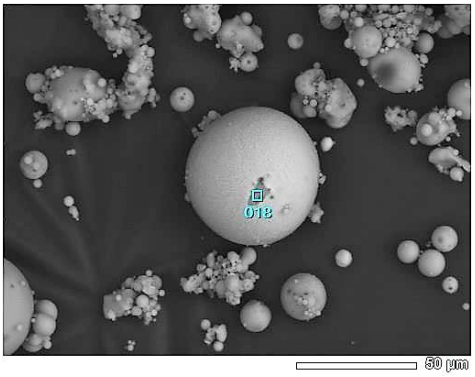

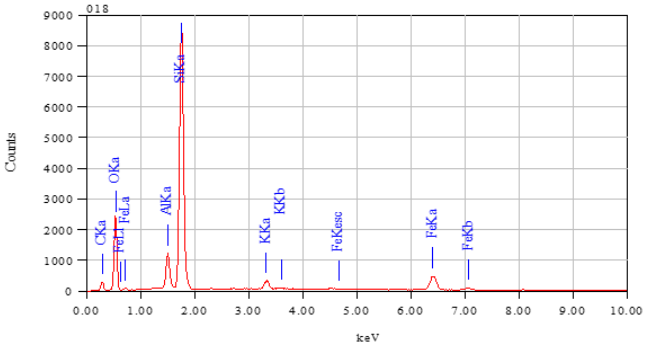

(a)

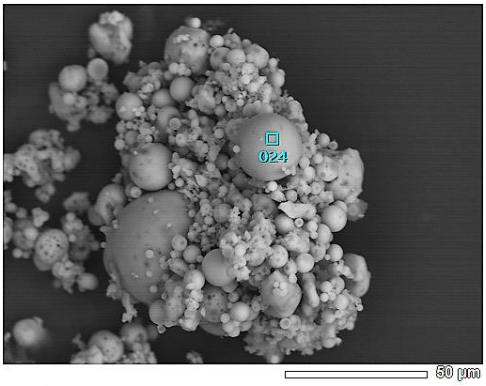

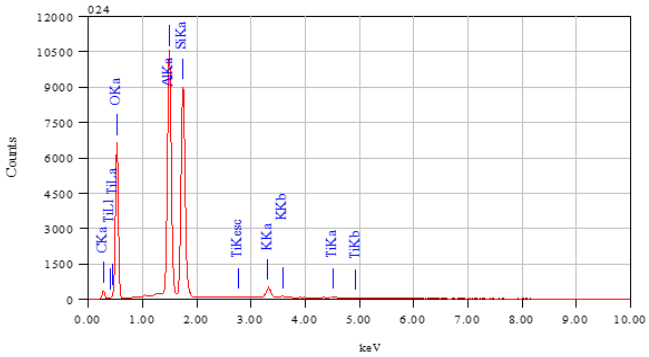

(b)

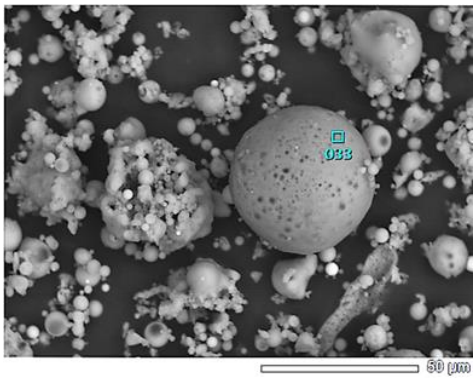

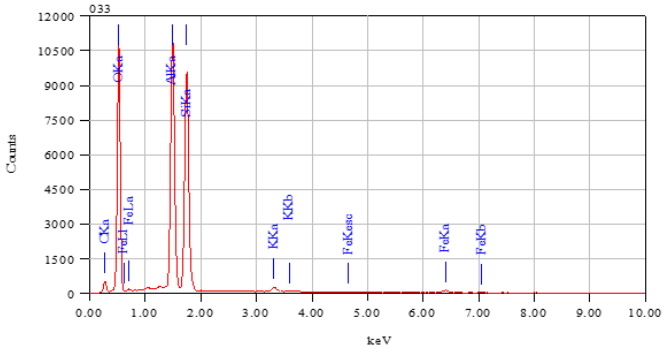

(c)

Figure 2.3 Backscattered electron micrographs with corresponding elemental spectra of (a) MPFA, (b) WWFA and (c) VPFA amorphous alumino-silicate spheres. These fly ash particles were found to differ in both size and in the amounts of elements such as Al, Si and O.

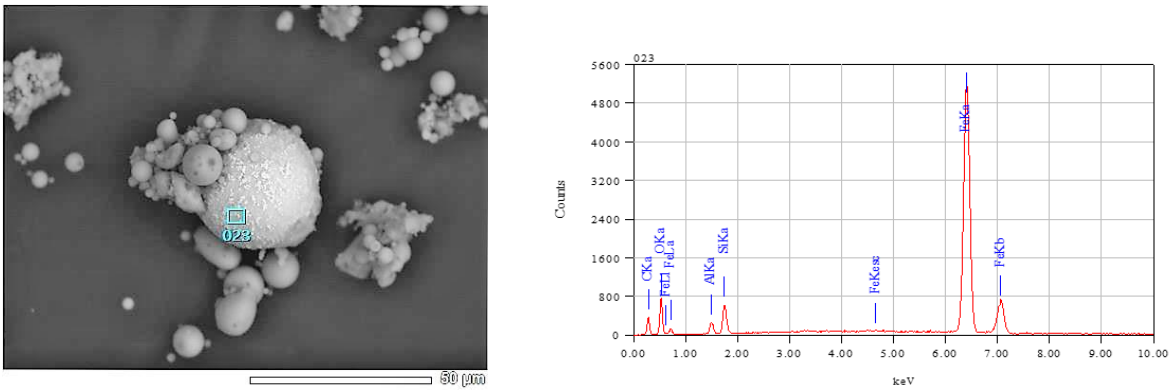

(a)

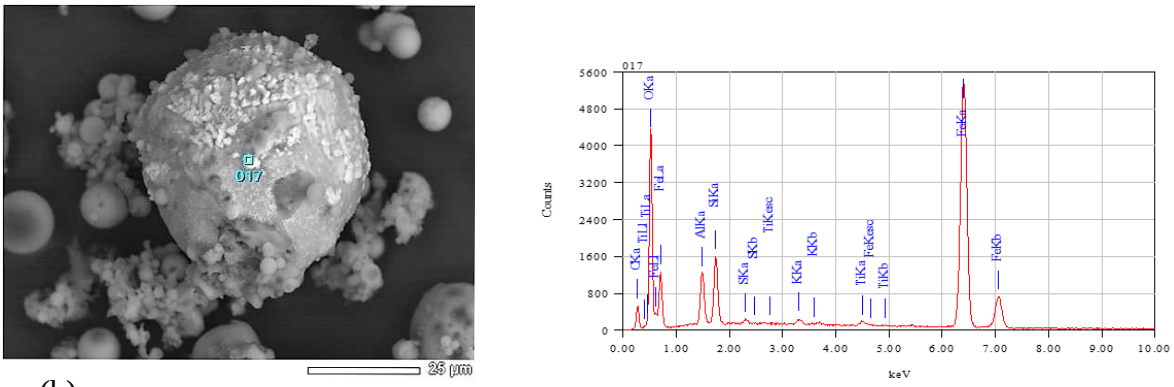

(b)

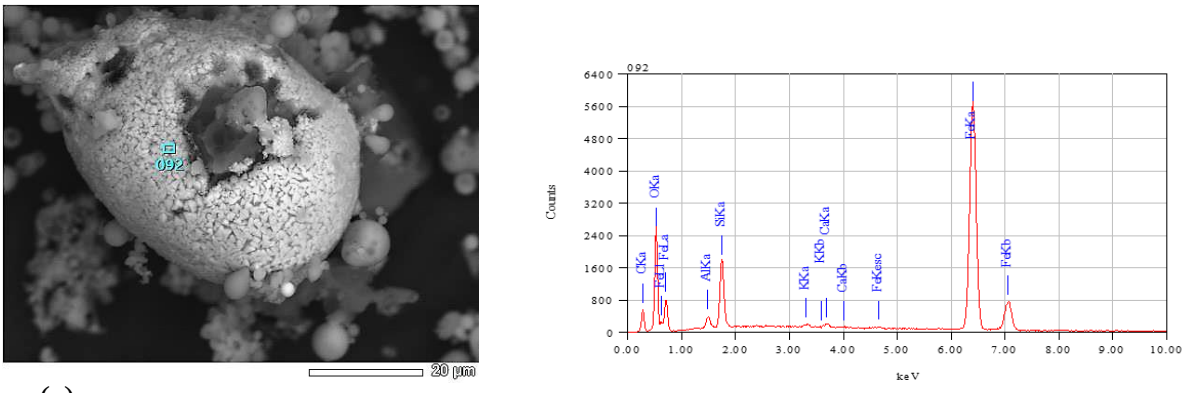

(c)

Figure 2.4 Backscattered electron micrographs with their corresponding elemental spectra of (a) MPFA, (b) WWFA and (c) VPFA fly ash samples; The darker area corresponds to the alumino-silicate phase; brighter areas are iron-rich phases.

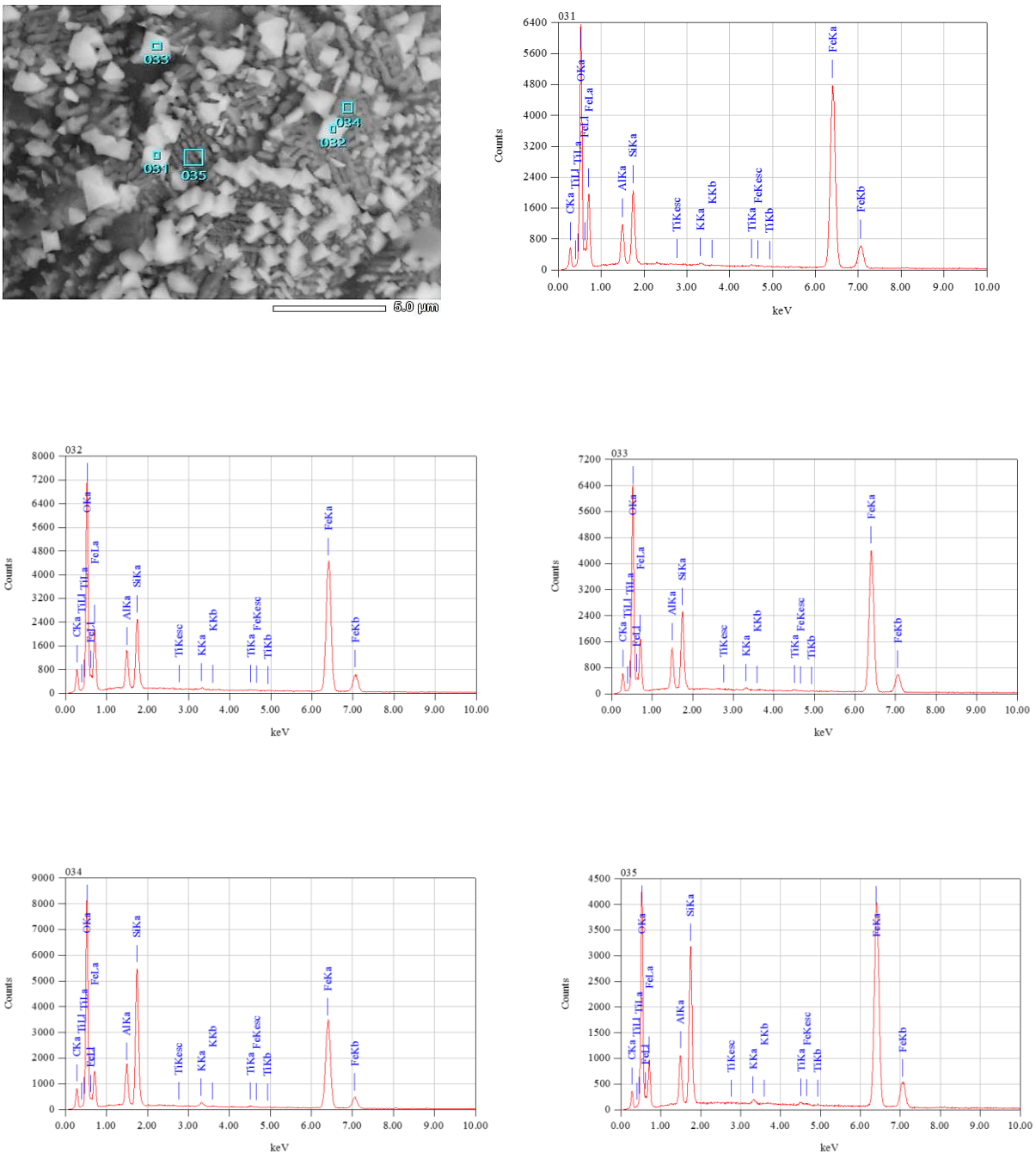

Figure 2.5 Backscattered electron micrographs with elemental spectra of a high magnification MPFA particle. These spectra demonstrate that the iron-rich phases are greater and brighter than the alumino-silicate phase.

2.3.3 Fly Ash leaching of As and Se

We have initially studied the role of initial solution pH used for leaching experiments on the final pH of fly ash leachate. More specifically, we focused on the effects of initial pH, contact time and solid: liquid ratio (S:L) on the mobility of As from fly ash. Then we have similarly assessed the impact of those variables on Se leaching from fly ash samples. These investigations were performed by batch leaching experiments in accordance with EPA procedure 1313 (USEPA, 2010). Finally, the respective maximum percentage removal of As and Se from the fly ash samples was evaluated as a mass unit of element (mg/kg) using Equation 2.3.

$$\text{Removal}(\%) = \left(\frac{\text{mass unit of element in leachate}}{\text{mass unit of element in digestion}} \right) \times 100 \qquad \text{Equation 2.3}$$

2.3.3.1 Fly Ash leachate demonstrates a strong pH buffering capacity

The results obtained in studying the initial pH and the final pH in fly ash leachates at two different S:L of 1:3.5 and 1:10 after 1 h and 24 h leaching time are shown in Table 2.5. According to the results in Table 2.5, at both S: L, compare to 1 h leaching, the acidic and neutral solutions produced leachates with the same or lower final pH values after leaching for 24 h, whereas the alkaline solution slightly increased the final pH. For example, at initial pH 4, the final pH value of MPFA at S: L of 1:3.5 decreased from 4.29 (1 h) to 4.27 (24 h), whilst at alkaline solution with pH 10, the final pH value of MPFA at the same S: L increased from 4.29 (1 h) to 4.33 (24 h). This observation may be due to the release of exchangeable ions attached to the clay minerals (Ward *et al.*, 2009). However, it was also found that at the lower S:L of 1:10, leachates of both acidic and alkaline fly ashes presented a wider pH range than the less dilute S:L of 1:3.5. Furthermore, the more dilute S:L (1:10) of the two acidic fly ashes,

MPFA and WWFA, resulted in higher final pH values than the 1:3.5 dilution for both leaching periods. On the other hand, the alkaline VPFA sample showed a general decrease in pH as a result of a greater S:L ratio. Interestingly, these results demonstrate that, regardless of the initial pH of the solutions used in leaching tests, the final pH values at both S:L are approximately the natural pH of the fly ash leachate after 1 h or 24 h. Those natural pH values were approximately 4.3 for MPFA, 3.8 for WWFA and 11.9 for VPFA. This indicates that the fly ash has a strong capacity for pH buffering and will tend to maintain its natural pH level regardless of the acidic or alkaline basis of the ash (Ward *et al.*, 2009).

Killingley *et al.*, determined that the initial pH of the ash-water system depends on the balance between the concentrations of Ca and Mg (alkaline-earth elements) in the ashes against the amount of SO_3 and P_2O_5 (potentially acid-generating) that are present (Killingley *et al.*, 2000). The data in Table 2.5 suggest that differences in the ratio of $CaO+MgO/SO_3+P_2O_5$ could be due to differences in each component, mainly SO_3 and CaO. In an acidic fly ash, the SO_3 level may be reduced due to removal of SO_4^{2-} ions from the surfaces of the ash particles following contact with water, therefore the final pH increased. However, in alkaline fly ash, the higher level of CaO in comparison to acidic samples may prevent the acid-generating effect of SO_3, thus decreasing the final pH (Ward *et al.*, 2009).

Table 2.5 Initial and final pH of fly ash samples following leaching at different S:L of 1:3.5 and 1:10 for 1 or 24 h.

Sample	Initial pH	Final leachate pH			
		1 h		24 h	
		S:L*=1:3.5	S:L=1:10	S:L=1:3.5	S:L=1:10
MPFA	4	4.29	4.37	4.27	4.39
	7	4.36	4.50	4.25	4.46
	10	4.29	4.54	4.33	4.66
WWFA	4	3.86	3.92	3.86	3.85
	7	3.88	3.99	3.82	3.95
	10	3.83	4.04	3.91	4.10
VPFA	4	11.97	11.52	11.68	11.52
	7	12.10	11.72	12.01	11.54
	10	11.98	11.64	12.06	11.78

*S:L is an abbreviation for solid: liquid ratio

Measurement uncertainty for all samples was (± 0.01)

2.3.3.2 Arsenic removal from fly ash leachate

In this section, we have initially determined the concentration of As (µg/L) in 50 mL of each fly ash leachate following a leaching experiment, which has been described earlier in section 2.2.2. Next, we have examined the relationship between initial pH and the concentration of As in fly ash leachate samples. As before, this experiment also tested for differences between S:L ratio of 1:3.5 and 1:10 after 1 or 24 h. The results, which are tabulated in Table 2.6, indicate that at a S:L of 1:10, As concentration in all leachates (except MPFA at pH 4) gradually decreases over time. Additionally, by decreasing the S:L from 1:3.5 to 1:10, the amount of As in all leachates (except WWFA) at all initial pH values moderately increased, regardless of contact

time. In this study, the initial pH of the leaching solution is a controlling factor in the leaching process. However, the pH was found to exert a variable effect on the concentration of soluble As in all cases tested. Furthermore, the concentrations of As in leachate from all fly ash samples appeared to be independent of the amount of As in the solid phase of fly ashes or their respective acidity/alkalinity.

Jankowski *et al.* (2006) have postulated that the majority of arsenic in fly ash may exist in a silicate matrix, with relatively lower levels linked with iron-rich phases or enriched on the fine particle surfaces (Jankowski *et al*., 2006). Thus, differences in particulate morphology and composition may explain the differences in As concentration between treatment conditions. Moreover, several researchers have stated that in acidic fly ashes, the iron-phase may be a significant factor in arsenate leaching process, while the Ca-phase may be a possible regulator in alkaline fly ashes (Van Der Hoek *et al.*, 1994, Huggins *et al.*, 2007b).

From the result in Table 2.6, when leaching at a S:L of 1:3.5 and 1 h, a greater concentration of As was released at a neutral pH for MPFA and VPFA. WWFA, on the other hand, showed the greatest As mobility under alkaline conditions at pH 10. Inspection of the data revealed a variable trend in As concentration with time in all fly ash leachates with initial pH values of 7 and 10, wherein the concentration of As gradually decreased over time. However, the acidic fly ashes MPFA and WWFA, arsenic mobility slightly increased at an initial pH of 4.

In terms of pH dependency in As mobility, Jegadeeson *et al.* (2008) suggested that, under acidic conditions (pH < 4), dissolution could be the main mechanism to mobilise As from fly ash, while desorption might occur at pH > 9, and adsorption and/or co-precipitation with iron (hydr)oxides potentially occurring at neutral pH (Jegadeesan *et al.*, 2008a). Additionally, several studies have indicated that maximum solubility of As as an oxyanion occurs in the pH range of 7-11 (Jankowski *et al.*, 2006, Izquierdo and Querol, 2012).

Table 2.6 Initial pH and concentration of As (µg/L) in fly ash leachates following leaching at S:L ratios of 1:10 and 1:3.5 for 1 or 24 h.

		As in 50 mL of fly ash leachate / µg/L					
Time / hr	Initial pH	MPFA 1:10	MPFA 1:3.5	WWFA 1:10	WWFA 1:3.5	VPFA 1:10	VPFA 1:3.5
1	4	21.4 (0.2)	4.4 (1.4)	40.1 (0.3)	74.0 (0.5)	21.0 (0.4)	13.4 (0.2)
	7	58.3 (0.1)	27.6 (0.1)	39.1 (0.1)	80.3 (0.1)	16.7 (1.1)	16.1 (0.2)
	10	35.4 (0.5)	12.7 (0.3)	32.8 (0.2)	81.8 (0.1)	21.4 (1.4)	15.8 (0.2)
24	4	37.3 (0.6)	8.1 (0.1)	23.5 (0.3)	81.4 (0.1)	15.4 (0.6)	6.4 (0.3)
	7	50.0 (0.1)	3.4 (0.4)	33.7 (0.2)	77.9 (0.2)	11.9 (0.3)	2.7 (0.2)
	10	23.4 (0.6)	7.2 (1.0)	31.5 (0.6)	77.0 (0.4)	13.8 (0.2)	6.0 (0.1)

Measurement uncertainty presented as standard deviation for 2 consecutive measurements

The most notable results from Table 2.6 indicated that by diluting the S:L from 1:3.5 to 1:10, the amount of As in all leachate (except WWFA) at all initial pH values moderately increased, independently of contact time. From earlier studies, it was suggested that As was mainly linked with amorphous and crystalline iron oxide (Jegadeesan *et al.*, 2008a). Therefore, a possible reason for higher amount of As observed in lower S:L could be that higher quantities of initial iron in MPFA and VPFA samples were released from fly ash at lower S:L of 1:10, and then oxidised and precipitated out of solution, thereby removing As from the leachate (Ward *et al.*, 2009).

Schwertmann and Taylor (1989) stated that a large surface area and pH dependency of surface charge (variable charge) are the most important properties of iron oxides, and adsorption of cations or anions can balance its surface charges (Schwertmann and Taylor, 1989). Additionally, the main geochemical mechanisms for controlling the solubility of trace metals in solutions are adsorption/desorption and co-precipitation of trace elements with iron (hydro)oxides, under various pH conditions (Sparks, 1995). Jegadeeson *et al.* (2008) indicated that, through the leaching process, As seemed to be associated with the precipitation of iron hydroxide and reported that the mobility of Fe and As was comparable in various pH solutions. At neutral pH, As co-precipitation with Fe may decrease its availability to undergo the leaching process. At a strongly alkaline pH, desorption might control arsenic mobility due to the weak association with iron (hydro)oxides because of the low attraction between the oxyanion and the surface of the iron mineral. Alternatively, at an acidic pH, a slight amount of Fe-carbonate was soluble whereas the iron oxide portions were persistent (Jegadeesan *et al.*, 2008a).

Supported by the information above, a potential explanation for different behavior of WWFA samples could be simplified by re-examining the results of XRF analysis (see Table 2.2). Here, WWFA was found to contain the lowest quantity of initial iron oxide (0.56 wt.%), which was nearly the half of that of iron observed in MPFA. Consequently, the lower mobilisation of As

that was observed in WWFA at a S:L of 1:10 may be due to the lowest quantities of iron that was simultaneously released from these samples. Moreover, the total amount of As leached from WWFA was higher than MPFA or VPFA. Iwashita *et al.*, stated that aluminum oxide, along with iron oxide, have a high capability for sorption of arsenate and selenite, and Ward *et al.*, have reported that the leaching solution with higher solid: liquid ratio included greater quantities of silicon and aluminium than less concentrated leachates (Iwashita *et al.*, 2005, Ward *et al.*, 2009). The results of XRF analysis showed that the amount of aluminum oxide in the WWFA sample was greater than that of the others. Therefore, with the leaching of greater amounts of Al, WWFA would be expected to show greater quantities of arsenic in its leachate than other fly ash samples, for both S:L of 1:3.5 1nd 1:10. However, the amount of As in more concentrated leachate was found to be higher than less concentrated ones. These results were also consistent with earlier reports by Ward *et al.* (Ward *et al.*, 2009).

In this study, the maximum percentage removal of As from fly ash samples were determined as 8.74% for MPFA, 9.01% for WWFA, and 6.24% for VPFA using data from leaching and digestion experiments and Equation 2.2. According to this result, essentially less than 10% of As may release from fly ash samples depends on our selected experimental conditions. Based on the annual amount of disposed fly ash (*i.e.*, approximately 7 Mt in Australia in 2010 (Heidrich *et al.*, 2013)), even this low amount of such a toxic element can cause environmental problems.

2.3.3.3 Selenium removal from fly ash leachate

In this section, at first, we have determined the amount of Se in 50 mL of each fly ash leachate following leaching experiment. The experimental procedure was as described in Section 2.2.2. Subsequently, we sought to examine the relationship between initial pH and the concentration

of Se in fly ash leachate samples. The obtained results are tabulated in Table 2.7. As before, this experiment also tested for differences between S:L ratios of 1:3.5 and 1:10 after 1 h and 24 h. As can be seen in Table 2.7, the amount of Se from the same ashes was found to be far lower in acidic fly ashes of MPFA and WWFA, relative to the alkaline VPFA sample, which conforms to the observations of previous studies (Ward *et al.*, 2003, Izquierdo and Querol, 2012).

According to Jankowski *et al.*, selenium primarily exists as silicates and oxyanions on fly ash surfaces, and whose concentrations are controlled by the pH of the leachates. Despite the lower levels of selenium in all fly ash samples, its concentration in leachates was found to be far higher, thus demonstrating that Se was more greatly mobilised than As, likely due to the lower availability of As for leaching (Van Der Hoek *et al.*, 1994, Jankowski *et al.*, 2006). Izquierdo and Querol reported that water (on its own) can remove 10–50% of Se from fly ash samples that have been collected from multiple countries. Additionally, according to Van Der Hoek *et al.*, at pH values between 4 and 10 in acidic fly ashes, "iron-phase" and in alkaline fly ashes "Ca-phase" were significant factors for both arsenate (AsO_4^{3-}, As(V)) and selenite (SeO_3^{2-}, Se(IV)) leaching processes. Previous studies have confirmed that selenium species in fly ashes and its leachates were mostly presented as selenite (Iwashita *et al.*, 2005, Luo *et al.*, 2011), therefore, alkaline fly ash with higher amounts of Ca in the leachate (especially at pH 10) could remove more selenite from the ashes.

Leaching at a S:L of 1:3.5 yielded the higher concentrations of Se release by initial pH 4 for MPFA, pH 7 for WWFA and pH 10 for VPFA after 24 h. Sample of VPFA showed the highest Se concentration (188 µg/L) at an alkaline pH. Interestingly, such behaviour from Se counters the discussion by Van Der Hoek *et al.*, who concluded that the highest amounts of Se could be leached at the pH opposite to the natural pH of the fly ash (Van Der Hoek *et al.*, 1994).

A possible reason for that behaviour might be presence of Se as oxyanions ($HSeO_3^-$ and SeO_3^{2-}) which would be less adsorbed by iron (hydr)oxides and aluminium oxides on the surface of ashes at alkaline pH, thus, Se could be more soluble (Izquierdo and Querol, 2012).

With more concentrated leachates, a variable trend in Se mobility with time was recognised. At all initial pH values, MPFA and VPFA leachates showed gradually increases in Se concentration over time may due to slow diffusion of interior of fly ash particles, while the mobility of Se from WWFA samples slightly decreased at all initial pHs due to the co-precipitation or adsorption on fly ash minerals (Neupane and Donahoe, 2013).

Greater Se mobility was observed at S:L of 1:10 following initial pH 10 for MPFA, pH 4 for WWFA and pH 7 for VPFA after 1 h. In all cases, the Se concentration from all initial pH increased steadily with time, with the exception of WWFA, which decreased. Iwashita *et al.* (2005) reported that iron oxide and aluminum oxide have a great adsorption capacity for selenite and arsenate which depends upon pH. Our XRF analysis (see Table 2.2) revealed that WWFA had the lowest amount of iron oxide, manganese oxide and silica but elevated amounts of aluminum oxide compared to MPFA and VPFA, and higher CaO than MPFA. Therefore, the higher Se concentration in WWFA leachate comparative to MPFA could be due to the greater amount of Al in WWFA fly ash and the possibility of more alumino-silicate within the leachate.

Table 2.7 Initial pH and concentration of Se (µg/L) in fly ash leachates following leaching at S:L of 1:10 and 1:3.5 for 1 h or 24 h.

		Se in 50 mL leachate / µg/L					
Time / hr	Initial pH	MPFA 1:10	MPFA 1:3.5	WWFA 1:10	WWFA 1:3.5	VPFA 1:10	VPFA 1:3.5
1	4	4.5 (0.1)	14.3 (0.1)	21.7 (0.2)	42.5 (0.1)	58.6 (0.1)	118.0 (0.1)
	7	6.9 (0.2)	15.0 (0.1)	20.4 (0.1)	42.5 (0.1)	76.7 (0.1)	132.6 (0.0)
	10	8.2 (0.3)	14.0 (0.1)	16.9 (0.1)	39.3 (0.1)	68.6 (0.1)	137.5 (0.0)
24	4	12.3 (0.3)	19.9 (0.2)	19.8 (0.2)	36.0 (0.1)	100.0 (0.0)	168.8 (0.0)
	7	8.2 (0.1)	17.8 (0.2)	17.1 (0.2)	40.2 (0.1)	99.1 (0.0)	165.8 (0.0)
	10	9.5 (0.2)	18.1 (0.3)	15.9 (0.1)	39.3 (0.1)	112.2 (0.0)	188.2 (0.0)

Measurement uncertainty presented as standard deviation in parenthesis for 2 replicate measurements

The results from Table 2.7 indicate that by decreasing the S:L ratio from 1:3.5 to 1:10, the amount of Se in all leachates at all initial pH moderately decreased to almost half of the amount, independent of contact time. These observations are consistent with the previous studies by Ward *et al.*, who determined that the leaching solution with S:L of 1: 3.5 included higher quantities of silicon and aluminium than less concentrated leachates, whilst the highest quantities of iron and manganese were observed in leachate from fresh fly ash with lower S:L ratio of 1:20 (Ward *et al.*, 2009). Another assumption by Ward *et al.* was related to the pH dependency of Al and Mn leaching behaviour, at pH >4.5. They found that the mobility of Al was limited in some ash resources and the lowest Al concentration observed at alkaline leachate with pH 7.5-8.7 (Ward *et al.*, 2009). Likewise, manganese followed such behaviour, for example, at acidic pH (reducing conditions) manganese was more mobilised than alkaline pH (oxidising conditions), in which Mn was more likely to precipitate. In addition, similar to iron oxides, manganese oxides could have a high sorption capacity for trace metals (Ward *et al.*, 2009).

The maximum percentage removal of Se from studied fly ash samples was estimated using data from leaching (Table 2.7) and digestion (Table 2.3) experiments and Equation 2.2.

Interestingly, the alkaline fly ash samples of VPFA was released up to 54.5% of its initial Se, whilst two acidic fly ash samples were released less than 10% of their preliminary Se (3.1% from MPFA, 5.2% from WWFA). As discussed earlier in this section, the alkaline fly ash with higher amounts of Ca in the leachate (especially at pH 10) could remove more selenite from the ashes in compare with acidic ones because of the correlation between Ca and Se (Ward *et al.*, 2003, Iwashita *et al.*, 2005).

2.4 Conclusion

Three class F fly ash samples including two acidic and one alkaline samples have been assessed to characterise their physical, chemical and morphological properties. In addition, this study performed an array of leaching experiments under several conditions (pH, S:L ratio, and contact time) to determine the As and Se content that was present in fly ash leachates.

This study yielded a number of valuable insights. Firstly, SiO_2, Al_2O_3 and Fe_2O_3 were found to comprise more than 70 wt % of fly ash particles, whilst the percentage of CaO was less than 3 wt.% in all fly ash samples. These results also confirmed that the samples were correctly categorised as class F fly ashes. Acidic fly ashes were found to contain the highest levels of both As (4.9-7.5 mg/kg) and Se (3.6- 3.8 mg/kg) while low levels (3.4 mg/kg As, and 2.1 mg/kg Se) were detected in alkaline fly ash. These fly ash particles varied in size, morphology and elemental composition. Leaching experiments determined that fly ashes had a strong buffering capacity and that the initial pH had a major but variable effect in As and Se mobility. High solubilities of As and Se were found mostly at a pH of 7 and 10, however the concentrations of As and Se were independent of their original level in the solid fly ashes. The higher mobility of As was observed at a lower S:L ratio of 1: 10, while the Se level moderately decreased down to the half in some cases. In agreement with previous studies, during the early stage of leaching, As and Se were quickly removed from enriched smaller particles with greater surface areas. However, the mobility of these element diminished with time, which may be due to sorption and/or co-precipitation of elements 'back into' the solid phase.

Despite the low As and Se levels in the studied fly ash sample leachates, the re-utilisation, and disposal or storage of massive quantity of fly ash in landfills or ponds may raise environmental issues related to the releasing toxic elements, especially As and Se. Therefore, it is crucial to reduce the amount of such toxic elements in fly ashes before reusing or even disposing them.

For this reason, biosorption of As and Se was considered to be a probable option for lowering the levels of these elements in fly ash leachate.

In the next two chapters, we have examined the possibility of using several tree bark species for biosorption of As(V), and then Se(IV), from synthetic solutions and leachates of fly ash samples.

Chapter 3

Evaluation of Tree Barks as a Biosorbent for As(V)

3.1 Introduction

A series of adsorption experiments was conducted on a range of tree barks in order to assess the significance of bark-type, pH, time, biosorption dosage, and arsenic concentration on arsenate adsorption to bark surfaces. The outer barks of different species were collected on-site from the Macquarie University campus (North Ryde, NSW, Australia) and examined to determine suitability for the adsorption study. The relative concentrations of all elements were determined using inductively coupled plasma-mass spectrometry (ICP-MS), except As, which was analysed by hydride generation atomic adsorption spectrophotometry (HG-AAS).

The objectives of this study are:

- to determine the extent of any potential adsorptive competition for As between barks. Specifically, this study will compare the adsorption capacities of As(V) on bark in a single-species system.
- to assess how changes in pH, time, bark dosage and elemental concentration influence biosorption in isothermal and kinetic experiments.

- to quantitatively determine As that can be removed from As(V)-loaded bark samples to regenerate bark.
- to investigate the utility of tree bark as an As biosorbent from fly ash leachate samples.

3.2 Experimental Method

As biosorption experiments were performed in two stages as shown in the two flow charts in Figure. 3.1 and Figure. 3.2. During the first stage (Figure. 3.1), two different Eucalyptus species, *Eucalyptus deanei* (*Ed*; Mountain Blue Gum) and *Eucalyptus amplifolia* (*Ea*; Cabbage Gum) bark, were chosen for use in determining the initial As concentration in bark, and quantitatively examining As removable from bark using Milli-Q. During the second stage (Figure. 3.2), *Eucalyptus deanei (Ed; Mountain Blue Gum), Lophostemon confertus (Lc; Brush Box) and Melaleuca quinquenervia (Mq; Paperbark)* barks were used (i) to quantitatively estimate As in bark before and after sorption, (ii) to compare selected physical and chemical properties of bark before and after As sorption, (iii) to determine the optimum conditions for As sorption for each kind of bark, and (iv) to examine the possibility of reusing As-loaded bark after removing the loaded As.

3.2.1 Biosorbents Collection and Preparation

The outer bark samples were collected from the campus grounds of Macquarie University (Sydney, NSW, Australia). Initially, *Ed* and *Ea* were used. As illustrated by the photographs in Figure. 3.3, the thick outer bark (rhytidome), which contains no living cells, cracks and peels away from the trunk in these tree species as a result of normal growth (Sakai, 2000). It should be noted that these trees grow next to a small, infrequently-used campus road.

Collected bark samples were washed several times with both tap and distilled water before being cut into small pieces and dried at room temperature for 7 days. Dried barks were

pulverised and sieved to obtain a particle size between 150 - 710 μm for use in adsorption experiments. Ground biomass samples were stored in sealed plastic bags until use in order to protect against contamination or moisture.

As depicted in Figure. 3.1, in addition to the use of raw bark, these barks were also subjected to several treatments prior to adsorption experiments. These pre-treatment methods included boiling, formaldehyde treatment and iron coating.

A boiling method reported by Palma *et al.* (Palma *et al.*, 2003) was adopted. Briefly, 7 g bark was added to 300 mL of Milli-Q water and boiled for 20 min prior to filtration of the solution by the decanting method. This process was repeated 6 times until the solution became clear. This treatment method enables the separation of all soluble organic compounds (*e.g.*, tannins) from the bark samples. Treated bark was then filtered and washed several times with Milli-Q water, before being dried overnight in an oven at 105°C, and stored in sealed plastic bags. In Palma *et al.*'s formaldehyde treatment method, after adding 10 g bark to 150 mL of 3% HNO_3 and 250 μL of 36% formaldehyde, the mixture was stirred in an 80°C water bath for 30 min. This process was aimed immobilising phenolic polymers in the bark, yielding a clear solution during adsorption tests. Treated bark samples were filtered with a Whatman #1 filter paper before being washed several times with Milli-Q water, desiccated overnight in a 50°C oven (18 h), and stored in sealed plastic bags.

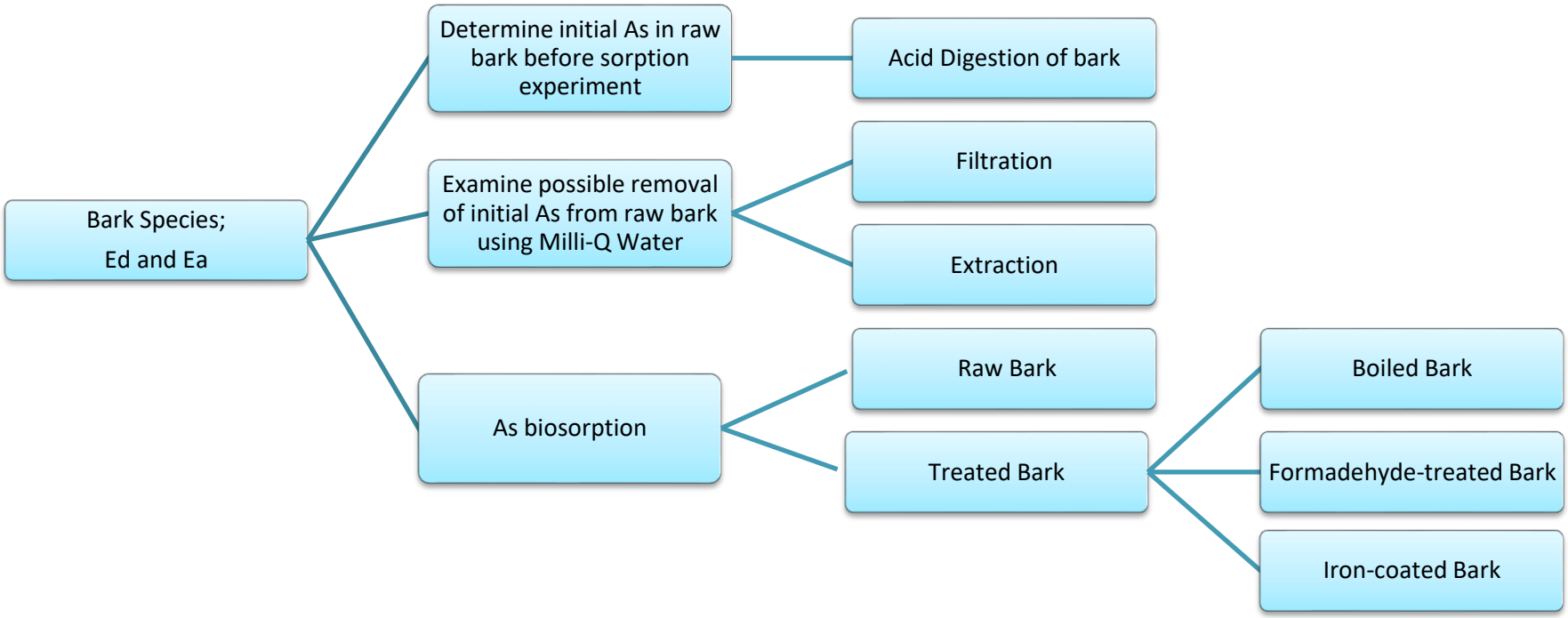

Figure. 3.1 First stage of current study

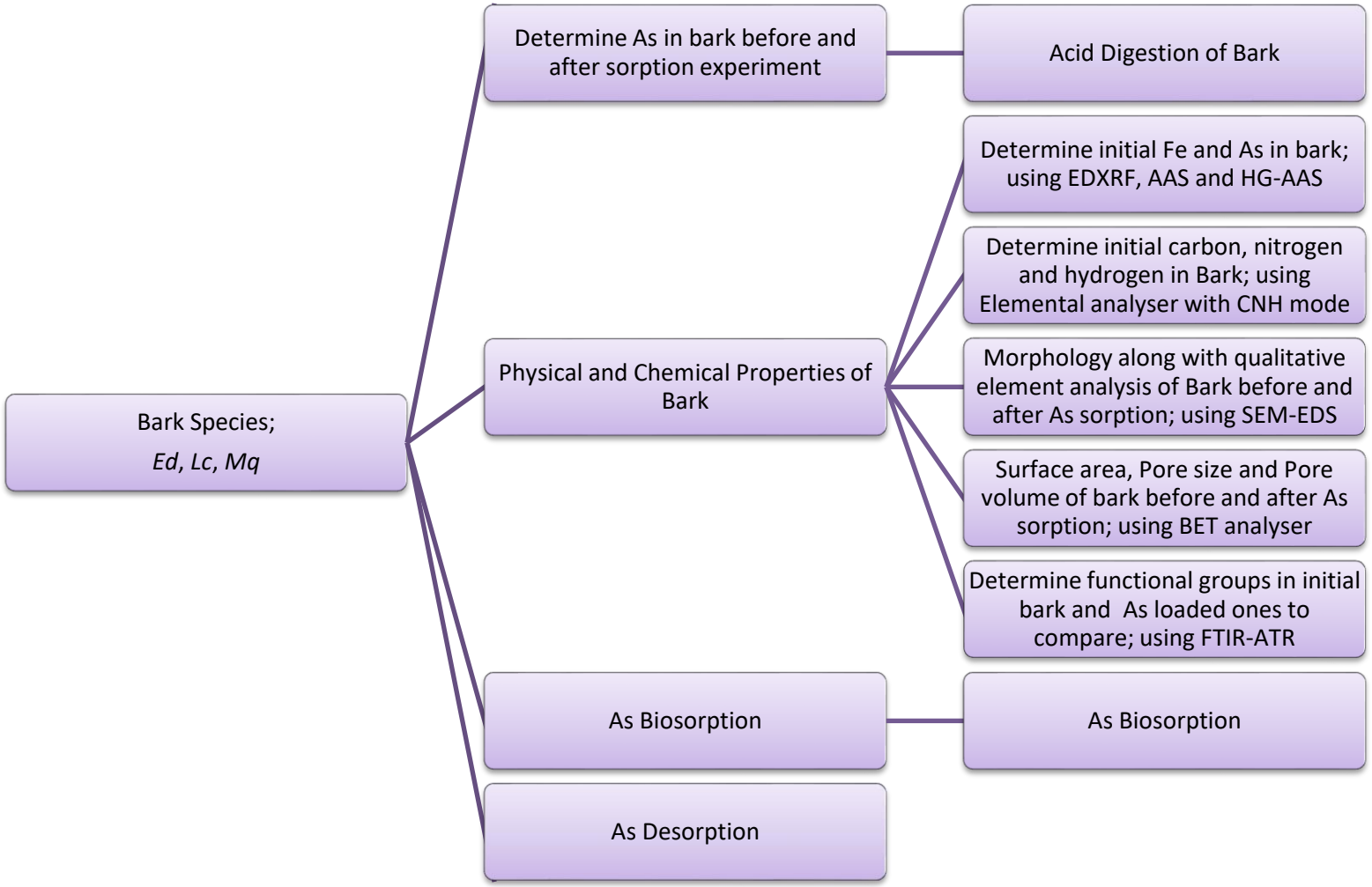

Figure. 3.2 Second stage of current study

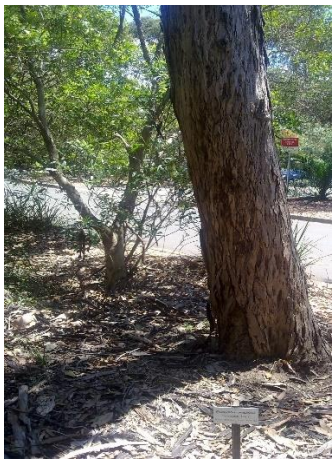

Figure. 3.3 Left: *Eucalyptus amplifolia* (*Ea*; Cabbage Gum), Right: *Eucalyptus deanei* (*Ed*; Mountain Blue Gum).

Based upon the iron-coating methods of sand (Lo and Chen, 1997, Thirunavukkarasu *et al.*, 2003) and eggshells (N. Yeddou Mezenner and Bensmaili, 2009, Rais Ahmad *et al.*, 2012), iron coating of bark samples was performed upon raw, boiled and formaldehyde-treated barks from both Eucalyptus species. In brief, 2 g of bark preparation was added to 10 mL of a 0.5 M ferric nitrate solution. Then, 7 mL of 3 M NaOH solution was added drop-wise to precipitate iron (hydr)oxide on the bark surface. Bark samples were then stirred at 300 rpm for 90 min at room temperature using a magnetic stirrer, then filtered, washed 10 times with Milli-Q water until the pH returned to pH 8-9, then dried overnight (18 h) at 100°C (Rais Ahmad *et al.*, 2012).

As it shown in Figure. 3.2, during the second stage of experiment, *Ed*, *Lc* and *Mq* barks (Figure. 3.4) were collected from campus grounds of Macquarie University, Sydney, NSW, Australia. After washing with tap and distilled water, bark samples were dried at room temperature for 7 days. Bark samples were then pulverised, sieved to a particle size of between 150 - 710 μm and stored in sealed plastic bags.

Figure. 3.4 Left to right: *Eucalyptus deanei* (*Ed*; Mountain Blue Gum), *Lophostemon confertus* (*Lc*; Brush Box) and *Melaleuca quinquenervia* (*Mq*; Paperbark).

3.2.2 Physical and Chemical Properties of Biosorbents

Physical properties such as size, surface area, pore size and morphology of unloaded or As-loaded bark were determined using sieves with defined mesh numbers, Brunauer-Emmett-Teller (BET) surface area analysis and scanning electron microscopy coupled with energy dispersive spectrometry (SEM-EDS). Meanwhile, elemental analysis of bark samples was performed using energy dispersive X-ray fluorescence (EDXRF), an elemental analyser in a carbon, nitrogen and hydrogen (CNH) mode, and atomic adsorption spectroscopy (AAS) with a hydride generation accessory (HG-AAS) for As determination. In addition, Fourier-transform infrared spectroscopy with attenuated total reflectance (FTIR-ATR) was used for identifying basic functional groups in the bark samples. Most of these instruments were explained in Section 2.2.3, Chapter 2. An outline will be given in Section 3.2.2.1 – 3.2.2.5.

3.2.2.1 BET Surface Area Analysis

As stated previously, the desired particle size between 150 - 710 μm was achieved using sieves with mesh numbers of 100 and 25, respectively. The BET surface area and pore size distribution of each kind of bark was measured using a Micromeritics Tristar II Plus Surface Area and Porosity Analyser. In brief, the samples were degassed under vacuum for 12 h prior to analysis on a Micromeritic Smart VacPrep unit in the Particles and Catalysis Research Group at University of New South Wales, Sydney, Australia. Surface area determination was achieved using the N_2 physisorption method. The BET model was used to determine the specific surface area and the Barrett-Joyner-Halenda (BJH) model was used to determine the pore size distribution.

3.2.2.2 Scanning Electron Microscopy with Energy Dispersive X-ray Microanalysis (SEM-EDS)

A JEOL-JSM-6480 LA scanning electron microscope equipped with EX-94300 SDD energy dispersive X-ray spectrometer (SEM-EDS) within the Microscopy Unit, Macquarie University, was employed for morphological observation, characterisation of particle surface texture and quantitative measurement of several elements within bark samples. Before and after biosorption, all bark samples (*Ed*, *Lc* and *Mq*) were coated by an evaporative coating using a QUORUM Q150T sputter coater/turbo evaporator and dried at 105°C overnight prior to SEM/EDS. SEM-EDS employed an accelerating voltage of 15-25 kV. EDS analyses were conducted on 5-10 points for each sample to obtain a more representative characterisation for the general structure of bark surface.

3.2.2.3 EDXRF and CNH Analysis

The major and minor elements (Fe, Cu, Ca, Zn, Mn, As and Se in their oxide forms) within bark samples were determined using Omnian software as part of the EDXRF experiment. Ease of use and sufficient estimation of quantities of elements were the important reasos to choose EDXRF analysis. The percentage of elements such as carbon, nitrogen and hydrogen within bark samples were determined using an Elemental Analyser, Model PE2400 CHNS/O (PerkinElmer, Shelton, CT, USA) with a PC-based data system, PE Data manager 2400 and a PerkinElmer AD-6 Ultra Micro Balance.

3.2.2.4 Hydride Generation Atomic Absorption Spectroscopy (HG-AAS)

All arsenic analyses were performed using a 932/933 atomic adsorption spectrophotometer, equipped with an HG3000 atomic hydride generator (GBC Scientific Equipment Pty Ltd, Victoria, Australia). An arsenic hollow cathode lamp from Photron Pty. Ltd. was employed as a radiation source (operated at 10 mA). The flame type was air/acetylene with the air flow rate 14.0 L/min and fuel flow rate 1.80 L/min. The analytical range of HG-AAS for these As experiments was 5 to 50 ppb at a 193.7 nm wavelength. For the determination of As(V), As(V) was pre-reduced to As(III) using 2 mL of concentrated HCl added to 5 mL of each sample, blank and standards along with 0.5 mL of a 10% solution of mixture of KI and ascorbic acid (HG-3000-GBC manual). Samples were mixed properly and left for 2 h to allow the complete reduction of all arsenate to arsenite. Finally, all samples, blanks and standards were passed through the hydride unit containing a 0.6% sodium borohydride solution and concentrated HCl. As mentioned in Section 3.2.2.5, hydride formation occurs when As(III) in an acidic solution reacts with $NaBH_4$ according to the following reaction:

$$3NaBH_4 + 4H_3AsO_3 \rightarrow 4AsH_3(g) + 3H_3BO_3 + 3NaOH$$

Arsenate, As(V), from arsenic acid (H_3AsO_4), is presented as $H_2AsO_4^-$ and $HAsO_4^{2-}$ and AsO_4^{3-} with $pKa_1 = 2.25$ and $pKa_2 = 6.83$, and $pKa_3 = 11.52$ (Wolthers Mariette *et al.*, 2005, Lizama *et al.*, 2011)

3.2.2.5 Fourier Transform Infrared Spectroscopy with Attenuated Total Reflectance (FTIR-ATR)

To identify the major functional groups within chosen barks, FTIR-ATR at the 4000 – 400 cm^{-1} and 1850-1550 cm^{-1} wavenumbers range was performed directly on the samples prior to and following biosorption using a Thermo Scientific iD5 ATR, Nicolet iS5 with Omnic software. This spectroscopic analysis was used to study the nature of cell–As ion interactions. All selected barks were oven dried at 105°C overnight and desiccated prior to spectroscopy.

3.2.3 Analytical Procedures: Acid Digestion and Water Base Extraction

Acid digestion and water based extraction procedures were performed on selected barks to determine the initial amounts of As and/or Fe contained within the respective barks.

Based on an open-vessel digestion method reported by Rodushkin, *et al*., bark digestion was performed by adding 10 mL of concentrated HNO_3 to 1 g of dried bark sample with a middle range of particle size between 150 - 710 µm in a Teflon beaker (Rodushkin *et al.*, 1999). It was found that particle size smaller than 150-710 µm generated sludge that would have made the filtration process very time consuming. The beaker was covered with a watch glass and left to cold soak for 30 min at room temperature. The sample was then heated on a hot plate at 120°C for 2 h. After cooling to room temperature, the digested sample was diluted to 100 mL with Milli-Q water, and stored in a sealed plastic bottle at 4°C. If there was any apparent residue, the

digested sample was centrifuged at 4,000 rpm for 5 min, and the supernatant was aspirated into a sealed plastic bottle (Rodushkin *et al.*, 1999).

Two procedures were employed for bark water based extraction. Firstly, a batch experiment where 20 g of either *Ed* and *Ea* bark was separately added to 200 mL of Milli-Q water (S:L = 1: 10) in a 500-mL beaker. The beaker was sealed and agitated on a magnetic stirrer at 200 rpm for 1 h at 23±2°C (Pandey *et al.*, 2009). Then, the solution was separated from the bark by filtration using Whatman#1 filter paper, and stored at 4°C.

To determine the effect of pH in the removal of As from biosorbent bark, all batch extractions were performed under the same conditions as above but at three different pH conditions (4, 7, and 10). The solutions were prepared using Milli-Q water with subsequent addition of 0.1 M NaOH or 0.1 M HCl in order to adjust to the desired pH using a Beckman pH meter, USA. All beakers were then sealed and agitated on a magnetic stirrer at 300 rpm for one hour at room temperature (23±2°C). Samples were filtered through a Whatman#2 filter paper and the filtrates stored at 4°C.

The second bark extraction method, utilised a Soxhlet apparatus. In this method, 15 g of either *Ed* or *Ea* bark was placed into a thimble undergoing Soxhlet extraction with 300 mL Milli-Q water in a 500 mL round bottom flask. During extraction, Milli-Q water was boiled and its vapour travelled upward into the condenser tube, where, after condensing, it dripped into a thimble containing a bark sample. By this method, soluble compounds moved into the condensed solvent in the thimble, and when the level of the liquid reached the bypass arm, it was returned to the flask. Therefore, the sample in the extraction thimble was continually exposed to fresh, hot solvent and consequently increased the extraction rate (Yang and Jaakkola, 2011). Extraction was carried out for 48 h, until the extracted solutions turned clear. The extracted solutions were collected in plastic bottles that were subsequently purged of air

using Argon gas and stored at 4°C. The extracted bark was collected and dried at room temperature for 7 days before being employed for As sorption.

3.2.4 Analytical Procedures: Biosorption in Batch Sorption Methods

As discussed in Section 1.3.8, previous studies (P. Jackson and P. Miller, 1998, Jackson and Miller, 1999, Narukawa *et al.*, 2005, Huggins *et al.*, 2007b, Bolanz *et al.*, 2012) have identified As(V) as the most predominant arsenic species in fly ash. Therefore, a stock solution containing a known concentration of As(V) was prepared for biosorption experiments on bark samples by dissolving sodium hydrogen arsenate ($Na_2HAsO_4.7H_2O$; Sigma-Aldrich) in Milli-Q water.

In a preliminary study (Figure. 3.1), 5 g of raw or treated bark samples from two Eucalyptus species, *Ea* and *Ed*, were treated with 50 mL of a 200 ppb As(V) solution. After being stirring at 300 rpmfor 2 h at room temperature, the bark was separated from the solution by filtration. The bark samples were washed several times before the solution was diluted to 100 mL and stored in plastic bottles at 4°C prior to HG-AAS analysis within 24 h.

In the main study (Figure. 3.2), batch sorption experiments were carried out to determine the optimum conditions for As(V) removal from synthetic solutions using *Ed*, *Lc* and *Mq* bark. All As sorption was performed at room temperature (23±2 ºC) in 100 mL plastic beakers containing 50 mL of an As(V) standard solution under a range of variable conditions including pH, contact time, As concentration and bark dosage. The experimental conditions are shown as a flow chart in Figure 3.5.

After all solutions were magnetically stirred at 300 rpm to achieve sorption equilibrium, they were separated from the biomass by filtration (Whatman#1 and 0.45 µm cellulose-acetate membrane). The filtrate was collected and the initial and the final arsenic concentrations were determined within 24 h by HG-AAS. Experiments were carried out in duplicate and the mean

result and standard deviation (SD) were recorded. Blank and control bark solutions were also analysed in parallel.

Batch sorption experiments were carried out to remove As(V) from actual fly ash leachates using the optimum biosorption conditions.

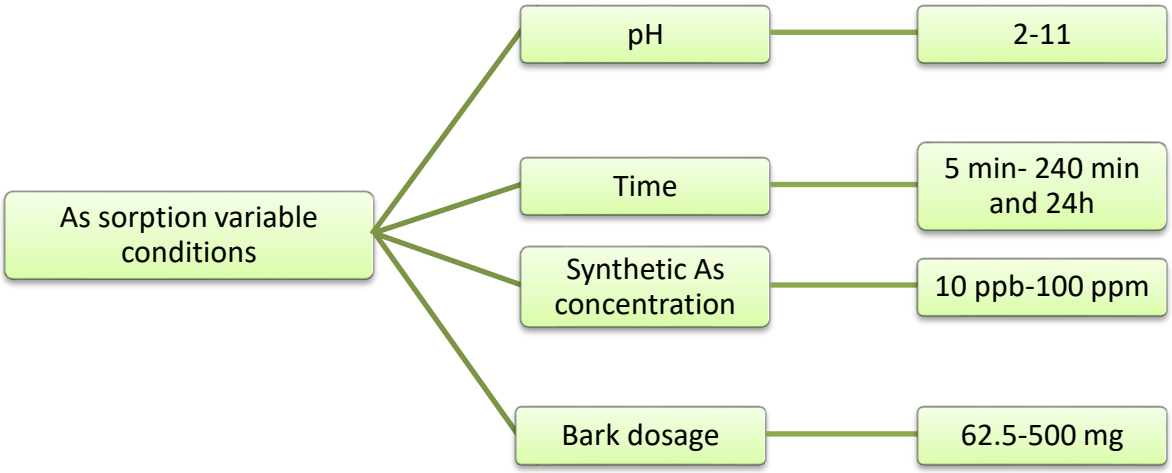

Figure. 3.5 Conditions applied for As sorption experiments

3.2.5 Isothermal and Kinetic Biosorption Experiments

In order to examine the role of treatment concentration in As adsorption, isothermal experiments were conducted on selected barks following a similar procedure outlined in Section 3.2.3. In brief, 25 mL of a known As solution ranging in concentration from 10 µg/L to 100 mg/L was added to 0.25 g of biomass (S:L=1:100) in 100 mL plastic beakers. The solution was stirred vigorously for 24 h at 300 rpm using a magnetic stirrer to reach equilibrium. These experiments were performed at optimum pH for each bark type and at room temperature (23±2

°C). Solutions of 0.01 M NaOH and HCl were used to adjust the pH as required for each bark type. After 24 h, the solution was separated from the biomass by filtration (Whatman#1 and 0.45 µm cellulose-acetate membrane). The arsenic concentrations of initial samples and samples after equilibrium were determined in duplicate within 24 h using HG-AAS. As discussed in Section 1.2.4.2, linear form of both the Langmuir isotherm model, Equation 3.1, and the Freundlich isotherm model, Equation 3.2, were used to describe the isotherms of biosorption.

$$\frac{1}{q_e} = \frac{1}{b q_{max} C_e} + \frac{1}{q_{max}} \qquad \text{Equation 3.1}$$

$$ln\, q_e = ln\, k + n\, ln\, C_e \qquad \text{Equation 3.2}$$

where, q_e is equilibrium amount of ion adsorbed by the sorbent (mg/g), q_{max} is the theoretical maximum amount of metal ions (mg/g) likely bound on the surface of biosorbent (monolayer adsorption capacity) in the equilibrium state, b is the Langmuir constant (L/mg), C_e is equilibrium concentration of sorbate in liquid phase (mg/L), k is Freundlich constant (L/mg), and n is Freundlich exponent or biosorption intensity (Ranjan *et al.*, 2009, Momčilović *et al*., 2011, Afroze *et al.*, 2016). In a Langmuir model, q_{max} and b were obtained from the slope and intercept of a $1/q_e$ versus $1/C_e$ plot, whilst k and n would be obtained from the slope and intercept of a ln q_e versus ln C_e plot.

Theoretically, in a Langmuir model, a monolayer of sorbate may homogeneously cover the surface of the sorbent, while in Freundlich model a multilayer sorption may occur on a heterogeneous surface of sorbent (Promthet and Mungkarndee, 2015).

In addition to these two models, the linear form of the Sips isotherm model, as represented by Equation 3.3, was used to clarify the biosorption isotherm.

$$ln\left(\frac{q_{max} K_s}{q_e}\right) = -\frac{1}{n_s} ln(C_e) + ln(K_s) \qquad \text{Equation 3.3}$$

In Equation 3.3, q_e is the adsorbed amount at equilibrium (mg/g), *Ce* the equilibrium concentration of the adsorbate (mg/L), q_{max} the Sips maximum adsorption capacity (mg/g), K_S the Sips equilibrium constant (L/mg), and n_s is the Sips model exponent. If n_s is close to 1, then the equation will present a Langmuir model, and if $C_e = 0$ or $K_s = 0$, the isotherm will follow the Freundlich model (Ebrahimian *et al.*, 2014)

In order to examine the role of treatment time in As adsorption, similar kinetic experiments to isothermal experiments were conducted. Briefly, 25 mL of a 100 µg/L As (V) solution was added to 0.25 g of biomass (S:L=1:100) in 100 mL plastic beakers and agitated at 300 rpm at room temperature (23±2°C). The sample was stirred vigorously for 5, 10, 15, 30, 60, 120, 180, 240 and 1440 min. Solutions of 0.01 M NaOH or HCl were used to adjust the pH to the desired value. After the designated treatment time had elapsed, the solution was separated from the biomass by filtration (Whatman#1 and 0.45 µm cellulose-acetate membrane). The arsenic concentrations of initial samples and samples after equilibrium were determined in duplicate within 24 h using HG-AAS. The quantity of As adsorbed was then plotted as a function of time to obtain the equilibration time of the adsorption process, the rate of adsorption and the equilibrium capacity of the adsorbent.

For kinetic model interpretation, the "q" value must be used until it reaches equilibrium. The quantity of As(V) at any time, equilibrium sorption capacity, and the percentage removal of As(V) were estimated using the following equations:

$$q_t = (C_i - C_t) \times \frac{V}{m} \qquad \text{Equation 3.4}$$

$$q_e = (C_i - C_e) \times \frac{V}{m} \qquad \text{Equation 3.5}$$

$$Removal\ \% = \frac{Ci - Ct}{Ci} * 100 \qquad \text{Equation 3.6}$$

In Equations 3.4, q_t corresponds to the quantity of adsorbed ion (µg/g) at any time t (min), C_i and C_t are the As(V) concentration (µg/L) before and after adsorption, respectively, V is the volume of the solution (L) and m is the mass of adsorbent (g). Meanwhile, in Equation 3.5, the experimental q_e value refers to the adsorbed quantity at equilibrium and C_e is concentration at equilibrium, which is the time wherein the C_t value is constant (Meunier *et al.*, 2003, Gadd, 2009, Ranjan *et al.*, 2009, Hansen *et al.*, 2010, Afroze *et al.*, 2016).

As discussed in Section 1.2.4.1, there are two kinetic models that can be applied, Lagergen Pseudo-first order (Equation 3.7) and Ho Pseudo-second order (Equation 3.8):

$$ln\ (q_e - q_t) = ln\ q_e - k_1 t \qquad \text{Equation 3.7}$$

$$t/q_t = (1/k_2 q_e^2) + (1/q_e)t \qquad \text{Equation 3.8}$$

where k_1 is the pseudo-first order rate constant (min) and k_2 is the pseudo-second order rate constant (g/mg min). The slope of linear $ln\ (q_e - q_t)$ versus t plot will then yield k_1, and the corresponding slope of a linear t/q_t versus t plot will yield k_2.

3.2.6 As Sorption Capacity of Bark

To determine the ability of bark species to adsorb As, 0.25 g of each bark sample was added to 50 mL of a 200 ppb As solution in separate 100 mL plastic beakers. These beakers were sealed and the solution was stirred at 300 rpm for 2 h at room temperature (23±2 ºC). The solution pH was adjusted to 6-7. These solutions were then filtered using Whatman#1 filter papers, and the filtered bark was washed several times with Milli-Q water. Finally, the solutions were diluted to 100 mL, and stored in plastic bottles at 4ºC. Duplication of samples along with blank and control bark solutions were analysed, and the mean result and standard deviation (SD) were

recorded. The initial and equilibrium arsenic concentrations in each sample were determined within 24 h using HG-AAS.

3.2.7 Desorption of Arsenic from Loaded Biomass

Batch desorption experiments were carried out in 100 mL plastic beakers. In brief, 0.50 g of As-loaded bark was introduced into a 50 mL solution containing 0.1 M NaCl, 0.1 M NaOH, 0.1 M $NaHCO_3$, 0.1 M Na_2CO_3, 0.1 M HCl and 0.1 M HNO_3. The solution was then stirred for 60 min at 300 rpm at 23±2 ºC. After a specified desorption time, the solution was separated from the biomass by filtration and the filtrated bark washed several times until a neutral pH of the washing solution was achieved. The solution was then diluted to 100 mL and stored at 4 ºC. All samples were studied in duplicate and the mean result and standard deviation (SD) were recorded. Blank and control bark solutions were also analysed in parallel. The initial and equilibrium arsenic concentrations in each sample were determined within 24 h using HG-AAS.

3.2.8 Removal of Arsenic from Fly Ash Leachate

In a set of batch sorption experiments, 500 mg of selected bark was added to 50 mL of selected fly ash leachate in 100 mL plastic beakers. After adjusting pH to the desired value determined from initial sorption experiments, the solution was magnetically stirred at 300 rpm. Following a desire contact duration for an effective As removal, samples were filtered and the concentrations of As(V) determined by HG-AAS within 24 h. All samples prepared in duplicate and the mean result and standard deviation (SD) were recorded. To minimise the error, blank and control bark solutions were also analysed in parallel.

3.3 Results and Discussion

Work reported in this chapter will closely follow the flow charts depicted in Figure. 3.1 and Figure. 3.2. At the first stage, the initial As concentration in two Eucalyptus species bark, and then the quantity of As removable from bark using Milli-Q water were determined. Moreover, As biosorption experiments on raw and treated bark of two Eucalyptus species were performed. At the second stage, some physical and chemical properties along with morphology of bark derive from different tree species were studied. Furthermore, the quantity of As within bark before and after sorption experiments was estimated, and a comparison of selected physical and chemical properties of bark before and after As sorption was performed. Finally, the effect of pH, contact time and bark dosage and initial concentration of As(V) solutions were evaluated using kinetic and isotherm models for As(V) sorption, and then the removal of As(V) from fly ash leachate was assessed. All results were compared with literature information to draw conclusions.

3.3.1 Initial Stage of As(V) Biosorption on Two Different Eucalyptus Species Bark

As highlighted in Section 3.2, arsenic adsorption experiments were firstly performed using the outer layer bark from two different Eucalyptus tree species, *Ed* and *Ea*.

3.3.1.1 Acid Digestion, Filtration and Extraction of Bark

Prior to adsorption experiments, it was imperative to first determine the natural amounts of As within the *Ed* and *Ea* bark digests, filtrates and extracts. The results obtained are tabulated in Table 3.1. For both *Ed* and *Ea* the lowest As concentration was found in their filtrates and the highest in their digests. Extraction was found to remove more As, compared to filtration, from both species. Water-soluble compounds such as tannins and terpenes are likely to have been removed by washing with Milli-Q water, whilst functional groups within the bark (*e.g.*, carboxyl and hydroxyl) are likely to be responsible for elemental adsorption (Pandey *et al.*, 2009).

However, the short duration and low temperature in the filtration process may have reduced the amount of water-soluble compounds from bark samples in contrast with the 48 h duration at high temperature (90^{o}C) used in extraction.

A potential explanation for the surprisingly high As concentrations observed in the *Ea* and *Ed* digests may be the result of soil contamination or possibly from air pollution due to the location of the growing trees (next to an infrequently-used campus road) or the proximity of the Macquarie University campus to the nearby high-traffic M2 motorway.

Table 3.1 Arsenic concentration in *Ea* and *Ed* bark digests, filtrates and extraction solutions (µg/kg)

Sample species	Process	As content / µg/kg bark
Ea	Digest	498.6 (10.4)
	Filtrate	42.9 (2.5)
	Extract	102.2 (7.6)
Ed	Digest	440.8 (8.0)
	Filtrate	10.8 (1.0)
	Extract	201.0 (7.6)

Measurement uncertainty presented as standard deviation in parenthesis for 2 consecutive measurements

3.3.1.2 Preliminary Biosorption Experiments Results

The first series of batch sorption experiments was conducted using raw *Ed* and *Ea* barks or barks that had been treated as outlined in Section 3.2.3. The barks were treated to enhance their As biosorption.

In Figure 3.6, the results of these biosorption experiments are illustrated as a percentage of As sorbed by bark in addition to the sorption capacity of the bark sample (in µg/g). According to the results in Figure 3.6, treated bark from either species demonstrated greater As sorption compared to raw bark. However, the maximum As sorption was found for *Ea* treated with formaldehyde, whilst *Ed* boiled showed the highest As sorption.

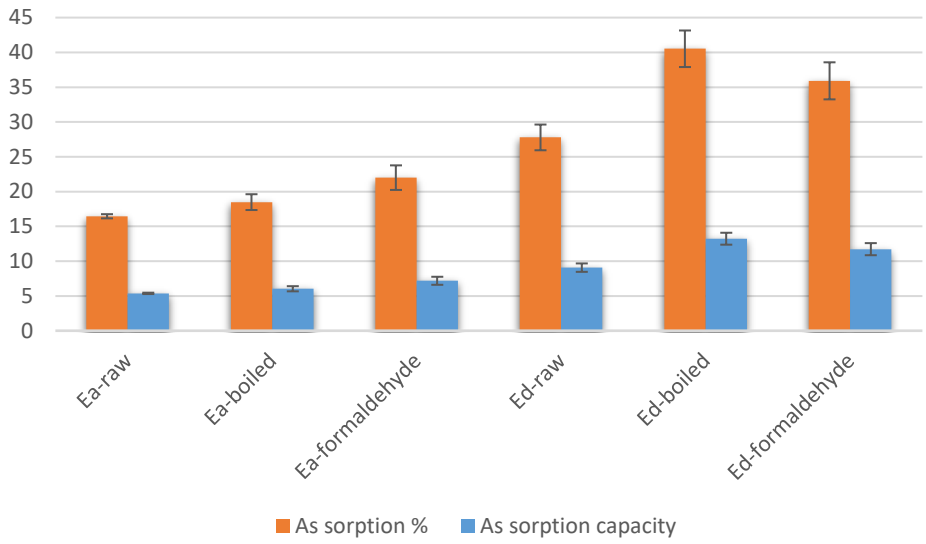

Figure 3.6 The percentage of As biosorption and sorption capacity of *Ea* and *Ed* bark samples at pH 6.

Both selected bark species showed some As sorption capacity. However, raw and treated *Ed* bark presented almost twice the sorption capacity compared to the raw and treated *Ea* bark. Therefore, raw and treated *Ed* barks were chosen to investigate the effect of pH in As sorption.

A second series of batch sorption experiments was performed using raw, boiled, formaldehyde- and iron-coated *Ed* barks as outlined in Section 3.2.2. The results obtained are shown in Figure 3.7. Notably, almost all raw and treated barks showed maximum As adsorption at pH 7, with the exception of formaldehyde-treated *Ed* bark showed maximum As adsorption at pH 4. The acidic solution might expand formaldehyde treatment, thus improve insolubility of tannins, which possibly is responsible for As sorption (Kumar and Dara, 1982, Deshicar *et al.*, 1990).

Ed-extracted bark, followed by boiled bark, demonstrated the least As adsorption of the treated barks, probably due to the removal of water-soluble compounds such as phenolic compounds (*i.e.*, tannins, terpenes and flavonoids), carbohydrates, glycosides, and soluble salts from the bark as a result of hot Soxhlet extraction (Yang and Jaakkola, 2011). Thus, if such bark-derived phenolic compounds (with functional groups such as carboxyl- and hydroxyl-groups) could be

responsible for As sorption, then their elimination in extracted or boiled bark would result in decreased As adsorption (Reddy *et al.*, 2011). However, boiling bark may increase the efficacy of the non-extractable compounds such as lignin, a polyphenol compound, thus increase the sorption capacity of elements, especially in acidic and alkaline conditions, in comparison with raw and extracted bark (Reddy *et al.*, 2011).

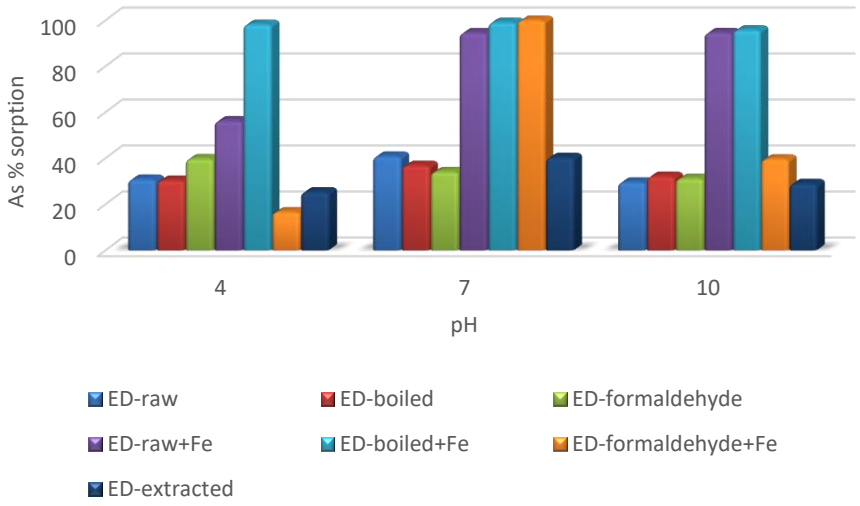

Figure 3.7 As biosorption of *Ed* bark samples at pH 4, 7 and 10.

Interestingly, Figure 3.7 shows that all iron-coated barks exhibited very high As adsorption of up to 99.9% at pH 7, and a high adsorption capacity relative to other bark treatments. This result can be explained by the high affinity of As for adsorption on iron compounds. Previously, iron oxide/hydroxides in granular form or nanoparticles were demonstrated to successfully adsorb both As(V) and As(III) from aqueous solutions (Litter *et al.*, 2010, Streat *et al.*, 2008).

According to Chil-Sung Jeon *et al.*, (Chil-Sung Jeon *et al.*, 2009), the adsorption of As(V) on iron-coated material could have occurred by ligand exchange reactions, in which the hydroxide groups are involved and resulted in the release of hydroxide through the following mechanism of the complex formation of As(V) with ferric hydroxide:

$$Fe - OH + H_2AsO_4^- \rightarrow Fe - OAsO_3H + OH^-$$

$$Fe - OH + HAsO_4^{2-} \rightarrow Fe - O_2AsO_2H^- + OH^-$$

$$2Fe - OH + HAsO_4^{2-} \rightarrow 2FeO - AsO_2H + 2OH^-$$

As(V) might be removed by iron-coated bark through the same ligand exchange reaction. Under strong alkaline condition, the iron-coated bark surface possibly became negatively charged, establishing electrostatic repulsion between iron-coated bark and $[H_2AsO_4]^-$, resulting in a decrease of adsorption. Alternatively, under strong acidic condition, arsenate may compete with hydrogen ions for the adsorption on iron coated bark (Chil-Sung Jeon *et al.*, 2009).

3.3.2 Biosorption of As(V) onto Tree Bark: Stage Two Studies

Although formaldehyde treatment and iron coating have significantly increased biosorptive capacity of the biomass, these strategies are neither cost effective nor safe for the environment. Based on our results indicating a higher arsenic adsorption affinity on iron-coated bark in synthetic solutions, this study was expanded the test the adsorption capacity of other tree species to investigate whether natural differences in iron concentration resulted in different biosorption capacities. Therefore, at the second stage of experimentation, which is also the main stage of the current Chapter, *Ed*, as the greater adsorbent compared to *Ea*, was selected for further sorption testing alongside two other species, *Lc* and *Mq*.

3.3.2.1 Physical and Chemical Data for Selected Biosorbents

Several physical and chemical characteristics of bark samples were studied prior to adsorption testing. These included BET surface area analysis, quantification of several elements using

EDXRF, CHN, and HG-AAS, morphology of bark by SEM-EDS, and assessing the type of functional groups present in bark using FTIR/ATR analysis. At later stages of the project, BET surface area, SEM-EDS, and FTIR-ATR analysis were repeated on As-loaded bark for comparison purposes.

3.3.2.1.1 BET Surface Area, Pore Size and Pore Volume Determination

For average size particles between 150-710 µm, their surface area (m^2/g), pore size (nm), and pore volume (cm^3/g) were determined using BET model, Barrett-Joyner-Halenda (BJH) model for the pore volume and average pore diameter as pore size distribution. The results, which are tabulated in Table 3.2, demonstrate that *Mq* exhibited the highest surface area of 1.25 m^2/g, which was approximately three times the surface area of *Ed* and *Lc* bark. Similarly, *Mq* showed the largest pore volume that is almost three times larger than that of the other two species. All these results support a more porous nature of *Mq*. However, *Ed* showed a 0.01-fold larger average pore diameter than that *Mq*, whilst *Lc*, exhibited the smallest pore size. All these features are likely to be related to the bark species nature, which is beyond the scope of this study.

3.3.2.1.2 EDXRF, CNH and HG-AAS Analysis

The results for elemental analysis by EDXRF for total concentration of Fe, As, Se, Cu, Ca, Zn and Mn, and the percentage of elemental data for C, N and H are shown in Table 3.3. However, no Mg or Al was detected by the EDXRF. As tabulated in Table 3.3, the quantity of iron within bark samples followed the order of *Mq* > *Lc* > *Ed*. Additionally, the quantity of As within the bark samples and the percentage of C, N and H also followed the same order.

Although *Mq* showed the highest quantity of Fe, As, C, N and H, it contained the lowest Ca and Se content. In contrast, *Ed* presented the lowest quantity of Fe and As, but the highest of Ca content. The highest concentration of Se was observed in *Lc* along with the highest Mn, Zn and Cu concentration. The reason for such behaviour may be related to the nature of tree species and structure of the plant, which is beyond our study.

Additionally, the concentration of Fe and As (mg/kg) in acid digests of bark samples was determined using AAS for Fe and with an HG accessory for As. All results from AAS, HG-AAS and EDXRF are tabulated in Table 3.4 for comparison. These results indicate a higher Fe content in *Mq* compared to *Lc* and *Ed*. Additionally, *Mq* showed greater initial As concentrations than *Lc* or *Ed*. This supports the explanation that the high Fe content enables an elevated affinity of As adsorption (Litter *et al.*, 2010).

Table 3.2 BET surface area analysis results for selected bark samples with average particle sizes of 150-710 µm

Bark Sample	BET Surface area / m^2/g	Pore size / nm	Pore volume / cm^3/g
Ed	0.46	6.35	0.004
Lc	0.43	6.30	0.003
Mq	1.25	6.31	0.009

Table 3.3 Elemental concentrations in counts/s (cps) within bark samples as determined by EDXRF and in % by CNH analysis.

Bark Sample	Fe	As	Se	Cu	Ca	Zn	Mn	C	N	H
Ed	51.8 (2.4)	0.3 (0.1)	0.3 (0.1)	2.4 (0.1)	18330.6 (9.6)	2.2 (0.1)	19.5 (1.2)	43.56 (0.14)	0.18 (0.01)	5.62 (0.09)
Lc	233.5 (12.1)	0.5 (0.1)	0.6 (0.1)	9.0 (0.9)	17039.4 (7.5)	22.8 (5.2)	39.6 (2.1)	45.81 (0.16)	0.19 (0.05)	5.87 (0.16)
Mq	960.9 (23.2)	1.2 (0.3)	0.2 (0.1)	5.6 (0.2)	1650.7 (4.3)	8.8 (1.4)	13.9 (0.6)	60.52 (0.84)	0.31 (0.03)	8.41 (0.13)

Measurement uncertainty as standard deviation presented in parenthesis for 2 or 3 consecutive measurements

Table 3.4 Acid digestion and EDXRF analysis of Fe and As concentrations within bark samples.

Bark Sample	Fe		As	
	AAS / mg/kg	XRF / cps	HG-AAS / mg/kg	XRF / cps
Ed	18.1 (1.9)	51.8 (2.4)	0.8 (0.1)	0.3 (0.1)
Lc	50.4 (4.3)	233.5 (12.1)	2.1 (0.2)	0.5 (0.1)
Mq	187.1 (3.4)	960.9 (23.2)	2.5 (0.2)	1.2 (0.3)

Measurement uncertainty as standard deviation presented for 3 measurements

Table 3.5 EDS results of bark sample analysis presented in mass%.

Unloaded Bark	Si	Al	Fe	Ca	Mg	Cu	O	N
Ed	0.1 (0.0)	0.1 (0.0)	ND	25.1 (6.4)	0.4 (0.1)	ND	55.0 (9.2)	ND
Mq	25.3 (1.4)	4.9 (1.0)	6.4 (1.2)	9.8 (0.6)	0.5 (0.2)	0.3 (0.0)	57.8 (10.3)	16.2 (1.4)
Lc	4.8 (0.0)	1.7 (0.9)	5.0 (0.0)	5.1 (1.7)	2.2 (0.7)	ND	51.6 (7.1)	ND

ND denotes not detected; Measurement uncertainty presented as standard deviation in parenthesis for 2 consecutive measurements

3.3.2.1.3 SEM-EDS Analysis

SEM was employed to examine the surface of unloaded bark. The corresponding micrographs of *Ed*, *Lc* and *Mq* are shown in Figures 3.11a, 3.11b and 3.11c. Notably, a rough surface and a large number of asymmetric and open pores in these micrographs may offer a greater opportunity for physical or chemical As biosorption. Micrographs with a 600× magnification particularly reveal a rough surface area which might offer more As binding sites (Reddy *et al*., 2011, Saqib *et al.*, 2013). However, *Lc* showed a more compact surface compared to the other two species. This feature could be associated with the structure of its cell wall, which may include more biopolymers such as lignins than two other species.

Variation in the biosorption capacity of three biosorbents is primarily due to differences in their surface porosity. Based on the scanning electron micrographs displayed in Figure 3.8, the abundant and notable unoccupied voids present on the *Mq* surface, make it to be visually much more porous compared to *Ed* and *Lc*. In addition, the surface of *Lc* seemed to be closely packed with potential 'biopolymers' such as lignins or tannins, which will yield a compact biosorbent surface (Wan Ngah and Hanafiah, 2008). The decreasing order of bark surface porosity can be determined as: *Mq* > *Ed* > *Lc*. According to the BET surface analysis results in Table 3.2, the pore volumes of such biosorbents follow the same decreasing order. Furthermore, difference in surface morphology or porosity will be responsible for different sorption capacities of biosorbents as well (Mishra *et al.*, 2010).

EDS results, which are tabulated in Table 3.5, indicate that the major elements in the bark samples were Si, Al, Fe, Ca, Mg and O in several compounds, which were consistent with the elemental compositions previously determined by EDXRF quantitative results in Table 3.4. However, As was not observed in unloaded bark samples, most likely due to the concentration of As being below the detection limit of the instrument. Notably, the data in Table 3.5 are

related to the maximum mass% of the elements collected from 6 to 54 spots of each bark species.

Almost all elements were observed in high quantities in the *Mq* samples except Ca, which was the highest in *Ed*, whilst Mg was most abundant in *Lc*. These results are in agreement with previous EDXRF results in Table 3.4. However, as SEM/EDS is not a sufficiently accurate quantitative analysis technique, these results only provide a semi-quantitative estimation of the realistic content of each element within the sample.

It must be emphasised that the practical quantity of elements observed in bark samples is inherently variable, as are the size of bark particles analysed. These values are therefore dependent upon the chosen spot. Alternatively, analysis may yield different signal intensities for elements such as Al, Si, Fe, Mg, Ca, Cu, K, Ti, Na, Cl, and S as a result of the presence of mineral compounds existing within the cell wall of tree bark (Gaballah and Kilbertus, 1998). Figures 3.9a, 3.9b and 3.9c display the BSE micrograph with corresponding elemental spectrum of unloaded *Ed*, *Mq*, and *Lc* bark samples. Several of these elements with low signal intensities indicate they were found in considerably low concentrations in the bark, while other elements with more intensive signal showed higher quantities in the bark. Oxygen presented a very intensive signal due to its high abundance in bark within organic compounds such as polysaccharides (cellulose, hemicellulose and pectin), polyphenolic compounds (lignin), aliphatic acids, and phenolic compounds (tannin and terpenes) that reside within the tree bark structure (Gaballah and Kilbertus, 1998).

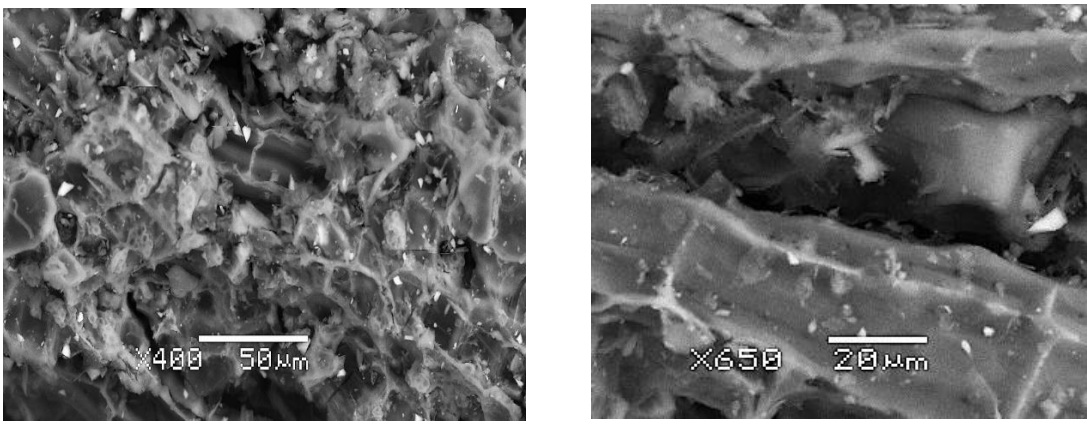

(a)

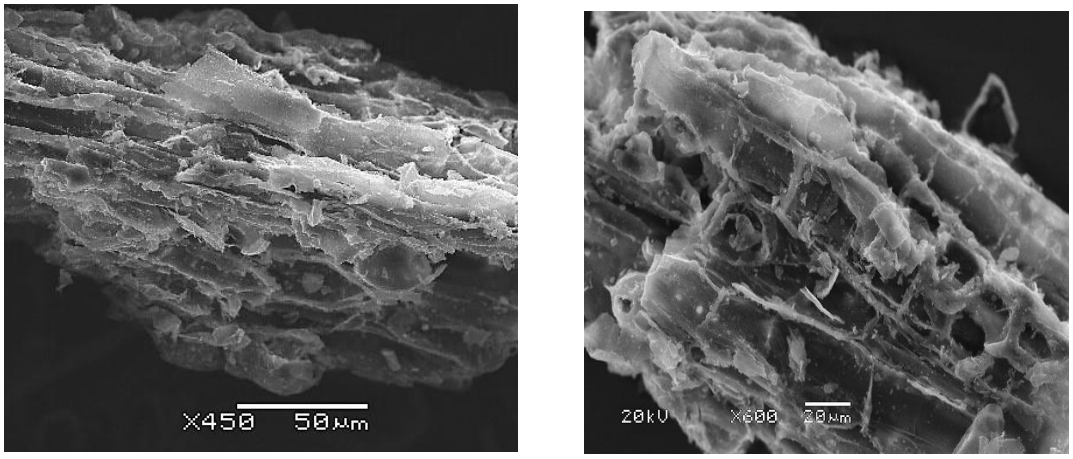

(b)

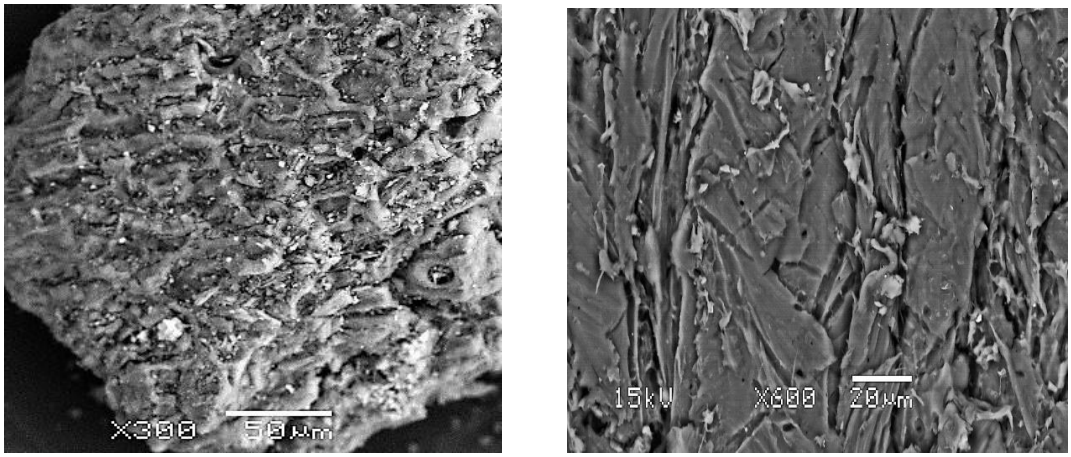

(c)

Figure 3.8 Scanning electron micrographs of raw bark: (a) *Ed*, (b) *Mq* and (c) *Lc*, at 300–450× (left) and 600–650× (right) magnifications.

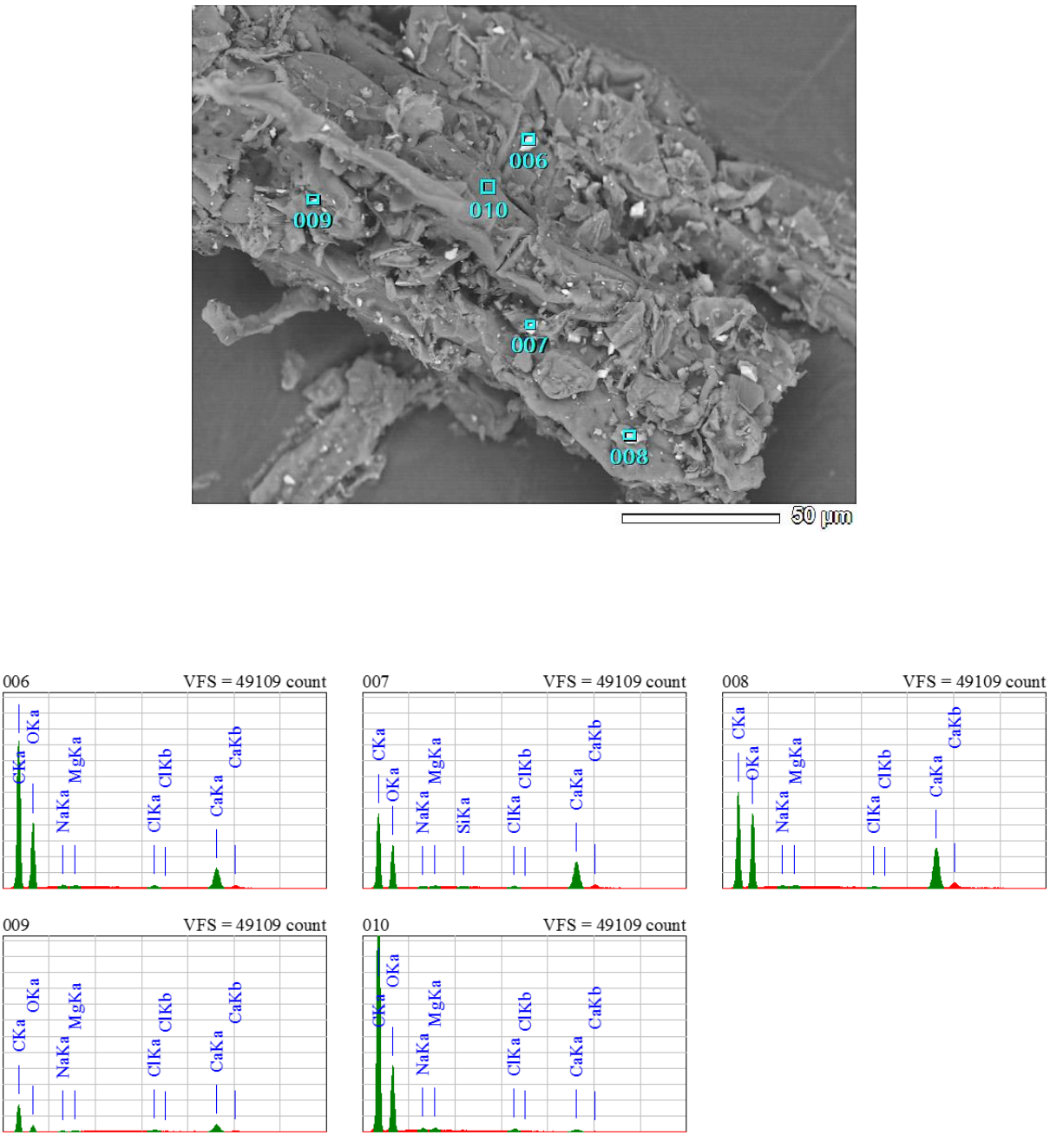

Figure 3.9 a) BSE micrograph with elemental spectra of raw *Ed* bark.

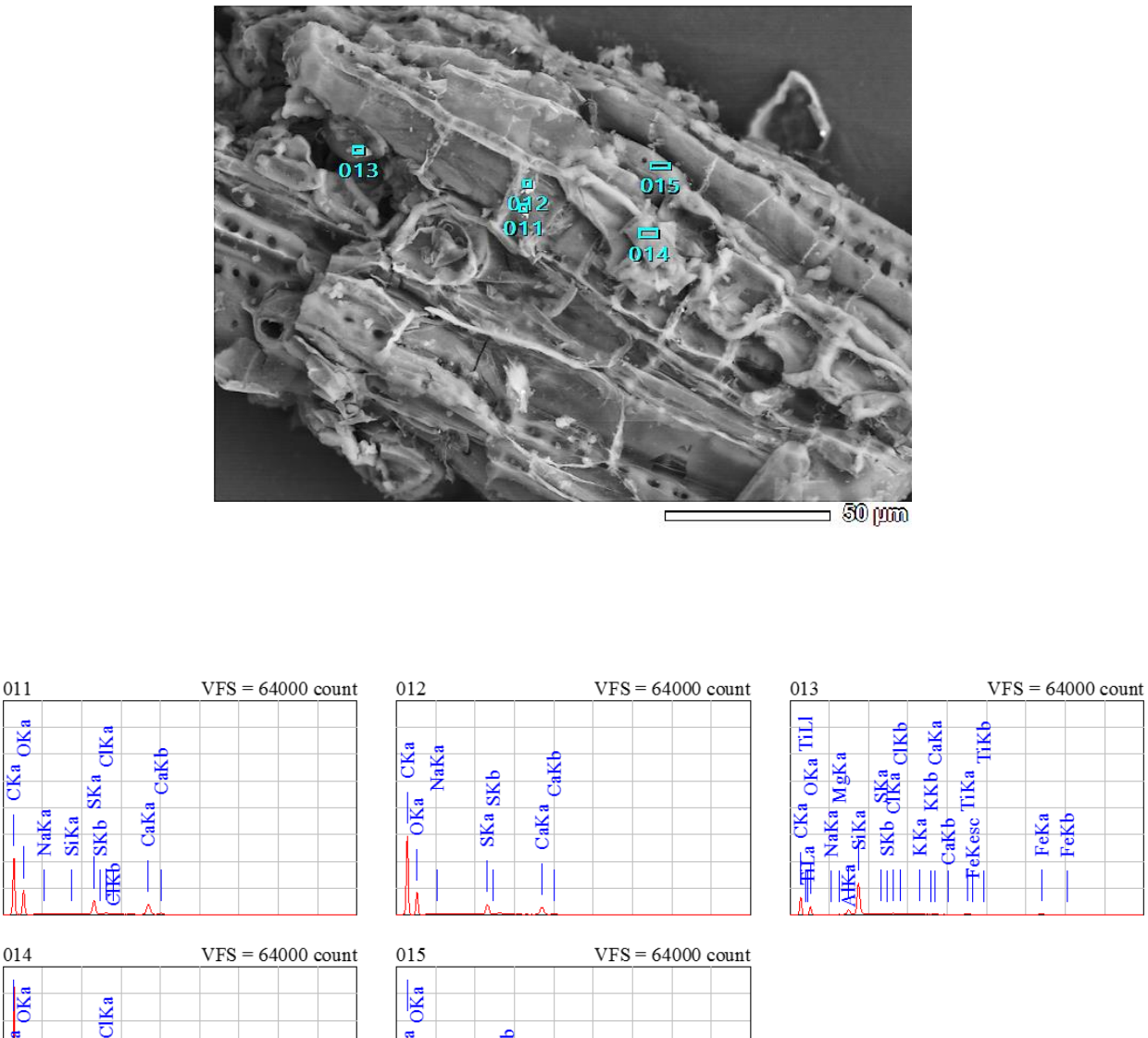

Figure 3.9 b) BSE micrograph with elemental spectra of raw *Mq* paper bark.

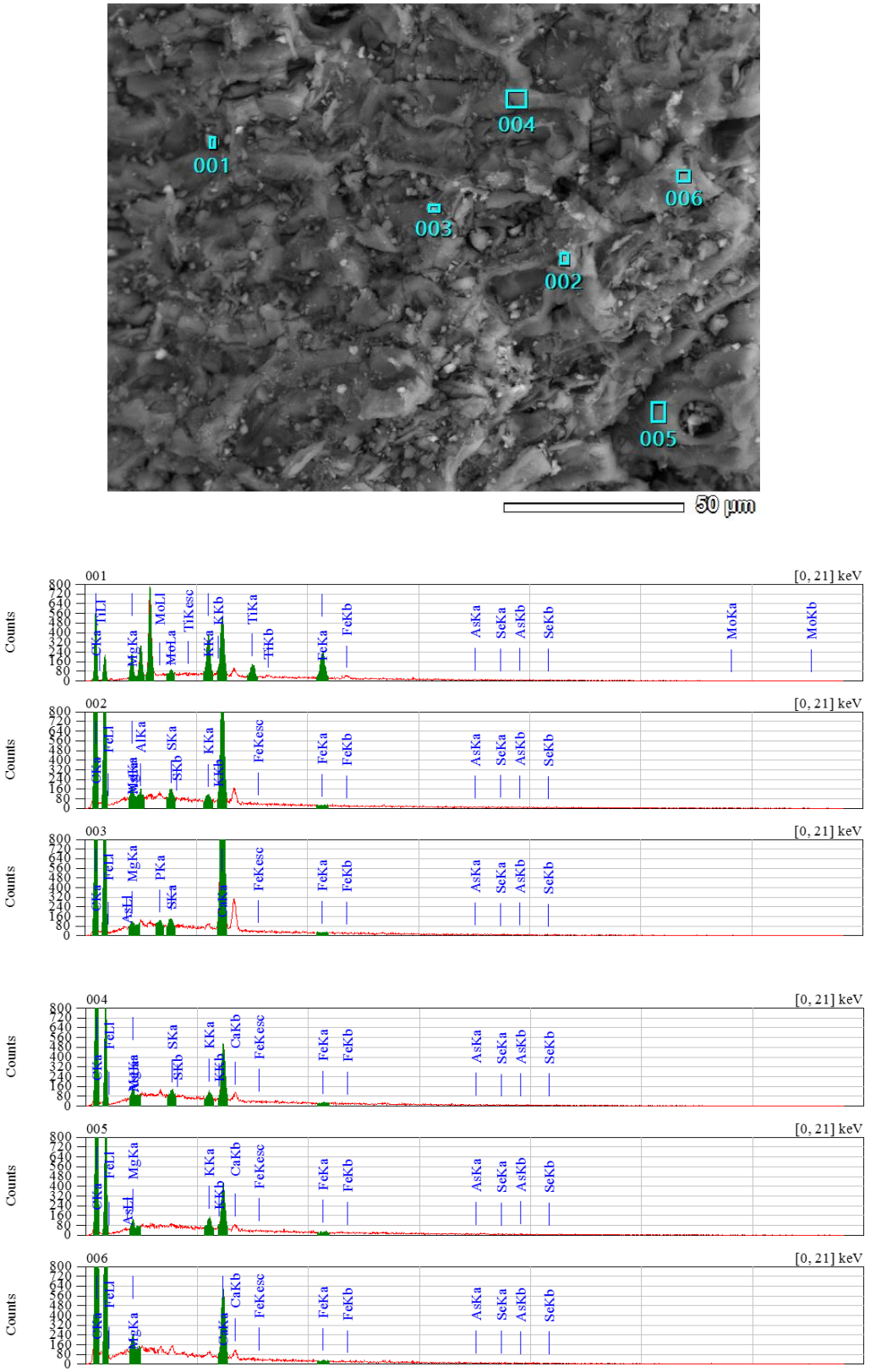

Figure 3.9 c) BSE micrograph with elemental spectra of raw *Lc* bark.

3.3.2.1.4 FTIR-ATR

FT-IR spectroscopy with an ATR accessory was employed to record the spectra of dried, unloaded or As(V)-loaded biomass in the 4000 – 400 cm^{-1} and 1850 – 1550 cm^{-1} wavenumber range. This spectroscopic analysis was used to seek information regarding the probable nature of cell–metal ion interactions. The FTIR spectra for raw barks, which are shown in Figure 3.10, suggest that raw *Ed*, *Mq*, and *Lc* bark consist of a mixture of functional groups. According to Mishra *et al.*, (Mishra *et al*., 2010), strong vibration peaks between 3,500 – 3,000 cm^{-1} in FTIR spectra of eucalyptus bark saw dust were assigned to the vibrations of O-H and −N-H functional groups and, broadening of these peaks arose from overlapping hydroxyl group and strong amide vibrations. By comparison, the broad and strong peaks at 3331.38, 3334.96 and 3327.81 cm^{-1} indicated the presence of hydroxyl and/or amide groups in *Ed*, *Mq* and *Lc* barks.

In their work, Mishra *et al*. (2010) assigned vibrations at 2921.55 and 2851.81 cm^{-1} in the FTIR spectrum of mango bark saw dust, 2921.23 cm^{-1} in that of eucalyptus bark saw dust, and 2917.14 and 2851.76 cm^{-1} in that of pineapple peel to symmetric or asymmetric CH stretching of aliphatic acids (Mishra *et al.*, 2010). Accordingly, the peaks at 2918.87 cm^{-1} in the spectra obtained for raw *Ed*, 2924.65 and 2852.62 cm^{-1} in that for raw *Mq*, 2923.15 and 2871.31 cm^{-1} for raw *Lc*, arose from the C–H stretching. In addition, the peaks at 1609.06 cm^{-1} for raw *Ed*, 1595.57 cm^{-1} for *Mq*, and 1614.85 cm^{-1} for raw *Lc* may be assigned to stretching vibration of carboxyl (C=O) groups, while the 1316.24, 1317.99 and 1318.11 cm^{-1} indicated the nitro (N=O) groups in *Ed*, *Mq* and *Lc* barks. These results are in a good agreement with the observed peaks at 1617.4 cm^{-1} and 1317.8 cm^{-1} in FTIR spectra of raw eucalyptus bark by Afroze *et al.*, (Afroze *et al*., 2016).

According to several previous studies (Pandey *et al.*, 2009, Mishra *et al.*, 2010, Tuzen and Sarı, 2010, Afroze *et al.*, 2016), the peaks in the range 1000-1300 cm^{-1} may be assigned to the C–O, C–C, or C–OH stretching of acidic groups, which are frequently observed in lignocellulosic biomasses. In addition, the peaks in the range of 1020-1340 cm^{-1} were used to support the presence of amine groups (Pandey *et al.*, 2009). Based on cited studies, the medium to strong peaks at 1230.12 cm^{-1} and 1029.38 cm^{-1} for *Ed*, 1239.70 cm^{-1} and 1032.87 cm^{-1} for *Mq*, and 1224.94 cm^{-1} and 1021.36 cm^{-1} for *Lc* suggest a possible acidic group and an amine group in these barks. Overall, analysis of FTIR-ATR results indicates that functional groups including carboxyl, hydroxyl, carbonyl, amine and other aromatics are present on the sorption sites of the bark surface.

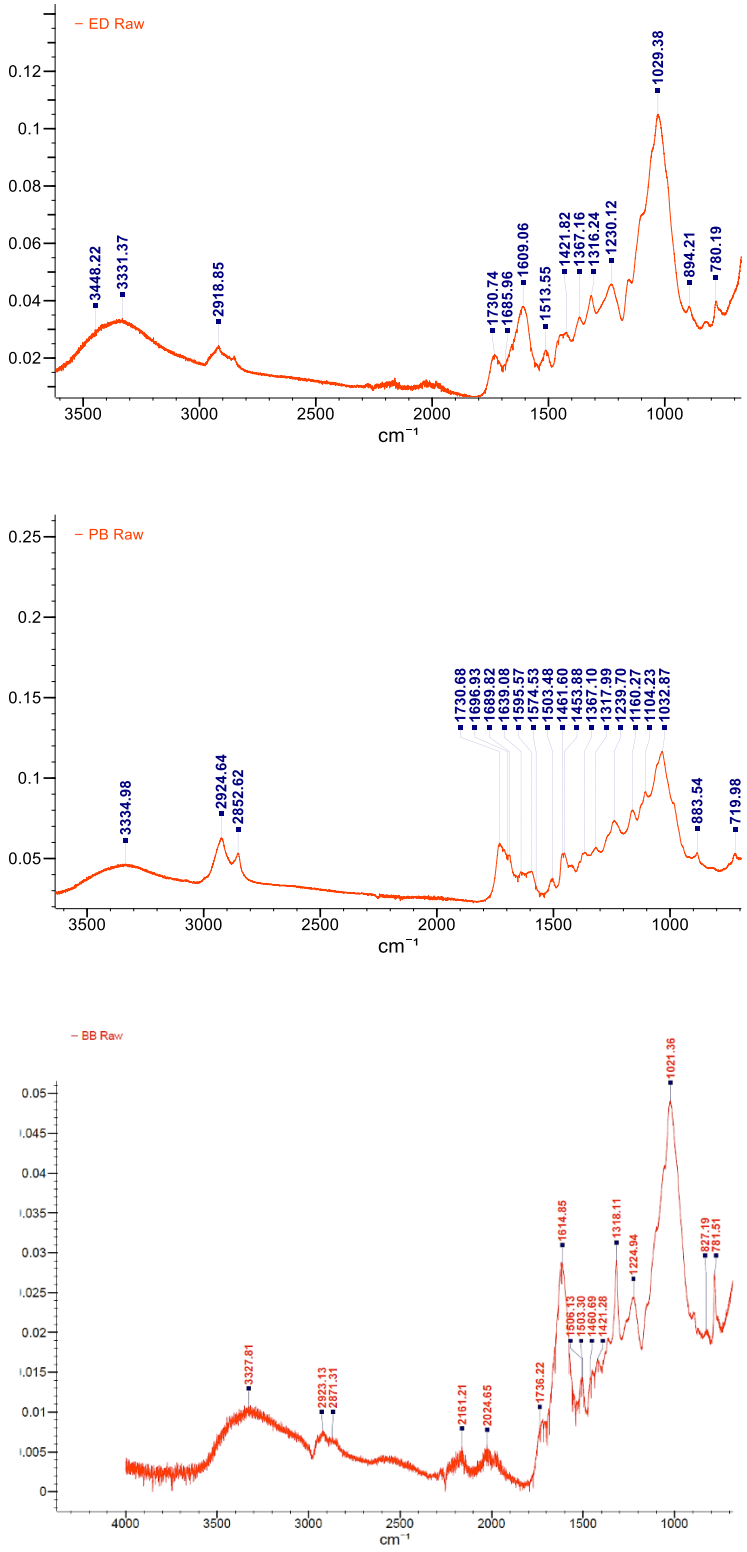

Figure 3.10 ATR spectrum of unloaded bark, from up to the bottom: raw *Ed*, raw *Mq* and raw *Lc*.

3.3.2.2 As Adsorption on Raw Bark

In this work, As sorption experiments were conducted on three different kinds of bark (*Ed*, *Mq*, and *Lc*), under several experimental conditions the solution pH from 2 to 11, initial As(V) solutions concentration of 0.01, 0.1, 1, 10 and 100 mg/L, bark dosage of 0.0625, 0.1250, 0.2500, and 0.5000 g in 25 mL of solution (S:L= 1:2.5, 1:5, 1:10, and 1:20), and contact times of 5, 10, 15, 30, 60, 120, 180, 240 and 1440 min. The obtained results for As(V) biosorption and the effect of changing conditions will be discussed in details below. Experiments were carried out in duplicate and the mean result and standard deviation (SD) were recorded. Blank and control bark solutions were also analysed in parallel.

3.3.2.2.1 pH Dependency for As(V) Biosorption

The effect of the pH range of 2–11 on the percentage removal of As(V) (Equation 3.5) for three biosorbents is shown in Figure 3.11. From pH 2 to 4, the As removal first increased, reached a maximum of 56.8% at pH 4 for *Mq*, and 47.7% for *Ed* and 27.8% for *Lc*, both at pH 5. Then with further pH increase, the percentage of As biosorption decreased up to pH 10, and then increased again at pH 11. Thus, the maximum percentage adsorption of As(V) occurred at pH 4 for *Mq*, and pH 5 for *Ed* and *Lc*.

Previously, Ranjan *et al.* (2009) showed that in the pH range of 3 to 6, the most prominent As(V) species present in solution is likely to be $H_2AsO_4^-$ with a small proportion of H_3AsO_4 near pH 2, whilst at pH > 8 $HAsO_4^{2-}$ and at pH range of 6-8, both $H_2AsO_4^-$ and $HAsO_4^{2-}$ are expected to be present (Ranjan *et al.*, 2009). According to the same report, the surface of biosorbent is protonated at low pH between 2 to 4 or 5, and therefore a strong attraction can occur between a positively charged biosorbent surface and oxyanion.

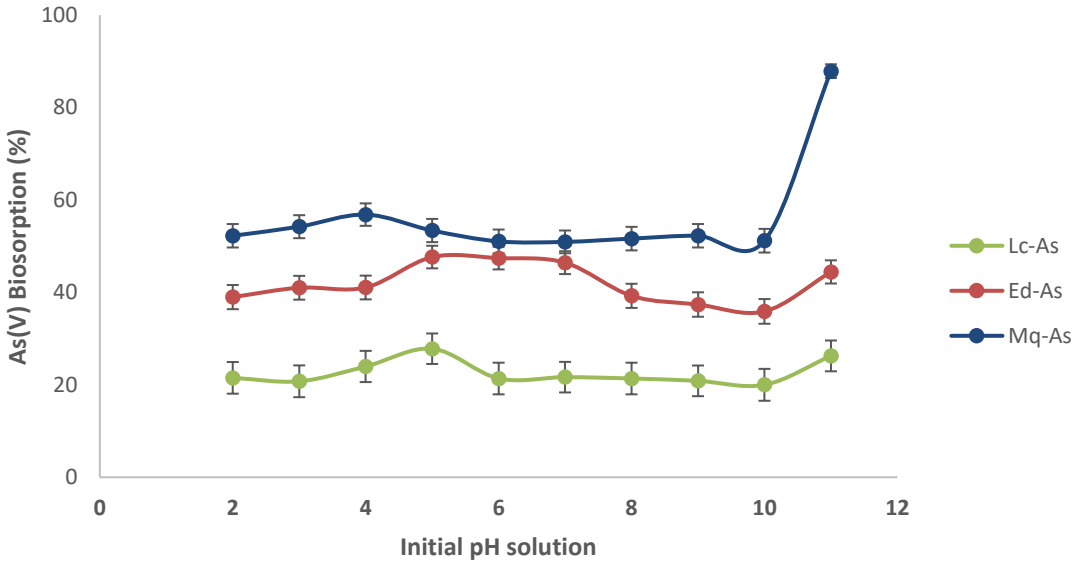

Figure 3.11 Effect of the pH on the adsorption of As(V) on *Ed*, *Mq* and *Lc* barks (conditions: mass of adsorbent=250 mg, volume of As(V) solution=25 mL, initial As(V) solution concentration=100 µg/L, temperature=23±2 °C, and contact time=120 min).

Additionally, an increase in $H_2AsO_4^-$ species over this pH range enhance As removal. At a pH from 5 to 10, a diminished As uptake might be caused by the negative charges of the sorbent surface. In this case, the biosorbent surface may adsorb hydroxyl ions, or some weak acidic functional groups on the sorbent surface ionize, or potentially both. Thus, a possible repulsive force between the negatively charged surface and the anions may decrease sorbent removal at higher pH (Ranjan *et al.*, 2009). Such increasing and decreasing patterns may also be due to a change of the As-bark interaction from mainly inner-sphere covalent bonds to weaker outer-sphere bonds at different pH (Simeoni, 2003).

As noted before, the chemistry of As(V) strongly depends on pH of solution. For example, in a strongly acidic solution, arsenic acid (H_3AsO_4) is formed, while under neutral and slightly alkaline conditions $H_2AsO_4^-$ and $HAsO_4^{2-}$ are the common As(V) species (Lizama *et al.*, 2011). Such negatively charged species are more easily removed than uncharged species due to the possibility of sorption, anion exchange or precipitation/coprecipitation (Henke and Hutchison, 2009). The reactions of arsenic acid and its anions along with their pKa values are shown below:

$$H_3AsO_4 \rightarrow H_2AsO_4^- + H^+ \qquad pKa_1 = 2.25$$

$$H_2AsO_4^- \rightarrow HAsO_4^{2-} + H^+ \qquad pKa_2 = 6.83$$

$$HAsO_4^{2-} \rightarrow AsO_4^{3-} + H^+ \qquad pKa_3 = 11.52$$

Additionally, the presence of iron oxides and iron hydroxides are highly affected in the speciation of As and its sorbing or coprecipitating in natural and synthetic environment (Henke and Hutchison, 2009). Coprecipitation possibly involves arsenic-bearing colloids adsorbed onto precipitated chemical species or absorbed in the precipitating compounds such as iron oxides, whilst sorption comprises the combination of selected ions on or within pre-existing solids (Henke and Hutchison, 2009). Sorption of As(V) on iron oxides mostly occurs in oxidising conditions in neutral to acidic pH, whilst at alkaline pH, As desorption occurs due to negative charge of sorbent surface (Lizama *et al.*, 2011). In high alkalinity, the buffer might deter re-solubilisation of undissolved As, as a rapid change in pH may release sorbed As by solubilisation. However, As can coprecipitate by increasing pH of solution due to precipitation of existing dissolved Fe (Lizama *et al.*, 2011). This could be the main reason for observing the high As removal at pH 11 in this study (see Figure 3.11) for the selected bark, especially *Mq* bark, which contains a high iron concentration compared to the other two other species (see Table 3.4). Moreover, the formation of brownish sludge during the sorption experiment may confirm the precipitation of iron oxide compound along with coprecipitation of As.

Another noticeable detail obtained from Figure 3.11 is that the percentage removal of As(V) using bark at every pH decreased in the order of *Mq* > *Ed* > *Lc*, which is the same as the order of porous surface and pore volume of biosorbents obtained from BET surface area analysis for particle size between 150-710 µm (Table 3.2). Moreover, the scanning electron micrograph of *Lc* bark (see Figure 3.8 (c)), shows a very compact surface, which is probably another reason for the least sorption capacity of this bark among other bark samples in this study. The lowest As removal of under 28% was found to be from the *Lc* bark at all examined pH range (see Figure 3.11), it was decided to not pursue the further experiments upon this species.

Furthermore, according to the obtained results, the optimum pH 4 for *Mq* bark and pH 5 for *Ed* bark were recognized and used for the next set of experiments.

3.3.2.2.2 Effect of Contact time on Arsenic Biosorption

The next step was to evaluate the effect of contact time (5 min to 240 min) on As biosorption using 0.25 g *Ed* and or 0.25 g *Mq*, and 25 mL of aqueous 100 µg/L As(V) at optimum pH obtained for each kind of bark. According to the results, which are depicted in Figure 3.12, the percentage removal of As increased with prolonged contact time. However, after a rapid increase in the early stage of contact (15 min), the rate of removal slowed with time, which is in agreement with other studies on removal of metal ions by various sorbents (Ranjan *et al.*, 2009, Kannan and Veemaraj, 2010, Afroze *et al.*, 2016). Nonetheless, there is a decrease at 30 min for *Mq* and 60 min for *Ed*, before the rate of removal gradually increased. However, *Ed* bark showed a diminishing As removal after 120 min up to 240 min. The reason for such a behaviour in this study is not clear and further investigation is needed. Overall, the percentage removal of As(V) reached a high value of 29.4% at 120 min for *Ed*, and 82.3% at 240 min for *Mq*.

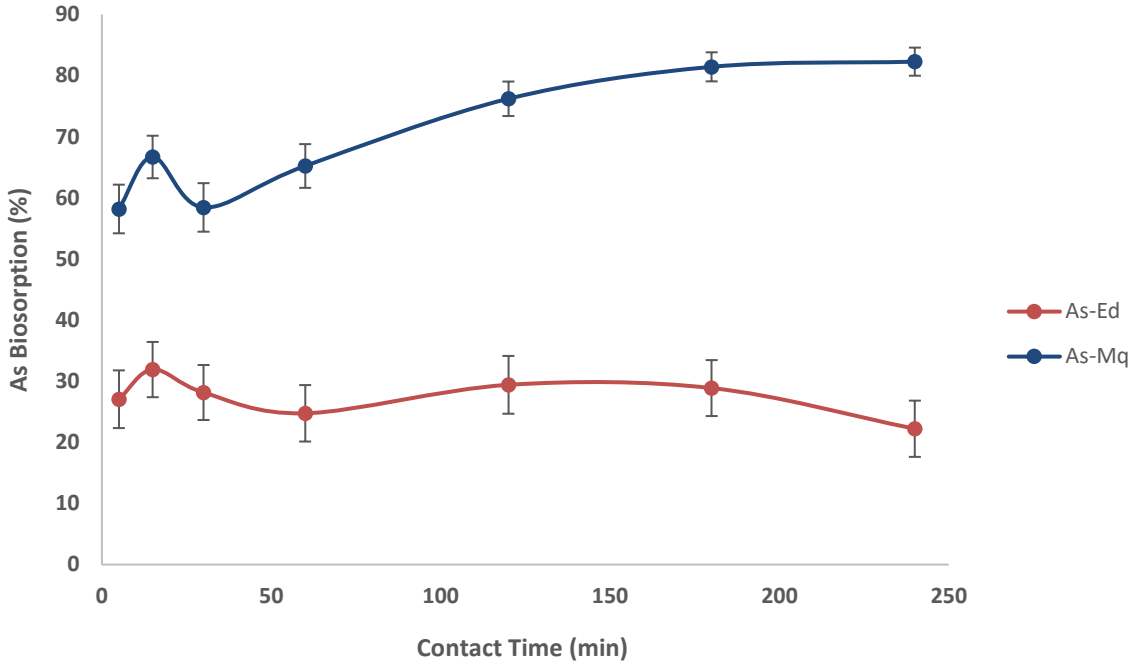

Figure 3.12 Effect of contact time on the adsorption of As(V) by *Ed* and *Mq* barks (conditions: mass of adsorbent=250 mg, volume of As(V) solution=25 mL, initial As(V) solution concentration=100 ppb, temperature=23±2 °C, and pH 4 for *Mq* and pH 5 for *Ed*).

The rapid adsorption at the initial contact period could have arisen from the availability of a more than required number of active sites on the surface of bark (Kannan and Veemaraj, 2010). However, over a longer time, the removal process becomes harder due to decreasing active sites on bark. Furthermore, sorption on bark might be a two-step process including firstly a very fast adsorption of certain ion on the external accessible surface sites of the sorbent, and then a slower intraparticle diffusion within a porous sorbent structure (Simeoni, 2003, Afroze *et al.*, 2016). As the maximum percentage removal of As(V) occurred at 120 min for *Ed* at pH 5, and at 240 min for *Mq* at pH 4, those contact times were chosen for the next set of experiments.

3.3.2.2.3 Effect of Biosorbent Dosage on Arsenic Biosorption

The adsorption of As(V) by selected barks was conducted with sorbent doses from 0.0625-0.500 g (2.5–20 g/L) under the previously found optimum conditions of 120 min contact time and pH 5 for *Ed*, 240 min and pH 4 for *Mq*, and initial As(V) concentration of 100 µg/L. The effect of biosorbent dosage on As(V) removal percentage (Equation 3.5), and the amount of As sorbed by bark (sorption, Equation 3.3), is shown in Figure 3.13. Here, the biosorption percentage of arsenic gradually increased with increasing dosage of bark, while the sorption efficiency decreased. The percentage removal of As was found to increase from approximately 44.7% to 79.2% for *Mq* and 27.9% to 32.2% for *Ed*.

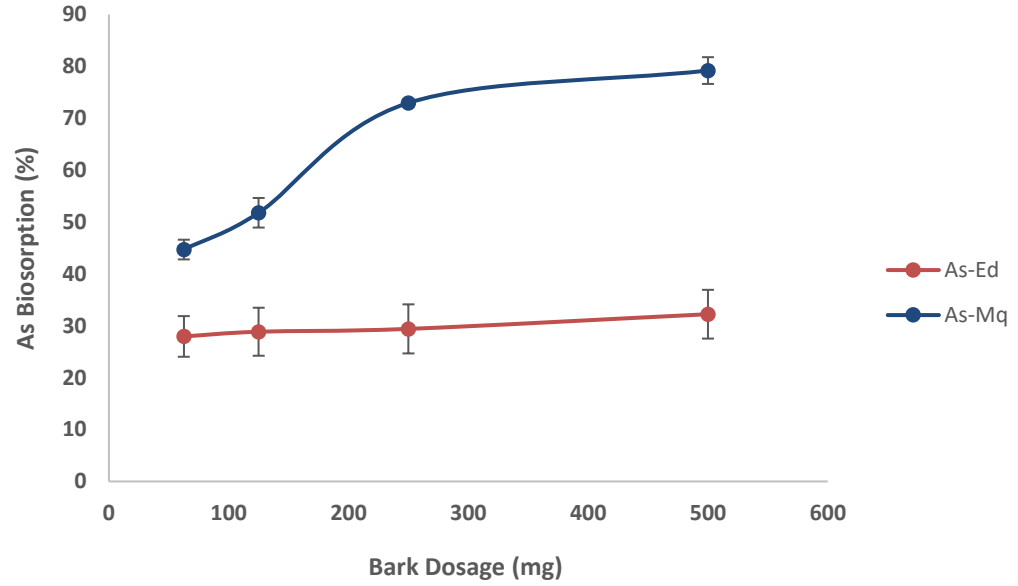

(a)

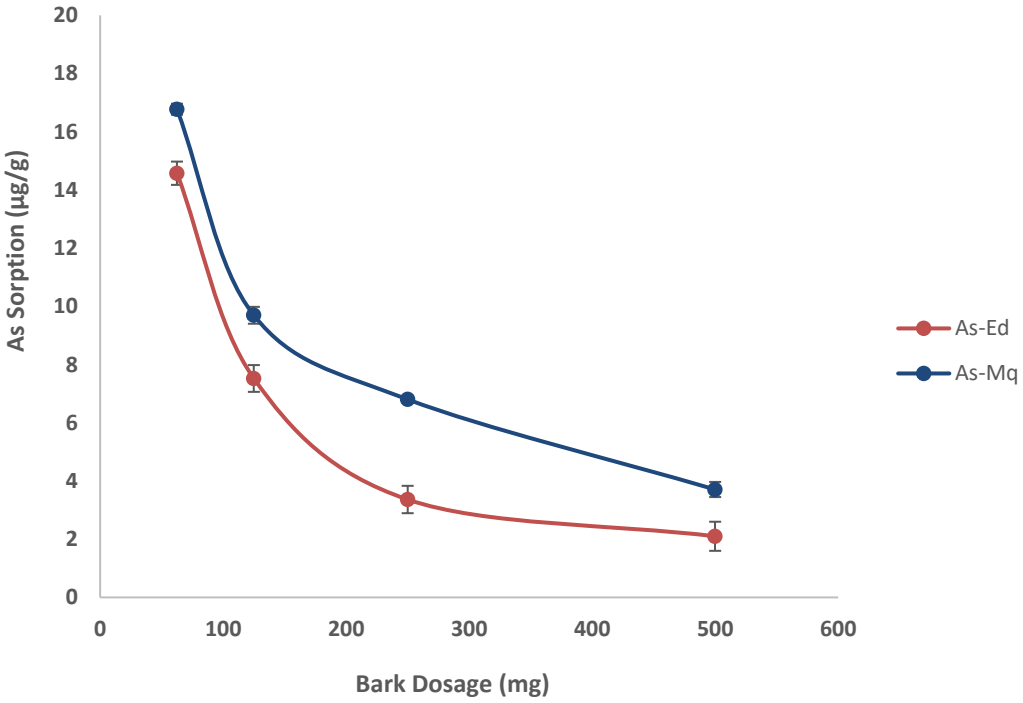

(b)

Figure 3.13 Effect of bark dosage on the (a) biosorption% of As(V) and(b) sorption (µg/g) by *Ed* and *Mq* barks (conditions: volume of As(V) solution=25 mL, initial As(V) solution concentration=100 ppb, temperature=23±2 °C, pH 4 and contact time 240 min for *Mq*, and pH 5 and contact time 120 min for *Ed*).

Very likely, by increasing the biosorbent dosage, surface area and the number of available active sites for elemental adsorption rapidly increase (Kannan and Veemaraj, 2010). Thus, the removal percentage increases with increasing sorbent dosage. However, in a fixed volume of solution, the amounts of ions sorbed on unit mass of sorbent reduce with increasing sorbent mass and therefore, a decrease in sorption efficiency occurs. This is probably due to the dissimilar concentration between solute concentration, in the solution and in the surface of the sorbent (Afroze *et al.*, 2016).

The maximum biosorbent dosage for 25 mL of 100 µg/L As(V) was found to be 500 mg (20 g/L) for both *Ed* and *Mq* bark. For this reason, the optimum dosage of 500 mg was selected for the following sections.

3.3.2.2.4 Effect of initial As(V) Concentration on Biosorption; Sorption Capacity Using Isotherms

A range of As concentrations from 10 µg/L to 100 mg/L was used to assess the effect of element concentration on arsenate biosorption to barks, while other parameters (bark dosage 20 g/L, pH 4 and contact time 240 min for *Mq*, and pH 5 and contact time 120 min for *Ed*) were kept unchanged. The results, as shown in Figure 3.14, indicate that (a) the percentage removal of As gradually decreased with increasing initial As(V) concentration from 10 µg/L to 100 mg/L, while (b) the amount of As adsorbed increased with increasing initial concentration of As(V).

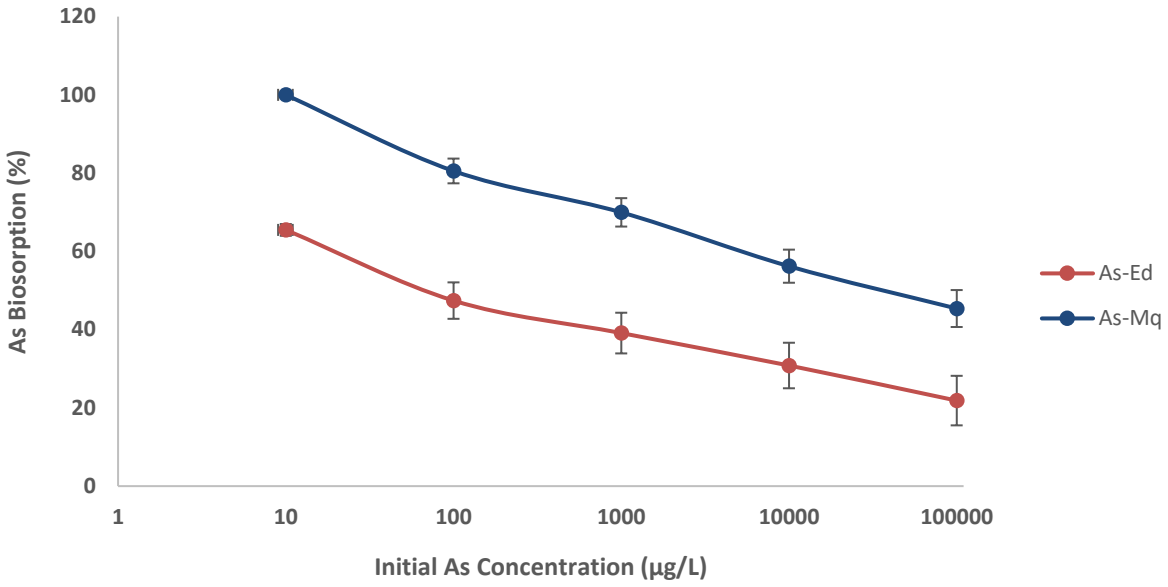

(a)

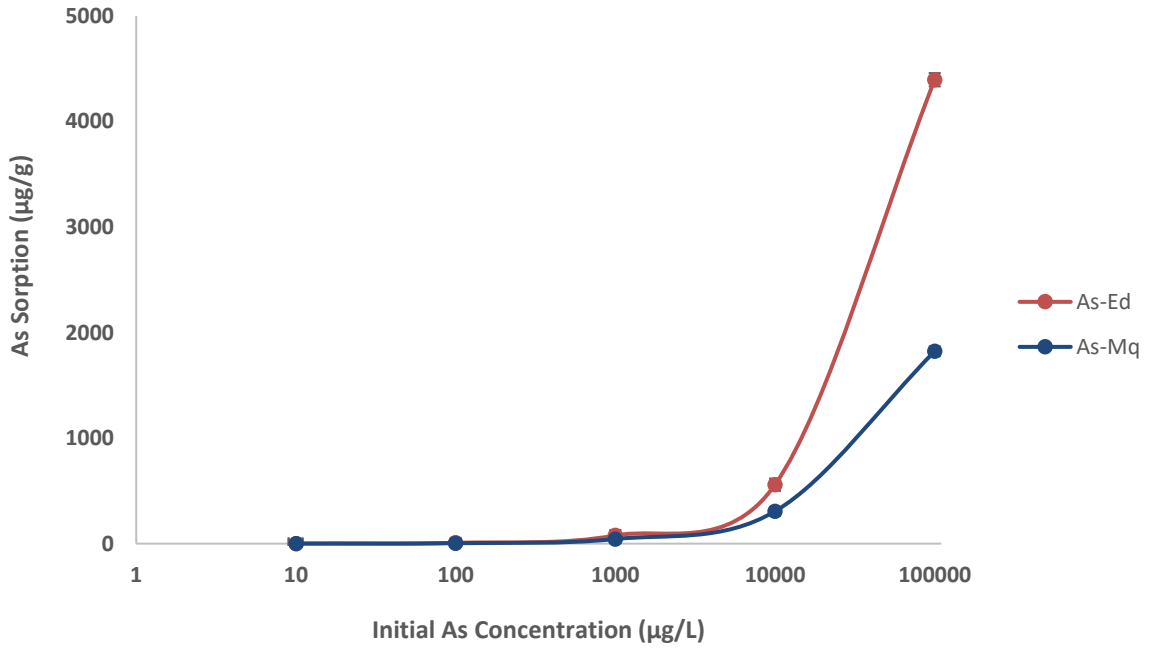

(b)

Figure 3.14 Effect of initial As concentration (µg/L) on (a) biosorption% of As(V) and (b) sorption (µg/g) by *Ed* and *Mq* barks (conditions: volume of As(V) solution=25 mL, bark dosage 0.25 g, temperature=23±2 °C, pH 4 and contact time 240 min for *Mq*, and pH 5 and contact time 120 min for *Ed*).

According to results in Figure 3.14(a), the As biosorption percentage decreased from 100% to 45.4% using *Mq* bark, and decreased from 65.5% to 21.9% when *Ed* bark was used. This is more likely due to the limited number of available active sites on the bark surface as part of the fixed dosage of bark used in the experiment. Therefore, increasing the initial As concentration reduced the capability of biosorption (Kannan and Veemaraj, 2010).

In Figure 3.14(b), by increasing the initial As(V) concentration from 10 µg/L to 100 mg/L, the amount of As(V) sorption (µg/g) on *Ed* bark was observed to increase from 0.74 µg/g to 1822.4 µg/g (1.82 mg/g), while *Mq* bark showed an increase from 1.00 µg/g to 4395.65 µg/g (4.40 mg/g). These results are in a good agreement with other studies (Ranjan *et al.*, 2009, Wang *et al.*, 2015, Afroze *et al.*, 2016), which indicated that the uptake of metal ions (sorption capacity) increased when the initial ion concentration increased. This could be due to a higher amount of As sorbed from a more concentrated solution as a result of increasing the interaction between As ions with sorbent, reducing the mass transfer resistance (Ranjan *et al.*, 2009, Wang *et al.*, 2015, Afroze *et al.*, 2016).

3.3.2.3 Adsorption Kinetics and Mechanism

In the present study, the adsorption kinetics of As(V) on *Ed* and *Mq* bark were investigated to evaluate the applicability of the Lagergen pseudo-first order (Equation 3.7), and Ho pseudo-second order (Equation 3.8), kinetic models using experimental data at various time points.

As noted in Section 3.2.5, in the pseudo-first order kinetic model, the values of K_1 (1/min) and q_e (µg/g) can be determined by the slope of a linear $\ln(q_e - q_t)$ versus t, which is shown in Figure 3.15 (a) for *Ed* and (b) for *Mq*. The values of determination coefficient (R^2) for the plots were 0.1948 for *Ed* and 0.873 for *Mq*, which are not adequately high. Additionally, the calculated amount of As sorbed per mass unit of bark (equilibrium sorption capacity, q_e) obtained from

this model (0.45 µg/g for Ed and 4.79 µg/g) are not robust enough in comparison with the experimental amount of sorbed As (3.83 µg/g and 7.72 µg/g). Therefore, the sorption process did not follow a pseudo-first order sorption rate.

In pseudo-second order kinetic model, the value of q_e (µg/g) and k_2 (g/(µg min)) could be determined from the slope and intercept of a linear t/q versus t plot, which is shown in Figure 3.16 for both *Ed* and *Mq*. The straight lines for both bark can confirm the applicability of the pseudo-second order model. The determination coefficient (R^2) of this model was found to be 0.9697 for *Ed* and 0.9960 for *Mq*, and the amount of As sorbed from this model was estimated to be 3.11 µg/g for *Ed* and 7.93 µg/g for *Mq*. Thus, the pseudo-second order model can better represent the sorption kinetics. This supports that the rate of the sorption procedure might be controlled by chemical process.

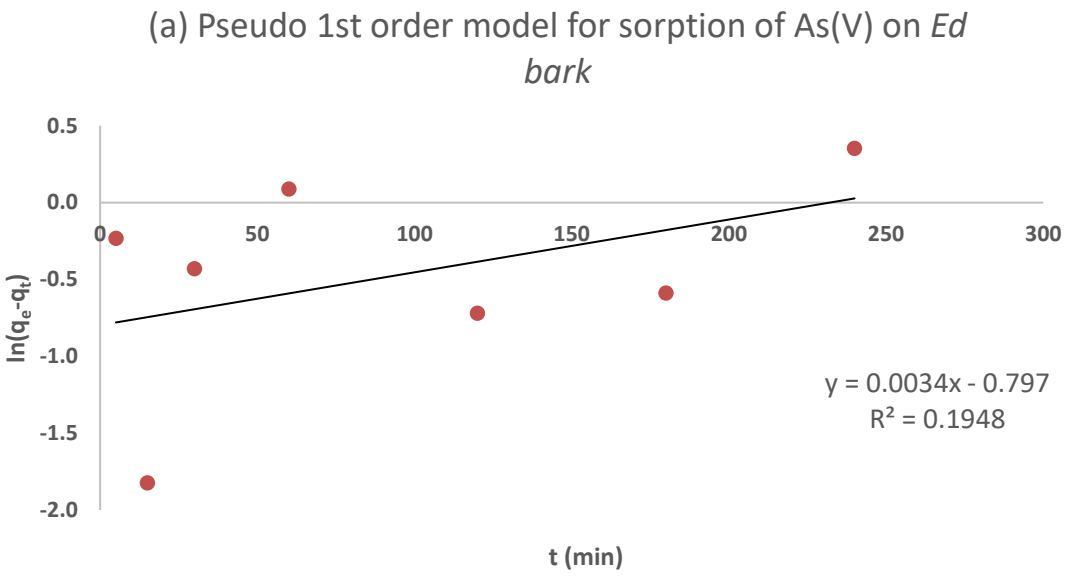

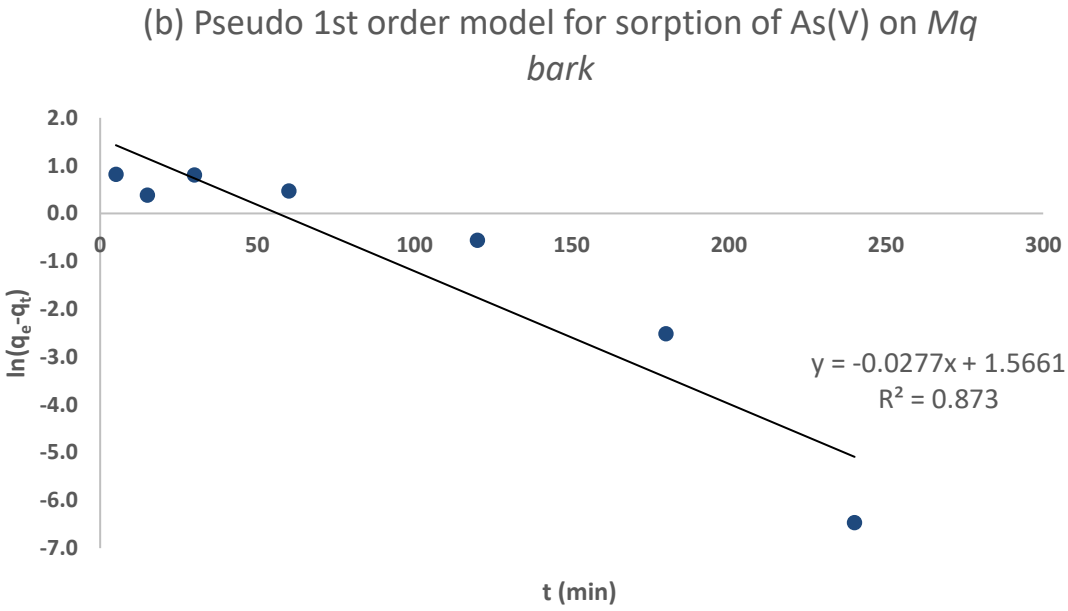

Figure 3.15 Pseudo-first order model of As(V) sorption by (a) *Ed*, and (b) *Mq* barks (conditions: mass of adsorbent=250 mg, volume of As(V) solution=25 mL, initial As(V) solution concentration=100 ppb, temperature=23±2 °C, and pH 4 for *Mq* and pH 5 for *Ed*).

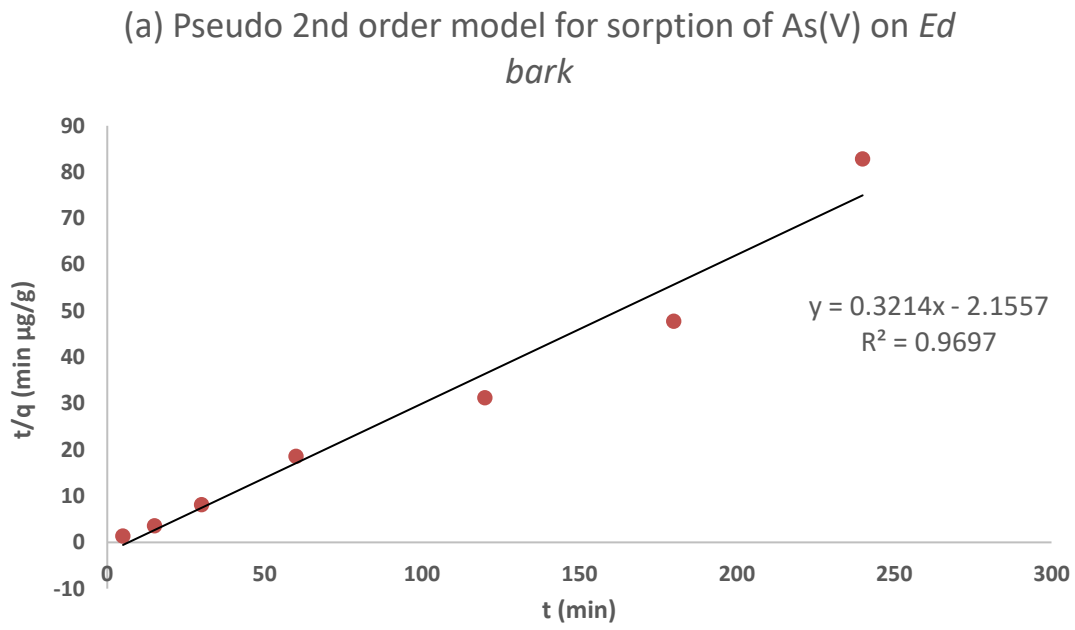

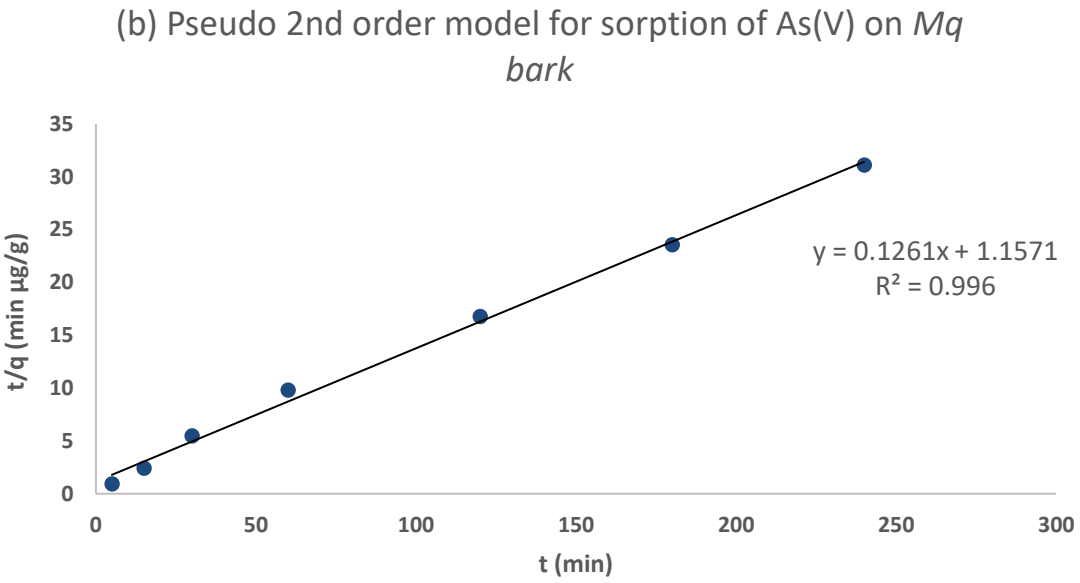

Figure 3.16 Pseudo-second order model of As(V) sorption by (a) *Ed*, and (b) *Mq* barks (conditions: mass of adsorbent=250 mg, volume of As(V) solution=25 mL, initial As(V) solution concentration=100 µg/L, temperature=23±2 °C, and pH 4 for *Mq* and pH 5 for *Ed*).

3.3.2.4 Adsorption Isotherm Studies

The capacity of the sorbent and the mechanism of the adsorption could be determined using equilibrium studies. Hence, the experimental data were fitted to the most common isotherm models of Langmuir, Freundlich and Sips within the As(V) concentration range of 10 to 100000 µg/L (10 µg/L to 100 mg/L) at equilibrium time 120 min for Ed and 240 for Mq using Figure 3.12, and isotherm parameters were evaluated. Then linear regression analysis was used to find the best fitted isotherm. Additionally, the non-linearized form of the Sips isotherm model was performed as a trial and error procedure using solver add-in, Microsoft Excel to evaluate the data from linear form (Kumar and Porkodi, 2006). The Solver function by employing an iterative least square can produce the optimum fitness between experimental data and theoretical model function describing data (Brown, 2001, Wong *et al*., 2004).

As noted in Section 3.2.5, in the Langmuir isotherm model, adsorption occurs homogenously on the active sites of the sorbent containing fixed numbers of similar sites with no transmigration of sorbate inside the surface (Afroze *et al.*, 2016). The maximum adsorption capacity, q_{max} (mg/g) and *b* values for Langmuir constants (Figure 3.17) were obtained from the slope and intercept of a linear $1/q_e$ versus $1/C_e$ using Equation 3.1. Accordingly, from Figure 3.17, the high value of linear correlation of determination (R^2) of the Langmuir isotherm is 0.9908 for *Ed* and 0.9905 for *Mq*, indicating the possibility of application of this model. The calculated values for Langmuir show that the monolayer capacities of *Ed* bark were 24.3 µg/g, and of *Mq* bark was 31.2 µg/g. These results indicated that monolayer adsorption capacity (µg/g) of *Mq* was higher in compared to *Ed*. Nevertheless, in Figure 3.17, the first three data points were mainly clumped together, therefore the high value of R^2 might be not accurate. For this reason, subsequently, other isotherm models were investigated.

In the Freundlich isotherm model, the *n* and *k* values, from Equation 3.2 could be obtained respectively from slope and intercept of a ln q_e versus ln C_e. The sorption equilibrium data

were fitted with experimental data for both *Ed* and *Mq* bark, and the obtained results are presented in Figure 3.18. The high value of linear correlation of determination (R^2) of the Freundlich isotherm is 0.972 for *Ed* and 0.9847 for *Mq* bark (Figure 3.18).

According to Demiral et al., (2008), the Freundlich constant (n) is an amount for measuring sorption affinity of the sorbent for a metal(oid) ion in solution. According to Demiral *et al.* (2008) and Afroze *et al*. (2016), a numerical value of 1/n for the sorbents greater than one indicates that the sorbent will favourably sorb a metal ion. In this study, the value of 1/*n* for *Ed* is 1.45, and for Mq is 1.41, which are greater than one, thus these barks have great potential for As(V) sorption.

In the Sips model, q_{max}, n and K_s were obtained from the nonlinear model using solver add-in function of the Microsoft Excel. Figure 3.19 shows the linear form of the Sips model obtained from the plot of $ln(q_{max}K_s/q_e)$ versus $ln(C_e)$ from Equation 3.3. Examination of data shows that the Sips model can well describe the sorption of As(V) on both *Ed* and *Mq* bark over the concentration ranges studied. Compared to Langmuir model in Figure 3.17, all data points in the Sips model, Figure 3.20, are well recognisable. The value of linear correlation coefficients (R^2) of the Sips isotherm is 0.98 for *Ed* and 0.99 for *Mq*, indicating the good fit of this model. Moreover, the value of exponent *n* for the Sips model is close to 1, therefore the sorption is relatively homogeneous (Kumar and Porkodi, 2006, Ebrahimian *et al*., 2014). In addition, the values of the maximum sorption capacity, q_{max}, obtained using the Sips equation are close to those evaluated using the Langmuir model.

All results for parameters obtained based on the Langmuir, Freundlich and Sips models for the sorption of As(V) on Ed and Mq bark are presented in Table 3.6.

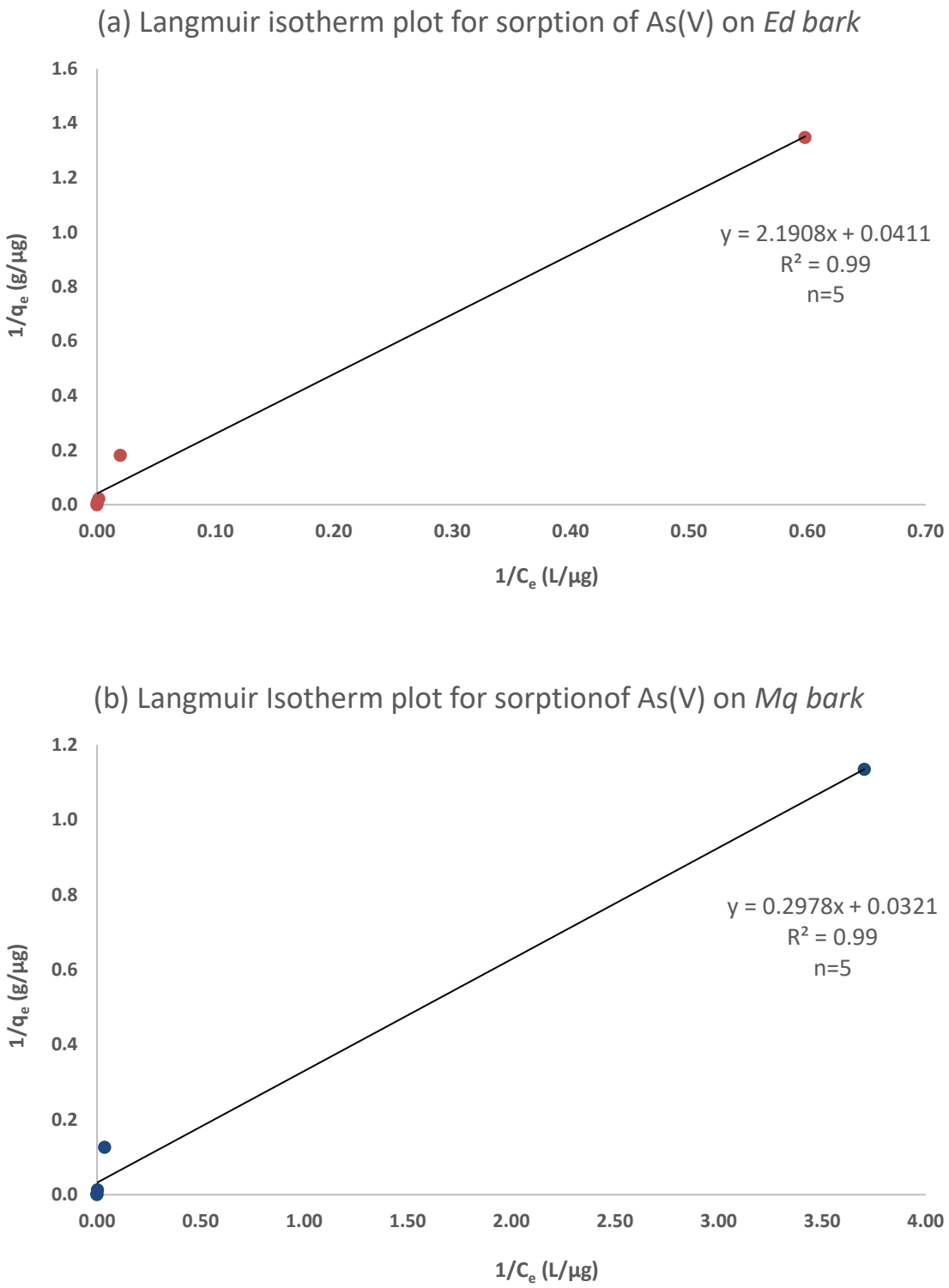

Figure 3.17 Langmuir isotherm model of As(V) sorption by (a) *Ed*, and (b) *Mq* barks (conditions: mass of adsorbent=250 mg, volume of As(V) solution=25 mL, initial As(V) solution concentration=10, 100, 1000, 10000, and 100000 µg/L, temperature=23±2 °C, and pH 4 and 240 min for *Mq* and pH 5 and 120 min for *Ed*).

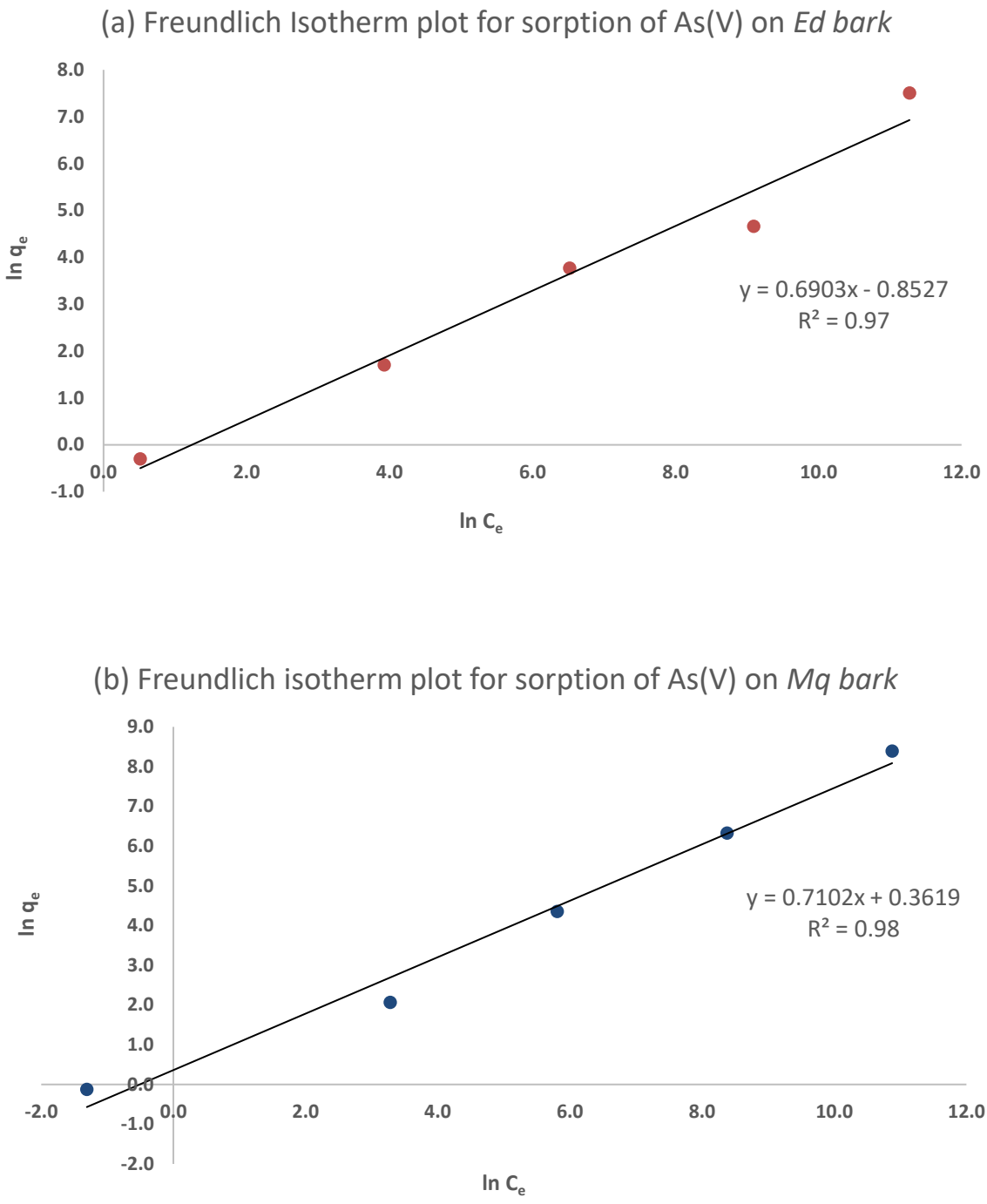

Figure 3.18 Freundlich isotherm model of As(V) sorption by (a) *Ed*, and (b) *Mq* barks (conditions: mass of adsorbent=250 mg, volume of As(V) solution=25 mL, initial As(V) solution concentration=10, 100, 1000, 10000, and 100000 µg/L, temperature=23±2 °C, and pH 4 and 240 min for *Mq* and pH 5 and 120 min for *Ed*).

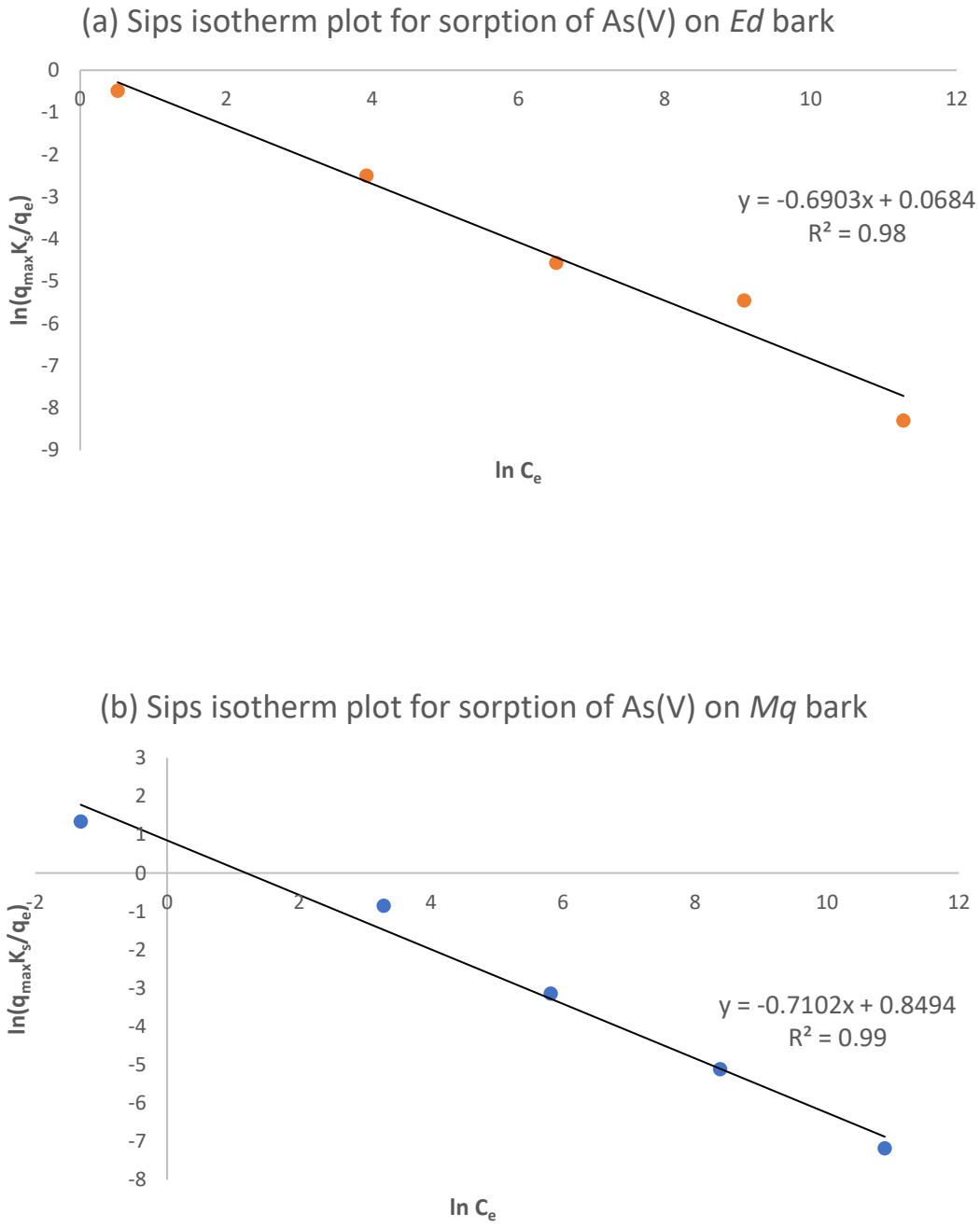

Figure 3.19 Sips isotherm model of As(V) sorption by (a) *Ed*, and (b) *Mq* barks (conditions: mass of adsorbent=250 mg, volume of As(V) solution=25 mL, initial As(V) solution concentration=10, 100, 1000, 10000, and 100000 µg/L, temperature=23±2 °C, and pH 4 and 240 min for *Mq* and pH 5 and 120 min for *Ed*).

Table 3.6 Summary of results for parameters based on the Langmuir, Freundlich and Sips models

Biosorbent	Model	Parameters	Values
Ed	Langmuir	q_{max} (µg/g)	24.3
		b (L/µg)	0.02
		R^2 (5 data points)	0.99
	Freundlich	*k* (L/µg)	2.35
		n	0.69
		R^2 (5 data points)	0.97
	Sips	q_{max} (µg/g)	24.7
		K_s ((L/µg)	0.02
		n_s	1.45
		R_2 (5data points)	0.98
Mq	Langmuir	q_{max} (µg/g)	31.2
		b (L/µg)	0.11
		R^2 (5 data points)	0.99
	Freundlich	*k* (L/µg)	1.44
		n	0.71
		R^2 (5 data points)	0.98
	Sips	q_{max} (µg/g)	31.1
		K_s ((L/µg)	0.10
		n_s	1.41
		R_2 (5data points)	0.99

Based on the larger R^2 in linear forms obtained for both *Ed* and *Mq*, the Sips isotherm models was found to be more suitable biosorption models. However, the R^2 values of Freundlich model for both bark species were still high, especially for *Mq*. Therefore, the As(V) sorption on the surface of the selected bark in solution with higher As concentration is likely to be as a monolayer coverage over the homogeneous surface of bark, whilst in solutions with lower As concentration a multilayer sorption on the heterogeneous surface of bark may have occurred.

3.3.2.5 Comparison of BET, SEM-EDS and FTIR-ATR Results before and after As Sorption on Bark

The BET surface area results for *Ed* and *Mq* bark before and after As sorption are presented in Table 3.7. Evidently, the surface area and pore volume of *Mq* bark before and after As loading was greater than that of *Ed* bark. In addition, after As sorption, surface area and porosity of both *Ed* and *Mq* loaded bark have both decreased. These results could be due to sorption of As on the bark surface as well as inside their pores, which may have blocked some existing pores. Similarly, pore size of both bark species have decreased after As sorption, supporting the possibility of congested of bark pores.

Table 3.7 BET surface area results for *Ed* and *Mq* bark before and after As sorption from 100 mg/L solution

	Raw *Ed*	As-loaded *Ed*	Raw *Mq*	As-loaded *Mq*
BET Surface Area (m^2/g)	0.46	0.14	1.25	0.59
Pore Volume (cm^3/g)	0.004	0.004	0.009	0.008
Pore Size (nm)	6.35	6.02	6.31	5.98

SEM-EDS results for selected bark before and after As(V) sorption are presented in Figure 3.20 and Figure 3.21. Visually, there was little difference in the morphology of bark after sorption. The rough surface and the large number of asymmetric and open pores in both raw and loaded bark appear to be similar. However, in a loaded bark, there seemed to be a decrease in the abundance of open pores due to coverage of As on the surface of selected bark. These results

are supported by the BET surface area results in Table 3.7, which showed decreased surface area and pore volume of selected bark after As(V) sorption.

Analysis of digested bark samples after reaction with 10 g/L As(V) revealed that ~50.5 mg/g and 29.7 mg/g As(V) was detected in the *Ed* and *Mq* bark, respectively. These results are higher than the SEM-EDS detection limit of 3000 mg/kg, however, we were unable to confirm the quantity of As in the bark samples using the EDS due to inaccurate quantitative analysis technique of EDS. More importantly, there is also a possibility of further internal sorbtion rather than just surface sorption of As by bark. This suggestion was confirmed by Freundlich isotherm model discussed above, which indicated a multilayer sorption on the heterogeneous surface of bark.

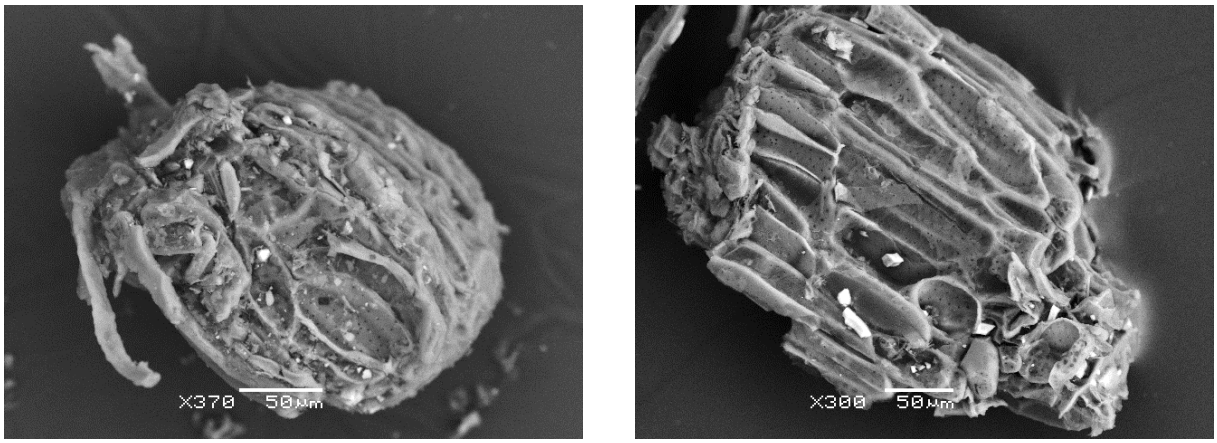

Figure 3.20 Scanning electron micrographs of *Ed* bark: left) before As sorption, and right) after As sorption.

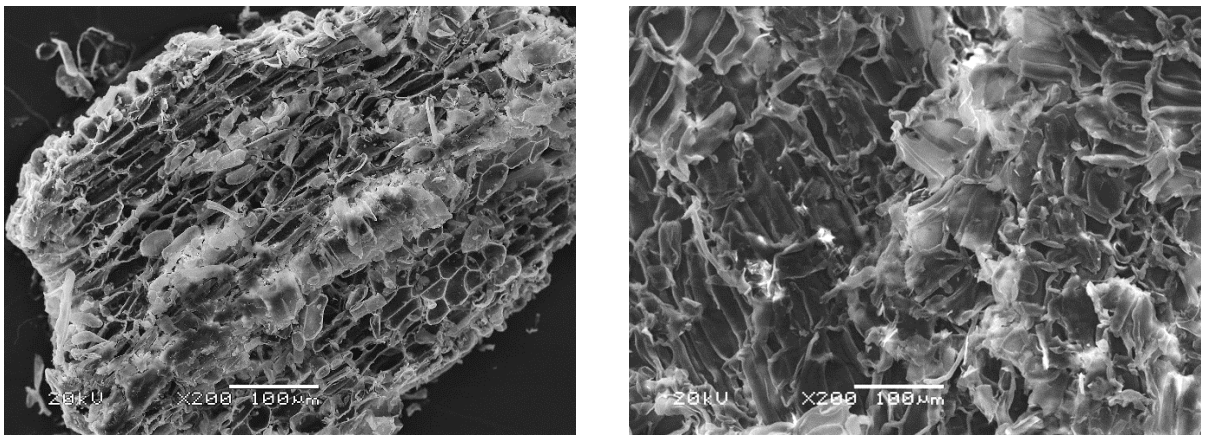

Figure 3.21 Scanning electron micrographs of *Mq* bark: left) before As sorption, and right) after As sorption.

FTIR-ATR was used to study bark samples before and after As sorption and the spectra obtained are displayed in Figure 3.22 and Figure 3.23. There was very little change in both intensity and shift in bands in the spectrum of As-loaded bark compared to raw bark. Regardless of correcting the baseline before every sample, the little changes in intensity and shift in band might be still within instrumental error. However, if those small changes are accepted to be significant, the following description may well be obtainable. As discussed in Section 3.3.2.1.4, the broad and strong peaks at 3331.38 cm^{-1} in the spectrum of raw *Ed* and 3334.96 cm^{-1} in the spectrum of raw *Mq* indicated the presence of possibly hydroxyl and/or amide groups (Mishra *et al.*, 2010, Afroze *et al.*, 2016). These peaks were observed to have shifted to 3332.51 cm^{-1} in the spectrum of As-loaded *Ed* and 3335.64 cm^{-1} in the spectrum of As-loaded *Mq*. In addition, the spectra of the raw *Ed* and the As-loaded *Ed* in Figure 3.22 showed the 1609.06 cm^{-1} peak in the former has shifted to 1606.71 cm^{-1} in the latter and its intensity has also increased. The peak at 1513.55 cm^{-1} shifted to 1508.96 cm^{-1}, while the peak at 1029.38 cm^{-1} shifted to 1025.94 cm^{-1}. Pandey *et al.*, (Pandey *et al.*, 2009), reported that the absorption in the region between 1080 and 1300 cm^{-1} indicated acidic groups in the biomass, while the absorption in the region of 1020–1340 cm^{-1} is associated with amine groups. Therefore, after As binding, any change in intensity and shift in bands in these regions of spectrum may correspond to the exchange of amine and or carboxylic groups by the As(V) (Pandey *et al.*, 2009).

Similar results were obtained for *Mq* bark as well. For example, in the spectra displayed in Figure 3.23, the intensity of band at 1595.57 cm^{-1} increased, accompanied by a shift to 1592.25 cm^{-1} after As loading. Additionally, increased intensity and a shift of the band at 1239.70 cm^{-1} to 1241.63 cm^{-1} were observed. These results indicated that the chemical interactions between the As(V) ions and the carboxyl and amine groups of the biomass might be involved in the biosorption.

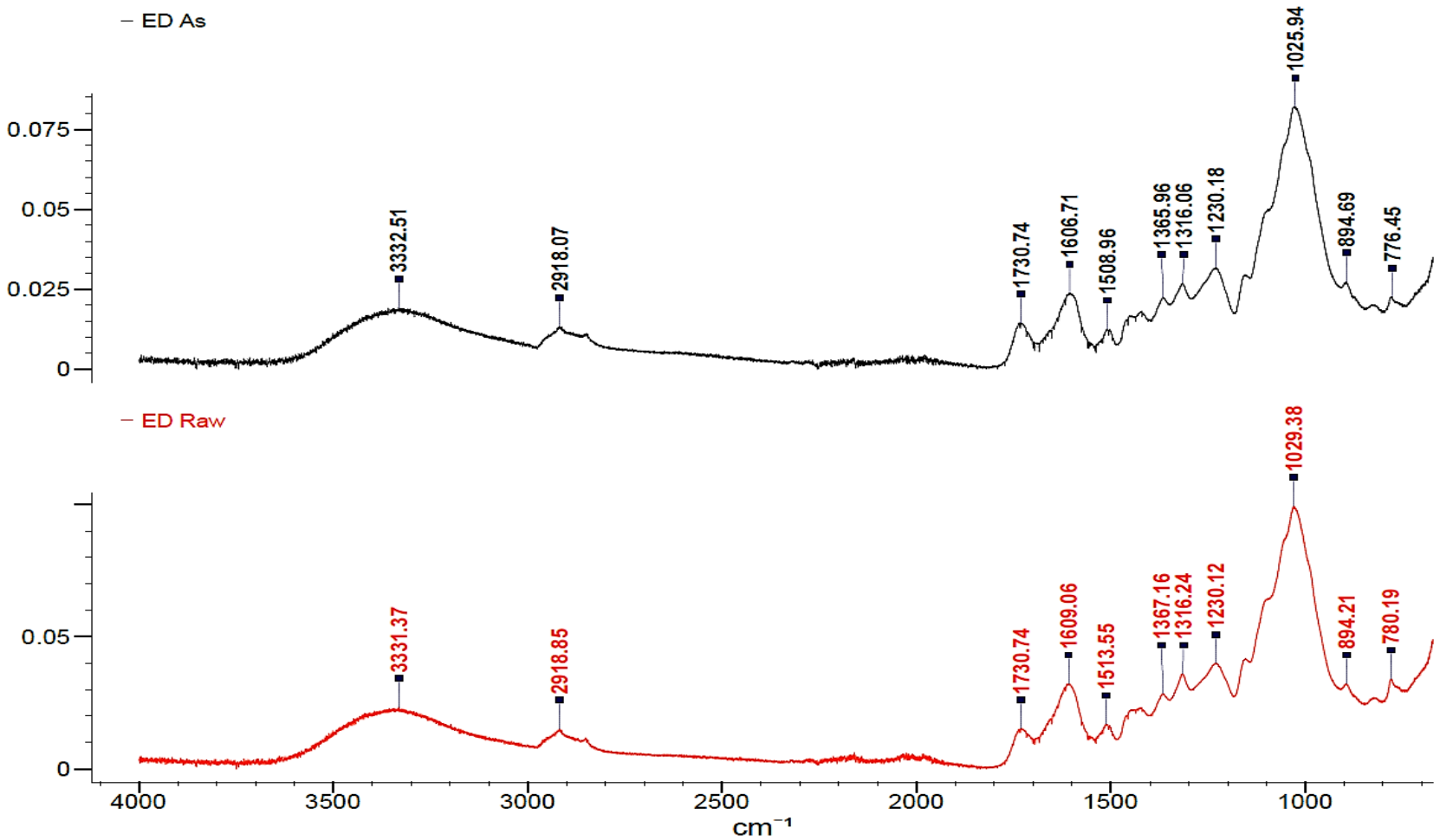

Figure 3.22 FTIR-ATR spectrum of *Ed* bark following As sorption (black), compared to raw bark (red).

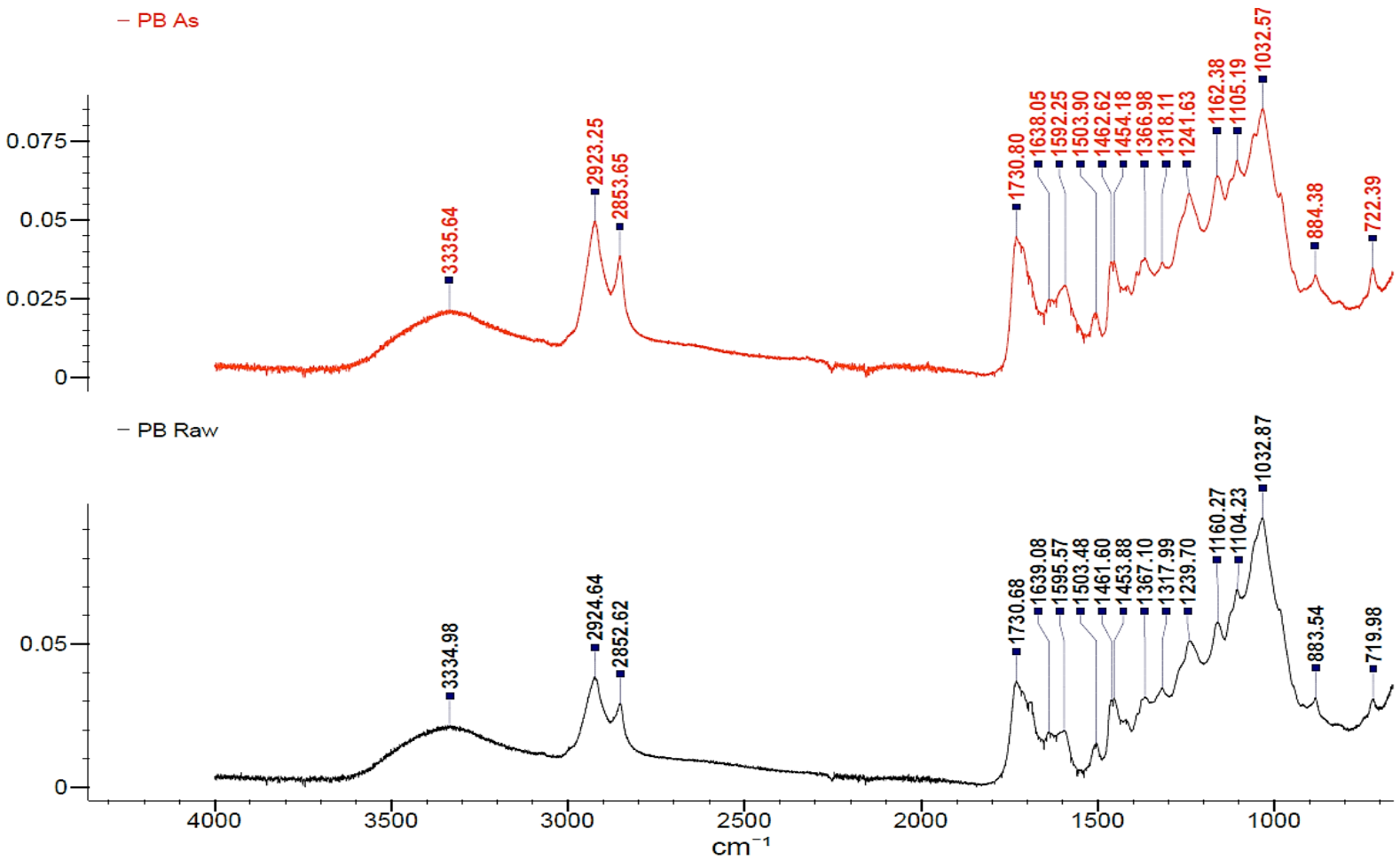

Figure 3.23 FTIR-ATR spectrum of *Mq* bark following As sorption (red), compared to raw bark (black).

3.3.2.6 Desorption and Regeneration Studies

Desorption of loaded bark facilitates re-use of the bark and recovery of sorbed materials. The results of desorption studies conducted in the presence of a list of electrolytes at 0.1 M each are tabulated in Table 3.8. Hence, the desorption percentage for each eluting agent was evaluated based on the ratio of the final released As(V) concentration to the initially sorbed concentration of As(V) as a percentage. Overall, less than 30% of As was desorbed from selected bark, with the lowest percentage obtained in the presence of neutral solutions of Milli-Q water and NaCl. In general, the acidic electrolytes were more effective for As removal in comparison to the alkaline Na_2CO_3 solution. Approximately 26% of the bound As(V) was recovered from *Ed* and 27% from *Mq* bark using HCl. The effectiveness of acidic electrolytes may be associated with metal desorption (Lorenzen *et al.*, 1995). Therefore, in a strong acidic condition As may be easily desorbed when Fe desorption has similarly occurred. Overall, the low desorption % of As(V) from *Ed* and *Mq* bark using selected 0.1 M electrolytes, may suggest the presence of a strong binding affinity, probably as a complex and/or ligand, between As(V) and bark composition (*i.e.*, Fe or some functional groups).

Regenerating or reusing the bark requires that the bound As(V) be eluted from the bark. However, as a result of low percentage desorption of As and low value of bark as a solid waste, regeneration of bark could be insignificant.

Table 3.8 Percentage of Sorption and Desorption of As(V) from *Ed* and *Mq* bark (As concentration of 100 ppm for sorption, and electrolyte concentration of 0.1 M for desorption)

Biosorbents	**Concentration of As(V) sorbed / mg/L**	**Sorption / %**	**Desorption / %**					
			Milli-Q water	NaCl	NaOH	Na_2CO_3	HCl	HNO_3
Ed	18.2	21.86	2.70	3.09	3.53	15.57	26.07	17.86
Mq	32.0	38.37	2.00	4.00	0.94	13.04	29.66	22.66

3.3.2.7 Comparison of Sorption Capacity of *Ed* and *Mq* bark with Other Sorbents

This study revealed the efficiency of the selected bark, *Ed* and especially *Mq*, as potential biosorbents for the removal of As(V) from aquatic solutions. The sorption capacity (q_m, mg/g) of arsenic in this study was found to be 1.82 mg/g using *Ed* bark at pH 5 and 4.40 mg/g using *Mq* bark at pH 4 at an initial As(V) solution of 100 mg/L. In Table 3.9, the sorption capacities from this study have been compared with other reported sorbents. The experimental data of the present study are comparable to data obtained by several other agricultural solid wastes and activated carbon adsorbents.

Table 3.9 Comparison of adsorption capacity (q_m in mg/g) of different sorbent for removal of As(V)

Sorbent	Sorbent Capacity / mg/g	References
***Ed* bark**	1.82	Present study
***Mq* bark**	4.41	Present study
Carbon, coconut shell	2.40	(Lorenzen *et al.*, 1995)
Orange juice residue	67.43	(Ghimire *et al.*, 2002)
Biomass, yeast	3.75	(Seki *et al.*, 2005)
Lamarak seed powder	2.14	(Kumari *et al.*, 2006)
Rice polish	0.15	(Ranjan *et al.*, 2009)

3.4 Application of Bark for the Removal of Arsenic from Fly Ash Leachate

In a set of batch sorption experiments (Section 3.2.8), *Ed* and *Mq* barks were used to remove As(V) from selected acidic and alkaline fly ash leachates. Optimum conditions determined above for As(V) biosorption were adopted for work involving either bark. For example, to remove As(V) from leachate, the pH of each leachate was maintained at 5 when using *Ed* bark as sorbent, and 4 for the *Mq* bark. Additionally, after adding 1 g of each bark separately into 50 mL of leachate (20 g/L), the experiment was completed in 120 min (2 h) when using *Ed* bark, and 240 min (4 h) when using *Mq* bark. The amount of initial As(V) in µg/L for 50 mL of 4 samples of each selected fly ash leachate using data from Table 2.6, along with quantities of final As(V) after biosorption, and percentage removal of As(V) are tabulated in Table 3.10. The results indicate that the percentage of As(V) removal was from approximately 69% to 100% for *Ed*, and 86% to 100% for *Mq*. In most cases, the quantity of As(V) in fly ash leachate samples after sorption experiment were not detectable, therefore, the percentage removal is assumed to be 100%. Another notable observation was that *Mq* bark could remove a higher quantity of As(V) from the same fly ash leachate compared to *Ed* bark, which is in agreement with the result of the higher sorption capacity of *Mq* bark than *Ed* bark, as reported in Table 3.9. As the amount of arsenic in all leachate was in the range of bark biosorption efficiency, such results are encouraging.

Table 3.10 Percentage removal and Concentration of As(V) in 50 mL of fly ash leachates before and after biosorption using *Ed* and *Mq* bark under optimum conditions

Fly ash leachate*	Initial As(V) in leachate / µg/L	Final As(V) in leachate after sorption with *Ed* / µg/L	Removal % using *Ed*	Final As(V) in leachate after sorption with *Mq* / µg/L	Removal % using *Mq*
MPFA-1	58.3	17.9	69.3	ND	100
MPFA-2	27.6	7.5	72.9	3.9	85.9
MPFA-3	37.3	ND	100	ND	100
MPFA-4	50.0	ND	100	ND	100
WWFA-1	40.1	3.4	91.4	ND	100
WWFA-2	81.4	ND	100	0.01	99.99
WWFA-3	80.3	ND	100	ND	100
WWFA-4	81.8	11.1	86.4	1.7	97.9
VPFA-1	15.4	2.3	85.3	1.0	93.4
VPFA-2	16.7	1.6	90.2	0.6	96.5
VPFA-3	21.4	2.2	89.9	0.8	96.5
VPFA-4	16.1	ND	100	ND	100

* In each fly ash leachate the description of numbers are as followed: S:L ratio of leaching, pH, and leaching time

MPFA-1: 10, 7, 1h, MPFA-2: 3, 7, 1h, MPFA-3: 10, 4, 24h, MPFA-4: 10, 7, 24h

WWFA-1: 10, 4, 1h, WWFA-2: 3, 4, 24h, WWFA-3: 3, 7, 1h, WWFA-4: 3, 10, 1h

VPFA-1: 10, 4, 24h, VPFA-2: 10, 7, 1h, VPFA-3: 10, 10, 1h, VPFA-4: 3, 7, 1h

3.5 Concluding Remarks

In this study, *Ed* and *Mq* bark were studied as potential biosorbents for As(V) removal. The arsenic sorption on bark was found to be highly dependent on solution pH. With increases in pH, sorption of As(V) followed several increasing and decreasing trends likely caused by changes of an As-bark bond that may exist as strong inner-sphere covalent bonds and weak outer-sphere hydrogen bonds at different pH conditions. Moreover, the optimum sorption occurred at pH 5 for *Ed* and pH 4 for *Mq* bark. The sorption of As(V) increased with increased bark dosage and contact time, but decreased with increased initial arsenic concentration.

The data for equilibrium sorption showed a good fit to the Sips isotherm models. Thus, the sorption is a monolayer on the homogeneous surface of bark in high concentration of As(V). The highest monolayer adsorption capacity was obtained as 24.7 µg/g at pH 5 for *Ed*, and 31.2 µg/g at pH 4 for *Mq* bark. Moreover, the maximum sorption capacity was found to be 1.2 mg/g for *Ed* bark, and 4.4 mg/g for *Mq* bark at an As(V) solution of 100 mg/L. A pseudo-second-order kinetic model was found to correlate most strongly with the experimental data for As(V) sorption from aqueous solutions. Therefore, surface sorption is an important factor in the arsenic sorption process. Desorption experiments indicated that sorption of As(V) might follow ion-exchange and strong physical-chemical sorption. It may be possible that concentrations of the acidic electrolytes have a positive effect in desorption of As(V).

Removal of As(V) from real-life acidic and alkaline fly ash leachates was conducted using tree bark species of *Ed* and *Mq* under optimised biosorption conditions (bark dosage of 20 g/L, pH 5 and contact time 2 h for *Ed*, and pH 4 and contact time 4 h for *Mq*). The percentage removal from selected fly ash leachates was greater than 70% and potentially reached up to 100%. Overall, the present study has demonstrated that the *Ed* and *Mq* bark may be effective sorbents for As(V) removal from other aqueous waste systems as well as fly ash leachate.

Chapter 4

Assessing Tree Barks as a Se Biosorbent

4.1 Introduction

Based on the findings reported in Chapter 3, a series of adsorption experiments was conducted on a range of barks to assess the significance of bark-type, pH, time, biosorption dosage, and selenium(IV) concentration on selenite adsorption to bark surfaces. In our work, the outer barks of several different species were collected on-site from the Macquarie University campus (North Ryde, NSW, Australia) and examined to determine their suitability for the adsorption study. The relative concentrations of all elements were determined using inductively coupled plasma-mass spectrometry (ICP-MS), except Se, which was analysed by hydride generation atomic adsorption spectrophotometry (HG-AAS).

Specifically, work conducted in this Chapter was aimed at:

- determining the extent of potential adsorptive competition for selenite between collected barks. This study will also target at comparing the adsorption capacities of Se(IV) on bark in a single-species system.
- assessing how changes in pH, time, bark dosage and elemental concentration influence biosorption in isothermal and kinetic experiments.
- determining the desorption of Se such that the bark can be regenerated.
- investigating the utility of bark in Se adsorption from fly ash leachate samples.

4.2 Experimental Method

Se biosorption experiments were predominantly performed on bark samples collected from three selected species, *Eucalyptus deanei* (*Ed*; Mountain Blue Gum), *Lophostemon confertus* (*Lc*; Brush Box) and *Melaleuca quinquenervia* (*Mq*; Broad-leaved Paperbark). During our experiments, the quantity of Se in bark before and after sorption was determined, along with comparisons of the physical and chemical properties of bark before and after Se sorption. The optimum condition of Se sorption for each kind of bark was determined, and finally, the possibility of reusing Se-loaded bark after Se removal was examined.

4.2.1 Biosorbents Collection and Preparation

Outer bark samples were collected from the campus grounds of Macquarie University, Sydney, NSW, Australia under the same conditions and procedures outlined in Figure 3.2. This study investigated biosorption of Se using the thick outer bark of *Ed*, *Lc* and *Mq* species (Figure 3.4 of Chapter 3).

In brief, bark samples were washed several times with both tap water and distilled water before being cut into small pieces and dried at room temperature for 7 days. For Se sorption experiments, dried barks were pulverised and sieved to obtain a particle size between 150 - 710 μm. To protect against contamination or moisture, the pulverised barks were stored in sealed plastic bags until use.

4.2.2 Biosorbents physical and chemical properties

Using the procedures outlined in Section 3.2.2, physical properties including size, surface area, pore size and morphology of unloaded and Se-loaded bark were determined by sieves with

known mesh numbers, Brunauer-Emmtt-Teller (BET) surface area analysis and scanning electron microscopy with energy dispersive spectrometery (SEM-EDS). In addition, elemental analysis of bark samples was performed using energy dispersive X-ray fluorescence (EDXRF) for total concentration of Fe, As, Se, Cu, Ca, Zn and Mn, a CHN analyser for carbon, nitrogen and hydrogen, and atomic adsorption spectroscopy (AAS) with a hydride generation accessory (HG-AAS) for Se determination. Further, Fourier-transform infrared spectroscopy with attenuated total reflectance (FTIR-ATR) was used for identifying basic functional groups in bark as explained in Section 3.2.2. Meanwhile, it will be also reported in Chapter 4 a modified procedure for Se analysis by HG-AAS due to a required pre-reduction of Se(VI) to Se(IV).

All Se analyses were performed on a 932/933 atomic adsorption spectrophotometer, equipped with a HG3000 atomic hydride generator (GBC Scientific Equipment PtY. Ltd., Victoria, Australia). A Se hollow cathode lamp from Photron Pty. Ltd. was employed as a radiation source (operated at 10 mA). The flame type was air/acetylene with the air flow rate 10.0 L/min and fuel flow rate 1.10 L/min. The analytical range of HG-AAS for these Se experiments was 5 – 100 µg/L (ppb) at a 196.0 nm wavelength. A pre-reduction procedure was performed to reduce all existing Se species to Se(IV). In this procedure, 5 mL of concentrated HCl was added to 5 mL of each sample, blank and standard solution. Each solution was mixed appropriately and heated for 1 h in a 70-80 °C water bath to reduce selenate to selenite (HG-3000-GBC manual). Finally, all samples, blanks and standards were passed through the hydride unit containing a 0.6% sodium borohydride solution and concentrated HCl. As mentioned in Section 4.2.2.5, hydride formation occurs when Se(IV) in an acidic solution reacts with $NaBH_4$ according to the following reaction:

$$3NaBH_4 + 4H_2SeO_3 \rightarrow 4SeH_2(g) + 3H_3BO_3 + 3NaOH$$

Selenite, Se(IV), is presented in solution as $HSeO_3^-$ and SeO_3^{2-} from selenious acid (H_2SeO_3) with pKa values of $pKa_1 = 2.54$ and $pKa_2 = 7.34$ (Kashiwakura *et al.*, 2011, Selim, 2011).

4.2.3 Analytical Procedures: Acid Digestion

Acid digestion of bark samples was performed by adopting the same procedure outlined in Section 3.2.3. In brief, 10 mL of concentrated HNO_3 was added to 1 g of dried bark sample with a particle size between 150 - 710 µm in a Teflon beaker (Rodushkin *et al.*, 1999). The beaker was covered with a watch glass and left to cold soak for 30 min at room temperature, prior to heating the sample on a hot plate at 120^{o}C for 2 h. After cooling to room temperature, the digested sample was diluted to 100 mL with Milli-Q water, and stored in a sealed plastic bottle at 4°C. If any residue became apparent, the digested sample was centrifuged at 4,000 rpm for 5 min, and the supernatant collected (Rodushkin *et al.*, 1999).

4.2.4 Biosorption and Analytical Procedures: Batch Sorption Experiments

Previous studies (P. Jackson and P. Miller, 1998, Jackson and Miller, 1999, Narukawa *et al*., 2005, Huggins *et al.*, 2007b) indicated that the most abundant selenium species in fly ash was Se(IV). Therefore, a stock solution containing 1000 ppm concentration of Se(IV) was prepared by dissolving anhydrous sodium selenite (Na_2SeO_3; Sigma-Aldrich) in Milli-Q water.

Batch biosorption experiments were performed on *Ed*, *Lc* and *Mq* barks to determine the optimum conditions for Se(IV) removal from synthetic selenite solutions at room temperature (23±2 ^{o}C). All experiments were carried out in 100 mL plastic beakers with 50 mL of a Se(IV) solution under a range of variable conditions, (the initial Se(IV) concentration of 10-200 µg/L, pH 2-11, bark dosage 0.0625-0.500 g in 25 mL with S: L from 1/400 to 1/20) and stirred at 300 rpm for a contact times 5- 1440 min. After sorption equilibrium, the solution was separated from the biomass by filtration (Whatman#1 and 0.45 µm cellulose-acetate membrane). The filtrate was collected and the initial and the final selenium concentrations determined within 24

h by HG-AAS. All samples were prepared in duplicates and the mean result and standard deviation (SD) were recorded. Blank and control bark solutions were also run in parallel.

Batch sorption experiments were carried out to remove Se(IV) from real-life fly ash leachates using the optimum biosorption conditions determined above.

4.2.5 Se(IV) Adsorption Isotherm and Kinetic Experiments

To examine the role of Se(IV) concentration in a sorption process, isothermal experiments were conducted on selected barks following a similar procedure outlined in Section 4.2.4. In brief, 25 mL of Se(IV) solution ranging in concentration from 10 µg/L to 200 µg/L was added to 0.25 g of biomass in 100 mL plastic beakers. The solution was stirred vigorously for 24 h at 300 rpm in order to reach equilibrium (Rajamohan and Rajasimman, 2015). These experiments were performed at an optimum pH and at room temperature (23±2 °C). Solutions of 0.01 M NaOH and HCl were used to adjust the pH as required for each bark type. After 24 h, the solution was separated from the biomass by filtration (Whatman#1 and 0.45 µm cellulose-acetate membrane). The selenium concentrations of initial samples and samples at equilibrium were determined in duplicates within 24 h using HG-AAS. As discussed in Section 1.2.4.2 and Section 3.2.5, the results obtained from isotherm experiments were plotted according to the Langmuir isotherm model (Equation 4.1), the Freundlich isotherm model (Equation 4.2), and the Sips isotherm model (Equation 4.3).

$$\frac{1}{q_e} = \frac{1}{bq_{\max}C_e} + \frac{1}{q_{\max}}; \text{ (plot } 1/q_e \text{ versus } 1/C_e) \qquad \text{Equation 4.1}$$

$$ln\, q_e = ln\, k + n\, ln\, Ce\,; \text{(plot } lnq_e \text{ versus } lnC_e) \qquad \text{Equation 4.2}$$

$$ln(\frac{q_{max}K_s}{q_e}) = -\frac{1}{n_s} ln(C_e) + l\, n(K_s)\,; \text{(plot } ln(\frac{q_{max}K_s}{q_e}) \text{ versus } ln\, C_e) \qquad \text{Equation 4.3}$$

where, q_e is equilibrium quantity of ion adsorbed by the sorbent (mg/g), q_{max} is the theoretical maximum quantity of metal ions (mg/g) likely bound on the surface of biosorbent (monolayer adsorption capacity) at equilibrium, b is the Langmuir constant (L/mg), C_e is the equilibrium concentration of sorbate in liquid phase (mg/L), k is the Freundlich constant (L/mg), n is the Freundlich exponent or biosorption intensity, K_s is the Sips constant (L/g), and n_s is the Sips exponent (Ranjan *et al.*, 2009, Momčilović *et al.*, 2011, Afroze *et al.*, 2016, Ebrahimian *et al.*, 2014). In the Langmuir model, q_{max} and b are correspondingly obtained from the slope and ordinate intercept of a linear $1/q_e$ vs. $1/C_e$ plot, whilst in the Freundlich model, k and n are correspondingly obtained from the slope and ordinate intercept of a linear ln q_e versus ln C_e plot. In the Sips model, q_{max}, K_s and n_s are obtained from the slope and intercepts of a linear $ln(q_{max}K_s/q_e)$ versus lnC_e.

Kinetic experiments were performed to examine the role of treatment time in Se adsorption. In these isothermal experiments, 25 mL of a 100 µg/L Se(IV) solution was added to 0.25 g of biomass in 100 mL plastic beakers and agitated at 300 rpm at room temperature (23±2°C). The sample was stirred vigorously for a desired period between 5 min and 240 min (5, 15, 30, 60, 120, 180, 240 min). Solutions of 0.01 M NaOH or HCl were used to adjust the pH to the desired value. After the selected contact time, the solution was separated from the biomass by filtration (Whatman#1 and 0.45 µm cellulose-acetate membrane). The Se(IV) concentrations of initial samples and samples at equilibrium were determined in duplicates within 24 h using HG-AAS. The quantity of Se(IV) sorbed was then plotted as a function of time to display the equilibration time of the adsorption process, the rate of adsorption and the equilibrium capacity of the adsorbent.

As noted in Section 3.2.5, for kinetic model interpretation, q_t, which is the quantity of Se(IV) sorbed (µg/g) at any time, t (min), q_e or equilibrium sorption capacity (µg/g), and the percentage removal of Se(IV) were evaluated using Equation 4.4, Equation 4.5, and Equation 4.6:

$$q_t = (C_i - C_t) \times \frac{V}{m}$$ Equation 4.4

$$q_e = (C_i - C_e) \times \frac{V}{m}$$ Equation 4.5

$$Removal\ \% = \frac{Ci - Ct}{Ci} * 100$$ Equation 4.6

where, C_i and C_t are the concentration (µg/L) of Se(V) before and after adsorption, respectively, V is the volume of the solution (L) and m is the mass of adsorbent (g). Moreover, the experimental q_e refers to the quantity adsorbed at equilibrium and C_e is concentration at equilibrium that is attained when C_t is constant (Meunier *et al.*, 2003, Gadd, 2009, Ranjan *et al.*, 2009, Hansen *et al.*, 2010, Afroze *et al.*, 2016)

As discussed in Section 1.2.4.1 and Section 3.2.5, Lagergen Pseudo-first order (Equation 4.7) and Ho Pseudo-second order (Equation 4.8) are the two most often applied models for characterising biosorption kinetics:

$$ln(q_e - q_t) = ln\ q_e - k_1 t$$ Equation 4.7

$$t/q_t = (1/k_2 q_e^2) + (1/q_e)t$$ Equation 4.8

where, q_e is the quantity of solute sorbed at equilibrium (mg/g), q_t is the quantity of solute sorbed at any time t, k_1 is the pseudo-first order rate constant (min) and k_2 is pseudo-second order rate constants (g/mg min). The data were then presented as a $ln\ (q_e - q_t)$ versus t plot to estimate k_1 from the slope of the plot, and a as t/q_t versus t plot to estimate k_2 from the slope of the plot (Kalavathy M. Helen *et al.*, 2005, Momčilović *et al.*, 2011).

4.2.6 Se(IV) Sorption Capacity of Bark

The ability of bark species for Se(IV) sorption was determined by adding 500 mg of each bark sample to 25 mL of a 100 ppm Se solution in a 100 mL plastic beaker. All beakers were then

sealed and the content was stirred at 300 rpm for 24 h at room temperature (23±2 ºC). The solution pH was adjusted to optimum value related to the selected bark. These solutions were then filtered using Whatman#1 filters, and the filtered bark washed several times with Milli-Q water. Finally, the solutions were diluted to 100 mL, and stored in plastic bottles at 4ºC. To minimise the errors, experiments were carried out in duplicate and the mean result and standard deviation (SD) were recorded. Moreover, blank and control bark solutions were analysed in similar way. The initial and equilibrium Se(IV) concentrations in each sample were determined within 24 h by HG-AAS.

4.2.7 Desorption of Selenite from Se-loaded Bark

Batch desorption experiments were carried out in 100 mL plastic beakers. In brief, 500 mg of Se-loaded bark was introduced into a 25 mL solution containing each of the following solutions: 0.1 M NaCl, 0.1 M NaOH, 0.1 M $NaHCO_3$, 0.1 M Na_2CO_3, 0.1 M HCl and 0.1 M HNO_3. The solutions were then magnetically stirred at 300 rpm for 60 min at room temperature at 23±2 ºC. Then, the solution was separated from the biomass by filtration and the filtrated bark washed several times until the pH of the washing solution became neutral. The solution was then diluted to 100 mL and stored at 4 ºC. The initial and equilibrium selenium concentrations in each sample were determined within 24 h using HG-AAS.

4.2.8 Removal of Se(IV) from Fly Ash Leachate

To test the practical application of the biosorbent, a set of batch sorption experiments was performed by adding 500 mg of each selected bark to 25 mL of fly ash leachate in 100 mL plastic beakers. After adjusting the pH to the desired value determined from the initial sorption

experiments, the solution was magnetically stirred at 300 rpm. After the optimum contact times for an effective Se removal, the samples were filtered and the concentrations of Se(IV) determined by HG-AAS within 24 h.

4.3 Results and discussion

This chapter sought to determine the quantity of Se(IV) within selected bark species before and after sorption experiments. During the study, we also evaluated the effect of pH, contact time and bark dosage and initial concentration of Se(IV) solutions using kinetic and isotherms models for Se(IV) sorption. Then, we also compared selected physical and chemical properties of bark before and after Se sorption and assessed their application to the removal of Se(IV) from fly ash leachate.

4.3.1 Physical and Chemical Data for Selected Barks

Similar to work reported in Chapter 3, *Ed*, *Lc* and *Mq* outer bark samples were selected for testing Se(IV) sorption. Hence, it was necessary to perform BET surface area, EDXRF, CHN, HG-AAS, SEM-EDS, and FTIR/ATR analysis to determine several physical and chemical characteristics of bark samples prior to Se(IV) adsorption testing. BET surface area, SEM-EDS, and ATR analysis results were then compared to those obtained using Se-loaded bark.

All physical and chemical results related to the selected bark species, *Ed*, *Mq* and *Lc*, before sorption procedure have already been discussed in Section 3.3.2.1. However, a summary of the data is tabulated in Table 4.1. As noted previously, the highest Fe, As, C, N and H content was found in *Mq* bark along with the Ca and Se content. In contrast, a higher Se, Ca and Mn content was determined in *Mq* bark than in *Ed* and *Lc* bark. A comparison in selected physical and

chemical data collected from barks before and after Se(IV) sorption will be discussed further in this chapter.

4.3.2 Selenite biosorption

Selenium sorption experiments were conducted on *Ed*, *Lc* and *Mq* barks in the pH range of 2-11, contact times of 5, 15, 30, 60, 120, 180, 240 and 1440 min, bark dosages of 62.5, 125.0, 250.0, and 500.0 mg/25 mL, and with initial Se(IV) concentrations of 10, 20, 40, 80, 100, 200 and 100×10^3 μg/L. The results will be discussed in detail below.

Table 4.1 Physical and chemical properties of selected bark samples with average size of 150-710 µm.

Bark Sample	BET surface area / m^2/g	Pore size / nm	Pore volume / cm^3/g	EDXRF / cps							CHN / %			HG-AAS /
				Fe	As	Se	Cu	Ca	Zn	Mn	C	N	O	Se
Ed	0.46	6.35	0.004	51.8 (2.4)	0.3 (0.1)	0.3 (0.1)	2.4 (0.1)	18330.6 (9.6)	2.2 (0.1)	19.5 (1.2)	43.5 (0.1)	0.2 (0.0)	5.6 (0.1)	0.5 (0.1)
Lc	0.43	6.30	0.003	233.5 (12.1)	0.5 (0.1)	0.6 (0.1)	9.0 (0.9)	17039.4 (7.5)	22.8 (5.2)	39.6 (2.1)	45.8 (0.2)	0.2 (0.1)	5.9 (0.2)	0.9 (0.1)
Mq	1.25	6.31	0.009	960.9 (23.2)	1.2 (0.3)	0.2 (0.1)	5.6 (0.2)	1650.7 (4.3)	8.8 (1.4)	13.9 (0.6)	60.5 (0.8)	0.3 (0.0)	8.4 (0.1)	0.1 (0.0)

Measurement uncertainty as standard deviation presented in parenthesis for 2 or 3 consecutive measurements

4.3.2.1 pH dependency of Se(IV) binding

The percentage sorption of Se(IV) using *Ed*, *Lc*, and *Mq* barks was estimated in synthetic solutions over a pH range of 2-11. Figure 4.1 shows the relation between Se(IV) biosorption% using the three selected barks, and initial pH of the solutions. These results indicate a somewhat fluctuating behaviour of Se(IV) sorption% for all bark species in response to pH. In general, from pH 2 to 6, the Se(IV) sorption% increased and reached a maximum of 85.8% at pH 6 for *Ed*, 84.5% at pH 5 for *Mq*, and 57.4% at pH 6 for *Lc* bark. Then, with further increases to pH 10, the Se(IV) biosorption% decreased, and then increased once again at pH 11. In summary, the maximum Se(IV) sorption% occurred at pH 5 for *Mq*, and pH 6 for both *Ed* and *Lc*.

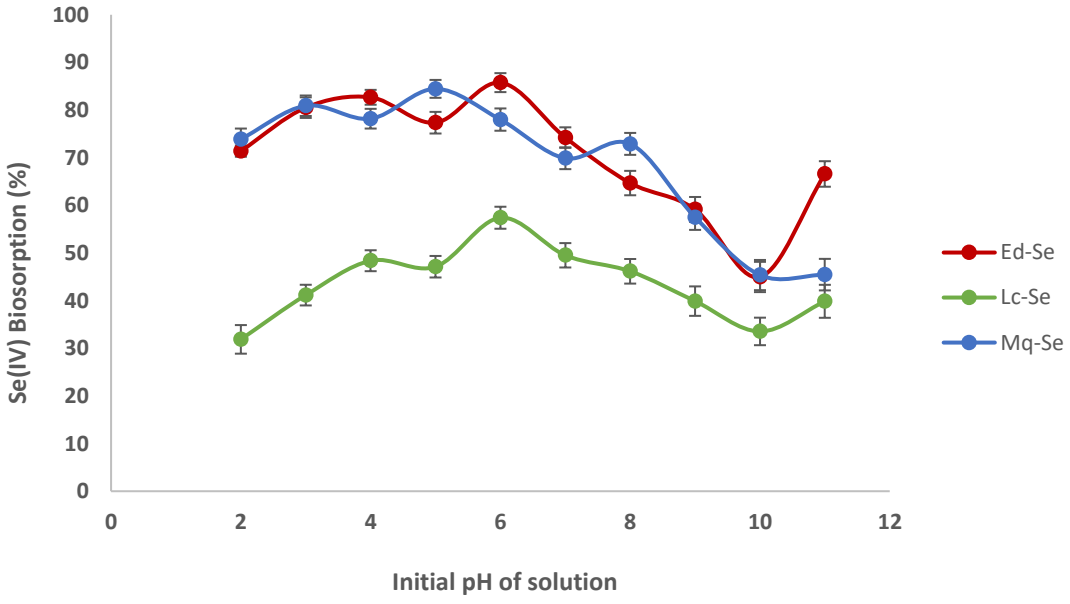

Figure 4.1 Effect of initial pH on the sorption of Se(IV) by *Ed*, *Mq* and *Lc* barks (Treatment conditions: mass of adsorbent=250 mg, volume of Se(IV) solution=25 mL, initial Se(IV) solution concentration=100 µg/L, temperature=23±2 °C, and contact time=120 min).

Tuzen and San reported that the solution pH strongly affects the metal binding sites of the sorbent surface, along with the metal ion chemistry in aqueous solution (Tuzen and Sarı, 2010, Khakpour *et al.*, 2014). Se(IV) species is known to exist in selenious acid (H_2SeO_3), biselenite ($HSeO_3^-$) and selenite (SeO_3^{2-}) in an aqueous solution (Duc *et al.*, 2006). Between pH 3.5 and 9.0, the biselenite ion is the predominant Se(IV) species in an aqueous solution, while above pH 9.0, selenite becomes the dominant species (Duc *et al.*, 2006, Tuzen and Sarı, 2010, Khakpour *et al.*, 2014). As pH decreases below pH 3.5, selenious acid becomes the more dominant Se species (El-Shafey, 2007, Khakpour *et al.*, 2014). Above pH 6, the negative charges on the bark surface may not favour the sorption of anions such as selenite and biselenite, therefore the Se(IV) sorption% decreases (Rajamohan and Rajasimman, 2015). At a pH of < 3.5, the low Se(IV) sorption% may be due to the inability of the neutral species (H_2SeO_3) to interact electrostatically with the biosorbent, while such species may react with some unprotonated amino groups (Tuzen and Sarı, 2010). On the other hand, at low pH, the ionisation of carboxyl groups of amino acids on the cell structure may increase the negative charges on the surface of bark, bark and these negative charges will prevent selenium ions sorption (Khakpour *et al.*, 2014). Thus, the high sorption% at pH 5 or 6 may be related to protons sufficiency, which allows more Se(IV) to reduce to elemental selenium and adsorb on the sorbent surface (Tuzen and Sarı, 2010, Khakpour *et al.*, 2014). Another reason for higher sorption% at low pH might be related to availability of more iron on sorbent surface, which can adsorb more Se(IV) (Lo and Chen, 1997).

Notably, during the sorption process in this study, the pH of the acidic solution increased, most probably due to acid catalysed hydrolysis of the bark matrix material (*i.e.*, proteins and carbohydrates) or interaction of Se(IV) with the bark that released OH^- (Gaballah and Kilbertus, 1998). Similarly, a decrease of pH for the pH 11 sample was also observed, likely due to the same mechanism.

Another noticeable feature in Figure 4.1 is that *Lc* bark showed the lowest Se(IV) removal percentage at every pH value compared to the other bark samples. This behaviour may have arisen from the fact that the *Lc* bark possesses the smallest pore surface and pore volume (see BET surface area analysis results in Table 4.1), and the very compact surface of this bark species, which was shown in the scanning electron micrograph in Figure 3.11c. However, *Ed* and *Mq* showed little difference in pH efficiency of Se sorption%. As a result of the ~20-30% lower Se removal for *Lc* bark than that of the other species over the entire pH range, no further experiments involving *Lc* bark were pursued in this work.

In addition, as we previously found that the maximum Se(IV) sorption% occurred at pH 5 for *Mq* bark and pH 6 for *Ed* bark, these are regarded as the optimum pH used in further experiments.

4.3.2.2 Effect of Contact time on Selenite Biosorption

To evaluate the effect of contact time (5 min to 240 min) on Se(IV) biosorption, 250 mg of each of *Ed* and *Mq* bark was added to 25 mL of aqueous 100 µg/L Se(IV) at the optimum pH of 6 for *Ed* and of pH 5 for *Mq* bark. Figure 4.2(a) displays the relationship between Se sorption% and contact time (min), whilst Figure 4.2(b) illustrates the Se uptake (µg/g) over different contact times (min). Accordingly, the sorption% of Se(IV) gradually increased with contact time, and reached a maximum of 92% at 120 min for *Ed* and 83% at 180 min for *Mq* bark. Similarly, the maximum sorption efficiency of *Mq* bark was found to be 7.8 µg/g at 180 min. However, *Ed* bark showed a slight decrease in Se uptake after reaching a maximum of 9.2 µg/g at 60 min. The results of this study are in agreement with those investigating removal of metal ions by various sorbents (Ranjan *et al.*, 2009, Kannan and Veemaraj, 2010, Tuzen and Sarı, 2010, Afroze *et al.*, 2016). We observed a slight decrease in Se(IV) sorption at 180 min for *Ed*, before the rate of removal increased again. *Mq* bark showed a slight decrease in Se(IV) removal

between 180 and 240 min. Overall, the percentage of Se(IV) removal reached a peak of 92.0% at 120 min for *Ed*, and of 83.0% at 180 min for *Mq* barks.

The process of retaining Se(IV) to the biosorbent surface is more complex than simple surface sorption. As noted in Section 3.3.2, the possible reason for quick adsorption during the initial contact time period could be the availability of more than the required number of active sites on the surface of bark (Kannan and Veemaraj, 2010). However, over a longer time the removal process slows down, likely due to decreasing numbers of active sites on the bark. Furthermore, sorption on bark might be a two-step process consisting of a very fast adsorption of an ion on the externally-accessible surface sites of the sorbent, followed by a slower intraparticle diffusion within the porous sorbent structure (Simeoni, 2003, Afroze *et al.*, 2016).

Interestingly, the results from Figure 4.3(a) and (b) show a higher Se(IV) sorption% and the amount of Se sorbed (µg/g) at the *Ed* bark than the *Mq* bark over the range of contact times. The reason for this may be related to the chemical composition of the *Ed* bark. Based on the EDXRF results in Table 4.1, an approximately ten-fold higher Ca level was present in the *Ed* bark (18330.6 cps) than in the *Mq* bark (1650.7 cps). Kashiwakura *et al.*, reported that Se is more likely to exist as calcium selenite ($CaSeO_3$) in a solid system and probably as a ferric selenite ($Fe_2(SeO_3)_3$) complex on the surface of a sorbent (Kashiwakura *et al.*, 2011). Elements including Al, Fe and especially Ca all showed strong affinity for selenite (Martens, 2003). Therefore, the *Ed* bark with the highest Ca level may be more capable of Se sorption compared with the *Mq* bark.

Based on a maximum percentage of Se(IV) removal at 120 min for *Ed* at pH 6, and at 180 min for *Mq* at pH 5, these contact times were adopted in all subsequent experiments.

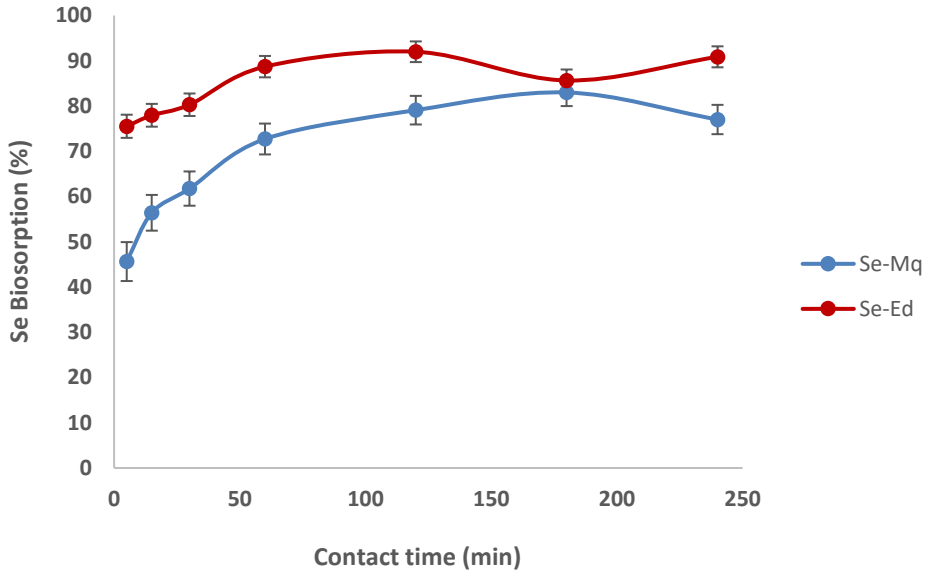

(a)

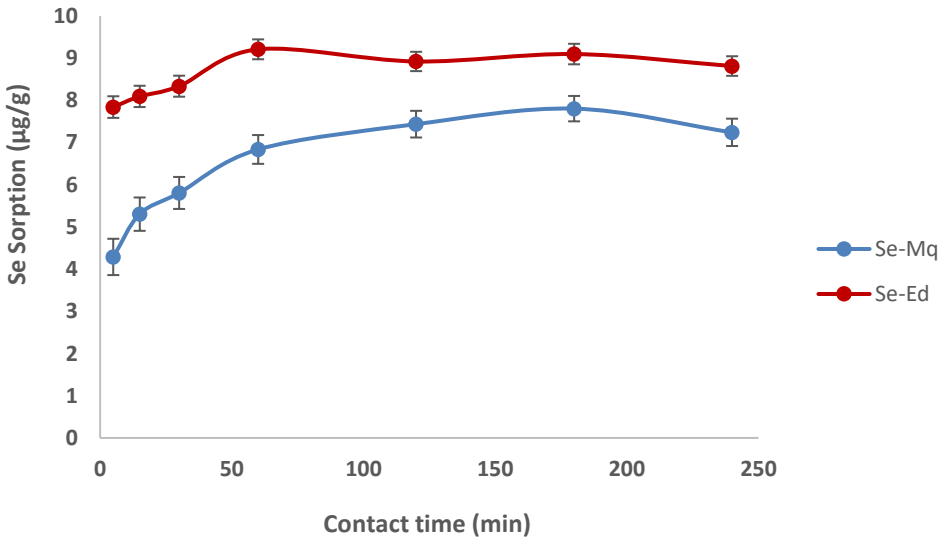

(b)

Figure 4.2 Effect of contact time on (a) the percentage sorption of Se(IV), and (b) Se(IV) sorption (µg/g) by *Ed* and *Mq* barks (conditions: mass of adsorbent=250 mg, volume of Se(IV) solution=25 mL, initial Se(IV) solution concentration=100 ppb, temperature=23±2 °C, and pH 5 for *Mq* and pH 6 for *Ed)*.

4.3.2.3 Effect of Biosorbent Dosage on Selenite Biosorption

Se(IV) adsorption experiments were then conducted on *Ed* and *Mq* barks with sorbent doses between 62.5-500 mg/25 mL (2.5–20 g/L). These experiments were performed under the previously-determined optimum conditions of contact time of 120 min and pH 6 for *Ed*, contact time of 180 min and pH 5 for *Mq*, and with an initial Se(IV) concentration of 100 µg/L. The effect of *Ed* and *Mq* bark dosage on Se(IV) removal, and the amount of Se sorbed by the bark, is shown in Figure 4.3(a) and (b). These results show that, by increasing bark dosage from 62.5 to 500 mg/25 mL (2.5-20 g/L), the biosorption of Se gradually increased from 15.9% to 76.8% for *Mq* and from 52.8% to 95.9% for *Ed* (Figure 4.3(a)). However, with increasing bark dosage, the sorption efficiency decreased from 21.9 to 5.0 µg/g for *Ed*, and from 6.2 to 3.7 µg/g for *Mq* bark (Figure 4.3(b)).

As discussed in Section 3.3.2.2.3, by increasing the biosorbent dosage, surface area and the number of available active sites for elemental adsorption rapidly increase. Therefore, the removal of Se increases with increasing sorbent dosage. However, at a low sorbent dosage, the sorbent surface may quickly become saturated with sorbate ions, resulting in large excess of ions remaining in solution (Tuzen and Sarı, 2010). Thus, in a fixed volume of solution, the quantity of ions that can be sorbed on the mass of sorbent reduces with increasing sorbent mass, leading to a decrease in sorption.

A solute concentration gradient between the solution and on the surface of the sorbent would also be a contributing factor (Afroze *et al.*, 2016). Moreover, according to Khakpour *et al.*, the number of charged binding sites available on the sorbent surface increases at high sorbent doses. However, these sorbents may collide with each other so frequently that this causes desorption of the adsorbate as a result of sorption and desorption process, giving rise to a reduced sorption (Khakpour *et al.*, 2014).

In summary, for a Se(IV) dosage of 25 mL at 100 µg/L, the optimal biosorbent dosage was found to be 500 mg (20 g/L) for both *Ed* and *Mq* barks. This optimum dosage of 500 mg was then adopted in further experiments.

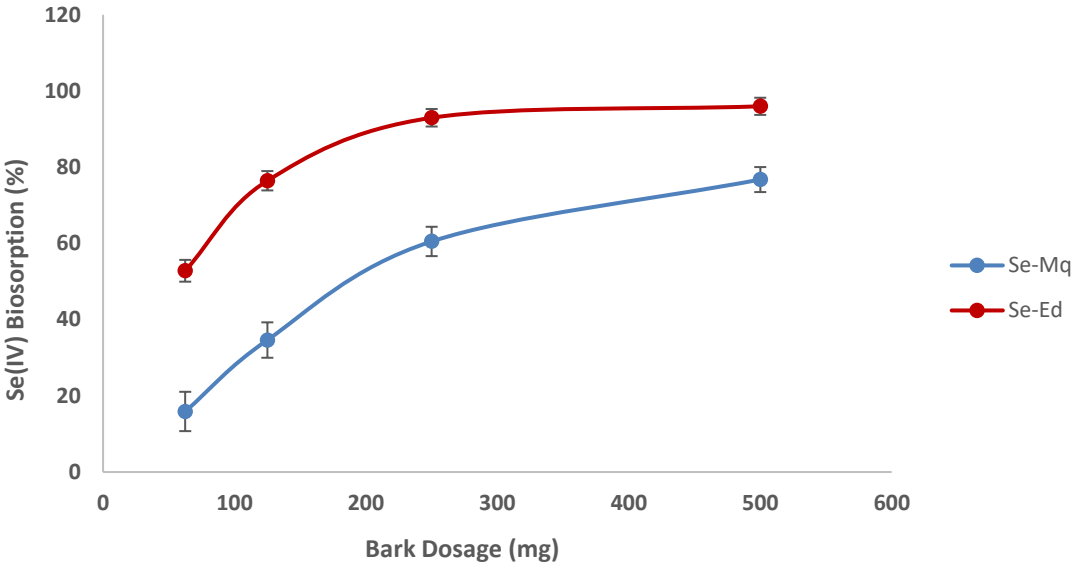

(a)

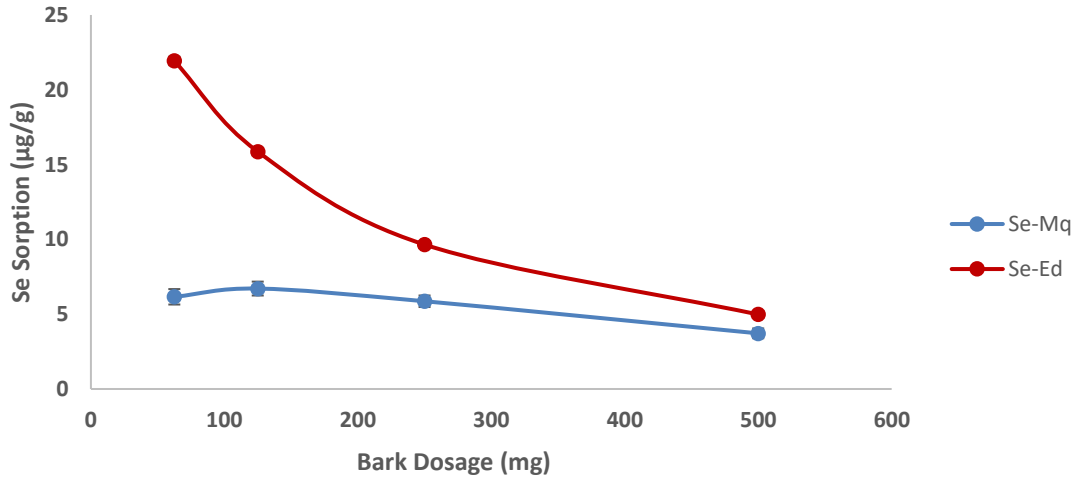

(b)

Figure 4.3 Effect of bark dosage on the (a) percentage of Se(IV) biosorption; and (b) Se (IV) sorption (µg/g) by *Ed* and *Mq* barks. (conditions: volume of Se(IV) solution=25 mL, initial Se(IV) solution concentration=100 ppb, temperature=23±2 °C, pH 5 and contact time 180 min for *Mq*, and pH 6 and contact time 120 min for *Ed*).

4.3.2.4 Effect of initial Se(IV) Concentration on Biosorption; Sorption Capacity Using Isotherms

A range of Se(IV) standard solutions ranging from 10 µg/L to 200 µg/L was prepared for use in assessing the effect of element concentration on selenite biosorption to barks. During these experiments, other parameters (*e.g.*, bark dosage 20 g/L, pH 5 and contact time 180 min for *Mq*, and pH 6 and contact time 120 min for *Ed*) were kept unchanged. Figure 4.4(a) and (b), respectively illustrate the effect of initial Se(IV) concentration on the percentage sorption of Se(IV), and the Se sorption efficiency (µg/g) of the *Ed* and *Mq* bark. The results, as shown in Figure 4.4, indicate that with increasing initial concentration of Se(IV) from 10 µg/L to 200 µg/L, the percentage removal of Se(IV) gradually decreased from approximately 93% to 62% for *Ed*, and from 100% to 62% for *Mq* bark (Figure 4.4(a)). Interestingly, the uptake of Se increased up to 12 µg/g for both *Ed* and *Mq* bark (Figure 4.4(b)).

Previous studies (Ranjan *et al.*, 2009, Khakpour *et al.*, 2014, Wang *et al.*, 2015, Afroze *et al.*, 2016), indicated that with increasing the initial metal ion concentration, the percentage of ion removal decreased, while the uptake capacity of metal ion sorption increased. The results from our study, which showed an increasing in Se sorption capacity has occurred when the initial Se(IV) concentration increased, are in a good agreement with those cited studies. Decreasing Se(IV) sorption might be due to the limited number of available active sites on the bark surface as part of the fixed dosage of bark in this experiment, thus, the capacity of bark reduces with increasing initial selenite concentration (Kannan and Veemaraj, 2010). In contrast, increasing Se(IV) sorption efficiency is possibly due to the initial selenite concentration acting as a "driving-force", which prevails over the mass transfer resistance between the selenite in solution and the biosorbent (Khakpour *et al.*, 2014). Hence, a Se(IV) solution with a higher concentration has resulted from an increased quantity of Se(IV) sorbed per unit mass of bark.

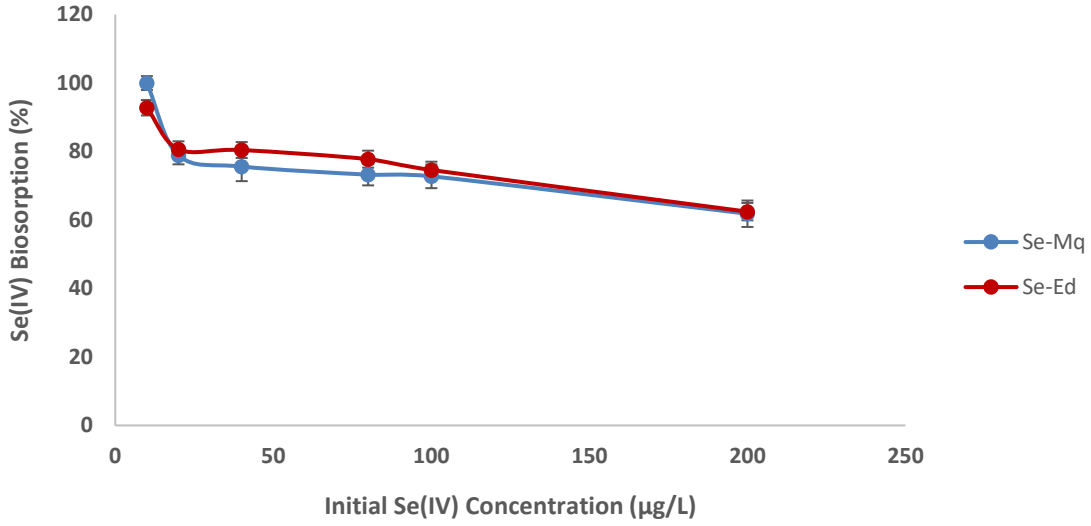

(a)

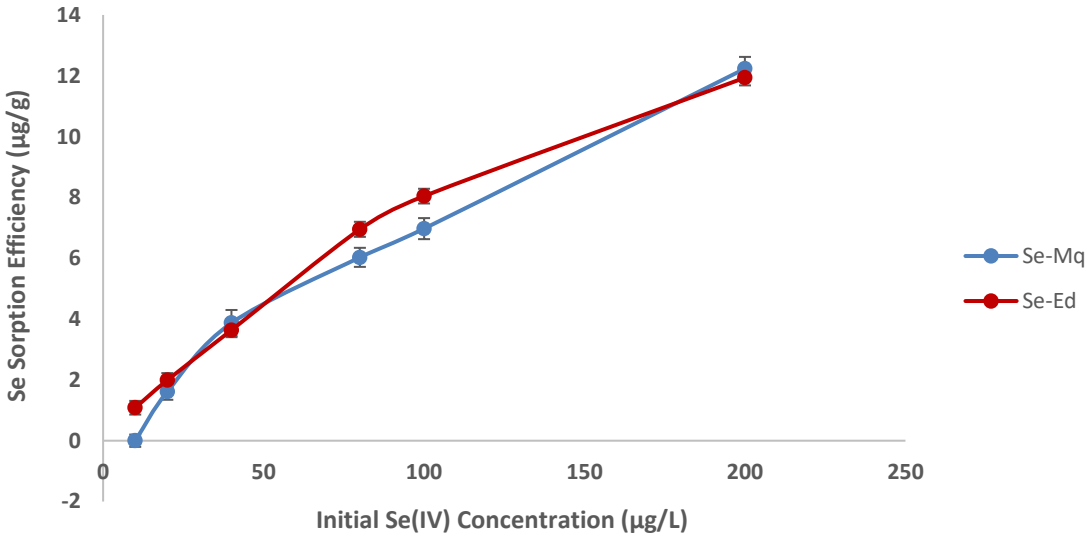

(b)

Figure 4.4 Effect of initial Se(IV) concentration (µg/L) on the (a) biosorption of Se(IV) and (b) sorption efficiency (µg/g) by *Ed* and *Mq* barks. (conditions: volume of Se(IV) solution=25 mL, bark dosage 0.50 g, temperature=23±2 °C, pH 5 and contact time 180 min for *Mq*, and pH 6 and contact time 120 min for *Ed*)

4.3.3 Se(IV) Adsorption Kinetics and Mechanism

The present study is aimed at investigating the sorption kinetics of Se(IV) on *Ed* and *Mq* bark, and also evaluating the applicability of the Lagergen pseudo-first order (Equation 4.7), Ho pseudo-second order (Equation 4.8), kinetic models to the experimental data.

As noted in Section 3.2.5, in the pseudo-first order kinetic model, K_1 (1/min) and q_e (µg/g) can be respectively determined from the slope and the ordinate intercept of a linear ln ($q_e - q_t$) versus t plot, as shown in Figure 4.5(a) for *Ed* and (b) for *Mq*. The determination coefficient (R^2) was estimated to be 0.3328 (7 data points) for Figure 4.5(a) and 0.5766 (7 data points) for Figure 4.5(b), which were not considered sufficiently valid. Additionally, the estimated quantity of Se sorbed per mass unit of bark (equilibrium sorption capacity, q_e) obtained from this model (1.39 µg/g for *Ed* and 2.26 µg/g for *Mq*) were not robust enough in comparison with the experimental data of 9.77 µg/g for *Ed* and 7.80 µg/g for *Mq*. Therefore, the sorption process did not follow a pseudo-first order sorption rate.

In a pseudo-second order kinetic model, q_e (µg/g) and k_2 (g/(µg min)) are respectively determined from the slope and the ordinate intercept of a linear t/q versus t plot. The corresponding plot obtained for *Ed* and *Mq* is shown in Figure 4.6(a) and Figure 4.6(b). A determination coefficient (R^2) of 0.9994 (7 data points) was estimated for Figure 4.6(a) and 0.9965 (7 data points) for Figure 4.6(b), and 8.94 µg/g of Se(IV) sorbed on *Ed* and 7.63 µg/g of Se(IV) sorbed on *Mq*. Thus, the pseudo-second order model better represents the sorption kinetics. This supports that the rate of the sorption procedure was controlled by the bark surface and involved physicochemical interaction between bark and Se(IV) (Rajamohan and Rajasimman, 2015).

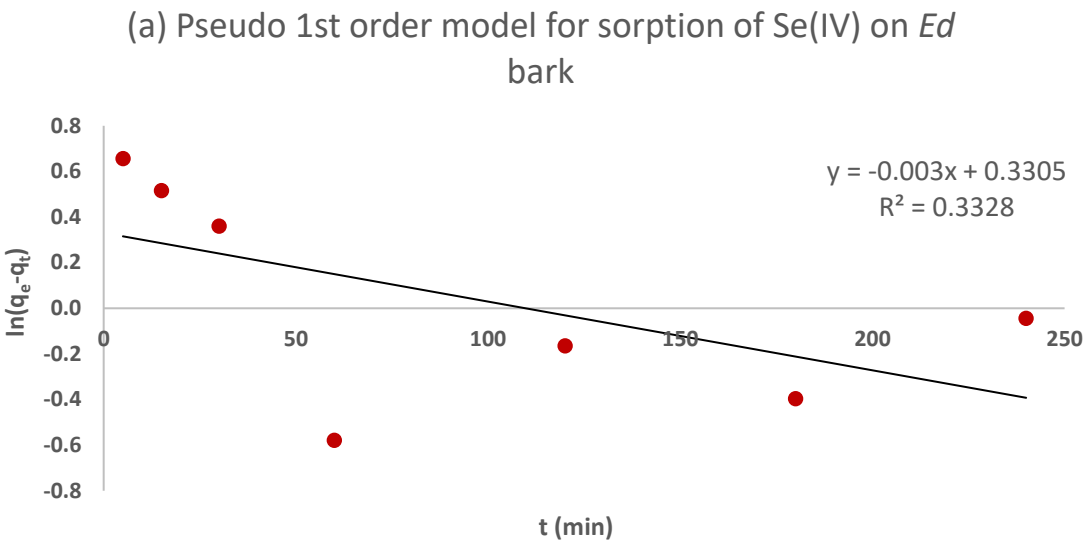

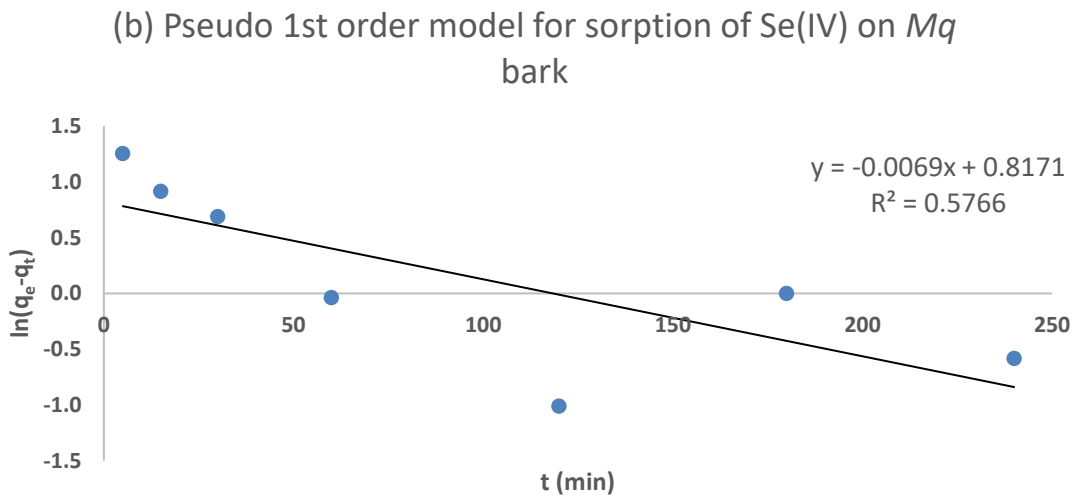

Figure 4.5 Pseudo-first order model of Se(IV) sorption by (a) *Ed*, and (b) *Mq* barks (conditions: mass of adsorbent=500 mg, volume of Se(IV) solution=25 mL, initial Se(IV) solution concentration=100 ppb, temperature=23±2 °C, and pH 5 for *Mq* and pH 6 for *Ed*).

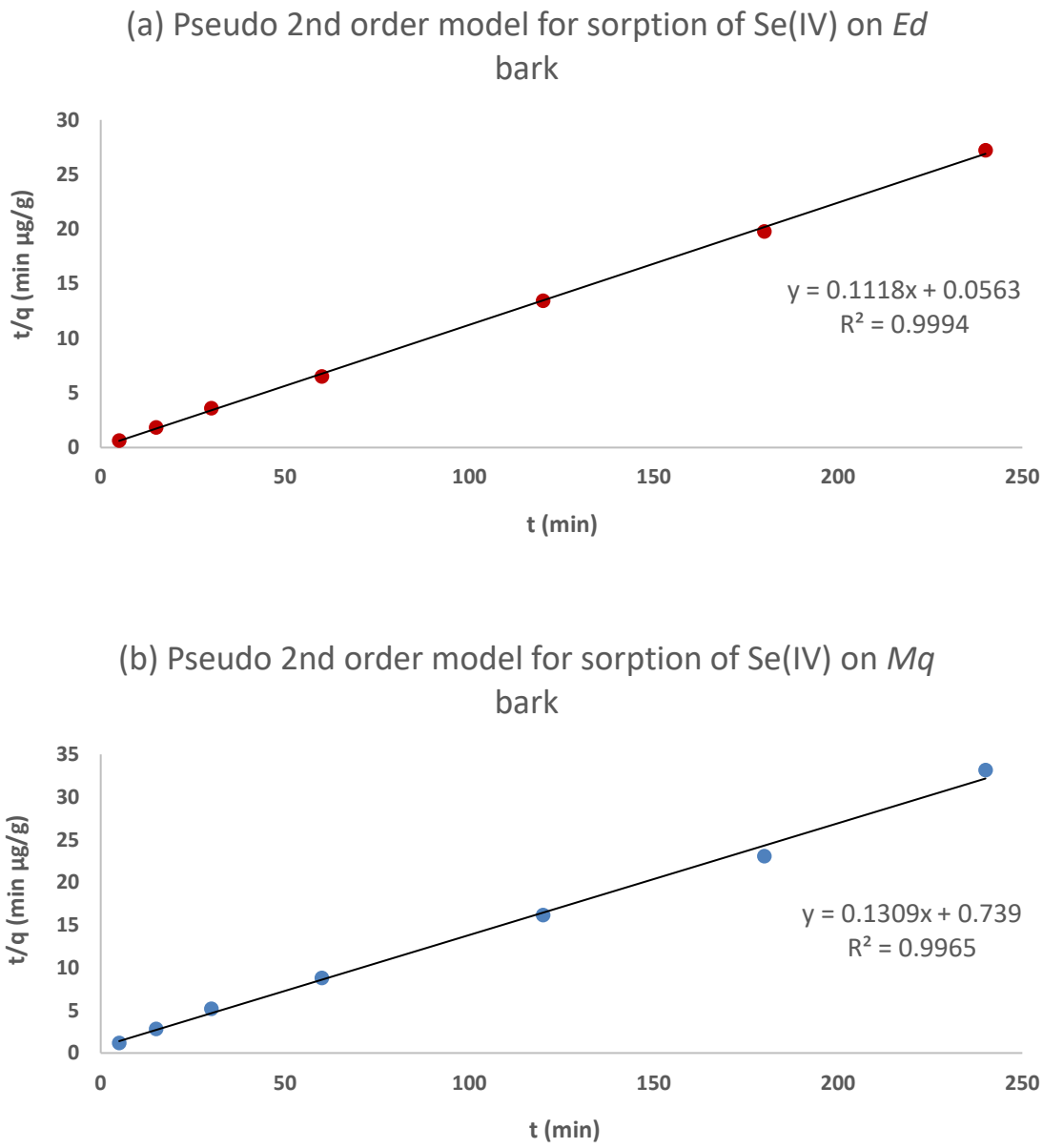

Figure 4.6 Pseudo-second order model of Se(IV) sorption by (a) *Ed*, and (b) *Mq* barks (conditions: mass of adsorbent=500 mg, volume of Se(IV) solution=25 mL, initial Se(IV) solution concentration=100 µg/L, temperature=23±2 °C, and pH 5 for *Mq* and pH 6 for *Ed*).

4.3.4 Se(IV) Adsorption Isotherm Studies

The capacity of the sorbent and the mechanism of adsorption were determined based on equilibrium studies. Hence, the experimental data were fitted to the most common isotherm models of Langmuir, Freundlich and Sips within the Se(IV)) concentration range of 20 to 200 µg/L, and isotherm parameters were estimated. Then, linear regression analysis was used to evaluate the best fitted isotherm.

As noted in Section 4.2.5, in a Langmuir isotherm model, adsorption occurs homogenously on the active sites of the sorbent containing a fixed number of similar sites with no transmigration of sorbate inside the surface (Afroze *et al.*, 2016). The maximum adsorption capacity, q_{max} (mg/g), and the Langmuir constant, *b*, were obtained from the slope and ordinate intercept of a linear $1/q_e$ versus $1/C_e$ plot, based on Equation 4.1. The results are depicted in Figure 4.7(a) for *Ed* and 4.7(b) for *Mq*. A high R^2 value of 0.9967 (5 data points) for *Ed*, in the Langmuir isotherm model (Figure 4.7(a)) suggests a valid assumption of a Se(IV) sorption monolayer on the *Ed* surface. Moreover, the Langmuir isotherm is well fitted to the experimental data for *Mq* bark (Figure 4.7(b)). A high determination coefficient (R^2) of 0.9994 (5 data points) for *Mq* indicates the applicability of this model. Nonetheless, the monolayer capacity of the *Ed* bark was evaluated to be 23.09 µg/g, which is higher than of 18.83 µg/g for the Mq bark.

In a Freundlich isotherm model, *n* and *k* in Equation 4.2 are obtained respectively from the slope and ordinate intercept of a linear ln q_e versus ln C_e. The sorption equilibrium data were linearly fitted with experimental data for both *Ed* and *Mq* bark, and the results are presented in Figure 4.9. A high R^2 value of 0.9598 (5 data points) and 0.9859 (5 data points) was estimated for *Ed* (Figure 4.8(a)) and *Mq* bark, respectively (Figure 4.8(b)).

As discussed in Section 3.3.2.4, the Freundlich constant (*n*) is a measure of the sorption affinity of the sorbent for a metal(oid) ion in solution. If the numerical value of $1/n$ for the sorbents is greater than one, the sorbent will favourably sorb on the metal ion (Demiral *et al.*, 2008, Afroze

et al., 2016). In this study, the value of 1/*n* is 1.51 for *Ed*, and 1.40 for *Mq*, demonstrating the potential of these barks for Se(IV) sorption.

As noted in Section 4.2.5, in the Sips model, q_{max}, n_s and *Ks* were obtained from nonlinear model using solver add-in function of the Microsoft Excel. In Figure 4.9 the linear form of the Sips model is displayed as a plot of $ln(q_{max}Ks/qe)$ versus $ln(Ce)$ based on Equation 4.3. The coefficient of determination (R^2) of the Sips isotherm is 0.96 for *Ed* and 0.99 for *Mq*, indicating the good fit of this model. Moreover, the value of exponent *n* for the Sips model is close to unity, indicating a homogeneous sorption (Kumar and Porkodi, 2006, Ebrahimian *et al.*, 2014). The value of the maximum sorption capacity, q_{max}, obtained using the Sips equation is also close to those evaluated by the Langmuir model.

All the Langmuir, Freundlich and Sips model parameters and their estimated values for the sorption of Se(IV) on *Ed* and *Mq* bark are presented in Table 4.2.

The higher R^2 values of 0.9994 and 0.9967 support the Langmuir isotherm as a suitable model for the Se(IV) sorption isotherm at the *Mq* and *Ed* bark, respectively. However, owing to a considerably high R^2 value of 0.9859, a Freundlich model may still be valid for the Se(IV) sorption isotherm at the *Mq* bark. Therefore, the Se(IV) sorption on the surface of selected bark is a monolayer coverage over the homogeneous bark surface.

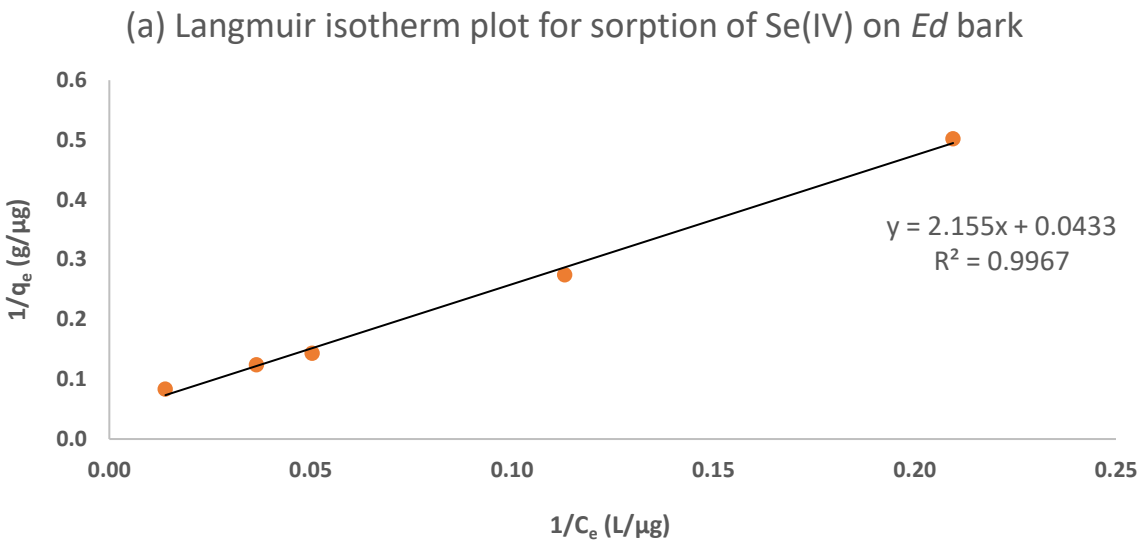

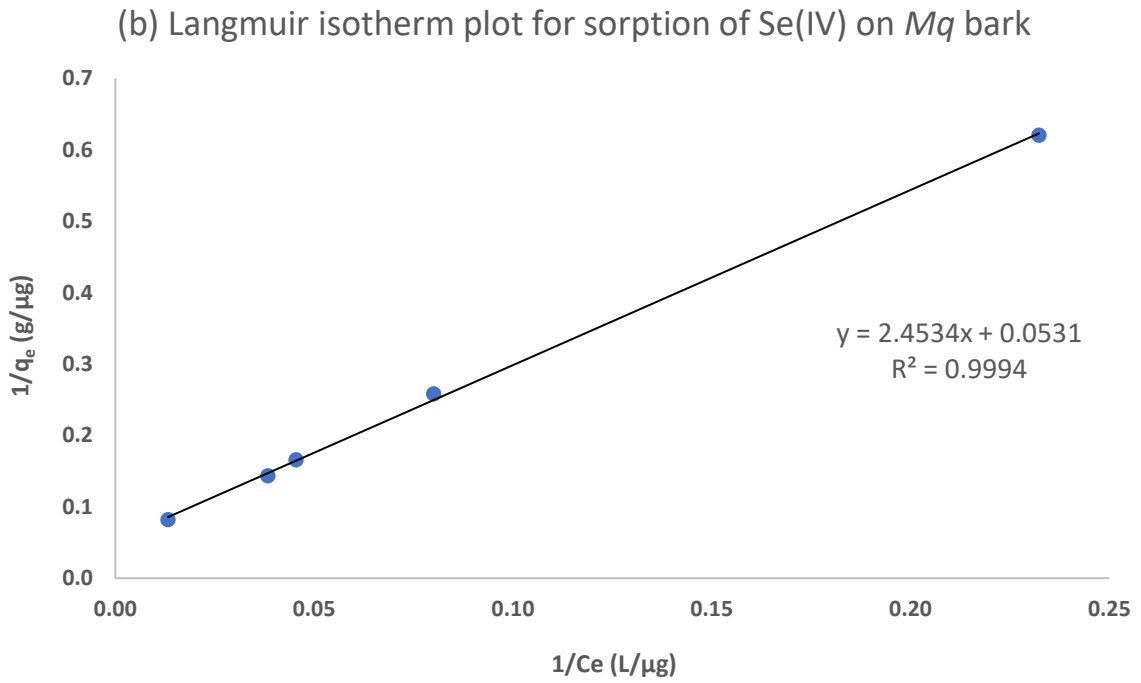

Figure 4.7 Langmuir isotherm model of Se(IV) sorption by (a) *Ed*, and (b) *Mq* barks (conditions: mass of adsorbent=250 mg, volume of Se(IV) solution=25 mL, initial Se(IV) solution concentration= 20, 40, 80, 100, and 200 µg/L, temperature=23±2 °C, and pH 5 and 180 min for *Mq* and pH 6 and 120 min for *Ed*).

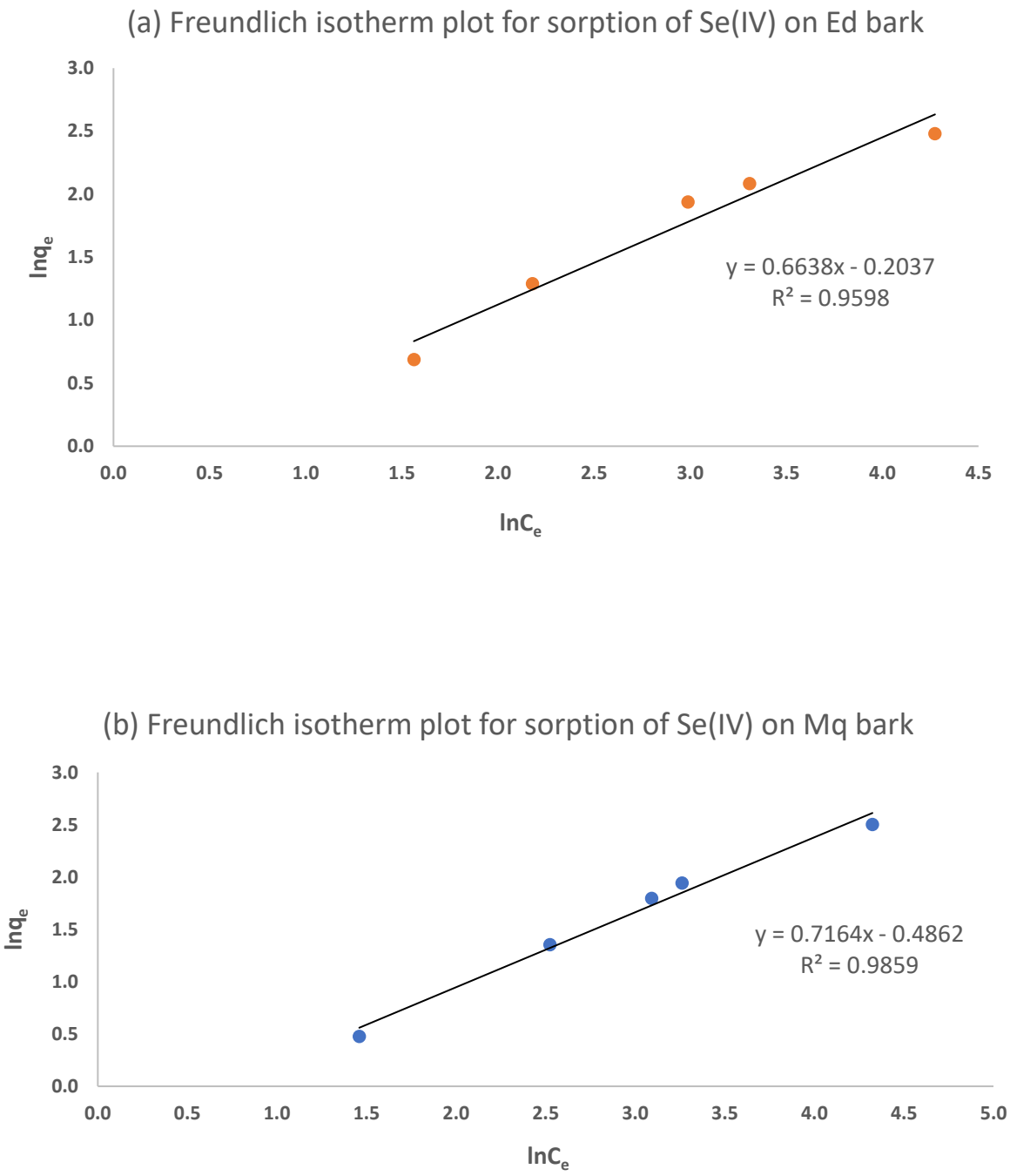

Figure 4.8 Freundlich isotherm model of Se(IV) sorption by (a) *Ed*, and (b) *Mq* barks (conditions: mass of adsorbent=250 mg, volume of Se(IV) solution=25 mL, initial Se(IV) solution concentration= 20, 40, 80, 100, and 200 µg/L, temperature=23±2 °C, and pH 5 and 180 min for *Mq* and pH 6 and 120 min for *Ed*).

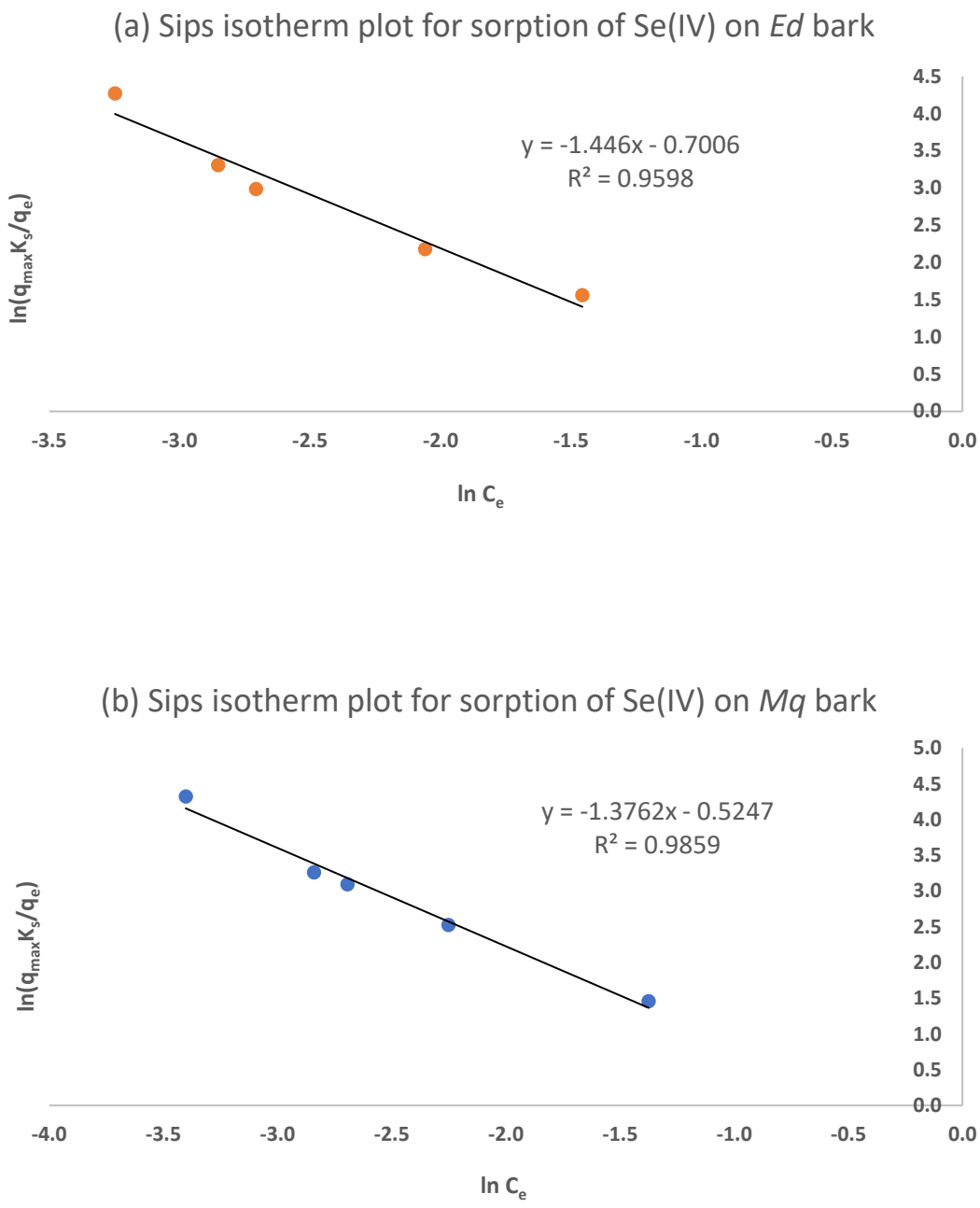

Figure 4.9 Sips isotherm model of Se(IV) sorption by (a) *Ed*, and (b) *Mq* barks (conditions: mass of adsorbent=250 mg, volume of Se(IV) solution=25 mL, initial Se(IV) solution concentration= 20, 40, 80, 100, and 200 µg/L, temperature=23±2 °C, and pH 5 and 180 min for *Mq* and pH 6 and 120 min for *Ed*).

Table 4.2 Summary of Langmuir, Freundlich and Sips calculated values for Se sorption

Biosorbent	Model	Parameters	Values
Ed	Langmuir	q_{max} (µg/g)	23.09
		b (L/µg)	0.02
		R^2 (5 data points)	0.99
	Freundlich	k (L/µg)	0.82
		n	0.66
		R^2 (5 data points)	0.96
	Sips	q_{max} (µg/g)	23.14
		K_s ((L/µg)	0.02
		$1/n_s$	1.45
		R^2 (5data points)	0.96
Mq	Langmuir	q_{max} (µg/g)	18.83
		b (L/µg)	0.02
		R^2 (5 data points)	0.99
	Freundlich	k (L/µg)	0.61
		n	0.72
		R^2 (5 data points)	0.99
	Sips	q_{max} (µg/g)	18.87
		K_s ((L/µg)	0.02
		$1/n_s$	1.38
		R^2 (5 data points)	0.99

4.3.5 Comparison of BET, SEM-EDS and FTIR-ATR Results before and after Se(IV) Sorption on Bark

The BET surface area results for *Ed* and *Mq* bark before and after Se(IV) sorption are presented in Table 4.3. The surface area and pore volume of *Mq* bark before Se loading were observed to be respectively ~60% and 55% larger than that of *Ed* bark, whilst after sorption of Se, both bark showed very similar surface area and pore volumes. Moreover, after Se sorption, the surface areas of both *Ed* and *Mq* Se-loaded barks decreased. These results could be due to sorption of Se on the surface of bark. Additionally, the porosity of *Mq* bark after Se sorption slightly decreased, while the pore size of *Mq* bark slightly increased. In contrast, although the pore volume of *Ed* bark slightly increased after Se sorption, its pore size remained approximately the same as unloaded *Ed* bark. The reason for lower BET surface area, pore volume or pore size of Se-loaded barks might be related to the removal of impurities during sorption process in a slightly acidic environment, which may have cleaned up unoccupied sites on the surface of bark, thus increase the porosity of bark surface (Khakpour *et al.*, 2014).

According to a unified pore size classification by Zdravkov *et al.*, materials with pore size between 3 to 50 nm are categorised as mesoporous (Zdravkov *et al.*, 2007). Both *Ed* and *Mq* barks with pore sizes of 6.35 nm and 6.31 nm, respectively, can therefore be classified as mesoporous. Therefore, beside BET surface area, other properties present on the bark such as functional groups may have an important role in its interaction with selenite ions in the sorption process.

Table 4.3 BET surface area results for *Ed* and *Mq* bark before and after Se(IV) sorption

Parameters	Raw *Ed*	Se-loaded *Ed*	Raw *Mq*	Se-loaded *Mq*
BET Surface Area / m^2/g	0.46	0.41	1.25	0.43
Pore Volume / cm^3/g	0.004	0.006	0.009	0.008
Pore Size / nm	6.35	6.28	6.31	6.45

The comparison of SEM-EDS results for selected bark before and after Se(IV) sorption are presented in Figure 4.10 and Figure 4.11. In these micrographs, there was a slight difference in the morphology of bark after Se sorption. The rough surface and large number of asymmetric and open pores are visibly similar in both raw and Se-loaded bark species. However, in Se-loaded bark, the sum of open pores seemed to have slightly decreased due to the possibility of Se coverage on the surface of selected bark. These results are supported by the BET surface area results (Table 4.3), which indicated that the surface area and pore volume of selected bark decreased after Se(IV) sorption.

As shown in Section 3.3.2.5, the EDS results of Se-loaded bark were found to be nearly the same as those of As-loaded bark. Although a very concentrated 10 g/L Se(IV) solution was used in the sorption process, the quantity of Se(IV) sorbed to the bark surface was not significant. The digestion of bark after reaction with 10 g/L Se(IV) revealed that the approximate amount of Se(IV) was 332.9 mg/g in *Ed*, and 537.4 mg/g in *Mq* bark, which were larger than the SEM-EDS detection limit of 3000 mg/kg. However, the EDS results could not confirm the quantity of Se in either of the selected barks due to inaccurate quantitative analysis by the EDS technique, or most importantly, the possibility of further internal sorption than surface sorption of Se(IV) by bark.

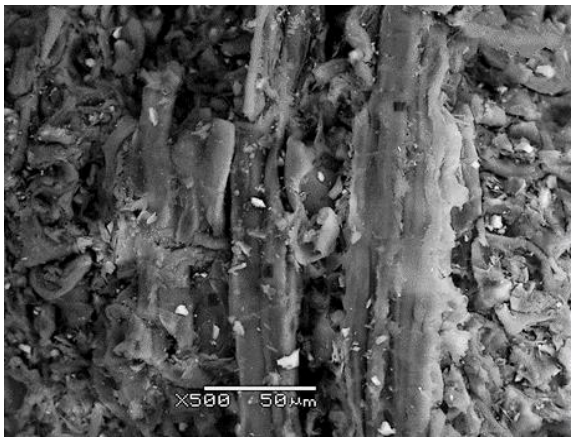

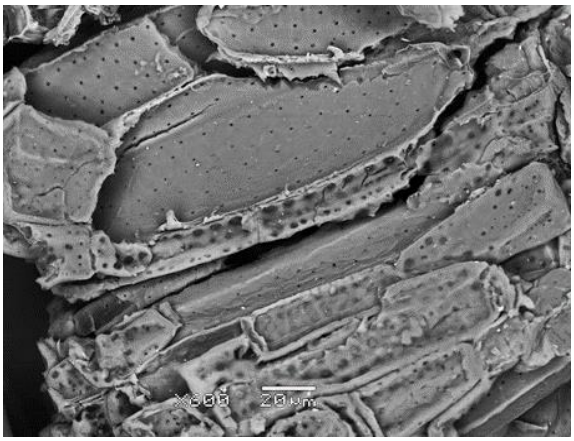

Figures 4.10 Scanning electron micrographs of *Ed* bark: left) before Se sorption, and right) after Se sorption

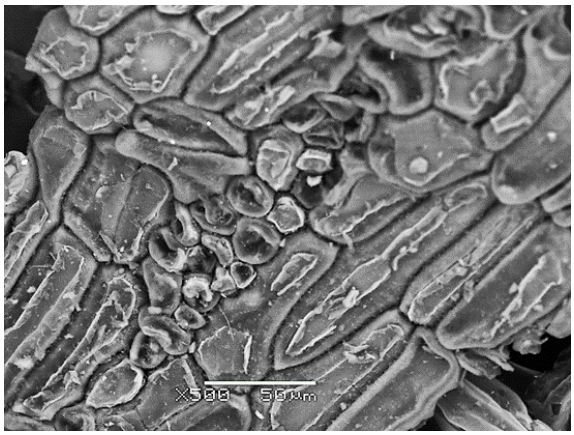

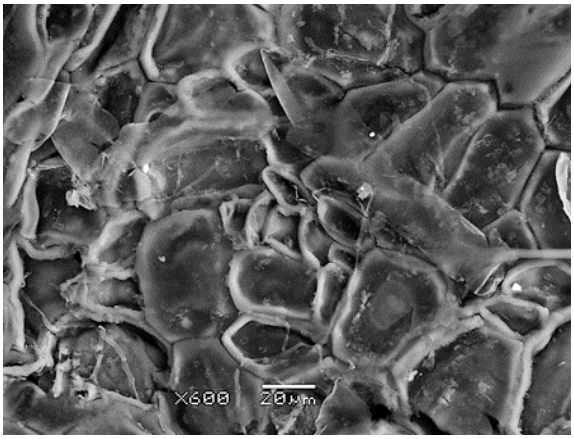

Figures 4.11 Scanning electron micrographs of *Mq* bark: left) before Se sorption, and right) after Se sorption

The FTIR-ATR spectra for the two types of barks before and after Se sorption are depicted in Figure 4.12 and 4.13. These spectra showed very little change in either the intensity or shifting of peaks between raw and Se-loaded barks. The broad and strong peaks at 3331.37 cm^{-1} in the spectrum of raw *Ed* have shifted to 3329.44 cm^{-1} in the spectrum of *Ed* Se-loaded, and the peak at 3334.96 cm^{-1} in raw *Mq* shifted to 3332.75 cm^{-1} in that of *Mq* Se-loaded. Based on explanation in Section 3.3.2.1.4, and Section 3.3.2.5, strong and wide vibration peaks in between 3,500 – 3,000 cm^{-1} in FTIR spectra were defined as the vibrations of O-H and −N-H functional groups, which indicate the presence of possibly hydroxyl and/or amide groups, and shifting peaks in this area may be related to sorption of Se on these functional groups (Pandey *et al.*, 2009, Mishra *et al.*, 2010, Afroze *et al.*, 2016). The spectra of *Ed* bark (see Figure 4.12) after interaction with Se(IV) showed increased intensity and shifted to asymmetrical stretching bands at 1604.91 cm^{-1}, compared with those observed in the spectra of raw *Ed* at 1609.06 cm^{-1}. The peak at 1513.55 cm^{-1} shifted to 1503.96 cm^{-1}, while the peak at 1029.38 cm^{-1} shifted to 1029.32 cm^{-1}. These results are in good agreement with those reported by Tuzan and San (Tuzen and Sarı, 2010). Based on Section 3.3.2.5, the absorption peaks in the region between 1080 and 1300 cm^{-1} indicated that the biomass may contain acidic groups, while the sorption in the region of 1020–1340 cm^{-1} would be associated with amine groups (Pandey *et al.*, 2009). Therefore, shifting peaks observed after Se loading in these areas can be a result of substitution of the hydrogen atoms of amine and or carboxylic groups by Se(IV).

Similar results were obtained for the *Mq* bark. For example, the intensity of peak at 1595.57 cm^{-1} increased, accompanied by a shift to 1592.37 cm^{-1} after Se loading (Figure 4.13). Additionally, increasing intensity and shifting to higher wavelengths can be observed for peak at 1160.27 cm^{-1} to 1159.19 cm^{-1}. Overall, these results indicate that the biosorption process may involve chemical interactions as ion-exchange between the Se(IV) ions and the hydrogen atoms of carboxyl, hydroxyl, amide and/or amine groups of the biomass.

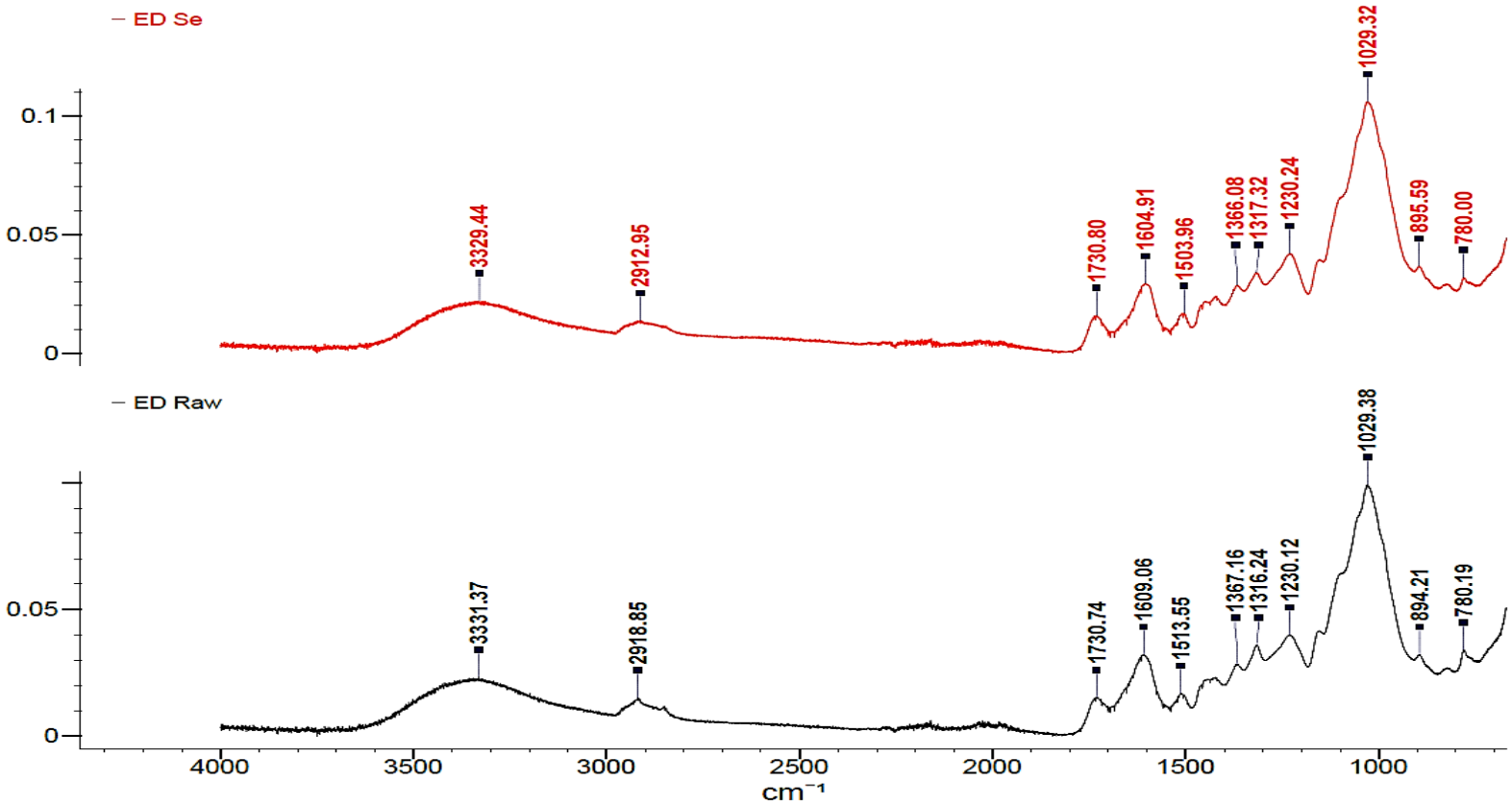

Figure 4.12 FTIR-ATR spectrum of Ed bark following Se sorption (red), compared to raw bark (black).

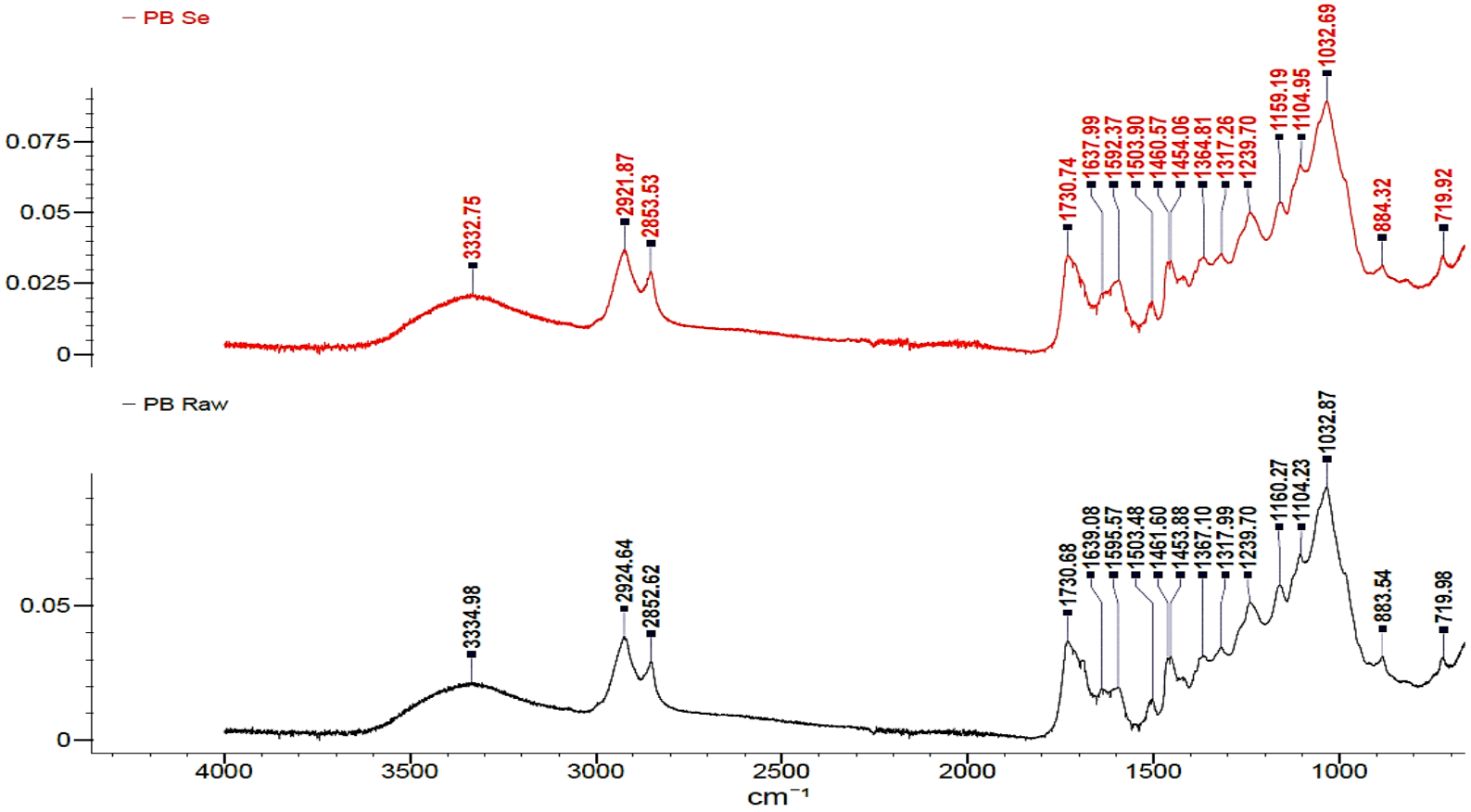

Figure 4.13 FTIR-ATR spectrum of Mq bark following Se sorption (red), compared to raw bark (black).

4.3.6 Desorption of Se(IV) and Regeneration Studies of Bark

Desorption of loaded biomass allows for the re-use of the sorbent, and recovery of sorbed materials. Desorption studies of Se(IV)-loaded *Ed* and *Mq* bark revealed that Se(IV) could be desorbed in very low quantities. The results of desorption studies are tabulated in Table 4.4. For each electrolyte used, the percentage desorption was estimated as final released Se(IV) concentration over initially sorbed concentration of Se(IV) (Afroze *et al.*, 2016). Overall, less than 20% of Se(IV) was desorbed from both *Ed* and *Mq* barks. The neutral solutions of Milli-Q water and NaCl could not remove any Se(IV) ions from Se-loaded *Ed* bark. Moreover, the lowest Se desorption was observed in the Se-loaded *Mq* bark following washing with neutral solutions of Milli-Q water and NaCl. In both bark species, the alkaline solutions of NaOH and Na_2CO_3, were more effective for Se desorption compared with acidic solutions of HNO_3 and HCl. Approximately 8% of the bound Se(IV) was recovered from *Ed* and 18% from *Mq* bark using NaOH solution. The efficacy of alkaline elution may be associated with hydroxylation of iron oxides on the surface of bark, which may cause the sorbed Se to be released (Lo and Chen, 1997). Overall, similar to the previous As desorption study, the low desorption of Se(IV) from *Ed* and *Mq* bark using selected 0.1 M electrolytes may be due to the presence of a strong binding affinity, probably as a complex and/or ligand, between Se(IV) and the biomolecular composition of the bark (*i.e.*, Fe or some functional groups such as carboxyl, hydroxyl or amine).

Regenerating or reusing the bark requires that the bound Se(IV) be appropriately eluted from the bark. Owing to the fact that the relative desorption of Se, and the value of bark as a solid waste were found to be very low, regeneration of bark could be an insignificant prospect.

Table 4.4 Percentage of Sorption and Desorption of Se(IV) from *Ed* and *Mq* bark (Se concentration of 100 ppm for sorption, and electrolyte concentration of 0.1 M for desorption)

Biosorbents	**Concentration of Se(IV) sorbed / mg/L**	**Sorption / %**	**Desorption / %**					
			Milli-Q water	NaCl	NaOH	Na_2CO_3	HCl	HNO_3
Ed	69.0	56.69	0	0	8.13	5.22	0	2.54
Mq	72.4	59.50	4.89	4.30	18.04	12.48	6.53	9.10

4.3.7 Comparison of Selenium Sorption Capacity of *Ed* and *Mq* bark with Other Sorbents

This study revealed the efficiency of the selected barks, *Ed* and *Mq*, as potential biosorbents for the removal of Se(IV) from aquatic solutions. The sorption capacity (q_m, mg/g) of selenite was found to be 6.90 mg/g for *Ed* bark at pH 6 and 7.24 mg/g for *Mq* bark at pH 5 using an initial Se(IV) solution of 100 mg/L, and a bark dosage of 20 g/L. The maximum sorption capacities from this study along with optimum pH values of the sorption procedure were compared with several reported sorbents values. They are tabulated in Table 4.5. The results show that *Ed* and *Mq* barks have the potential to act as mid-range biosorbents, demonstrating a greater capacity than reported data for other biomass sorbents such as *Aspergillus sp. J2*, and aquatic weed species. The sorption capacity and more than 70% sorption efficiency of selenium in this study indicate that *Ed* and *Mq* bark can be suitable biosorbents for Se(IV) removal from aquatic solutions including fly ash leachate.

4.4 Application of Bark for the Removal of Se(IV) from Fly Ash Leachate

In a set of batch sorption experiments (Section 4.2.8), *Ed* and *Mq* barks were used to remove Se(IV) from selected acidic and alkaline fly ash leachates. The acquired optimum condition for Se(IV) biosorption was operated for both bark species. For example, to remove Se(IV) from leachate, the pH of each leachate was maintained at 6 when the *Ed* bark was used as a sorbent, and 5 when the Mq bark was used. Additionally, after separately adding 1 g of each bark into 50 mL of leachate (20 g/L), the experiment was completed in 240 min (4 h) when using *Ed* bark, and 180 min (3 h) when using *Mq* bark.

Table 4.5 Comparison of adsorption capacity (q_m in mg/g) of different sorbent for removal of Se(IV)

Sorbent	Sorbent Capacity / mg/g	pH	References
***Ed* bark**	6.9	6	Present study
***Mq* bark**	7.2	5	Present study
***Eichhornia crassipes*, aquatic weed**	0.3 (µg/g)	6	(Rodríguez-martínez *et al.*, 2016)
***Lemna minor*, aquatic weed**	0.2 (µg/g)	6	(Rodríguez-martínez *et al.*, 2016)
***Eucalyptus camaldulensis*, Carbon**	36.5	5	(Rajamohan and Rajasimman, 2015)
Aspergillus sp. J2	6.3	5	(Li *et al.*, 2013)
***Saccharomyces Cerevisiae*, baker's yeast biomass**	39.0	5	(Khakpour *et al.*, 2014)
***Cladophora hutchinsiae*, green algae**	74.9	5	(Tuzen and Sarı, 2010)
Rice husk treated with sulfuric acid (wet sorbate)	40.9	1.5	(El-Shafey, 2007)
Iron oxide coated sand	1.3	4.5-6	(Lo and Chen, 1997)

The amount of initial Se(IV) in 50 mL of selected fly ash leachates with the highest Se(IV) concentration, along with the final concentration of Se(IV) in the leachate after biosorption, was determined within 24 h of biosorption experiment and in triplicates. The initial and final concentration of Se(IV) for each selected leachate and the percentage removal of Se(IV) using *Ed* and *Mq* bark are tabulated in Table 4.6. These results indicate approximately 65% to 100% Se(IV) removal in using *Ed*, and from 63% to 85% in using *Mq*. In some cases, the quantity of Se(IV) in fly ash leachate samples after sorption experiment was not detectable, therefore, the percentage removal is assumed to be 100%.

Another notable observation was that *Ed* bark demonstrated a higher Se(IV) removal from the same fly ash leachate compared to the *Mq* bark, which is in agreement with previous results of a higher sorption capacity using *Ed* bark than Mq bark within the range of 20 to 200 µg/L (Section 4.3.2.4, Figure 4.4(a)). For example, Se(IV) concentrations in all MPFA leachates were in the range of 20 µg/L, thus the percentage removal of selenium using *Ed* bark was higher than 95% compared to the *Mq* bark with approximately 79% removal. However, the percentage sorption of Se(IV) from WWFA and VPFA leachates with Se(IV) in the concentration range of 40 to 200 µg/L was found to be slightly greater in using *Mq* bark compared to *Ed* bark. Overall, the present study supports the proposition that *Ed* and *Mq* bark for Se(IV) may be suitable for the removal of Se(IV) from fly ash leachate under the selected range of operating conditions.

Table 4.6 Percentage removal and Concentration of As(V) in 50 mL of fly ash leachates before and after biosorption using *Ed* and *Mq* bark in their optimum conditions

Fly ash leachate*	Initial Se(IV) in leachate / µg/L	Final Se(IV) in leachate after sorption with *Ed* / µg/L	Removal % using *Ed*	Final Se(IV) in leachate after sorption with *Mq* / µg/L	Removal % using *Mq*
MPFA-1	19.6	ND	100	4.2	78.5
MPFA-2	19.3	1.0	95.1	4.2	78.1
MPFA-3	26.7	2.7	89.8	11.2	58.2
WWFA-1	46.6	10.1	78.4	10.1	78.4
WWFA-2	63.5	10.0	84.2	9.3	85.4
WWFA-3	57.5	11.0	81.0	10.5	81.7
VPFA-1	184.9	58.9	68.2	60.0	67.6
VPFA-2	174.9	52.3	70.1	56.7	67.6
VPFA-3	195.4	69.1	64.7	72.3	63.0

* All fly ash leachates are selected from S:L ratio of 1:3.5 but different pH, and leaching time as follow:

MPFA-1: 4, 24 h, MPFA-2: 7, 24 h, MPFA-3: 10, 24 h

WWFA-1: 4, 1 h, WWFA-2: 7, 1 h, WWFA-3: 10, 1 h

VPFA-1: 4, 24 h, VPFA-2: 7, 24 h, VPFA-3: 10, 24 h

4.5 Concluding Remarks

In this study, *Ed* and *Mq* bark have been found to be potential biosorbents for use in Se(IV) removal. The selenium sorption on bark was highly dependent on solution pH. With increases in pH, sorption of Se(IV) followed somewhat fluctuating trends, possibly arising from changes of an Se-bark bond that exists as a strong inner-sphere covalent bond and a weak outer-sphere hydrogen bond at different pH. Moreover, the maximum sorption occurred at pH 6 for *Ed* and pH 5 for *Mq* bark. The sorption of Se(IV) was found to increase with bark dosage and contact time, but decrease with the initial selenium concentration.

The data for sorption equilibrium demonstrated a good fit to the Freundlich isotherm model. Thus, the sorption may be a multilayer sorption on the heterogeneous surface of the biosorbent. However, from Langmuir and Sips isotherm model, the highest monolayer sorption capacity on the homogeneous surface of bark was obtained as 23.09 µg/g at pH 6 for *Ed*, and 18.83 µg/g at pH 5 for *Mq* bark. Moreover, the maximum sorption capacity was found to be 6.9 mg/g for *Ed* bark, and 7.2 mg/g for *Mq* bark using 100 mg/L Se(IV) solution under optimum conditions. The pseudo-second-order kinetic model was found to correlate most strongly with the experimental data for Se(IV) sorption from aqueous solutions. Therefore, surface sorption is crucial in the selenium sorption process. Desorption experiments indicated that sorption of Se(IV) might follow an ion-exchange and strong physical-chemical sorption. The concentrations of the alkaline (NaOH and Na_2CO_3) may have a positive effect in desorption of Se(IV).

Furthermore, removal of Se(IV) from real-life acidic and alkaline fly ash leachates was demonstrated using *Ed* and *Mq* tree bark under optimised conditions of the biosorption process (bark dosage of 20 g/L, pH 6 and contact time 240 min for *Ed*, and pH 5 and contact time 180 min for *Mq*). The percentage removal from selected fly ash leachates was greater than 63% and potentially reached up to 100%. Overall, the present study has demonstrated that the

sorption potential and biosorption efficiency of *Ed* and *Mq* bark may be effective sorbents for Se(IV) removal from other aqueous waste systems as well as fly ash leachate.

Chapter 5

Conclusion and Future Directions

5.1 Summary and Conclusions

Coal fly ash is a very fine, powdery material that consists of a heterogeneous composition of amorphous aluminosilicate spheres and slightly iron rich spheres. Coal fly ash is primarily produced from the combustion of coal in thermal power plants during energy production. Globally, between 3 – 57% of all fly ash by-products are re-used in the forms of cement and concrete, mine backfill, land filling, soil treatment, production of synthetic zeolites, ceramic filters for hot gas cleaning, and adsorbents (Blissett and Rowson, 2012). However, the majority of coal fly ash is temporarily buried in lagoons or within dry ash landfills. Even though some trace elements such as As and Se are present in coal in low amounts, during the combustion process, the quantity of these elements increases on the surface of the fly ash particles. Therefore, when concentrated on these fly ash particles, uncontained fly ashes have the potential to release an excessive portion of As and Se trace elements into the surrounding environment (Neupane and Donahoe, 2013). In their most common oxyanion speciation of arsenate and selenite in fly ash (Kashiwakura *et al.*, 2011, Izquierdo and Querol, 2011), As and Se are highly soluble in aquatic solutions in a pH range of 7 to 10 (Jankowski *et al.*, 2006), rendering these toxic trace metals highly mobile in surface and ground waters. Despite several methods having been reported for As and Se removal from fly ash, the biosorption has not been investigated. The current study investigates the potential utility of the outer layer of selected tree barks as biosorbents for removing both As(V) and Se(IV) from fly ash leachates.

Tree bark is a non-living biosorbent with the capacity to bind and remove trace elements from dilute aqueous solutions by providing a wide range of ion exchange sites such as hydroxyl, carboxyl and amine groups through their complex biochemical composition of tannins, lignin, cellulose, proteins, carbohydrates and phenolic compounds (Gaballah and Kilbertus, 1998). Moreover, tree barks are readily available, low cost, and are a renewable resource with a large surface area. In conjunction with the possibility of regeneration and metal recovery, the use of tree barks can be justified as an economical and environmentally-friendly biosorbent.

This study achieved three main objectives, the respective conclusions of which are presented in the following sub-sections.

5.1.1 Conclusion 1

Physical, chemical and morphological properties were characterised for three fly ash samples, including two acidic (MPFA and WWFA; intrinsic pH<5) and one alkaline (VPFA; intrinsic pH>11). The results of this study indicated that these fly ashes possessed BET surface areas between 0.5 – 1.1 m^2/g (Table 2.1), and were categorized as Class F fly ashes since they contained > 70 wt.% of total SiO_2, Al_2O_3 and Fe_2O_3, and < 3 wt.% CaO (Table 2.2). The study showed that the fly ash samples contained an estimated concentration of 3.4 – 7.5 mg of As per kg, and 2.1 – 3.8 mg of Se per kg (Table 2.3). Scanning electron micrographs (Figure 2.1-2.5) established that a large proportion of fly ash particles was spherical in shape and included amorphous cenosphere iron-rich particles, along with irregularly-shaped particles composed of alumino-silicates.

Results from batch leaching experiments performed on these fly ash samples led to the following remarks.

- Regardless of the initial pH of the solution, fly ash leachate demonstrated a powerful buffering capacity by maintaining its natural pH level (Table 2.5) (Ward *et al.*, 2009).
- Acidic fly ashes released nearly twice the amount of As compared to the alkaline fly ash leachate (Table 2.6). On the other hand, > 50% of Se was removed from alkaline fly ash, nearly 10-fold the amount obtained in acidic fly ash leachate (Table 2.7), most likely due to the correlation between Ca-phase and Se (Ward *et al.*, 2003, Iwashita *et al.*, 2005).
- The initial pH of the fly ash exhibited a profound but variable effect on As(V) and Se(IV) mobility. The greatest As mobility occurred under neutral to alkaline conditions for MPFA and VPFA (Table 2.6), likely due to As co-precipitating with Fe and the desorption of weak As associations with iron hydroxide or iron oxide at alkaline pH (Jegadeesan *et al.*, 2008a). WWFA exhibited a different behaviour, likely due to the fly ash containing the least initial iron oxide (0.56 wt.%), resulting in the lowest release of Fe from this sample (Table 2.2). For all fly ash leachates, the greatest Se mobility (Table 2.7) was observed at a similar pH to the intrinsic pH of the fly ash samples.
- The mobility of As(V) was observed to be greater at a lower solid: liquid ratio of 1: 10 than more concentrated leachate for the MPFA and VPFA samples (Table 2.6), which may be due to greater Fe solubility. Alternatively, WWFA released more As at a solid:liquid ratio of 1:3.5 due to greater quantities of Si (64.3 wt.%) and Al (27.0 wt.%) (Table 2.2), which can be further released in more concentrated leachate (Iwashita *et al.*, 2005, Ward *et al*., 2009). In contrast to As, the quantity of Se in lower solid:liquid ratios of 1:10 decreased to almost half of that of the more concentrated leachate (Table 2.7). This may be due to the absence of Fe or Mn and higher concentrations of Si and Al in the more concentrated leachate (Iwashita *et al.*, 2005, Ward *et al*., 2009).
- During the early stage of leaching (1 h), As(V) was quickly removed from the surface of fly ash particles (Table 2.6), but the rate of removal decreased over longer time

periods. This effect may be due to sorption and/or co-precipitation of elements back into the solid phase (Jankowski *et al.*, 2006). However, the mobility of Se(IV) gradually increased in MPFA and VPFA leachates of all initial pH values over time (Table 2.7), which may be due to slow dissolution from within fly ash particles (Neupane and Donahoe, 2013).

5.1.2 Conclusion 2

In this study, the outer barks of *Eucalyptus deanei* (*Ed*) and *Melaleuca quinquenervia* (*Mq*) were applied as potential biosorbents for both As(V) and Se(IV) removal. Following the determination of physical, chemical and morphological characterisation of these barks, a series of adsorption experiments was conducted to assess the effects of bark-type, pH, contact time, biosorption dosage, and initial As(V) and Se(IV) concentration on the adsorption process. From the results of this study, the following remarks are made:

- *Mq* bark exhibited a larger BET surface area and pore volume than *Ed* bark, whilst the pore size of each bark was nearly the same (Table 3.2). However, after As(V) and/or Se(IV) sorption, surface area and porosity of both *Ed* and *Mq* barks decreased (Table 3.7 and Table 4.3).
- The quantity of Fe in *Mq* bark was found to be approximately 20 times greater than that in *Ed* bark, whilst the Ca level in *Ed* bark was nearly 10 times greater in *Mq* bark (Table 3.3). *Mq* was found to contain more As than *Ed* bark (Table 3.3), whilst *Ed* bark contained more Se than *Mq*, which may be related to the presence of Fe in *Mq* bark, which has an affinity to sorb As, whilst the greater Ca level *Ed* bark may assist in sequestering Se.
- Scanning electron micrographs revealed that both bark species possessed rough surfaces and large numbers of asymmetric, open pores (Figure 3.8 (a) and (b)), which may

provide greater availability for As and Se sorption. However, after sorption of As (Figures 3.20 and 3.21), and Se (Figures 4.10 and 4.11) slight differences in texture of bark surface became recognisable.

- From the FTIR-ATR results (Figure 3.10), the broad and strong bands at 3331.38 cm^{-1} for *Ed*, and 3334.96 cm^{-1} for *Mq* indicated the presence of potential hydroxyl and/or amide groups in both bark species. The peaks at 2918.87, and 2924.65 cm^{-1}, respectively, implied the C–H stretching in unloaded *Ed* and *Mq* bark. The medium to strong C–O bands at 1230 cm^{-1} and 1029 cm^{-1} for *Ed*, and 1239 cm^{-1} and 1032 cm^{-1} for *Mq* confirmed a possible ether structure of these barks. However, after loading As or Se on the bark, slight increases in intensity and shifting bands were observed, potentially as a result of substitution of hydrogen atoms of amine and/or carboxylic groups (Pandey *et al.*, 2009) by As (Figure 3.22 and 3.23) or Se (Figure 4.12 and 4.13).
- The sorption of As(V) and Se(IV) on bark was found to be highly dependent on solution pH. By increasing pH, sorption of As(V) and Se(IV) was observed to fluctuate (Figure 3.11 and Figure 4.1), which may be due to changes of an element-bark bond, which is likely to exist as strong inner-sphere covalent bonds and weak outer-sphere hydrogen bonds at different pH conditions (Simeoni, 2003). The maximum percentage of As(V) sorption was observed at pH 5 for *Ed* bark (47.7%), and at pH 4 for *Mq* bark (56.8%), whilst Se(IV) was found to be maximally sorbed at pH 6 for *Ed* bark (85.8%), and pH 5 for Mq bark (84.5%).
- The percentage sorption of both As(V) and Se(IV) was found to increase as a function of contact time and bark dosage owing to increasing surface area and the number of available active sites for elemental sorption. However, this effect was levelled off with higher initial As(V) and Se(IV) concentrations, which may be due to the limited number of available active sites on the bark surface (Kannan and Veemaraj, 2010, Rajamohan and Rajasimman, 2015). Interestingly, the sorption uptake and efficiency was found to

follow the opposite pattern. The maximum sorption% of As(V) was observed at 82.3% for *Mq* at 240 min, and 29.4% for *Ed* at 120 min (Figure 3.12). Furthermore, by using 20 g/L bark, 79.2% As(V) was removed at pH 4 by *Mq* bark whilst 32.2% was removed at pH 5 by *Ed* bark (Figure 3.13). Also, As biosorption was found to decrease with increased initial concentrations of As(V) from about 100% to 45.4% when using *Mq* bark, and from 65.5% to 21.9% when using *Ed* bark (Figure 3.14). The percentage of Se(IV) removal was found to reach a maximum between 92% to 95.9% when utilising *Ed* bark, and 76.8% to 83% for *Mq* bark (Figure 4.2 and Figure 4.3). Furthermore, the percentage of Se(IV) removal was found to decrease from approximately 93% for *Ed*, and 100% for *Mq* bark down to 62% for both barks when the initial concentration of Se(IV) was increased from 10 µg/L to 200 µg/L (Figure 4.4).

- The data for sorption equilibrium were found to demonstrate a good fit to the Sips isotherm models for As(V) sorption, whilst both the Langmuir and the Sips isotherm models presented appropriate Se(IV) sorption isotherm. Accordingly, we have proposed here a sorption model consisting of a monolayer on a homogeneous bark surface in higher element concentration, whilst in solutions with lower element concentration a multilayer sorption on the heterogeneous surface of bark may have occurred. The linear values of maximum As(V) sorption efficiency were estimated from Langmuir and Sips isotherm models to be 24.7 µg/g for *Ed* and 31.2 µg/g for *Mq* bark (Table 3.6), whilst the maximum Se(IV) sorption efficiency was 23.1 µg/g for *Ed* and 18.8 µg/g for *Mq* bark (Table 4.2). A pseudo-second-order kinetic model correlated most strongly with the experimental data for As(V) and Se(IV) sorption from aqueous solutions. Therefore, surface sorption is crucial in the As and Se sorption process.
- Overall, < 30% As(V) was recovered from *Ed* and *Mq* bark using 0.1 M HCl as the electrolyte (Table 3.8), whilst < 20% Se(IV) was recovered using 0.1 M NaOH (Table 4.4). Therefore, these desorption experiments indicate that sorption of As(V) and

Se(IV) might follow an ion-exchange and strong physical-chemical binding affinity between such elements and the bark.

- The sorption capacity of arsenate was found to be 1.8 mg/g for *Ed* bark at pH 5 and 4.4 mg/g for Mq bark at pH 4 (Table 3.9), whilst the sorption capacity of selenite was observed as 6.9 mg/g for *Ed* bark at pH 6 and 7.2 mg/g for *Mq* bark at pH 5 (Table 4.5). These results were obtained when testing an initial As(V) or Se(IV) solution of 100 mg/L, and bark dosage of 20 g/L. These results were comparable with the reported data from other agricultural solid wastes and activated carbon adsorbents.

5.1.3 Conclusion 3

Finally, the results of this study support the possibility of removing As(V) and Se(IV) from selected acidic and alkaline fly ash leachates using the outer bark of *Ed* and *Mq* under optimised conditions of the biosorption process. This method was able to remove 69% – 100% of As(V) using *Ed* bark and 86% – 100% of As(V) using *Mq* bark (Table 3.10). This method was also able to remove 65% – 100% of Se(IV) when utilising *Ed* bark, or 63% – 85% of Se(IV) when using *Mq* bark (Table 4.6). In summary, the removal of least 63% of As(V) and Se(IV) was achievable from the selected fly ash leachates and potentially up to 100%. Overall, the present study has demonstrated that both the *Ed* bark and *Mq* bark are effective sorbents for As(V) and Se(IV) removal from fly ash leachates prior to reutilisation or disposal in landfills or detention lagoons.

5.2 Recommendations and Future Directions

There are several limitations during the study, resulting in possible avenues for future work to expand the study. These potential studies include:

- The repetition of leaching and biosorption experiments using mixture of both As(V) and Se(IV) in order to determine the presence of any sorption competition between the two elements.
- An evaluation of As and Se sorption in response to changes in temperature rather than solely at room temperature.
- An evaluation of As and Se sorption in presence of other anions such as SO_4^{2-}, PO_4^{3-}, CO_3^{2-}, and/or cations such as Fe^{3+}, Al^{3+}, Ca^{2+}, would be required to determine the effects of inorganic ions on As and Se sorption.
- Repeat sections of the study utilizing the dynamic column method for leaching and sorption experiments in parallel with static batch method to determine whether there are any method-dependent differences.
- Perform further characterisation studies on these biosorbents to better understand their mechanism and ability to accumulate As(V) and Se(IV).

References

ADRIANO, D. C., PAGE, A. L., ELSEEWI, A. A., CHANG, A. C. & STRAUGHAN, I. 1980. Utilization and Disposal of Fly Ash and Other Coal Residues in Terrestrial Ecosystems: A Review1. *Journal of Environmental Quality,* 9**,** 333-344.

AFROZE, S., SEN, T. K. & ANG, H. M. 2016. Adsorption removal of zinc (II) from aqueous phase by raw and base modified Eucalyptus sheathiana bark: Kinetics, mechanism and equilibrium study. *Process Safety and Environmental Protection,* 102**,** 336-352.

AHMARUZZAMAN, M. 2010. A review on the utilization of fly ash. *Progress in Energy and Combustion Science,* 36**,** 327-363.

AKINYEMI, S. A., GITARI, W. M., AKINLUA, A. & PETRIK, L. F. 2012. Mineralogy and Geochemistry of Sub-Bituminous Coal and Its Combustion Products from Mpumalanga Province, South Africa. *In:* KRULL, I. S. (ed.) *Analytical Chemistry.* InTech, 47-70.

AKSU, Z. 2001. Equilibrium and kinetic modelling of cadmium(II) biosorption by C. vulgaris in a batch system: effect of temperature. *Separation and Purification Technology,* 21**,** 285-294.

AMIN, M. N., KANECO, S., KITAGAWA, T., BEGUM, A., KATSUMATA, H., SUZUKI, T. & OHTA, K. 2006. Removal of Arsenic in Aqueous Solutions by Adsorption onto Waste Rice Husk. *Industrial & Engineering Chemistry Research,* 45**,** 8105-8110.

ARULRAJAH, A., MOHAMMADINIA, A., HORPIBULSUK, S. & SAMINGTHONG, W. 2016. Influence of class F fly ash and curing temperature on strength development of fly ash-recycled concrete aggregate blends. *Construction and Building Materials,* 127**,** 743-750.

AUSTIN, D. E. & NEWLAND, L. 1985. Time-resolved leaching of cadmium and manganese from lignite and incinerator fly ash. *Chemosphere,* 14**,** 41-51.

BAYLEY, C. & ROSE, G. R. 1960. Metal-organic complexes formed during the treatment of wood with metal salts. *Nature,* 185**,** 313-314.

BAYSAL, Z., ÇINAR, E., BULUT, Y., ALKAN, H. & DOGRU, M. 2009. Equilibrium and thermodynamic studies on biosorption of Pb(II) onto Candida albicans biomass. *Journal of Hazardous Materials,* 161**,** 62-67.

BELFORD, D. & PRESTON, R. 1960. Copper-cellulose complexes. *Nature,* 185**,** 911-911.

BLAND, D. E. 1963. Sorption of copper by wood constituents. *Nature,* 200**,** 267-267.

BLISSETT, R. S. & ROWSON, N. A. 2012. A review of the multi-component utilisation of coal fly ash. *Fuel,* 97**,** 1-23.

BOLANZ, R. M., MAJZLAN, J., JURKOVIČ, L. & GÖTTLICHER, J. 2012. Mineralogy, geochemistry, and arsenic speciation in coal combustion waste from Nováky, Slovakia. *Fuel,* 94**,** 125-136.

BROWN, A. M. 2001. A step-by-step guide to non-linear regression analysis of experimental data using a Microsoft Excel spreadsheet. *Computer Methods and Programs in Biomedicine,* 65**,** 191-200.

CERVERA, M. L., ARNAL, M. C. & DE LA GUARDIA, M. 2003. Removal of heavy metals by using adsorption on alumina or chitosan. *Analytical and Bioanalytical Chemistry,* 375**,** 820-825.

CHANG, A. C., LUND, L. J., PAGE, A. L. & WARNEKE, J. E. 1977. Physical Properties of Fly Ash-Amended Soils1. *Journal of Environmental Quality,* 6**,** 267-270.

CHEN, W., KIRKELUND, G. M., JENSEN, P. E. & OTTOSEN, L. M. 2017. Comparison of different MSWI fly ash treatment processes on the thermal behavior of As, Cr, Pb and Zn in the ash. *Waste Management,* 68**,** 240-251.

CHIL-SUNG JEON, KITAE BAEK, JOON-KYU PARK, YOUNG-KI OH & LEE, S.-D. 2009. Adsorption characteristics of As(V) on iron-coated zeolite. *Journal of Hazardous Materials,* 163**,** 804-808.

CLARK, R., RITCHEY, K. & BALIGAR, V. 2001. Benefits and constraints for use of FGD products on agricultural land. *Fuel,* 80**,** 821-828.

CRINI, G. & BADOT, P.-M. 2008. Application of chitosan, a natural aminopolysaccharide, for dye removal from aqueous solutions by adsorption processes using batch studies: A review of recent literature. *Progress in Polymer Science,* 33**,** 399-447.

CRIST, R. H., MARTIN, J. R. & CRIST, D. R. 1999. Interaction of Metal Ions with Acid Sites of Biosorbents Peat Moss and Vaucheria and Model Substances Alginic and Humic Acids. *Environmental Science & Technology,* 33**,** 2252-2256.

CUTILLAS-BARREIRO, L., ANSIAS-MANSO, L., FERNÁNDEZ-CALVIÑO, D., ARIAS-ESTÉVEZ, M., NÓVOA-MUÑOZ, J. C., FERNÁNDEZ-SANJURJO, M. J., ÁLVAREZ-RODRÍGUEZ, E. & NÚÑEZ-DELGADO, A. 2014. Pine bark as bio-adsorbent for Cd, Cu, Ni, Pb and Zn: Batch-type and stirred flow chamber experiments. *Journal of Environmental Management,* 144**,** 258-264.

CUTILLAS-BARREIRO, L., PARADELO, R., IGREXAS-SOTO, A., NÚÑEZ-DELGADO, A., FERNÁNDEZ-SANJURJO, M. J., ÁLVAREZ-RODRIGUEZ, E., GARROTE, G., NÓVOA-MUÑOZ, J. C. & ARIAS-ESTÉVEZ, M. 2016. Valorization of biosorbent obtained from a forestry waste: Competitive adsorption, desorption and transport of Cd, Cu, Ni, Pb and Zn. *Ecotoxicology and Environmental Safety,* 131**,** 118-126.

DAVIS, T. A., VOLESKY, B. & MUCCI, A. 2003. A review of the biochemistry of heavy metal biosorption by brown algae. *Water Research,* 37**,** 4311-4330.

DEMIRAL, H., DEMIRAL, I., TUMSEK, F. & KARABACAKOGLU, B. 2008. Adsorption of chromium(VI) from aqueous solution by activated carbon derived from olive bagasse and applicability of different adsorption models. *Chemical Engineering Journal,* 144**,** 188-196.

DESHICAR, A. M., BOKADE, S. S. & DARA, S. S. 1990. Modified hardwickia binata bark for adsorption of mercury (II) from water. *Water Research,* 24**,** 1011-1016.

DHANKHAR, R. & HOODA, A. 2011. Fungal biosorption – an alternative to meet the challenges of heavy metal pollution in aqueous solutions. *Environmental Technology,* 32**,** 467-491.

DUC, M., LEFÈVRE, G. & FÉDOROFF, M. 2006. Sorption of selenite ions on hematite. *Journal of Colloid and Interface Science,* 298**,** 556-563.

DUDAS, M. J. 1981. Long-term leachability of selected elements from fly ash. *Environmental Science & Technology,* 15**,** 840-843.

DUNN, E. 2015. *Why is coal ash important to you and me?* [Online]. ENGL 105 Fall 2015. Available: http://engl105062.web.unc.edu/2015/09/17/coal-ash/ [Accessed 08/04/2017.

EAST, J. & MATTHIAS, R. 2016. *National Coal Resources Data System (NCRDS)* [Online]. The U.S. Geological Survey (USGS). Available: http://energy.er.usgs.gov/products/databases/CoalQual/intro.htm [Accessed 04/04/2017 2017].

EBRAHIMIAN, A., SABERIKHAH, E., EMAMI, M. S. & SOTUDEH, M. 2014. *Study of biosorption parameters: Isotherm, kinetics and thermodynamics of basic blue 9 biosorption onto Foumanat tea waste*.

EL-MOGAZI, D., LISK, D. J. & WEINSTEIN, L. H. 1988. A Review of Physical, Chemical, and Biological Properties of Fly Ash and Effects on Agricultural Ecosystems. *The Science of the Total Environment,* 74**,** 1-37.

EL-SHAFEY, E. I. 2007. Sorption of Cd(II) and Se(IV) from aqueous solution using modified rice husk. *Journal of Hazardous Materials,* 147**,** 546-555.

ENERGYAUSTRALIA. 2016. *Coal Electricity Generation* [Online]. Available: https://www.energyaustralia.com.au/about-us/media-centre/educational-resources [Accessed 5/12/2016].

EPRI 2010. Comparison of Coal Combustion Products to Other Common Materials: Chemical Characteristics. *Technical Results.* Electric Power Research Institute, Doc number 1020556 .

ESPOSITO, A., PAGNANELLI, F. & VEGLIÒ, F. 2002. pH-related equilibria models for biosorption in single metal systems. *Chemical Engineering Science,* 57**,** 307-313.

FERNÁNDEZ-TURIEL, J. L., DE CARVALHO, W., CABAÑAS, M., QUEROL, X. & LÓPEZ-SOLER, A. 1994. Mobility of heavy metals from coal fly ash. *Environmental Geology,* 23**,** 264-270.

FISHER, G., PRENTICE, B., SILBERMAN, D., ONDOV, J., BIERMANN, A., BAGAINI, R. & MCFARLAND, A. 1978. Physical and Morphological Studies of Size-Classified Coal Fly Ash. *Environmental Science and Technology,* 12**,** 444.

FISHMAN, N. S., RICE, C. A., BREIT, G. N. & JOHNSON, R. D. 1999. Sulfur-bearing coatings on fly ash from a coal-fired power plant: composition, origin, and influence on ash alteration. *Fuel,* 78**,** 187-196.

FLOMINA, E. 1967. Chemistry of interaction of CCA-235 antiseptic with wood. *Izvestiya Vysshikh Uchebnykh Zavedenii Les. Zhurnal,* 10**,** 118-122.

FOMINA, M. & GADD, G. M. 2014. Biosorption: current perspectives on concept, definition and application. *Bioresource Technology,* 160**,** 3-14.

FOO, K. Y. & HAMEED, B. H. 2010. Insights into the modeling of adsorption isotherm systems. *Chemical Engineering Journal,* 156**,** 2-10.

FRISBIE, S. H., MITCHELL, E. J. & SARKAR, B. 2013. World Health Organization increases its drinking-water guideline for uranium. *Environmental Science: Processes & Impacts,* 15**,** 1817-1823.

FURR, A. K., KELLEY, W. C. & BACHE, C. A. 1976. Multielement uptake by vegetables and millet grown in pots on fly ash amended soil. *Journal of agricultural and food chemistry,* 24**,** 885-888.

FURR, A. K., PARKINSON, T. F., BACHE, C. A., GUTENMANN, W. H., PAKKALA, I. S. & LISK, D. J. 1981. Elemental content of vegetables and millet grown in potted soil amended with lignite fly ash. *Archives of environmental contamination and toxicology,* 10**,** 647-651.

FURR, A. K., PARKINSON, T. F., ELFVING, D. C., GUTENMANN, W. H., PAKKALA, I. S. & LISK, D. J. 1979. Elemental content of apple, millet, and vegetables grown in pots of neutral soil amended with fly ash. *Journal of agricultural and food chemistry,* 27**,** 135-138.

GABALLAH, I. & KILBERTUS, G. 1998. Recovery of heavy metal ions through decontamination of synthetic solutions and industrial effluents using modified barks. *Journal of Geochemical Exploration,* 62**,** 241-286.

GADD, G. M. 2009. Biosorption: critical review of scientific rationale, environmental importance and significance for pollution treatment. *Journal of Chemical Technology and Biotechnology,* 84**,** 13-28.

GARRETT, N. E., CAMPBELL, J. A., STACK, H. F., WATERS, M. D. & LEWTAS, J. 1981. Utilization of the rabbit alveolar macrophage and Chinese hamster ovary cell for evaluation of the toxicity of particulate materials. II. Particles from coal-related processes. *Environmental Research***,** 366-376.

GAVRILESCU, M. 2004. Removal of Heavy Metals from the Environment by Biosorption. *Engineering in Life Sciences,* 4**,** 219-232.

GHIMIRE, K. N., INOUE, K., MAKINO, K. & MIYAJIMA, T. 2002. Adsorptive Removal of Arsenic Using Orange Juice Residue. *Separation Science and Technology,* 37**,** 2785-2799.

GHODBANE, I. & HAMDAOUI, O. 2008. Removal of mercury(II) from aqueous media using eucalyptus bark: Kinetic and equilibrium studies. *Journal of Hazardous Materials,* 160**,** 301-309.

GIBBS, B. M., THOMPSON, D. & ARGENT, B. B. 2008. Mobilisation of trace elements from assupplied and additionally cleaned coal: Predictions for Ba, Be, Cd, Co, Mo, Nb, Sb, V and W. *Fuel,* 87**,** 1217-1229.

GIUSTI, L. 2009. A review of waste management practices and their impact on human health. *Waste Management,* 29**,** 2227-2239.

GOODARZI, F., HUGGINS, F. E. & SANEI, H. 2008. Assessment of elements, speciation of As, Cr, Ni and emitted Hg for a Canadian power plant burning bituminous coal. *International Journal of Coal Geology,* 74**,** 1-12.

GREIST, W. H. & B.A. TOMKINS 1986. Influences of carbonaceous particles on the interaction of coal combustion stack ash with organic matter. *Environmental Science and Technology* 20**,** 291-295.

GUTENMANN, W. H. & LISK, D. J. 1979. Absorption of selenium from coal fly ash-amended soil byAstragalus racemosus. *Bulletin of environmental contamination and toxicology,* 23**,** 104-106.

HANSEN, H. K., ARANCIBIA, F. & GUTIÉRREZ, C. 2010. Adsorption of copper onto agriculture waste materials. *Journal of Hazardous Materials,* 180**,** 442-448.
HANSEN, L. D. & FISHER, G. L. 1980. Elemental distribution in coal fly ash particles. *Environmental Science and Technology* 14**,** 111-117.
HARRIS, W. R., E.K. CHESS, D. OKAMOTO, J.F. RAMSEN & D.W. LATER 1984. Contribution of nitropyrene to the mutagenic activity of coal fly ash. *Environmental Mutagenesis,* 6**,** 131-144.
HASSETT, D. J., PFLUGHOEFT-HASSETT, D. F. & HEEBINK, L. V. 2005. Leaching of CCBs: observations from over 25 years of research. *Fuel,* 84**,** 1378-1383.
HEIDRICH, C., FEUERBORN, H.-J. & WEIR, A. 2013. Coal Combustion Products: a Global Perspective. *2013 World of Coal Ash (WOCA).* Lexington, KY.
HENKE, K. R. & HUTCHISON, A. 2009. Arsenic chemistry. *In:* HENKEN, K. R. (ed.) *Arsenic: Environmental Chemistry, Health Threats and Waste Treatment.* John Wiley & Sons Ltd.
HOLLIS, J., KEREN, R. & GAL, M. 1988. Beron Release and Sorption by Fly Ash as Affected by pH and Particle Size,. *Journal of Environmental Ouality,* 17**,** 181.
HUANG, T. Y., CHIUEH, P. T. & LO, S. L. 2017. Life-cycle environmental and cost impacts of reusing fly ash. *Resources, Conservation and Recycling,* 123**,** 255-260.
HUGGINS, F. E., SENIOR, C. L., CHU, P., LADWIG, K. & HUFFMAN, G. P. 2007b. Selenium and Arsenic Speciation in Fly Ash from Full-Scale Coal-Burning Utility Plants. *Environmental Science & Technology,* 41**,** 3284-3289.
HULETT, L. D., WEINBERGER, A. J., NORTHCUTT, K. J. & FERGUSON, M. 1980. Chemical Species in Fly Ash from Coal-Burning Power Plants. *Science,* 210**,** 1356-1358.
INTERNATIONAL ENERGY STATISTICS, U. E. I. A. 2012. US Energy Information Administration [online]. Available: http://www.eia.gov/cfapps/ipdbproject/iedindex3.cfm [Accessed 10/03/2016].
IWASHITA, A., SAKAGUCHI, Y., NAKAJIMA, T., TAKANASHI, H., OHKI, A. & KAMBARA, S. 2005. Leaching characteristics of boron and selenium for various coal fly ashes. *Fuel,* 84**,** 479-485.
IZQUIERDO, M. & QUEROL, X. 2011. Leaching behaviour of elements from coal combustion fly ash: An overview. *International Journal of Coal Geology*.
IZQUIERDO, M. & QUEROL, X. 2012. Leaching behaviour of elements from coal combustion fly ash: An overview. *International Journal of Coal Geology,* 94**,** 54-66.
JACKSON, B. P. & MILLER, W. P. 1998. Arsenic and selenium speciation in coal fly ash extracts by ion chromatography-inductively coupled plasma mass spectrometry. *Journal of Analytical Atomic Spectrometry,* 13**,** 1107-1112.
JACKSON, B. P. & MILLER, W. P. 1999. Soluble Arsenic and Selenium Species in Fly Ash/Organic Waste-Amended Soils Using Ion Chromatography−Inductively Coupled Plasma Mass Spectrometry. *Environmental Science & Technology,* 33**,** 270-275.
JALA, S. & GOYAL, D. 2006. Fly ash as a soil ameliorant for improving crop production—a review. *Bioresource Technology,* 97**,** 1136-1147.
JANKOWSKI, J., WARD, C., FRENCH, D. & GROVES, S. 2006. Mobility of trace elements from selected Australian fly ashes and its potential impact on aquatic ecosystems. *Fuel,* 85**,** 243-256.
JEGADEESAN, G., AL-ABED, S. R. & PINTO, P. 2008a. Influence of trace metal distribution on its leachability. *Fuel,* 87**,** 1887-1893.
KALAVATHY M. HELEN, KARTHIKEYAN T., RAJGOPAL S. & ROSE, M. L. 2005. Kinetic and isotherm studies of Cu(II) adsorption onto H_3PO_4-activated rubber wood sawdust. *Journal of Colloid and Interface Science,* 292**,** 354-362.
KALYONCU, R. S. 2001. Coal combustion products. *U.S. Geological Survey Minerals Yearbook.* Reston, VA.
KANNAN, N. & VEEMARAJ, T. 2010. Cadmium (II) ions removal by adsorption onto *Eucalyptus globules* bark, *Bambusa glucescens* dust and commercial activated carbons. *Electronic Journal of Environmental, Agricultural and Food Chemistry,* 9**,** 129-137.
KASHIWAKURA, S., OHNO, H., KUMAGAI, Y., KUBO, H., MATSUBAE, K. & NAGASAKA, T. 2011. Dissolution behavior of selenium from coal fly ash particles for the development of an acid-washing process. *Chemosphere,* 85**,** 598-602.

KASHIWAKURA, S., OHNO, H., MATSUBAE-YOKOYAMA, K., KUMAGAI, Y., KUBO, H. & NAGASAKA, T. 2010. Removal of arsenic in coal fly ash by acid washing process using dilute H2SO4 solvent. *Journal of Hazardous Materials,* 181**,** 419-25.

KEATING, M., BAUM, E. & ROUND, M. 2000. Laid to Waste; The Dirty Secret of Combustion Waste from America's Power Plants. USA: Citizens Coal Council, Hoosier Environmental Council, Clean Air Task Force.

KHAKPOUR, H., YOUNESI, H. & MOHAMMADHOSSEINI, M. 2014. Two-stage biosorption of selenium from aqueous solution using dried biomass of the baker's yeast Saccharomyces cerevisiae. *Journal of Environmental Chemical Engineering,* 2**,** 532-542.

KILLINGLEY, J., MCEVOY, S., DOKUMCU, C., STAUBER, J. & DALE, L. 2000. Trace Element Leaching From Fly Ash from Australian Power Stations. CSIRO Energy Technology, Project C8051.

KLEIN, D. H., ANDREN, A. W., CARTER, J. A., EMERY, J. F., FELDMAN, C., FULKERSON, W., LYON, W. S., OGLE, J. C., TALMI, Y., VAN HOOK, R. I. & BOLTON, N. 1975. Pathways of thirty-seven trace elements through coal-fired power plant. *Environmental Science and Technology,* 9**,** 973-979.

KRATOCHVIL, D., PIMENTEL, P. & VOLESKY, B. 1998. Removal of Trivalent and Hexavalent Chromium by Seaweed Biosorbent. *Environmental Science & Technology,* 32**,** 2693-2698.

KRIEGER, H. & JACOBS, B. 1978. Analysis of radioactive contaminants in by-product from coal-fires power plant operations. U.S. Environmental Protection Agency (USEPA), EPA-600-/4-78-039.

KRISHNAMURTHY, S. & FREDERICK, R. M. 1994. Using biopolymers to remove heavy metals from soil and water. *Remediation Journal,* 4**,** 235-244.

KÜBEL, H. & PIZZI, A. 1982. The chemistry and kinetic behavior of copper-chromium-arsenic/boron wood preservatives. Part 5. Reactions of a copper-chromium-boron (CCB) preservative with cellulose, lignin and their simple model compounds. *Holzforsch. Holzverwert,* 34**,** 75-83.

KUMAR, K. V. & PORKODI, K. 2006. Relation between some two- and three-parameter isotherm models for the sorption of methylene blue onto lemon peel. *Journal of Hazardous Materials,* 138**,** 633-635.

KUMAR, P. & DARA, S. 1980. Modified barks for scavenging toxic heavy metal ions. *Indian Journal of Environmental Health,* 22**,** 196-202.

KUMAR, P. & DARA, S. S. 1982. Utilisation of agricultural wastes for decontaminating industrial/domestic wastewaters from toxic metals. *Agricultural Wastes,* 4**,** 213-223.

KUMAR, V., MATHUR, M. & KHARIA, P. 2003. Fly ash management: Vision for the New Millenium, . Technology Information Forecasting and Assessment Council, News and Views, 25, March, 2003.

KUMARI, P., SHARMA, P., SRIVASTAVA, S. & SRIVASTAVA, M. M. 2006. Biosorption studies on shelled Moringa oleifera Lamarck seed powder: Removal and recovery of arsenic from aqueous system. *International Journal of Mineral Processing,* 78**,** 131-139.

KUTCHKO, B. & KIM, A. 2006. Fly ash characterization by SEM–EDS. *Fuel,* 85**,** 2537-2544.

LARCHER, W. 2003. *Physiological Plant Ecology: Ecophysiology and Stress Physiology of Functional Groups*, Springer Science & Business Media.

LI, A., CLARK, C., HANSON, R., HENDERSON, T. & HOBBS, C. 1983. Comparative mutagenicity of a coal combustion fly ash extract in Salmonella typhimurium and Chinese hamster ovary cells. *Environmental and Molecular Mutagenesis,* 5**,** 263-272.

LI, K., ZHANG, Y., DANG, Y., WEI, H. & WANG, Q. 2014. Removal of Cr(VI) from Aqueous Solutions Using Buckwheat (Fagopyrum esculentum Moench) Hull through Adsorption–Reduction: Affecting Factors, Isotherm, and Mechanisms. *CLEAN – Soil, Air, Water,* 42**,** 1549-1557.

LI, Z., LI, H., YANG, X., ZHANG, H., LIU, C. & CAO, B. 2013. Characterization of Se(IV) removal from aqueous solution by Aspergillus sp. J2. *Chemical Engineering Journal,* 220**,** 67-71.

LIEM, H., SANDSTROM, M., T. WALLIN, A. CARNE, U. RYDEVIK, THURENIUS, B. & P.O. MOBERG 1983. Studies on leaching and weathering processes of coal ashes. *Water Science and Technology,* 15**,** 163-191.

LITTER, M. I., MORGADA, M. E. & BUNDSCHUH, J. 2010. Possible treatments for arsenic removal in Latin American waters for human consumption-Review. *Environmental Pollution,* 158**,** 1105-1118.

LIU, K., XIE, W., ZHAO, Z.-B., PAN, W.-P. & RILEY, J. T. 2000. Investigation of Polycyclic Aromatic Hydrocarbons in Fly Ash from Fluidized Bed Combustion Systems. *Environmental Science & Technology,* 34**,** 2273-2279.

LIU, W. K., WONG, M. H. & TAM, N. F. Y. 1986. Comparison of hemolytic activities of coal fly ash and its soluble and insoluble fractions. *Environmental Research***,** 459-469.

LIZAMA, A. K., FLETCHER, T. D. & SUN, G. 2011. Removal processes for arsenic in constructed wetlands. *Chemosphere,* 84**,** 1032-43.

LO, S.-L. & CHEN, T.-Y. 1997. Adsorption of Se(IV) and Se(VI) on an iron-coated sand from water. *Chemosphere,* 35**,** 919-930.

LORENZEN, L., VAN DEVENTER, J. S. J. & LANDI, W. M. 1995. Factors affecting the mechanism of the adsorption of arsenic species on activated carbon. *Minerals Engineering,* 8**,** 557-569.

LUO, Y., GIAMMAR, D. E., HUHMANN, B. L. & CATALANO, J. G. 2011. Speciation of Selenium, Arsenic, and Zinc in Class C Fly Ash. *Energy & Fuels,* 25**,** 2980-2987.

MARTTIGOD, S. V., RAI, D., EARY, L. E. & AINSWORTH, C. C. 1990. Geochemical factors controlling the mobilization of inorganic constituents from fossil fuel combustion residues: I. Review of the major elements. *Journal of Environmental Quality,* 19**,** 188-201.

MATSUNAGA, T., KIM, J. K., HARDCASTLE, S. & ROHATGI, P. K. 2002. Crystallinity and selected properties of fly ash particles. *Materials Science and Engineering,* A325**,** 333-343.

MATTIGOD, S. V. 1983. Chemical composition of aqueous extracts of fly ash: Ionic speciation as a controlling factor. *Environmental Technology Letters,* 4**,** 485-490.

MEIJ, R. 1994. Trace element behavior in coal-fired power plants. *Fuel Processing Technology,* 39**,** 199-217.

MEUNIER, N., LAROULANDIE, J., BLAIS, J. F. & TYAGI, R. D. 2003. Cocoa shells for heavy metal removal from acidic solutions. *Bioresource Technology,* 90**,** 255-263.

MICHALAK, I. & CHOJNACKA, K. 2009. Edible macroalga Ulva prolifera as microelemental feed supplement for livestock: the fundamental assumptions of the production method. *World Journal of Microbiology and Biotechnology,* 25**,** 997-1005.

MICHALAK, I., CHOJNACKA, K. & WITEK-KROWIAK, A. 2013. State of the Art for the Biosorption Process—a Review. *Applied Biochemistry and Biotechnology* 170**,** 1389-1416.

MICHALAK, I. C., K. 2010. The New Application of Biosorption Properties of Enteromorpha prolifera. *Applied Biochemistry and Biotechnology,* 160**,** 1540-1556.

MISHRA, V., BALOMAJUMDER, C. & AGARWAL, V. K. 2010. Biosorption of Zn (II) onto the Surface of Non-living Biomasses: A Comparative Study of Adsorbent Particle Size and Removal Capacity of Three Different Biomasses. *Water, Air, and Soil Pollution,* 211**,** 489-500.

MOMČILOVIĆ, M., PURENOVIĆ, M., BOJIĆ, A., ZARUBICA, A. & RANĐELOVIĆ, M. 2011. Removal of lead(II) ions from aqueous solutions by adsorption onto pine cone activated carbon. *Desalination,* 276**,** 53-59.

MORITA, M., HIGUCHI, M. & SAKATA, I. 1987. Binding of heavy metal ions by chemically modified woods. *Journal of Applied Polymer Science,* 34**,** 1013-1023.

MUMFORD, J. L. & LEWTAS, J. 1982. Mutagenicity and cytotoxicity of coal fly ash from fluidized bed and conventional combustion. *Journal of Toxicology and Environmental Health,* 10.

MURPHY, V., HUGHES, H. & MCLOUGHLIN, P. 2007. Cu(II) binding by dried biomass of red, green and brown macroalgae. *Water Research,* 41**,** 731-740.

N. YEDDOU MEZENNER & BENSMAILI, A. 2009. Kinetics and thermodynamic study of phosphate adsorption on iron hydroxide-eggshell waste. *Chemical Engineering Journal,* 147**,** 87-96.

NARUKAWA, T., TAKATSU, A., CHIBA, K., RILEY, K. W. & FRENCH, D. H. 2005. Investigation on chemical species of arsenic, selenium and antimony in fly ash from coal fuel thermal power stations. *Journal of Environmental Monitoring,* 7**,** 1342-8.

NEPA 1999. National Environment Protection (Assessment of Site Contamination) Measure 1999. *Schedule B3, Guidline on Laboratory Analysis of Potentially Contaminated Soils.* Canberra, NSW: Office of Parliamentary Counsel.

NEUPANE, G. & DONAHOE, R. J. 2013. Leachability of elements in alkaline and acidic coal fly ash samples during batch and column leaching tests. *Fuel,* 104**,** 758-770.

NIMZ, H. 1974. Das Lignin der Buche — Entwurf eines Konstitutionsschemas. *Angewandte Chemie,* 86**,** 336-344.
OPENSHAW, S. C. 1992. *Utilization of Coal Fly Ash.* Master of Engineering, University of Florida.
OTERO-REY, J. E. R., MATO-FERN´ANDEZ, M. ı. J., MOREDA-PI˜NEIRO, J., ALONSO-RODR´ıGUEZ, E., MUNIATEGUI-LORENZO, S., L´OPEZ-MAH´ıA, P. O. & PRADA-RODR´ıGUEZ, D. ı. 2005. Influence of several experimental parameters on As and Se leaching from coal fly ash samples. *Analytica Chimica Acta,* 531**,** 299-305.
P. JACKSON, B. & P. MILLER, W. 1998. Arsenic and selenium speciation in coal fly ash extracts by ion chromatography-inductively coupled plasma mass spectrometry. *Journal of Analytical Atomic Spectrometry,* 13**,** 1107-1112.
PAGE, A. L., ELSEEWI, A. A. & STRAUGHAN, I. R. 1979. Physical and chemical properties of fly ash from coal fired power plants with special reference to environmental impacts. *Residue Reviews,* 71**,** 83-120.
PAGNANELLI, F., MAINELLI, S., VEGLIÒ, F. & TORO, L. 2003. Heavy metal removal by olive pomace: biosorbent characterisation and equilibrium modelling. *Chemical Engineering Science,* 58**,** 4709-4717.
PALMA, G., FREER, J. & BAEZA, J. 2003. Removal of metal ions by modified Pinus radiata bark and tannins from water solutions. *Water Research,* 37**,** 4974-80.
PANDEY, P. K., CHOUBEY, S., VERMA, Y., PANDEY, M. & CHANDRASHEKHAR, K. 2009. Biosorptive removal of arsenic from drinking water. *Bioresource Technology,* 100**,** 634-7.
PARK, D., YUN, Y.-S. & PARK, J. M. 2008. XAS and XPS studies on chromium-binding groups of biomaterial during Cr(VI) biosorption. *Journal of Colloid and Interface Science,* 317**,** 54-61.
PARK, D., YUN, Y.-S. & PARK, J. M. 2010. The past, present, and future trends of biosorption. *Biotechnology and Bioprocess Engineering,* 15**,** 86-102.
PATRA, K. C., RAUTRAY, T. R. & NAYAK, P. 2012. Analysis of grains grown on fly ash treated soils. *Applied Radiation and Isotopes*.
PEFFER, J. 1982. Fly Ash Disposal in a Limestone Quarry. *Ground Water,* 20**,** 267.
PETERS, G. & PARAMESWARAN, N. 1980. Transmission electron microscopical localization of salt preservative components in wood cell walls. *Wood Science and Technology,* 14**,** 81-88.
PLACKETT, D., AINSCOUGH, E. & BRODIE, A. 1987. The examination of preservative-treated radiata pine using electron spin resonance spectroscopy. *Patent Number IRG/WP,* 3423**,** 1987.
PROMTHET, P. & MUNGKARNDEE, P. 2015. Biosorption of nickel (II) ions from aqueous solutions by tapioca peel. *African Journal of Environmental Science and Technology,* 9**,** 662-670.
RAIS AHMAD, RAJEEV KUMAR & HASEEB, S. 2012. Adsorption of Cu2+ from aqueous solution onto iron oxide coated eggshell powder: Evaluation of equilibrium, isotherms, kinetics, and regeneration capacity. *Arabian Journal of Chemistry,* 5**,** 353-359.
RAJAMOHAN, N. & RAJASIMMAN, M. 2015. Biosorption of Selenium using activated plant based sorbent – Effect of variables, isotherm and kinetic modeling. *Biocatalysis and Agricultural Biotechnology,* 4**,** 795-800.
RAMÍREZ-PAREDESA, F., I., MANZANO-MUÑOZB, T., GARCIA-PRIETOB, J., J, F.B., ZHADANC, G.G., SHNYROVC, V.L., KENNEDYD, J.F. & ROIGA, M.G. 2013. Biosorption of Heavy Metals from Acid Mine Drainages onto Pig Bristles, Poultry Feathers and Crustacean Shells Industrial Biowastes. *Journal of Basic & Applied Sciences,* 9**,** 510-524.
RANDALL, J., GARRET, V., BERMANN, R. & WAISS, A. 1974. Removal and recycling of heavy metal ions from waste solutions. *Forest Products Journal,* 24**,** 80-84.
RANDALL, J. & HAUTALA, E. Removal of heavy metal ions from waste solutions by contact with agricultural byproducts. Proceedings Industrial Wastes Conference, Purdue University, 1977.
RANDALL, J., HAUTALA, E., WAISS JR, A. & TSCHERNITZ, J. 1976. Modified barks as scavengers for heavy metal ions. *Forest Products Journal,* 24.
RANJAN, D., TALAT, M. & HASAN, S. H. 2009. Biosorption of arsenic from aqueous solution using agricultural residue 'rice polish'. *Journal of Hazardous Materials,* 166**,** 1050-9.
REATEGUI, M., MALDONADO, H., LY, M. & GUIBAL, E. 2010. Mercury(II) Biosorption Using Lessonia sp. Kelp. *Applied Biochemistry and Biotechnology,* 162**,** 805-822.

REDDY, D. H. K., LEE, S.-M. & SESHAIAH, K. 2012. Biosorption of Toxic Heavy Metal Ions from Water Environment Using Honeycomb Biomass—An Industrial Waste Material. *Water, Air, & Soil Pollution,* 223**,** 5967-5982.

REDDY, H. K. D., RAMANA, D. K. V., SESHAIAH, K. & REDDY, A. V. R. 2011. Biosorption of Ni(II) from aqueous phase by Moringa oleifera bark, a low cost biosorbent. *Desalination,* 268**,** 150-157.

REIJNDERS, L. 2005. Disposal, uses and treatments of combustion ashes: a review. *Resources, Conservation and Recycling,* 43**,** 313-336.

RIBEIRO, J., SILVA, T. F., MENDONCA FILHO, J. G. & FLORES, D. 2014. Fly ash from coal combustion – An environmental source of organic compounds. *Applied Geochemistry,* 44**,** 103-110.

RODRÍGUEZ-MARTÍNEZ, C. E., GONZÁLEZ-ACEVEDO, Z. I., OLGUÍN, M. T. & FRÍAS-PALOS, H. 2016. Adsorption and desorption of selenium by two non-living biomasses of aquatic weeds at dynamic conditions. *Clean Technologies and Environmental Policy,* 18**,** 33-44.

RODUSHKIN, I., RUTH, T. & HUHTASAARI, Å. 1999. Comparison of two digestion methods for elemental determinations in plant material by ICP techniques. *Analytica Chimica Acta,* 378**,** 191-200.

ROY, W. R. & BERGER, P. M. 2011. Geochemical Controls of Coal Fly Ash Leachate pH. *Coal Combustion and Gasification Products,* 3**,** 63-66.

ROY, W. R. & GRIFFIN, R. A. 1984. Illinois Basin coal fly ashes. 2. Equilibria relationships and qualitative modeling of ash-water reactions. *Environmental Science & Technology,* 18**,** 739-742.

ROY, W. R., THIERY, R. G., SCHULLER, R. M. & SULOWAY, J. J. 1981. *Coal fly ash : a review of the literature and proposed classification system with emphasis on environmental impacts* Champaign, IL (615 E. Peabody Dr., Champaign 61820) : Illinois State Geological Survey.

SAKAI, K. 2000. Chemistry of Bark. *In:* HON, D. N. S. & SHIRAISHI, N. (eds.) *Wood and Cellulosic Chemistry, Second Edition, Revised, and Expanded.* Second ed. New York . Basel: Marcel Dekker, Inc.

SAQIB, A. N. S., WASEEM, A., KHAN, A. F., MAHMOOD, Q., KHAN, A., HABIB, A. & KHAN, A. R. 2013. Arsenic bioremediation by low cost materials derived from Blue Pine (Pinus wallichiana) and Walnut (Juglans regia). *Ecological Engineering,* 51**,** 88-94.

SARKAR, A., RANO, R., MISHRA, K. K. & SINHA, I. N. 2005. Particle size distribution profile of some Indian fly ash—a comparative study to assess their possible uses. *Fuel Processing Technology,* 86**,** 1221-1238.

SCHRAMKE, J. A. 1992. Neutralization of alkaline coal fly ash leachates by CO2(g). *Applied Geochemistry,* 7**,** 481-492.

SCHURE, M. R. 1985. Surface area and porosity of coal fly ash. *Environ. Sci. Technol.;(United States),* 19.

SCHWERTMANN, U. & TAYLOR, R. M. 1989. Iron Oxides. *In:* DIXON, J. B. & WEED, S. B. (eds.) *Minerals in Soil Environments.* 2 ed. Madison, WI, USA: Soil Science Society of America Book Series

SEKI, H., SUZUKI, A. & MARUYAMA, H. 2005. Biosorption of chromium(VI) and arsenic(V) onto methylated yeast biomass. *Journal of Colloid and Interface Science,* 281**,** 261-266.

SELATNIA, A., MADANI, A., BAKHTI, M. Z., KERTOUS, L., MANSOURI, Y. & YOUS, R. 2004. Biosorption of Ni2+ from aqueous solution by a NaOH-treated bacterial dead Streptomyces rimosus biomass. *Minerals Engineering,* 17**,** 903-911.

SELIM, H. M. 2011. *Dynamics and Bioavailability of Heavy Metals in the Rootzone*, CRC Press.

SHAH, P., STREZOV, V. & NELSON, P. F. Trace Element Speciation under Coal Fired Power Station Conditions. 2nd IASME / WSEAS International Conference on Energy & Environment (EE'07), 2007 Portoroz, Slovenia. 194-202.

SILVA, L. F. O., WARD, C. R., HOWER, J. C., IZQUIERDO, M., WAANDERS, F., OLIVEIRA, M. L. S., LI, Z., HATCH, R. S. & QUEROL, X. 2010. Mineralogy and Leaching Characteristics of Coal Ash from a Major Brazilian Power Plant. *Coal Combustion and Gasification Products,* 2**,** 51-65.

SIMEONI, M. A. 2003. *The effect of Fulvic Acid on the Adsorption of Arsenate to Minerals and Soils.* Doctor of Philosophy, Macquarie University.

SINHA, R. K. 2004. *Modern Plant Physiology,* England, CRC Press.

SPARKS, D. L. 1995. *Environmental Soil Chemistry*, Academic Press.
SPEARS, D. & LEE, S. 2004. Geochemistry of leachates from coal ash. *Geological Society, London, Special Publications,* 236**,** 619-639.
SRIVASTAVA, S., AGRAWAL, S. B. & MONDAL, M. K. 2015. A review on progress of heavy metal removal using adsorbents of microbial and plant origin. *Environmental Science and Pollution Research,* 22**,** 15386-15415.
STREAT, M., HELLGARDT, K. & NEWTON, N. L. R. 2008. Hydrous ferric oxide as an adsorbent in water treatment Part 3: Batch and mini-column adsorption of arsenic, phosphorus, fluorine and cadmium ions. *Process Safety and Environmental Protection,* 86**,** 21-30.
SU, T. & WANG, J. 2011. Modeling batch leaching behavior of arsenic and selenium from bituminous coal fly ashes. *Chemosphere,* 85**,** 1368-1374.
SUGANYA, E., RANGABHASHIYAM, S., LITY, A. V. & SELVARAJU, N. 2016. Removal of hexavalent chromium from aqueous solution by a novel biosorbent Caryota urens seeds: equilibrium and kinetic studies. *Desalination and Water Treatment,* 57**,** 23940-23950.
SUN, G. & SHI, W. 1998. Sunflower Stalks as Adsorbents for the Removal of Metal Ions from Wastewater. *Industrial & Engineering Chemistry Research,* 37**,** 1324-1328.
TEMPLETON, D. & HOPEY, D. 2010. *A debate over fly ash disposal* [Online]. Available: http://carbonwaters.org/2010/12/a-debate-over-fly-ash-disposal/ [Accessed 08/04/2017].
THEIS, T. & GARDNER, K. 1990. Environmental Assessment of Ash Disposal, Critical Reviews. *Environmental Control,* 20**,** 21.
THEIS, T. L. & WIRTH, J. L. 1977. Sorptive behavior of trace metals on fly ash in aqueous systems. *Environmental Science & Technology,* 11**,** 1096-1100.
THIRUNAVUKKARASU, O. S., VIRARAGHAVAN, T. & SUBRAMANIAN, K. S. 2003. Arsenic Removal from Drinking Water using Iron Oxide-Coated Sand. *Water, Air, and Soil Pollution,* 142**,** 95-111.
TOMECZEK, J. & PALUGNIOK, H. 2002. Kinetics of mineral matter transformation during coal combustion. *Fuel,* 81**,** 1251-1258.
TORREY, S. 1978. *Trace contaminants from coal,* Park Ridge, NJ, Noyes Data Corporation, 294.
TRADELINK, L. 2015. *Pond Ash* [Online]. Available: http://lakulishtradelink.com/pondash.html [Accessed 08/04/2017].
TUZEN, M. & SARı, A. 2010. Biosorption of selenium from aqueous solution by green algae (*Cladophora hutchinsiae*) biomass: Equilibrium, thermodynamic and kinetic studies. *Chemical Engineering Journal,* 158**,** 200-206.
UCUN, H., BAYHAN, Y. K., KAYA, Y., CAKICI, A. & FARUK ALGUR, O. 2002. Biosorption of chromium(VI) from aqueous solution by cone biomass of Pinus sylvestris. *Bioresource Technology,* 85**,** 155-158.
USEPA. 2009. *National Primary Drinking Water Regulation Table* [Online]. United States Environmental Protection Agency. Available: https://www.epa.gov/ground-water-and-drinking-water/table-regulated-drinking-water-contaminants#Inorganic [Accessed 08/02/2017].
USEPA 2010. Liquid-Solid partitioning as a function of extract pH using a parallel batch extraction. United States Environmental Protection Agency.
USEPA. 2016a. *Coal Ash Basics* [Online]. Available: https://www.epa.gov/coalash/coal-ash-basics [Accessed 01/04/2016].
USEPA. 2016b. *Final Rule: Disposal of Coal Combustion Residuals from Electric Utilities* [Online]. Available: https://www.epa.gov/coalash/coal-ash-rule [Accessed 01/04/2016].
VAGEESH, T. & SIDDARAMAPPA, R. Leachate composition and soil quality assessment in coal fly ash amended soils. 17. World congress of soil science,, Bangkok (Thailand), 14-21 Aug 2002, 2002.
VAN DER HOEK, E. E., BONOUVRIE, P. A. & COMANS, R. N. J. 1994. Sorption of As and Se on mineral components of fly ash: relevance for leaching processes. *Applied Geochemistry,* 9**,** 403-412.
VASSILEV, S. V., KITANO, K. & VASSILEVA, C. G. 1997. Relations between ash yield and chemical and mineral composition of coals. *Fuel,* 76**,** 3-8.

VASSILEV, S. V. & VASSILEVA, C. G. 2007. A new approach for the classification of coal fly ashes based on their origin, composition, properties, and behaviour. *Fuel,* 86**,** 1490-1512.
VILLAESCUSA, I., FIOL, N., MARTíNEZ, M. A., MIRALLES, N., POCH, J. & SERAROLS, J. 2004. Removal of copper and nickel ions from aqueous solutions by grape stalks wastes. *Water Research,* 38**,** 992-1002.
VOLESKY, B. 1990. *Biosorption of Heavy Metals*, Taylor & Francis.
VOLESKY, B. & HOLANT, Z. R. 1995. Biosorption of Heavy Metals. *Biotechnol. Prog.,* 11**,** 235-250.
WAN NGAH, W. S. & HANAFIAH, M. A. K. M. 2008. Removal of heavy metal ions from wastewater by chemically modified plant wastes as adsorbents: A review. *Bioresource Technology,* 99**,** 3935-3948.
WANG, L., CHEN, Z., YANG, J. & MA, F. 2015. Pb(II) biosorption by compound bioflocculant: performance and mechanism. *Desalination and Water Treatment,* 53**,** 421-429.
WANG, S. 2008. Application of solid ash based catalysts in heterogeneous catalysis. *Environmental Science and Technology,* 42**,** 7055-7063.
WANG, S., BOYJOO, Y., CHOUEIB, A., ESTHER NG, WU, H. & ZHU, Z. 2005. Role of unburnt carbon in adsorption of dyes on fly ash *Journal of Chemical Technology and Biotechnology,* 80**,** 1204-1209.
WANG, S. & WU, H. 2006b. Environmental-benign utilisation of fly ash as low-cost adsorbents-Review. *Journal of Hazardous Materials,* B136**,** 482-501.
WANG, S. & ZHU, Z. H. 2007. Humic acid adsorption on fly ash and its derived unburned carbon. *Journal of Colloid and Interface Science,* 315**,** 41-46.
WANG, W., QIN, Y., SONG, D. & WANG, K. 2008. Column leaching of coal and its combustion residues, Shizuishan, China. *International Journal of Coal Geology,* 75**,** 81-87.
WARD, C. R., FRENCH, D. & JANKOWSKI, J. 2003. Comparative evaluation of leachability test methods and element mobility for selected Australian fly ash samples. *Technical Note, 22.* Co-operative Research Centre for Coal in Sustainable Development.
WARD, C. R., FRENCH, D., JANKOWSKI, J., DUBIKOVA, M., LI, Z. & RILEY, K. W. 2009. Element mobility from fresh and long-stored acidic fly ashes associated with an Australian power station. *International Journal of Coal Geology,* 80**,** 224-236.
WEI, C., RAABE, O. G. & ROSENBLATT, L. S. 1982. Microbial detection of mutagenic nitro-organic compounds in filtrates of coal fly ash. *Environmental Mutagenesis* 4**,** 249-58.
WILD, S. R. & JONES, K. C. 1995. Polynuclear aromatic hydrocarbons in the United Kingdom environment: A preliminary source inventory and budget. *Environmental Pollution,* 88**,** 91-108.
WITEK-KROWIAK, A. 2012. Analysis of temperature-dependent biosorption of Cu2+ ions on sunflower hulls: Kinetics, equilibrium and mechanism of the process. *Chemical Engineering Journal,* 192**,** 13-20.
WITEK-KROWIAK, A. 2013. Application of beech sawdust for removal of heavy metals from water: biosorption and desorption studies. *European Journal of Wood and Wood Products,* 71**,** 227-236.
WITEK-KROWIAK, A., DARIA PODSTAWCZYK, CHOJNACKA, K., DAWIEC, A. & MARYCZ, K. 2013. Modelling and optimization of chromium III biosorption on soybean meal. *Central European Journal of Chemistry* 11**,** 1505-1517.
WOLTHERS MARIETTE, CHARLET LAURENT, VAN DER WEUDEN CONELIS H., VAN DER LINDE PETER R. & DAVID, R. 2005. Arsenic mobility in the ambient sulfidic environment: Sorption of arsenic(V) and arsenic(III) onto disordered mackinawite. *Geochimica et Cosmochimica Acta,* 69**,** 3483-3492.
WONG, Y. C., SZETO, Y. S., CHEUNG, W. H. & MCKAY, G. 2004. Adsorption of acid dyes on chitosan—equilibrium isotherm analyses. *Process Biochemistry,* 39**,** 695-704.
YANG, G. & JAAKKOLA, P. 2011. Wood chemistry and isolation of extractives from wood. *BIOTULI Project.* Finland: Saimaa University of Applied Sciences.
YANG, J. & VOLESKY, B. 1999. Modeling Uranium-Proton Ion Exchange in Biosorption. *Environmental Science & Technology,* 33**,** 4079-4085.

YANG, X., IKEHATA, K., LERNER, R., HU, Y., JOSYULA, K., CHANG, S.X. & LIU, Y. 2010. Agricultural Wastes. *Water Environment Research,* 82**,** 1396-1425.

ZDRAVKOV, B. D., ČERMÁK, J. J., ŠEFARA, M. & JANKŮ, J. 2007. Pore classification in the characterization of porous materials: A perspective. *Central European Journal of Chemistry,* 5**,** 385-395.

ZIELINSKI, R. A. & FINKELMAN, R. B. 1997. Radioactive Elements in Coal and Fly Ash: Abundance, Form, and Environmental Significance, FS-163-97.

ZIELINSKI, R. A., FOSTER, A. L., MEEKER, G. P. & BROWNFIELD, I. K. 2007. Mode of occurrence of arsenic in feed coal and its derivative fly ash, Black Warrior Basin, Alabama. *Fuel,* 86**,** 560-572.

Appendix

Tabulations of Isotherm Results

Tables of raw data of isotherm experiments

Ed-As(V) and *Mq*-As(V): Isotherm models of As(V) sorption by Ed, and Mq barks (conditions: mass of adsorbent=250 mg, volume of As(V) solution=25 mL, initial As(V) solution concentration=10, 100, 1000, 10000, and 100000 µg/L, temperature=23±2 °C, and pH 4 and 240 min for Mq and pH 5 and 120 min for Ed).

Ed-Se(IV) and *Mq*-Se(IV): Isotherm models of Se(IV) sorption by Ed, and Mq barks (conditions: mass of adsorbent=250 mg, volume of Se(IV) solution=25 mL, initial Se(IV) solution concentration= 20, 40, 80, 100, and 200 µg/L, temperature=23±2 °C, and pH 5 and 180 min for Mq and pH 6 and 120 min for Ed).

Ed-As(V)

Initial Concentration calculated (µg/L)	Concentration calculated after equilibrium sorption (µg/L)	$q_e = (C_i - C_e)*V/m$ (µg/g)	Langmuir model for Ed; y=2.1908x+0.0411		Freundlich model for Ed; y=0.6903x-0.8527		Sips model for Ed; y=-0.6903x+0.0684	
C_i	C_e	q_e	$1/q_e$	$1/C_e$	$ln(q_e)$	$ln(C_e)$	$ln(q_{max}*b/q_e)$	$ln(c_e)$
9.09	1.67	0.74	1.35	0.60	-0.30	0.51	-0.49	0.51
105.74	50.60	5.51	0.18	0.02	1.71	3.92	-2.49	3.92
1113.48	677.91	43.56	0.02	0.00	3.77	6.52	-4.56	6.52
9941.30	8876.73	106.46	0.01	0.00	4.67	9.09	-5.45	9.09
96847.83	78623.69	1822.41	0.00	0.00	7.51	11.27	-8.29	11.27

Mq-As(V)

Initial Concentration calculated (µg/L)	Concentration calculated after equilibrium sorption (µg/L)	$q_e = (C_i - C_e)*V/m$ (µg/g)	Langmuir model for Mq; y=0.2978x+0.0321		Freundlich model for Mq; y=0.7102x+0.3619		Sips model for Mq; y=-0.7102x+0.8494	
C_i	C_e	q_e	$1/q_e$	$1/C_e$	$ln(q_e)$	$ln(C_e)$	$ln(q_{max}*b/q_e)$	$ln(c_e)$
9.09	0.27	0.88	1.13	3.70	-0.13	-1.31	1.34	-1.31
105.74	26.63	7.91	0.13	0.04	2.07	3.28	-0.86	3.28
1113.48	334.35	77.91	0.01	0.00	4.36	5.81	-3.14	5.81
9941.30	4353.26	558.80	0.00	0.00	6.33	8.38	-5.11	8.38
96847.83	52891.30	4395.65	0.00	0.00	8.39	10.88	-7.18	10.88

Ed-Se(IV)

Initial Concentration calculated (µg/L)	Concentration calculated after equilibrium sorption (µg/L)	$q_e = (C_i - C_e)*V/m$ (µg/g)	Langmuir model for Ed; y=2.155x+0.0433		Freundlich model for Ed; y=0.6638x-0.2037		Sips model for Ed; y=-1.446x-0.7006	
C_i	C_e	q_e	$1/q_e$	$1/C_e$	$ln(q_e)$	$ln(C_e)$	$ln(q_{max}*b/q_e)$	$ln(c_e)$
24.68	4.77	1.99	0.50	0.21	0.69	1.56	-1.46	1.56
45.21	8.84	3.64	0.27	0.11	1.29	2.18	-2.06	2.18
89.37	19.86	6.95	0.14	0.05	1.94	2.99	-2.71	2.99
107.79	27.37	8.04	0.12	0.04	2.08	3.31	-2.85	3.31
191.16	71.79	11.94	0.08	0.01	2.48	4.27	-3.25	4.27

Mq-Se(IV)

Initial Concentration calculated (µg/L)	Concentration calculated after equilibrium sorption (µg/L)	$q_e = (C_i - C_e)*V/m$ (µg/g)	Langmuir model for Mq; y=2.4534x+0.0531		Freundlich model for Mq; y=0.7164x-0.4862		Sips model for Mq; y=-1.3762x-0.5247	
C_i	C_e	q_e	$1/q_e$	$1/C_e$	$ln(q_e)$	$ln(C_e)$	$ln(q_{max}*b/q_e)$	$ln(c_e)$
20.412	4.30	1.61	0.62	0.23	0.48	1.46	-1.37	1.46
51.216	12.49	3.87	0.26	0.08	1.35	2.52	-2.25	2.52
82.314	22.02	6.03	0.17	0.05	1.80	3.09	-2.69	3.09
95.843	26.11	6.97	0.14	0.04	1.94	3.26	-2.84	3.26
197.853	75.51	12.23	0.08	0.01	2.50	4.32	-3.40	4.32